AGARD-AR-256

AGARD

ADVISORY GROUP FOR AEROSPACE RESEARCH & DEVELOPMENT

7 RUE ANCELLE 92200 NEUILLY SUR SEINE FRANCE

AGARD ADVISORY REPORT No.256

Technical Status Review on Drag Prediction and Analysis from Computational Fluid Dynamics: State of the Art

NORTH ATLANTIC TREATY ORGANIZATION

DISTRIBUTION AND AVAILABILITY
ON BACK COVER

NORTH ATLANTIC TREATY ORGANIZATION

ADVISORY GROUP FOR AEROSPACE RESEARCH AND DEVELOPMENT

(ORGANISATION DU TRAITE DE L'ATLANTIQUE NORD)

AGARD Advisory Report No.256

TECHNICAL STATUS REVIEW

on

DRAG PREDICTION AND ANALYSIS FROM COMPUTATIONAL FLUID DYNAMICS: STATE OF THE ART

The information in this report was presented at an AGARD Fluid Dynamics Panel Technical Status Review on Drag Prediction and Analysis from Computational Fluid Dynamics: State of the Art, held at the Laboratorio Nacional de Engenharia Civil, Lisbon, Portugal, on 5 May 1988

THE MISSION OF AGARD

According to its Charter, the mission of AGARD is to bring together the leading personalities of the NATO nations in the fields of science and technology relating to aerospace for the following purposes:

— Recommending effective ways for the member nations to use their research and development capabilities for the common benefit of the NATO community;

— Providing scientific and technical advice and assistance to the Military Committee in the field of aerospace research and development (with particular regard to its military application);

— Continuously stimulating advances in the aerospace sciences relevant to strengthening the common defence posture;

— Improving the co-operation among member nations in aerospace research and development;

— Exchange of scientific and technical information;

— Providing assistance to member nations for the purpose of increasing their scientific and technical potential;

— Rendering scientific and technical assistance, as requested, to other NATO bodies and to member nations in connection with research and development problems in the aerospace field.

The highest authority within AGARD is the National Delegates Board consisting of officially appointed senior representatives from each member nation. The mission of AGARD is carried out through the Panels which are composed of experts appointed by the National Delegates, the Consultant and Exchange Programme and the Aerospace Applications Studies Programme. The results of AGARD work are reported to the member nations and the NATO Authorities through the AGARD series of publications of which this is one.

Participation in AGARD activities is by invitation only and is normally limited to citizens of the NATO nations.

Published June 1989

ISBN 92-835-0516-6

Printed by Specialised Printing Services Limited
40 Chigwell Lane, Loughton, Essex IG10 3TZ

FOREWORD AND CONCLUSIONS

by
J.W.Slooff
National Aerospace Laboratory, NLR,
Amsterdam, Netherlands

In the past 10—20 years Computational Fluid Dynamics (CFD) has emerged as an indespensible tool in aircraft design. Methods based on linearized theory (Panel Methods) and Full Potential theory with or without inclusion of viscous effects are being used on a routine basis in industry and research establishments. Methods based on the Euler equations and Reynolds Averaged Navier-Stokes equations, at least for simple configurations, are approaching this status. The status is reflected in, a.o., the proceedings (ref. 1) on "Applications of Computational Fluid Dynamics in Aeronautics", held in Aix-en-Provence, in the spring of 1986.

One of several observations made at the Aix-en-Provence meeting (ref. 2) was that the computation of drag was given only secondary treatment in almost all of the papers presented. This in spite of the importance of drag for aircraft performance. In the Round Table Discussion terminating the Aix meeting both the accuracy of drag prediction and the breakdown of drag into its basic components (viscous, induced and wave drag) emerged as being very important but not satisfactorily dealt with. It was concluded that the topic should receive more attention in the future.

In order to stimulate such attention the FDP decided to organize a Technical Status Review (TSR) on the topic of "Drag Prediction and Analysis from Computational Fluid Dynamics".The primary objective was to obtain a survey of the state-of-the-art in the NATO countries. The TSR was to take place in conjunction with the FDP Symposium on "Validation of Computational Fluid Dynamics" to be held in the spring of 1988 in Lisbon because this symposium was expected to address also the aspect of validation with respect to drag. Since the symposium was expected to draw a large audience it was decided that the TSR would be of "open" character allowing all symposium participants to become aware of the current status of CFD-based drag prediction. In this way attention to the subject would be stimulated within a large group of researchers.

Contributions to the TSR were made by:

J.J.Thibert	(France)
W.Schmidt and P.Sacher	(Germany)
K.Papailiou	(Greece)
M.Borsi and G.Bucciantini	(Italy)
J.van der Vooren	(Netherlands)
P.Ashill	(UK)
T.Holst	(USA)
C.Boppe	(USA)

In the opinion of the FDP the presentations contained very valuable information on the subject. For this reason the authors were requested to provide written versions. These have been collected in the present volume.

At the meeting there was, unfortunately, very little time for discussion. However, the main conclusions can be summarized as follows.

1. Accurate and consistent computation through CFD of (absolute) drag levels for complex configurations is, not surprisingly, beyond reach for a considerable time to come. Pacing items are basically the same as those of CFD in general (grid generation, turbulence modelling, grid resolution, speed and economics of computation). However, for drag prediction purposes the importance of some factors, such as grid resolution and speed/economics of computation, is amplified by one or several orders of magnitude.

2. For attached flow about simple configurations (2D airfoils, wings, wing-bodies, isolated bodies, isolated nacelles) CFD drag prediction has met with some, though limited, success.

   It appears that for 2D airfoils most but not all codes can now predict drag with an accuracy of within about 5%. For 3D wings this figure appears to be the order of 10%; possibly somewhat less for transport aircraft wings, probably higher for combat aircraft.

3. For body or nacelle-type components there is little information but some can be found in the papers by Ashill, Boppe and Schmidt & Sacher. The latter mention prediction of supersonic wave drag and afterbody drag as particularly challenging topics.

4. Prediction through Euler codes of drag-due-to-lift for combat aircraft wings with leading-edge vortices has met with some success (Schmidt & Sacher).

5. For separated flows inadequate turbulence modelling in combination with inappropriate grid clustering and refinement are problem areas even in 2D airfoil flow.

6. Navier-Stokes codes typically do not (yet) involve drag prediction except for 2D airfoil flows. Even then they do not do a better job than zonal methods involving potential flow or Euler schemes coupled with boundary layers.

7. The application for drag prediction purposes of the current generation of Euler codes, in particular in 3D, is hampered by (over) sensitivity to grid density and quality through spurious (artificial) dissipation. For 3D wings and wing-bodies with attached flow only full potential methods with or without boundary layers appear to have met with some success.

8. Most authors seem to agree that a "far-field" type of drag assessment based on application of the momentum theorem is to be preferred over a "near-field" type of procedure (pressure and skin friction integration), both for reasons of accuracy as well as for the purpose of identifying the viscous, induced (vortex) and shock-wave related components of drag.

9. Identification and quantification through CFD of the viscous, induced and shock-wave components of drag seems to be fairly well established for potential flow models (with or without boundary layers). For Euler flow models the principles seem to be clear but not the technical/numerical code implementation. For (Reynolds-averaged) Navier-Stokes methods the identification and quantification of the viscous, induced and wave drag components is as yet unclear and might even be impossible without introducing certain assumptions with respect to the asymptotic structure of the flow field.

10. There is no or insufficient experimental material available for validation of CFD procedures for predicting the viscous, induced and shock-wave components of drag.

11. In spite of the limitations mentioned above CFD-based drag prediction has proven to be useful when embedded in an increment/decrement procedure involving experimental (W/T) results for the complete configuration and CFD results for simplified configurations, the latter even as far down as 2D. A symbolic algorithm for such a procedure might be written as

$$C_{D_{complex}}^{(new)} = C_{D_{complex}}^{(old)} + C_{D_{simple}}^{(new)} - C_{D_{simple}}^{(old)}$$

Here $C_{D_{complex}}^{(old)}$ is to be obtained through W/T testing

and $C_{D_{simple}}$ (old and new) through CFD

It is recommended that the Fluid Dynamics Panel considers possibilities for further stimulation of progress in the field of CFD-based drag prediction and analysis, in particular with respect to pts. 3,4,5,6,7, and 9 (Euler and Navier-Stokes codes) and pt. 10. One possibility to be considered is a Working Group with the objective to collect and document suitable experimental data (pt. 10). Another suggestion is to consider the possibility of organising a specialists' meeting within a 3 to 5 years time frame.

References

1. "Applications of Computational Fluid Dynamics in Aeronautics". AGARD-CP-412, 1986

2. W.J.McCroskey "Technical Evaluation Report on the Fluid Dynamics Panel Symposium on Applications of Computational Fluid Dynamics in Aeronautics". AGARD-AR-240, 1987

PRÉFACE ET CONCLUSIONS

par
J.W.Slooff
National Aerospace Laboratory (NLR)
Amsterdam
Pays-Bas

Au cours des 10 à 20 dernières années le calcul en dynamique des fluides (CFD) s'est affirmé comme un outil indispensable dans la conception des aéronefs. Des méthodes basées sur la théorie linéarisée (Les Méthodes de Panel) et sur l'équation complète du potentiel avec ou sans incorporation des effets visqueux, sont couramment employées dans l'industrie et dans les établissements de recherche. Les méthodes basées sur les équations d'Euler et sur la moyenne des équations Navier-Stokes établie à partir des nombres de Reynolds, atteignent le même niveau d'acceptation, du moins pour les configurations simples.

Cet état de fait est confirmé entre autres, par le compte rendu de la conférence sur "Les applications du calcul en dynamique des fluides dans le domaine de l'aéronautique" (ref. 1) tenue à Aix en Provence au printemps de l'année 1986.

L'un des participants à la réunion d'Aix en Provence (ref. 2) a constaté qu'il n'avait été accordée qu'une importance secondaire au calcul de la traînée dans la quasi-totalité des communications présentées, et ceci en dépit de son importance pour la détermination des performances des aéronefs. Lors de la table ronde organisée en fin de séance à Aix, l'exactitude de la prévision de la traînée et sa partition en éléments de base (la traînée visqueuse, la traînée induite, la traînée d'onde) se sont révelés comme des sujets très importants. Malheureusement ils n'ont été examinés que partiellement ou pas du tout lors de la réunion. Les participants sont convenus qu'une plus grande attention devrait être portée sur ce sujet à l'avenir.

Le Panel FDP a décidé de faire le point de l'état des techniques dans ce domaine, avec pour titre "Les techniques de prévision et d'analyse de la traînée par le calcul en dynamique des fluides". Le Panel s'est fixé comme objectif principal de faire le point de l'état de l'art dans les pays membres de l'OTAN. Cette étude devait être réalisée conjointement avec le symposium FDP sur "La validation du calcul en dynamique des fluides" prévu au printemps de l'année 1988 à Lisbonne, puisque ce symposium devait examiner aussi la question de la validation par rapport à la traînée.

Vu le fait qu'un grand nombre de participants était annoncé pour ce symposium, il a été décidé de communiquer les résultats de cette étude aux participants afin de les informer sur l'état actuel des connaissances dans le domaine de la prévision de la traînée par le calcul en dynamique des fluides. Le Panel a voulu ainsi promouvoir la recherche dans ce domaine, auprès d'un grand groupe de chercheurs.

Les personnalites ayant participé à ces travaux sont:

J.J.Thibert (France)
W.Schmidt & P.Sacher (République Fédérale d'Allemagne)
K.Papailiou (Grèce)
M.Borsi et G.Bucciantini (Italie)
J.van der Vooren (Pays-Bas)
P.Ashill (Grande Bretagne)
T.Holst (Etats-Unis)
C.Boppe (Etats-Unis)

De l'avis du FDP, les présentations comportaient des informations précieuses sur ce sujet. Par conséquent il a été demandé aux auteurs d'en fournir des versions écrites pour les présenter dans ce recueil.

Malheureusement, il n'est resté que très peu de temps pour la table ronde en clôture de séance dont les principales conclusions peuvent être resumées comme suit:

1. Le calcul précis et répétitif des niveaux absolus de traînée pour des configurations complexes au moyen du CDF, n'est envisageable que dans un avenir relativement lointain. L'avancement dans ce domaine dépend essentiellement des mêmes éléments que pour le CDF en général soit: (la génération des maillages, la modélisation de la turbulence, la résolution des maillages, la vitesse et la rentabilité de calcul). Pourtant, dans le cas de la prévision de la traînée, l'importance de certains facteurs, tels que la résolution des maillages et la vitesse/rentabilité de calcul, est amplifiée d'un ou de plusieurs ordres de grandeur.

2. En ce qui concerne les écoulements attachés autour de configurations simples (profils bidimensionnels, voilures, corps isolés, nacelles isolées) la prévision de la traînee par CDF a eu un certain succès, dont l'impact a pourtant été limité. Il semblerait que pour les profils bidimensionnels, la plupart des codes permettent désormais la prévision de la traînée avec une précision d'au moins 5%. Pour les voilures tridimensionnelles ce chiffre serait de l'ordre de 10%: peut-être un peu moins pour les voilures des aéronefs de transport et probablement un peu plus pour les aéronefs de combat.

3. Très peu d'informations existent pour les éléments de fuselage ou de nacelle à part celles qui figurent aux études de ASHILL, BOPPE, SCHMIDT & SACHER. Ces auteurs parlent de la prévision de la traînée d'ondes supersoniques et de la traînée de l'arrière corps comme étant des sujets particulièrement intéressants.

4. La prévision de la traînée due à la portance par codes Euler pour les voilures des aéronefs de combat présentant des tourbillons du bord d'attaque a connu un certain succès (SCHMIDT & SACHER).

5. Dans les cas des écoulement décollés, des problèmes se posent en raison des imperfections dans la modélisation de la turbulence et de groupement et de l'épuration peu appropriés des maillages, même en ce qui concerne les écoulements bidimensionnels autour des profils aérodynamiques.

6. En général, les codes Navier-Stokes ne s'appliquent pas (encore) à la prévision de la traînée, sauf pour les écoulements bidimensionnels autour des profils aérodynamiques. Dans ces cas, même les résultats obtenus ne sont guère mieux que ceux fournis par les méthodes zonales qui font appel à l'écoulement potentiel ou aux schémas d'Euler, combinés aux couches limites.

7. L'application de la présente génération de codes Euler à la prévision de la traînée, et en tridimensionnel en particulier est entravée par une sensibilité excessive à la densité et à la qualité du maillage occasionnée par de fausses pertes (artificielles).

Pour ce qui est des voilures tridimensionnelles et des configurations voilure-fuselage avec écoulements attachés, seules les méthodes à potentiel entier, avec ou sans couches limites ont eu du succès.

8. La majorité des auteurs sont de l'avis que la prévision de la traînée du type "champ lointain", basée sur l'application du théorème des moments est préférable à l'approche "champ proche" (intégration de la pression et du frottement superficiel) tant pour des raisons de précision que pour permettre l'identification des raisons de précision que pour permettre l'identification des éléments constitutifs de la traînée ayant rapport aux ondes de choc et aux phénomènes visqueux, induits (tourbillons).

9. Il semble que l'identification et la quantification de ces éléments constitutifs par l'intermédiaire des techniques du CDF soient acquises pour la modélisation de l'écoulement potentiel (avec ou sans couches limites). Pour les modèles Euler les principes semblent assez clair, ce qui n'est pas le cas pour la mise en oeuvre des codes techniques/numériques. Pour les méthodes Navier-Stokes (Moyenne des nombres de Reynolds) l'identification et la quantification des éléments visqueux, induits et de traînée d'onde ne sont pas encore bien définies et pourraient même s'avérer impossibles sans introduire certaines hypothèses ayant trait à la structure asymptotique de l'écoulement.

10. Selon le cas, il existe peu ou pas de matériel experimental pour la validation des procédures CDF en vue de la prévision des éléments constitutifs de la traînée visqueuse induite et d'onde de choc.

11. Malgré les contraintes indiquées plus haut, la prévision de la traînée par CDF s'est avérée très efficace, à condition d'être intégrée dans une procédure d'incrément/decrément faisant appel à des résultats expérimentaux (en soufflerie) pour l'ensemble de la configuration et des résultats CDF pour les configurations simplifiées, allant même jusqu'au bidimensionnel. Un algorithme symbolique pour une telle procédure pourrait s'écrire:

$$C_{D_{complexe}}^{(nouveau)} = C_{D_{complexe}}^{(ancien)} + C_{D_{simple}}^{(nouveau)} - C_{D_{simple}}^{(ancien)}$$

où $C_{D_{complexe}}^{(ancien)}$ est à définir par des essais en soufflerie

et $C_{D_{simple}}$ (ancien et nouveau) par CDF

Il est recommandé au Panel AGARD de la Dynamique des Fluides de réfléchir aux moyens qui existent pour faire avancer les travaux dans le domaine de la prévision et l'analyse de la traînée par CDF, et en particulier les points 3,4,5,6,7 et 9 (Codes Euler et Navier-Stokes) et le point 10. L'une des possibilités consisterait à envisager la formation d'un groupe de travail qui aurait pour mission de recueillir et de classer les données expérimentales appropriées (point 10).

Le Panel pourrait également envisager l'organisation d'une réunion de specialistes sur ce sujet, d'ici 3 a 5 ans.

Références:

1. "Applications of Computational Fluid Dynamics in Aeronautics" AGARD-CP-412, 1986

2. W.J.McCroskey "Technical Evaluation Report on the Fluid Dynamics Panel Symposium on Applications of Computational Fluid Dynamics in Aeronautics" AGARD-AR-240, 1987

AGARD FLUID DYNAMICS PANEL

Chairman: Mr D.H.Peckham
Superintendent AE2 Division
Royal Aerospace Establishment
R141 Building
Farnborough Hants GU14 6TD
U.K.

Deputy Chairman: Dr J.W.McCroskey
Senior Staff Scientist
US Army Aero Flightdynamics
Directorate (AVSCOM)
NASA Ames Research Center
Moffett Field, CA 94035—1099
U.S.A.

PROGRAMME COMMITTEE MEMBERS

Professor Ir. J.W.Slooff (Chairman)
National Aerospace Laboratory NLR
Anthony Fokkerweg 2
1059 CM Amsterdam
Netherlands

Major Z.Gikas
Hellenic Air Force Tech. Res. Center
KETA
Terpsithea
16501 Glyfada
Athens, Greece

Mr L.H.Ohman
Head High Speed Aerodynamics Lab.
National Aeronautical Establishment
National Research Council
Montreal Road
Ottawa, Ontario K1A 0R6
CanadaItaly

Dr Ing. G.Bucciantini
Aeritalia-Societa Aerospaziale
Italiana
Gruppo Velivoli Combattimento
Corso Marche 41
10146 Torino

M. l'Ing. Général B.Monnerie
Directeur Adjoint
Direction Aérodynamique
B.P. 72
ONERA
92322 Châtillon
France

Mr A.Vint
APM Tornado IDS Development-W182C
British Aerospace PLC
Warton Aerodrome
Warton
Preston PR4 1AX
United Kingdom

Dr W. Schmidt
Deputy Director, Dornier 328 Program
Dornier GmbH, EY
P.O.Box 1420
D-7990 Friedrichshafen 1
Federal Republic of Germany

Mr D.L.Bowers
Aeromechanics Division,
Flight Dynamics Laboratory
AFWAL/FIMM
Wright Patterson AFB, Ohio 45433
United States

Professor Dr G. Georgantopoulos
Hellenic Air Force Academy
Dekelia Airbase
Athens,
Greece

PANEL EXECUTIVE

M.C.Fischer
Fluid Dynamics Panel
AGARD
7 rue Ancelle
92200 Neuilly-sur-Seine
France

CONTENTS

	Page
FOREWORD AND CONCLUSIONS	iii
AGARD FLUID DYNAMICS PANEL OFFICERS AND PROGRAMME COMMITTEE	vii
	Reference
PREVISION DE LA TRAINEE A PARTIR DES METHODES DU CALCUL. ETAT DE L'ART EN FRANCE by J.J.Thibert	1
DRAG PREDICTION AND ANALYSIS FROM CFD. STATE-OF-THE-ART IN GERMANY by W.Schmidt and P.Sacher	2
SOME RESULTS ON FLOW CALCULATIONS INVOLVING DRAG PREDICTION by K.D.Papailiou	3
STATE OF THE ART OF AIRCRAFT DRAG PREDICTION IN ITALY BY MEANS OF THEORETICAL METHODS by G.Bucciantini and M.Borsi	4
AIRCRAFT DRAG PREDICTION FOR TRANSONIC POTENTIAL FLOW by J.van der Vooren	5
CFD METHODS FOR DRAG PREDICTION AND ANALYSIS CURRENTLY IN USE IN UK by P.R.Ashill	6
COMPUTATIONAL FLUID DYNAMICS DRAG PREDICTION – RESULTS FROM THE VISCOUS TRANSONIC AIRFOIL WORKSHOP by T.L.Holst	7
CFD DRAG PREDICTION FOR AERODYNAMIC DESIGN by C.W.Boppe	8

PREVISION DE LA TRAINEE A PARTIR DES METHODES DE CALCUL. ETAT DE L'ART EN FRANCE

(Drag Prediction and Analysis From Computational Fluid Dynamics.State of the Art in FRANCE)

par
J.J. THIBERT
Chef de la division Aérodynamique Appliquée
Avions de Transport
Office National d'Etudes et de Recherches Aérospatiales (ONERA)
B.P. N° 72 - 92322 CHATILLON CEDEX (France)

RESUME

Les approches de l'industrie et de la recherche en matière de prévision de traînée sont différentes. L'industrie est confrontée au difficile problème de la prévision de la traînée de configurations complètes ce qui est actuellement impossible uniquement à l'aide des méthodes de calcul existantes.

Cependant des prévisions de traînée doivent être effectuées soit au cours de la phase de définition d'un projet pour choisir entre différentes solutions, soit pour évaluer la traînée d'un projet donné. Dans le premier cas la connaissance du niveau absolu de la traînée n'est pas nécessaire et les choix sont effectués en comparant les traînées calculées. Dans le second cas les méthodes de prévision utilisées sont basées sur la connaissance de la traînée en soufflerie et en vol d'un avion pris comme référence. La traînée du nouveau projet est alors estimée en terme d'écart par rapport à l'avion de référence en utilisant les résultats d'essais en soufflerie et les calculs.

Il existe cependant des différences au niveau du type des méthodes de calcul ainsi que dans leur mode d'utilisation entre les constructeurs civils ou militaires.

Des efforts importants ont été consacrés ces dernières années dans les instituts de recherche et en particulier à l'ONERA dans le but de déterminer pour chaque type de méthode de calcul le meilleur processus de calcul de la traînée. Ces différentes approches ont été validées à l'aide de comparaisons avec des essais effectués sur des configurations géométriques simples telles que des profils ou des ailes.

Quelques exemples d'analyse des différents termes de traînées issus des méthodes fluide parfait bidimensionnelles et tridimensionnelles résolvant l'équation du potentiel ou les équations d'Euler sont présentés. Pour les méthodes couplées des comparaisons avec les essais montrent que les méthodes potentielles utilisées habituellement pour les applications permettent d'atteindre des niveaux de précision en 2D et 3D de quelques pour cent. Beaucoup d'efforts restent à faire en ce qui concerne les nouvelles méthodes de calcul comme les méthodes Euler couplées ou Navier-Stokes pour obtenir, voire améliorer ce niveau de précision.

L'amélioration encore nécessaire de la précision de la prévision des différents termes de traînée nécessite des résultats d'essais détaillés et précis qui ne sont pas disponibles en 3D et un effort devrait être effectué en ce sens.

ABSTRACT

The industry and the research institutes approaches for drag prediction based on CFD are different.

Industry works mainly on complete configurations the drag prediction of which are impossible at this time with existing CFD codes. However drag predictions have to be made for performance comparisons of several designs and for the drag prediction of a given project. In the first case the knowledge of the absolute value of the drag is not necessary and only the differences in drag prediction by CFD are taken into account.

For the second case drag prediction techniques are based on the knowledge in wind tunnel and in flight of the drag of a given aircraft which is taken as a reference. The drag of a new project is then estimated in term of difference with the reference aircraft using CFD and wind tunnel data. However differences in CFD codes as well as in the way they are used for drag prediction appear between civil or military aircraft manufacturers.

Much effort has been devoted these last years in the research institutes in order to determine for each type of theoretical modeling the best way to compute drag taking into account the assumptions included in the models.

These approaches have been checked by comparisons with experiments carried out on simple configuration like airfoils or wings.

Some examples of drag component analysis for inviscid flow methods solving the potential equation or the Euler equations are presented. For the viscous methods comparisons of drag prediction with experimental data show that the potential codes which are currently used for performance prediction give an accuracy of the drag within a few percent. Much effort has to be done in the next future in order to obtain with the new viscous Euler codes or Navier-Stokes codes under development the same or even a better degree of accuracy.

The necessary improvement of the different drag component prediction which still has to be made needs detailed experiments which are not yet available for 3D configurations.

1 - INTRODUCTION

Le développement de la puissance des ordinateurs associé aux progrès réalisés en analyse numérique ont permis l'élaboration ces dernières années de programmes de calcul performants, résolvant des systèmes d'équations de plus en plus complexes et permettant l'étude théorique de configurations pour lesquelles jusqu'alors seule une étude expérimentale était envisageable. Malgré ces progrès il faut bien reconnaître que pour ce qui est de la prévision de la traînée la situation actuelle n'est pas satisfaisante. Il est en effet plus facile d'obtenir de bonnes corrélations entre les calculs et les essais en ce qui concerne les répartitions de pression ou le développement des couches limites sur une voilure par exemple que de

prédire la traînée avec une précision suffisante pour une estimation correcte des performances. Les constructeurs, pour l'évaluation de la traînée d'un nouvel appareil civil ou militaire utilisent donc encore largement les essais en soufflerie en s'aidant toutefois des calculs soit pour comparer diverses solutions soit pour transposer plus ou moins directement les résultats de soufflerie aux conditions de vol. Des études plus détaillées sur des configurations plus simples (profils et voilures) ont été effectuées à l'ONERA avec pour objectif de déterminer en fonction des méthodes de calcul utilisées la meilleure technique de calcul de la traînée en s'appuyant sur des résultats expérimentaux.

Dans une première partie sera présentée la méthodologie utilisée, tant en ce qui concerne les avions civils que militaires, pour la prévision de la traînée. Dans une seconde partie les principaux résultats des études effectuées à l'ONERA en matière de bilan de traînée et des possibilités actuelles des méthodes de calcul seront discutés.

2 - PREVISION DE LA TRAINEE : L'APPROCHE INDUSTRIELLE

Les industriels sont confrontés au difficile problème d'optimiser la forme d'une configuration complète d'avion en prenant en compte de nombreuses contraintes. Cette optimisation se fait progressivement au fur et à mesure de l'avancement d'un projet en utilisant à la fois les calculs et les essais en soufflerie. Selon le type d'avion, civil ou militaire, les méthodes de calcul utilisées ainsi que la méthodologie retenue pour l'évaluation de la traînée diffèrent sensiblement.

2.1 - Avions civils

Les méthodes de calcul couramment utilisées sont des méthodes irrotationnelles :

- méthodes de singularités,
- méthodes linéarisées compressibles,
- méthodes potentielles transsoniques (différences finies ou éléments finis),
- méthodes potentielles couplées avec des calculs de couches limites tridimensionnelles.

Ces méthodes de calcul sont utilisées au stade de l'avant projet pour comparer les performances de diverses solutions concernant des éléments de l'appareil : profils, voilure, installation motrice, hypersustentation.

Les comparaisons sont effectuées plutôt en terme de répartitions de pression ou de charge en envergure qu'en terme de traînée proprement dit bien que pour des géométries voisines une certaine confiance soit accordée à la prévision de la traînée (en terme d'écarts) pour les profils et les voilures.

Pour le projet proprement dit la prévision du C_x n'est pas possible à l'aide des méthodes de calcul (maillages, temps de calcul...). Elle est basée sur la technique de l'avion de référence selon la méthodologie suivante :

- pour l'avion de référence (qui est généralement l'avion précédent ou un avion de géométrie voisine) les traînées en vol et en soufflerie sont connues ;

- sur cet avion un bilan de traînée au point de croisière basé sur les essais en soufflerie permet d'extraire les trois principales composantes :
  . C_x minimum
  . C_x compressibilité
  . C_x induit

- le C_x minimum est ensuite corrigé des effets Reynolds en utilisant des calculs de couche limite, par contre les deux autres termes sont généralement conservés ;

- le bilan ainsi transposé aux conditions de vol est comparé au C_x de vol et les écarts constatés sont imputés au terme C_x compressibilité + C_x induit ;

- pour le nouvel avion le même procédé est utilisé à partir des essais en soufflerie et le ΔC_x constaté sur l'avion de référence est utilisé pour corriger l'estimation ainsi effectuée.

Cette technique suppose que le nouvel avion et l'avion de référence aient des géométries voisines et que les conditions de croisière (nombre de Mach, portance) soient proches. Elles n'est de plus valable que pour des conditions proches de la croisière c'est-à-dire en l'absence de décollements. Les précisions ainsi obtenues sont de l'ordre de quelques pour cent à condition toutefois que la précision des résultats d'essais en soufflerie soit excellente.

2.2. - Avions militaires

Bien que la précision requise pour l'évaluation de la traînée soit un peu moins élevée que pour les avions civils, la complexité des formes et le domaine de vol plus étendu rendent cette estimation encore plus difficile. Les méthodes de calcul couramment utilisées sont :

- méthodes de singularité,
- méthodes potentielles transsoniques (différences finies),
- méthodes Euler (volumes finis et éléments finis),
- méthodes de calcul des couches limites tridimensionnelles.

Pour un projet d'avion nouveau l'évaluation de la traînée se fait au départ avec des méthodes simples, cette évaluation étant affinée au fur et à mesure du développement du projet par l'utilisation de méthodes de calcul plus complexes. Cette évaluation se fait toujours par comparaison avec un avion de référence dont la traînée en vol et en soufflerie est connue. Cet avion permet de valider les modèles de prévision dans les conditions de soufflerie et de vol, la prévision du C_x du nouvel avion se faisant en termes d'écarts par rapport à l'avion de référence.

Si une relative confiance est accordée aux méthodes de calcul pour ce qui est de la prévision de la traînée d'onde et de la traînée de frottement, par contre des termes tels que la traînée des arrière-corps ou la traînée due aux charges sont encore inaccessibles aux calculs.

Par ailleurs des bilans de traînée tels que ceux effectués sur les avions civils ne sont généralement pas utilisés, les essais en soufflerie ou en vol ne permettant pas de valider ces bilans ; de plus la transposition en vol de certains termes comme cela est pratiqué pour les avions civils notamment pour la traînée induite n'est pas toujours considérée comme un processus fiable.

3 - PREVISION DE LA TRAINEE : ETUDES EFFECTUEES A L'ONERA

Les organismes de recherche tels que l'ONERA n'ont pas pour mission de définir des configurations complètes. Leurs principales activités concernent :

- le développement de nouvelles méthodes de calcul,
- la validation de ces méthodes sur des éléments d'avions (profils, voilures, configurations voilures-fuselage...).

Comme ces organismes ne disposent généralement pas de mesures en vol ces validations sont effectuées à l'aide d'essais en soufflerie.

Parmi les nombreuses méthodes de calcul développées à l'Office les plus utilisées au niveau des applications en aérodynamique externe sont :

- les méthodes de singularités,
- les méthodes potentielles,
- les méthodes Euler.

Les méthodes Navier-Stokes initialement développées pour les écoulements internes sont utilisées depuis peu en aérodynamique externe et de ce fait leurs possibilités en matière de prévision de la traînée ne sont pas encore établies. Par contre pour les autres méthodes et notamment les méthodes potentielles l'expérience acquise depuis de nombreuses années permet de faire un bilan quant à leur capacité à prévoir la traînée.

3.1 - Ecoulement bidimensionnel de fluide parfait

Ce cas le plus simple que l'on puisse envisager met toutefois en évidence la difficulté de la prévision du C_x pression. La figure 1 montre l'éventail des valeurs obtenues en utilisant la plupart des méthodes fluide parfait disponibles sur le profil NACA0012 à $M = 0,8$ et $\alpha = 0$. Les valeurs de C_x obtenues par intégration des pressions s'étagent entre 52 10^{-4} et 127 10^{-4}, la valeur généralement admise étant voisine de 90 se trouve donc approximativement au milieu de la plage.

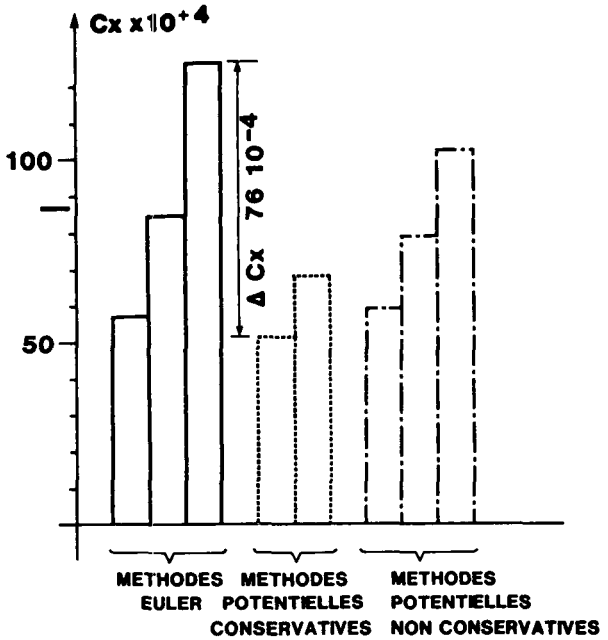

Fig. 1 - Prévision de la traînée de pression
Fluide parfait 2D. Profil NACA0012
$M = 0,8$ $\alpha = 0$.

Les causes de ces écarts sont évidemment multiples :

. maillage,
. convergence des calculs,
. type d'équations résolues (Potentiel, Euler),
. schéma numérique (conservatif ou non),
. viscosité artificielle.

Ces différents paramètres n'étant généralement pas complètement indépendants une étude systématique de leur influence n'est pas toujours possible néanmoins un certain nombre de tendances ont été dégagées.

3.1.1 - Influence du maillage

Cette étude effectuée avec une méthode potentielle différences finies utilisant un maillage en C montre figure 2 que même aux basses vitesses pour atteindre une précision de l'ordre de 10^{-4} un maillage d'environ 40000 points serait nécessaire.

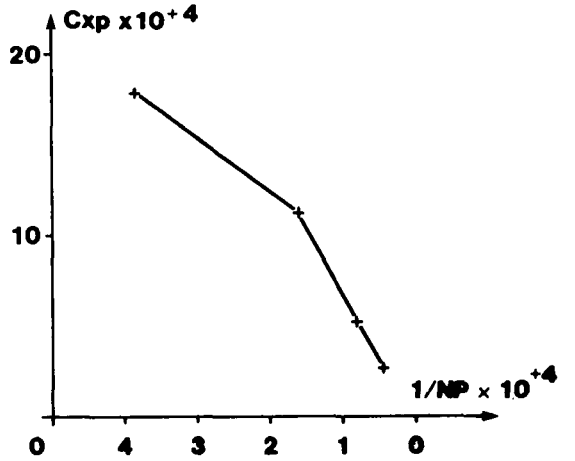

Fig. 2 - Influence du nombre de points de maillage
Fluide parfait 2D. Profil NACA0012
$M = 0,1$ $\alpha = 0$.

Ce nombre de points de maillage dépend de la topologie utilisée (C, H ou O) et de la viscosité artificielle de la méthode. Les maillages couramment utilisés et qui comportent de l'ordre de 5000 à 7000 points selon les méthodes ne permettent donc pas d'obtenir une précision du C_{xp} par intégration des pressions supérieure à 10 10^{-4}. Pour ce qui est de l'extension du maillage, son influence est présentée figure 3 pour deux valeurs de la densité de points. Une extension de l'ordre de 25 habituellement retenue permet d'atteindre un niveau de précision sur le C_{xp} d'un ordre de grandeur supérieur à celui lié au nombre de points.

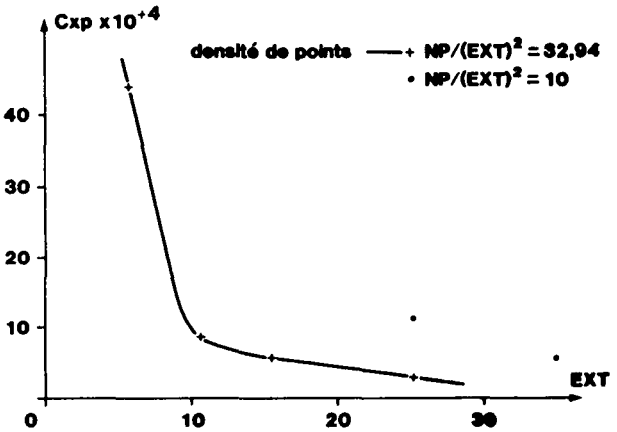

Fig. 3 - Influence de l'extension du maillage
Fluide parfait 2D. Profil NACA0012
$M = 0,1$ $\alpha = 0$.

Outre les problèmes de maillages il faut également une convergence du calcul excellente ce qui conduit pour certaines méthodes de calcul utilisées et notamment les méthodes de relaxation à un grand nombre d'itérations.

3.1.2 - Influence du schéma numérique

Sur la figure 4 sont tracées les répartitions de pressions obtenues sur le profil NACA0012 à M = 0,8 et $\alpha = 0$ avec trois méthodes potentielles. Les nombres de points de maillages sont voisins et les algorithmes sont du type SLOR. Les deux méthodes non conservatives [1] et la version 2D de [2] donnent des positions de choc voisines avec cependant un écart sur le C_x de 20 10^{-4}. La position du choc obtenue avec la méthode conservative dérivée de la méthode [2] est bien entendu plus reculée et son intensité plus forte.

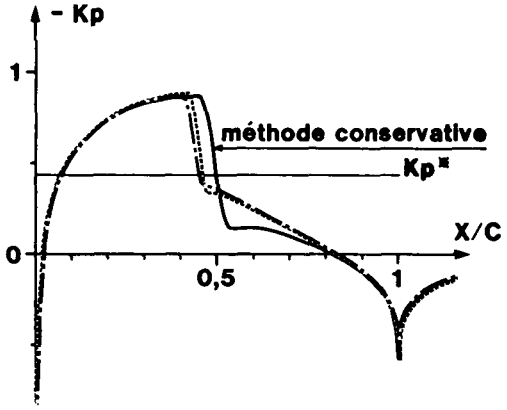

Fig. 4 - Répartitions des pressions
Profil NACA0012 M = 0,8 $\alpha = 0$.
Méthodes de calcul potentielles.
Fluide parfait.

Ces différences de position et d'intensité de choc bien connues avec les méthodes potentielles existent également avec les méthodes Euler. Ainsi la figure 5 montre les mêmes répartitions de pression calculées avec deux méthodes Euler implicites [3] et [4] ne différant que par le schéma numérique et la viscosité artificielle liée au schéma.

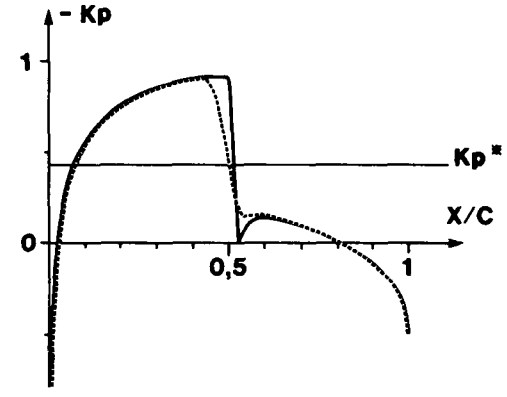

Fig. 5 - Répartitions des pressions
Profil NACA0012 M = 0,8 $\alpha = 0$.
Méthodes Euler implicites.

Si les positions de choc sont voisines les sauts de pression à travers le choc sont très différents et l'écart sur le C_x est de 42 10^{-4}. On retrouve également un ΔC_x de 30 10^{-4} entre la méthode [3] et la méthode [5] qui est une méthode Euler explicite utilisant un schéma du type Mac Cormack, cette dernière méthode donnant une position de choc voisine de celle obtenue avec les méthodes potentielles non conservatives.

La tendance généralement admise attribuant aux solutions Euler des positions de choc et des sauts de pression à travers le choc intermédiaires entre les solutions potentielles non conservatives et conservatives n'est donc pas générale.

3.1.3 - Méthodes d'estimation du C_{xp}

Pour pallier les difficultés mentionnées précédemment concernant l'estimation du C_x de pression à partir de l'intégration des pressions deux techniques sont utilisées dans les méthodes potentielles.

La première technique vise à réduire les erreurs dues à l'imprécision du schéma numérique. Elle consiste à corriger la valeur du C_{xp} (=$C_x$choc) obtenu par intégration des pressions de l'intégrale de la quantité de mouvement calculée sur un contour entourant la région subsonique de l'écoulement, intégrale qui devrait en principe être nulle en écoulement subcritique. Ceci est équivalent à un calcul de la traînée de choc à l'aide d'un bilan de quantité de mouvement sur un contour entourant les régions supersoniques de l'écoulement. Cette technique d'évaluation du C_{xp} utilisée dans la version 2D de [6] permet d'obtenir des valeurs plus réalistes comme le montrent les figures 6 et 7.

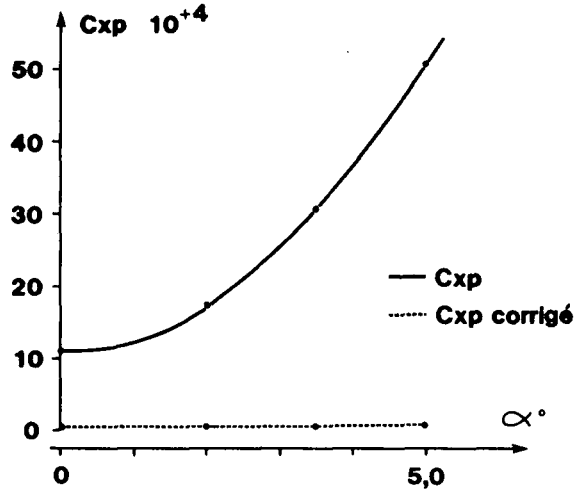

Fig. 6 - Amélioration du calcul du C_x pression
Profil NACA0012 M = 0,1. Fluide parfait
Méthodes de calcul potentielles.

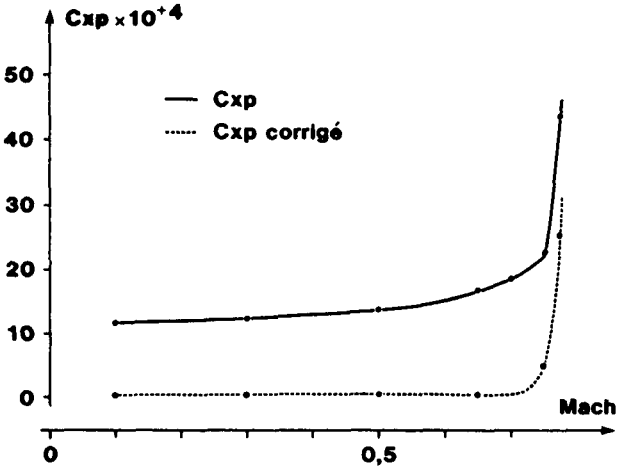

Fig. 7 - Amélioration du calcul du C_x pression
Profil NACA0012 $C_z = 0$. Fluide parfait
Méthodes de calcul potentielles.

La deuxième technique utilisée dans les méthodes [1] [7] consiste à calculer le C_{xp} en utilisant les valeurs du nombre de Mach calculées sur la face amont du choc et en utilisant les relations de choc. Cette seconde technique nécessite une technique fiable de détection du ou des chocs dans l'écoulement. Elle est en outre difficilement transposable en écoulement tridimensionnel.

La figure 8 présente pour le profil NACA0012 à M = 0,7 une comparaison de ces deux techniques de calcul du C_{xp}. La deuxième technique conduit à des valeurs de C_{xp} plus faibles que la première mais les écarts obtenus tout au moins dans la plage de C_z pour laquelle les méthodes potentielles sont raisonnablement utilisables sont nettement plus faibles que ceux obtenus à partir de l'intégration des pressions.

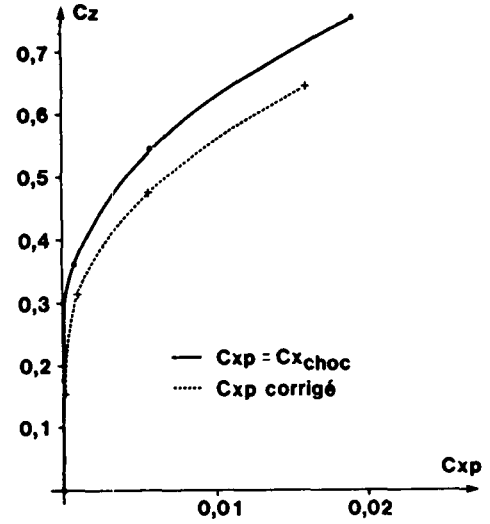

Fig. 8 - Comparaison des techniques de calcul de la traînée de pression.
Profil NACA0012 M = 0,7.
Méthodes de calcul potentielles non conservatives.

3.2 - Méthodes de calcul couplées bidimensionnelles

Quatre méthodes potentielles couplées sont habituellement utilisées pour l'estimation des performances des profils. Deux de ces méthodes utilisent une technique de couplage faible soit par engraissement du profil [1] soit par modification de la condition de glissement sur le contour initial [6]. Ces deux méthodes sont non conservatives et ne comportent pas de calcul de sillage. Dans les deux autres méthodes [7] qui ne diffèrent que par le schéma numérique non conservatif ou conservatif le couplage est réalisé à l'aide d'une technique de couplage fort [8] [9]. Ces deux dernières méthodes comportent par ailleurs un calcul de sillage.

3.2.1 - Estimation du C_x à l'aide des méthodes "couplage faible"

Dans la méthode [1] le C_x est obtenu selon le processus suivant : $C_x = C_{xchoc} + C_{xf} + C_{xpv}$

- le terme C_{xchoc} est calculé selon la deuxième technique décrite au paragraphe 3.1.3,
- le terme C_{xf} est calculé par intégration du frottement,
- le terme C_{xpv} (traînée de pression visqueuse) est obtenu par différence de l'intégration du champ de pression sur le profil "engraissé" et sur le profil initial.

Dans la méthode [6] les différents termes sont évalués de la manière suivante :

- le terme C_{xchoc} est calculé selon la première technique décrite au paragraphe 3.1.3,
- le terme C_{xf} est obtenu par intégration du frottement,
- le terme C_{xpv} est évalué par intégration des injections de quantité de mouvement à la paroi du profil.

Une comparaison des C_x calculés à l'aide de ces deux méthodes est présentée figure 9 pour le profil NACA0012 à M = 0,7 et un nombre de Reynolds de 3,6 10^6 en transition naturelle.

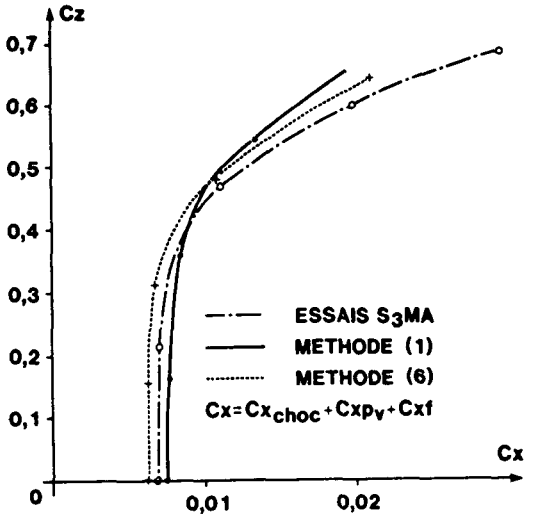

Fig. 9 - Prévision de la traînée. Profil NACA0012 M = 0,7 R_e = 3,6 10^6. Méthodes potentielles couplées (couplage faible). T.N.

Pour des $C_z < 0,3$ des écarts de l'ordre de 6 10^{-4} apparaissent entre les deux méthodes, écarts provenant principalement du terme C_{xf} par suite de positions de transition différentes. Les valeurs expérimentales déduites des essais effectués à la soufflerie S3MA et également reportées sur la figure se situent pour cette gamme de C_z entre les deux valeurs théoriques. A plus fort C_z le C_x donné par la méthode [1] devient inférieur à celui donné par la méthode [6] du fait du terme C_{xchoc}. On notera le bon comportement de la méthode [6] pour laquelle l'écart avec l'expérience est sensiblement constant pour une large plage de la portance.

3.2.2 - Estimation du C_x à l'aide des méthodes "couplage fort"

Dans ces méthodes qui comportent un calcul de sillage le C_x peut être calculé de deux manières différentes :

$C_{xa} = C_{xp} + C_{xf}$

- le terme C_{xp} étant obtenu par intégration des pressions,
- le terme C_{xf} est obtenu par intégration du frottement,

$C_{xb} = C_{xchoc} + C_{xv}$

- le terme C_{xchoc} est évalué à l'aide de la deuxième technique décrite au paragraphe 3.1.3,

- le terme C_{xv} (traînée visqueuse) est déduite de l'épaisseur de quantité de mouvement du sillage à l'aval du profil.

La figure 10 présente pour le profil CAST 7 à M = 0,7 une comparaison des C_x évalués selon les deux techniques précédentes à l'aide des méthodes conservative et non conservative [7].

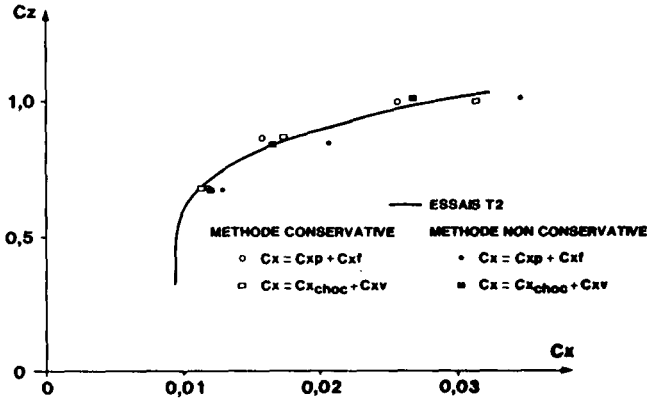

Fig. 10 - Prévision de la traînée. Profil CAST 7 M = 0,7 R_e = 4,5 10^6. Méthodes potentielles couplées (couplage fort). T.D.

Ces valeurs sont également comparées aux résultats expérimentaux obtenus dans la soufflerie à parois adaptables T2 du CERT/DERAT en transition déclenchée et pour un nombre de Reynolds de 4,5 10^6.

Les écarts entre le C_{xa} et le C_{xb} sont plus élevés pour la méthode non conservative. En outre du fait de l'imprécision sur le terme C_{xp} les meilleures corrélations avec les essais sont obtenues avec le C_{xb}.

En conclusion de ce paragraphe consacré à la prévision du C_x en écoulement bidimensionnel les remarques suivantes peuvent être effectuées:

- Les méthodes potentielles "couplage fort" [7] fournissent dans la plupart des cas des prévisions de C_x acceptables (de l'ordre de 3 %) lorsque le C_x est évalué à partir de la traînée de choc et à partir de l'épaisseur de quantité de mouvement dans le sillage.

- Les méthodes potentielles "couplage faible" et notamment la méthode [6] permettent d'atteindre pour des configurations non décollées des précisions voisines avec des temps de calcul beaucoup plus faibles.

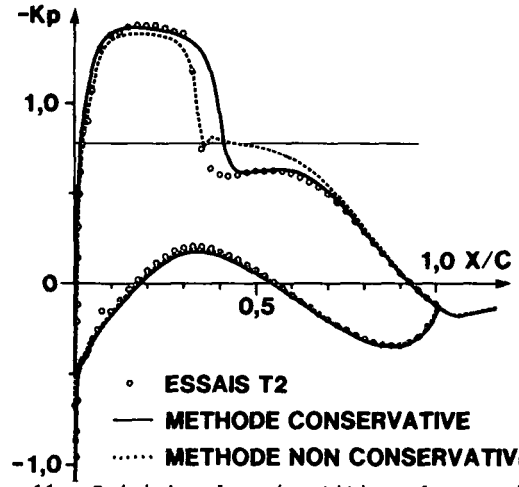

Fig. 11 - Prévision des répartitions de pression. Profil CAST 7 M = 0,7 α = 2°. Méthodes potentielles couplées (couplage fort). T.D. R_e = 4,5 10^6.

- L'utilisation de versions conservatives couplage fort assure généralement une meilleure prévision des répartitions de pression après le choc (figure 11) et par conséquent une meilleure prévision des coefficients aérodynamiques à incidence fixée.

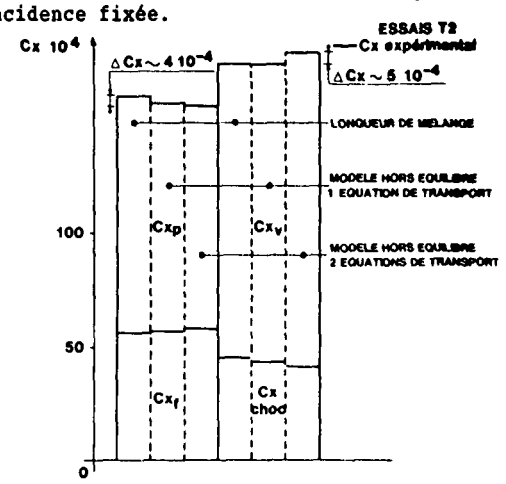

Fig. 12 - Prévision de la traînée. Influence du modèle de turbulence. Méthode potentielle conservative (couplage fort). Profil CAST 7 M = 0,7 α = 2° R_e = 4,5 10^6.

- Pour ce qui est de l'influence du modèle de turbulence la figure 12 montre que l'utilisation d'un modèle d'équilibre de type longueur de mélange ou de modèles hors équilibre à 1 ou 2 équations de transport ne conduit pas à des écarts importants sur les valeurs du C_x.

- En ce qui concerne les méthodes Euler leur stade de développement actuel et notamment l'absence de version avec "couplage fort" ne permet pas de porter un jugement sur leurs possibilités en matière de prévision du C_x. Il est vraisemblable cependant que seules les méthodes traitant correctement l'interaction choc couche limite permettront dans le cas de chocs forts d'améliorer les prévisions du C_x actuellement obtenues avec les méthodes potentielles.

3.3 - Ecoulements tridimensionnels de fluide parfait

Les principales méthodes de calcul tridimensionnelles utilisées en aérodynamique externe transsonique sont :

- une méthode potentielle différences finies [2],
- une méthode potentielle éléments finis [10],
- une méthode Euler [5].

La méthode [2] est une méthode non conservative avec un algorithme de type SLOR. Les maillages utilisés sont de type C-H.

La méthode [10] est une méthode potentielle éléments finis structurés conservative.

La méthode [5] est une méthode Euler pseudo-instationnaire explicite utilisant un schéma du type Mac Cormack. Les deux dernières méthodes sont utilisées avec des maillages du type H-H.

3.3.1 - Evaluation de la traînée de pression

Le terme traînée de pression englobe en tridimensionnel la traînée induite et la traînée de choc.

Cette intégration des pressions déjà fort imprécise en bidimensionnel l'est encore plus en tridimensionnel. Les principaux paramètres

influençant la précision sont comme en bidimensionnel :

- le maillage,
- la convergence des calculs,
- le type d'équations résolues,
- le schéma numérique.

3.3.1.1 - Influence du maillage

Les figures 13 et 14 montrent les évolutions du $C_x$pression calculé sur une voilure d'avion de transport dans un cas subsonique et un cas transsonique à l'aide des méthodes potentielles [2] et [10].

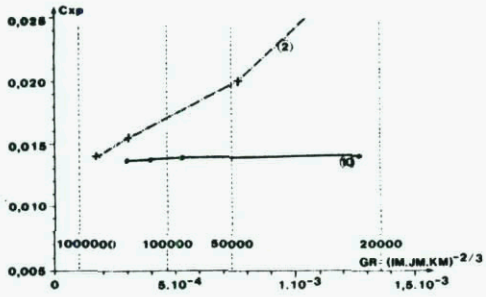

Fig. 13 - Influence du nombre de points de maillage sur le C_{xp}. Fluide parfait 3D. Méthodes potentielles. Cas subsonique.

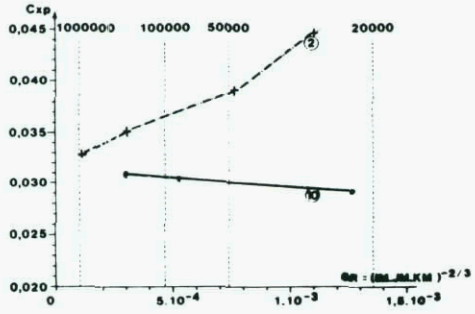

Fig. 14 - Influence du nombre de points de maillage sur le C_{xp}. Fluide parfait 3D. Méthodes potentielles. Cas transsonique.

La sensibilité de la méthode [2] avec maillage en C (figure 15) est plus importante que celle de la méthode [10] avec maillage en H (figure 16), ce type de maillage assurant même avec un nombre de points réduit une densité relativement importante aux bords d'attaque et de fuite.

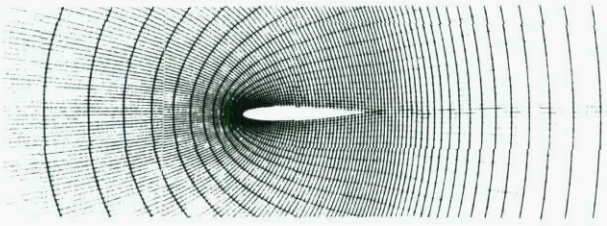

Fig. 15 - Schéma du maillage. Méthode potentielle différences finies 3D.

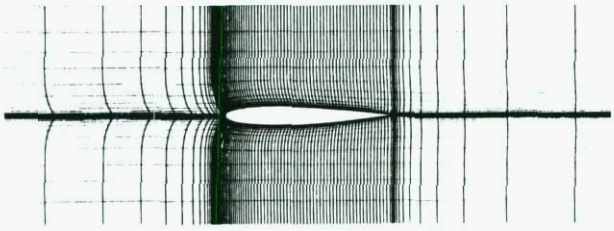

Fig. 16 - Schéma du maillage. Méthode potentielle éléments finis 3D.

Avec la méthode [2] il faut environ 400 000 points pour obtenir une précision de l'ordre de 5 % sur le C_x de pression.

Des calculs effectués avec diverses extensions de maillage n'ont pas montré une grande sensibilité du C_x pression à ce paramètre.

Le maillage au bord de fuite et la manière dont est écrite la condition de non contournement sont également des paramètres qui influencent la précision du C_x pression.

3.3.1.2 - Influence de la convergence

En dehors de la qualité du maillage une excellente convergence des calculs est nécessaire, cette convergence étant atteinte plus ou moins rapidement selon le type d'algorithme utilisé. Les figures 17 et 18 montrent que l'algorithme de la méthode potentielle éléments finis qui comporte une boucle externe non linéaire traitée par une méthode de point fixe et une boucle interne résolue par une méthode de gradient conjugué dans laquelle la matrice est préconditionnée par la factorisée incomplète de Cholesky est beaucoup plus efficace que l'algorithme du type SLOR utilisé dans la méthode différences finies.

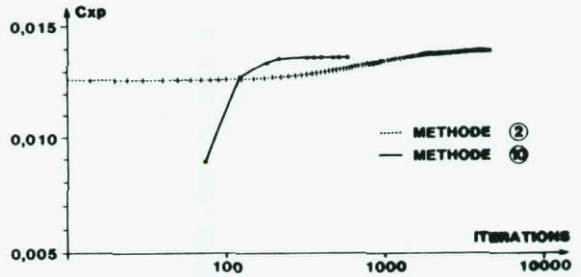

Fig. 17 - Convergence de la traînée de pression. Fluide parfait 3D. Méthodes potentielles. Cas subsonique.

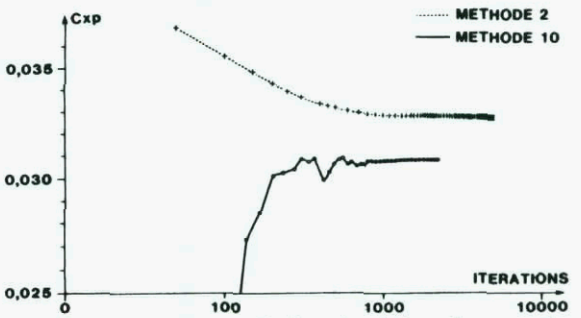

Fig. 18 - Convergence de la traînée de pression. Fluide parfait 3D. Méthodes potentielles. Cas transsonique.

3.3.1.3 - Influence du schéma numérique

Sur les planches 17 et 18 les valeurs du C_x pression à convergence des calculs sont voisins pour le cas subsonique mais diffèrent d'environ 5 % pour le cas transsonique du fait de la différence de schéma numérique, conservatif ou non conservatif.

3.3.1.4 - Influence du type d'équation

La figure 19 présente un exemple de dispersion de valeurs du C_x pression obtenue avec les différentes méthodes de calcul tridimensionnelles [2] [5] et [10].

Le cas traité est pourtant simple puisqu'il s'agit d'une aile elliptique de grand allongement (10,2) à $M = 0,6$ équipée du profil NACA 0012 pour deux incidences 0° et 2° pour lesquelles l'écoulement est entièrement subsonique.

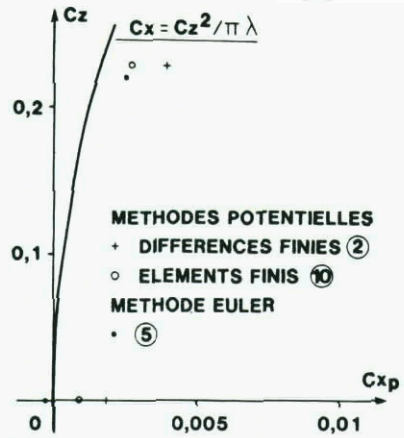

Fig. 19 - Prévision de la traînée de pression. Fluide parfait 3D. Aile elliptique M = 0,6 λ = 10,2.

A incidence nulle les méthodes potentielles donnent les valeurs de C_x de l'ordre de 10 ou 20 10^{-4}, la méthode Euler étant par contre assez proche de la valeur théorique $C_x = 0$.

A $\alpha = 2°$ les trois méthodes surestiment la traînée de l'ordre de $\Delta C_x = 10\ 10^{-4}$ pour les méthodes Euler et potentiel éléments finis et de plus de 20 10^{-4} pour la méthode potentiel différences finies.

3.3.2 - Amélioration de la prévision du C_x pression

Les exemples présentés précédemment montrent que même en prenant beaucoup de précautions tant au niveau du maillage que de la convergence, la précision que l'on peut espérer obtenir sur le C_x de pression par intégration des pressions est faible. De ce fait une technique de calcul du C_{xp} a été mise au point et intégrée dans la méthode potentielle différences finies [2] la plus utilisée actuellement au niveau des applications.

Cette technique déjà présentée au paragraphe 3.1.3 consiste à éliminer les erreurs dues au schéma numérique en déduisant de la valeur du C_x obtenue par intégration des pressions, l'intégrale de la quantité de mouvement calculée sur un contour entourant la région subsonique de l'écoulement (intégrale qui est en principe nulle en écoulement subcritique).

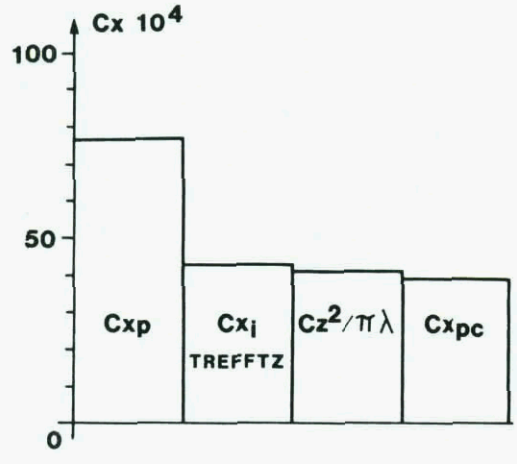

Fig. 20 - Prévision de la traînée de pression. Aile elliptique M = 0,1 λ = 21 α = 5°. Méthode potentielle non conservative 3D. Fluide parfait.

Cette technique appliquée au cas d'une aile elliptique d'allongement 21 équipée du profil NACA0012 conduit à un C_x pression à M = 0,1 et 5° d'incidence de 43 10^{-4}, la valeur théorique correspondante est de 41,3 10^{-4} et la valeur déduite de l'intégration des pressions de 77 10^{-4} (figure 20). On a reporté sur la figure la valeur de la traînée induite déduite de l'intégration de la quantité de mouvement sur le plan de Trefftz et qui est de 39,2 10^{-4}. Les deux valeurs ainsi obtenues sont voisines toutefois l'intégration dans le plan de Trefftz dépend en fait du choix (arbitraire) qui est effectué.

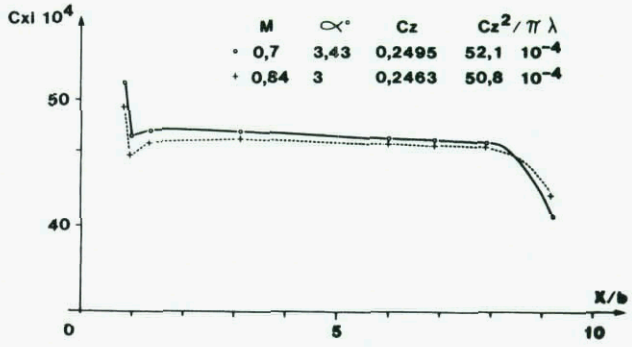

Fig. 21 - Influence de la position du plan aval sur le calcul de la traînée induite. Aile M6 λ = 3,8. Méthode potentielle non conservative 3D. Fluide parfait.

Ainsi la figure 21 montre que la distance choisie en aval de l'aile pour effectuer l'intégration influe sur la valeur de la traînée induite avec notamment une forte diminution au niveau du dernier plan de maillage provenant des conditions aux limites non rigoureuses imposées sur la frontière aval du domaine de calcul. Le plan de Trefftz retenu dans les calculs est le plan précédant cette frontière aval.

En écoulement transsonique la technique décrite précédemment donne la somme de la traînée induite et de la traînée de choc. La traînée de choc est évaluée par un bilan de quantité de mouvement sur un contour entourant la région supersonique de l'écoulement.

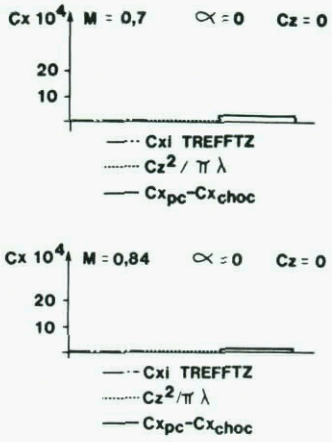

Fig. 22 - Prévision de la traînée induite. Aile M6 $C_z = 0$. Méthode potentielle non conservative 3D.

Cette technique de décomposition de la traînée a été utilisée sur l'aile M6, aile symétrique

d'allongement 3,8.

A M = 0,7 et 0,84 et incidence nulle (figure 22) la traînée calculée par intégration sur le plan de Trefftz est effectivement nulle. Les valeurs obtenues à partir de la traînée de pression corrigée à laquelle est soustraite la traînée de choc éventuelle sont de l'ordre de 1 à 2 10^{-4} ce qui est également tout à fait correct compte tenu des intégrations effectuées.

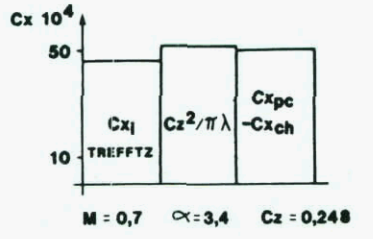

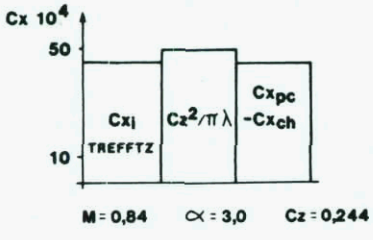

Fig. 23 - Prévision de la traînée induite Aile M6. Méthode potentielle non conservative 3D.

A M = 0,7 et α = 3,4° les deux méthodes d'évaluation de la traînée induite donnent des valeurs inférieures à $C_z^2/\pi\lambda$ ce qui indique une sous estimation de ce terme qui est d'ailleurs plus importante avec l'intégration sur le plan de Trefftz, figure 23.

A M = 0,84 et α = 3° figure 23 la sous évaluation de la traînée induite augmente mais dans ces conditions sur l'aile externe au voisinage du bord d'attaque les nombres de Mach locaux sont voisins de 1,6, ce qui explique la moins bonne précision du calcul.

Les valeurs de la traînée de choc calculées pour ces différentes conditions sont données figure 24.

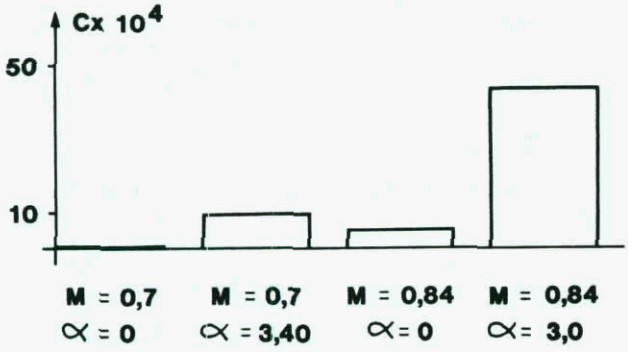

Fig. 24 - Prévision de la traînée de choc Aile M6 Méthode potentielle non conservative 3D.

Ces techniques de calcul de la traînée induite et de la traînée de choc à partir de bilans de quantités de mouvement donnent donc des valeurs beaucoup plus précises que l'intégration des pressions sur la voilure. Il est difficile de chiffrer la précision atteinte mais l'on peut raisonnablement estimer qu'elle est de l'ordre de quelques pour cent.

3.4 - Ecoulements tridimensionnels de fluide visqueux

Dans la méthode non conservative aux différences finies [2] a été inclus un calcul des couches limites laminaire et turbulente avec une technique de couplage par transpiration [6]. La méthode ne comportant pas de calcul de sillage la traînée visqueuse est évaluée par l'intermédiaire de la traînée de frottement et de la traînée de pression visqueuse (C_{xpv}) obtenue par intégration des quantités de mouvement à la paroi.

$$C_{xv} = C_{xf} + C_{xpv}$$

Une évaluation du terme C_{xv} à partir de l'épaisseur de quantité de mouvement de la couche limite au bord de fuite est également effectuée.

La traînée totale résulte donc de la somme de la traînée visqueuse, de la traînée de choc et de la traînée induite, ces deux derniers termes étant calculés comme indiqué au paragraphe 3.3.2.

Il est difficile de valider à l'aide d'essais ce bilan de traînée car certains termes ne sont pas connus expérimentalement et les comparaisons sont donc effectuées sur la traînée totale.

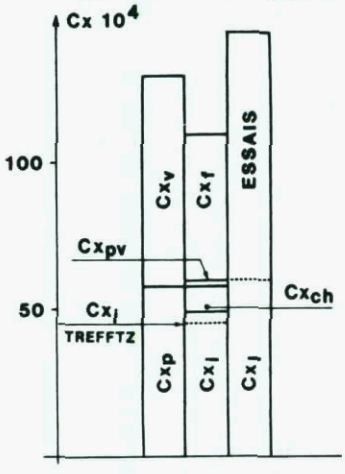

Fig. 25 - Prévision de la traînée. Aile M6 λ = 3,8 M = 0,7 C_z = 0,245 R_e = 7, 3 10^6 T.N. Méthode potentielle couplée 3D.

La figure 25 présente pour l'aile M6 à M = 0,7 et α = 3,4° la comparaison des traînées calculées et expérimentales. Le C_x calculé à l'aide des termes C_{xp} et C_{xv} *(Sqire et Young) est plus faible que* le C_x mesuré d'environ 15 %. L'écart est encore plus important avec $C_x = C_{xp} + C_{xf}$. D'autres bilans effectués sur la même aile pour d'autres conditions d'essais ainsi que les évolutions des différents termes avec le Mach et le C_z ont permis d'attribuer cet écart principalement aux termes C_x *induit et* C_{xpv}.

Pour cette incidence les répartitions de pression tracées figure 26 font apparaître des survitesses importantes au bord d'attaque suivies d'une forte recompression. Ce type de répartitions de pression conduit inévitablement à une mauvaise précision de l'intégration des pressions sur l'aile et par conséquent du terme C_x induit. Par ailleurs le C_x visqueux représente environ 54 % de la traînée totale ce qui est important et il est vraisemblable que l'absence de calcul de sillage ainsi que la technique du couplage faible conduisent dans ces conditions à une sous estimation des effets visqueux.

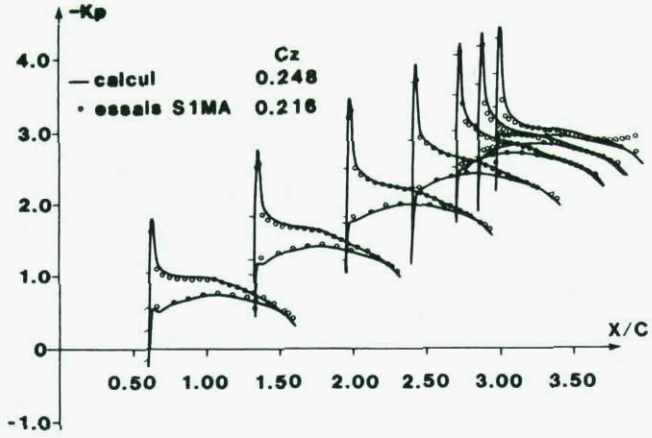

Fig. 26 - Répartitions des pressions. Aile M6 $\lambda = 3,8$ $M = 0,7$ $C_z = 0,245$ $R_e = 7,3\ 10^6$ T.N.

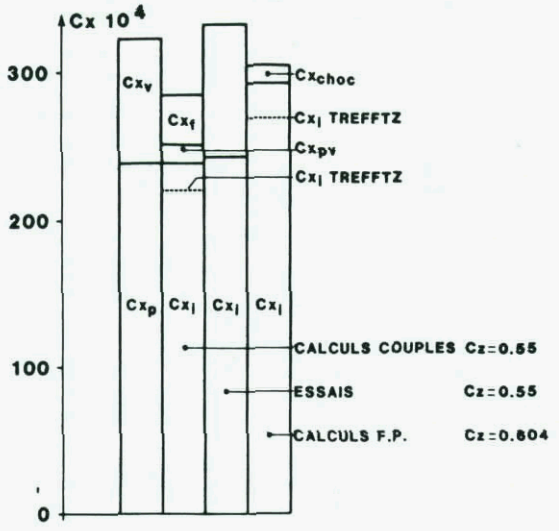

Fig. 27 - Prévision de la traînée. Aile non symétrique $\lambda = 4$ $M = 0,8$ $C_z = 0,55$ $R_e = 3,7\ 10^6$ T.D. Méthode potentielle couplée 3D.

Un autre exemple est présenté figure 27. Il s'agit d'une aile non symétrique d'allongement 4. Le bilan de traînée est effectué à $M = 0,8$ et à un niveau du C_z de 0,55 en transition déclenchée et pour un nombre de Reynolds de $3,7\ 10^6$. L'accord calcul expérience est très bon dans ce cas puisque le ΔC_x n'est que de 3 % avec $C_x = C_{xp} + C_{xv}$.

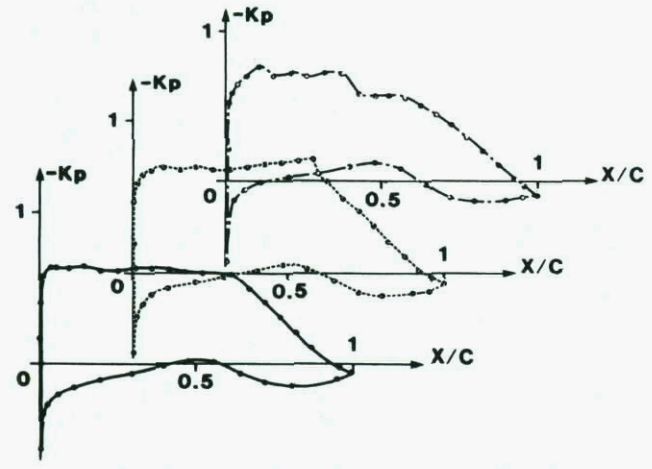

Fig. 28 - Répartition des pressions. Aile non symétrique $\lambda = 4$ $M = 0,8$ $C_z = 0,55$ $R_e = 3,7\ 10^6$ T.D.

Les répartitions de pression tracées figure 28 montrent que cette voilure contrairement à l'exemple précédent ne comporte pas de zones à fort gradient ce qui explique la bonne prévision du C_x induit. On a également reporté sur la figure 27 le C_x induit provenant de l'intégration de la quantité de mouvement sur le plan de Trefftz qui est comme pour l'aile M6 trop faible. Pour ce cas le C_x visqueux ne représente que 24 % de la traînée totale, l'écart calcul expérience correspond donc à une erreur de 10 % sur ce terme soit du même ordre de grandeur que l'erreur estimée pour l'aile M6 et qui provient essentiellement de la traînée de pression visqueuse qui est sous estimée.

Ces quelques exemples de calcul de la traînée en écoulement tridimensionnel à l'aide de méthodes potentielles montrent qu'il est possible d'atteindre des précisions de quelques pour cent en calculant les différents termes à l'aide de bilans de quantité de mouvement :

- un bilan sur un contour entourant la région subsonique dont la valeur est soustraite du C_x obtenu par intégration des pressions permet d'obtenir la somme du C_x induit et du C_{xchoc},

- un bilan sur un contour entourant la région supersonique donne le C_{xchoc},

- un bilan de quantité de mouvement des injections à la paroi permet de calculer le C_x de pression visqueuse,

Par ailleurs une intégration du frottement donne le C_x correspondant.

La précision pourrait sans doute être améliorée en évaluant le terme C_x visqueux à partir d'un calcul de sillage tridimensionnel. Pour ce qui est de la traînée induite la technique utilisée assure dans la plupart des cas des précisions correctes; toutefois lorsque de forts gradients de pression sont présents sur la voilure la précision devient moins bonne.

Pour ce qui est des méthodes Euler elles devraient permettre d'améliorer le calcul de la traînée de choc à condition toutefois que la viscosité artificielle de ces méthodes ne soit pas trop élevée.

En outre les gains de précision que l'on peut espérer avec les méthodes Euler ne seront effectives que lorsque ces méthodes seront couplées avec des méthodes de calcul des écoulements visqueux et en utilisant des techniques de couplage fort permettant de traiter correctement les interactions choc-couche limite.

4 - CONCLUSION

La prévision de la traînée de configurations complètes avec une précision de quelques pour cent est encore hors de portée des méthodes de calcul actuelles. De ce fait les constructeurs utilisent largement les essais en soufflerie dans leurs méthodes de prévision.

L'estimation de la traînée d'un nouvel appareil est effectuée à partir de la traînée connue d'un "avion de référence" en terme d'écart. Dans ce processus les calculs sont utilisés pour ce qui est des avions civils pour estimer la traînée de frottement en soufflerie et en vol alors que pour les avions militaires les modèles de prévision concernent l'avion complet. Les méthodes de calcul (Potentiel ou Euler) servent à comparer les traînées de diverses solutions pendant la phase de

définition du projet.

Pour des configurations aérodynamiques plus simples telles que les profils ou les voilures les études effectuées à l'ONERA à l'aide des diverses méthodes de calcul servant au niveau des applications à la prévision des performances amènent les conclusions suivantes:

- L'intégration des pressions ne permet pas une estimation correcte du terme traînée de pression. De ce fait celle-ci est remplacée en bidimensionnel par la traînée de choc et en tridimensionnel par la somme de la traînée induite et de la traînée de choc.

- Pour une même configuration la valeur de la traînée de choc dépend du processus d'évaluation utilisé mais aussi, très largement de la méthode numérique (équations résolues, viscosité artificielle).

- L'estimation de la traînée induite à partir des données dans le plan de Trefftz conduit généralement à une sous estimation de ce terme.

- Pour ce qui est de la traînée visqueuse les meilleurs évaluations sont obtenues à l'aide de calculs des sillages.

Les comparaisons calcul expérience effectuées avec les méthodes potentielles couplées montrent qu'il est possible d'atteindre pour des configurations ne comportant pas de zones décollées importantes des niveaux de précision de quelques pour cent en bidimensionnel et en tridimensionnel. Cette précision est obtenue en introduisant des techniques d'évaluation des diverses composantes de la traînée les mieux adaptées aux méthodes de calcul utilisées.

L'on peut ainsi effectuer un parallèle entre les techniques d'évaluation de la traînée à partir des résultats de calcul et les méthodes de corrections des effets de parois et de support pour les essais en soufflerie. Pour chaque soufflerie, chaque type de montage, les corrections sont différentes et il en est de même pour l'évaluation de la traînée à partir de méthodes de calcul différentes. De plus pour toute nouvelle soufflerie de nombreux essais sont nécessaires pour l'étalonnage de la veine d'essais et la mise au point des méthodes de correction. Ceci est également vrai pour l'évaluation de la traînée à l'aide d'une nouvelle méthode de calcul et explique l'écart qu'il y a entre les méthodes existantes et celles qui sont réellement utilisées au stade des applications pour la prévision des performances.

Les nouvelles méthodes de calcul en cours de développement telles que les méthodes Euler couplées ou Navier Stokes seront-elles comparables pour ce qui est de la prévision du C_x aux souffleries à parois adaptables pour lesquelles les corrections de paroi sont supprimées ? Au stade actuel de leur développement il est impossible de répondre et beaucoup d'efforts devront être consacrés à la validation de ces méthodes pour obtenir une réponse.

Ce travail de validation des méthodes de prévision des diverses composantes de la traînée nécessite des résultats d'essais détaillés et précis sur des configurations bidimensionnelles ou tridimensionnelles variées qui n'existent pas actuellement et un effort dans ce sens est nécessaire.

REFERENCES

[1] - J. BOUSQUET. Calculs bidimensionnels transsoniques avec couche limite. AAAF 11ème Colloque, 1974.

[2] - J.J. CHATTOT, C. COULOMBEIX, C. DA SILVA TOME. Calculs d'écoulements transsoniques autour d'ailes. La Recherche Aérospatiale 1978 N° 4.

[3] - A. LERAT, J. SIDES, V. DARU. An Implicit finite Volume Method for Solving the Euler Equations. Lecture Notes in Physics vol. 170 TP ONERA 1982-59.

[4] - A. LERAT, J. SIDES. Implicit Transonic Calculations without Artificial Viscosity or upwinding. Notes on Numerical Fluid Mechanics. Springer Verlag TP ONERA 1987-195.

[5] - H. VIVIAND, J.P. VEUILLOT. Méthodes pseudo instationnaires pour le calcul d'écoulements transsoniques. ONERA Publication N° 1978-4.

[6] - M. LAZAREFF, J.C. LE BALLEUR. Calcul des écoulements visqueux tridimensionnels sur ailes transsoniques par interaction fluide parfait couche limite. La Recherche Aérospatiale 1983 N° 3.

[7] - J.C. LE BALLEUR. Calcul par couplage fort des écoulements visqueux transsoniques incluant sillages et décollements. Profils d'ailes portants. La Recherche Aérospatiale 1981-3.

[8] - J.C. LE BALLEUR. Computation of Flows Including Strong Viscous Interactions with Coupling Methods. AGARD CP 291 or TP ONERA 1980-121.

[9] - J.C. LE BALLEUR. Viscous Inviscid Interaction solvers and Computation of Highly Separated Flows. Proceedings of ICASE Workshop on Vortex Dominated flows. NASA Langley (July 9-10, 1985), Springer Verlag. ONERA TP 1986-4.

[10] - M. BREDIF. Finite Element Calculation of Potentiel flow Around wings. 9ème Congrès ICNMFD Saclay 25-29 juin 1984.

DRAG PREDICTION AND ANALYSIS FROM CFD STATE-OF-THE-ART IN GERMANY

Wolfgang Schmidt
Dornier Luftfahrt GmbH
D-7990 Friedrichshafen 1

Peter Sacher
Messerschmitt-Bölkow-Blohm GmbH
D-8000 München 80

Summary

Consistent and accurate prediction of absolute drag for aircraft configurations is currently beyond reach computationally as well as experimentally using wind tunnel model testing. This is attributed to several elements ranging from lack of physical understanding up to limitations in numerical methods and scaling laws. To access drag by computational methods, drag components and the overall drag built-up have to be specified. For the individual drag component semi-empirical as well as theoretical estimates are discussed. Problems and limitations in drag estimates using computational fluid mechanics (CFD) are demonstrated for different types of flowfields. Within the scope of the present conference, our survey over the state-of-the-art in Germany will cover industrial aspects for commuter and transport aircraft, trainer, as well as fighter configurations, missiles, and space vehicles.

1. INTRODUCTION

The topic of drag prediction and consequently drag reduction will remain a high priority challenge for engineering design and analysis in order to improve cruise and/or manouevring performance and to reduce fuel consumption. The traditional sources for drag and the terminology of are described in Fig. 1.

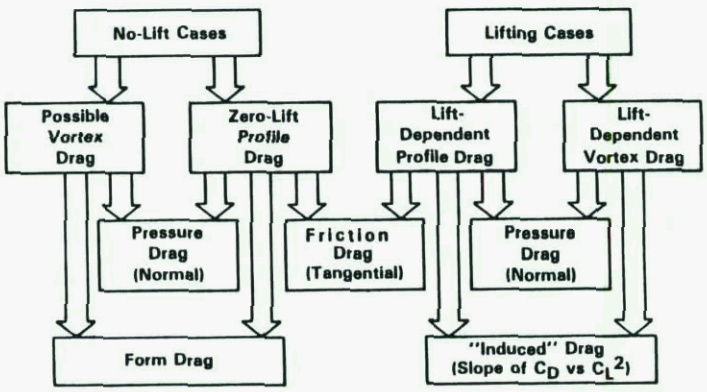

Fig. 1: Sources and Terminology of Drag Contribution

Those different drag sources can play quite different important roles depending on the type of air vehicle considered. Fig. 2 is illustrating the difference in drag-build up for the three very different configurations supersonic fighter aircraft, supersonic transport, and subsonic transport aircraft.

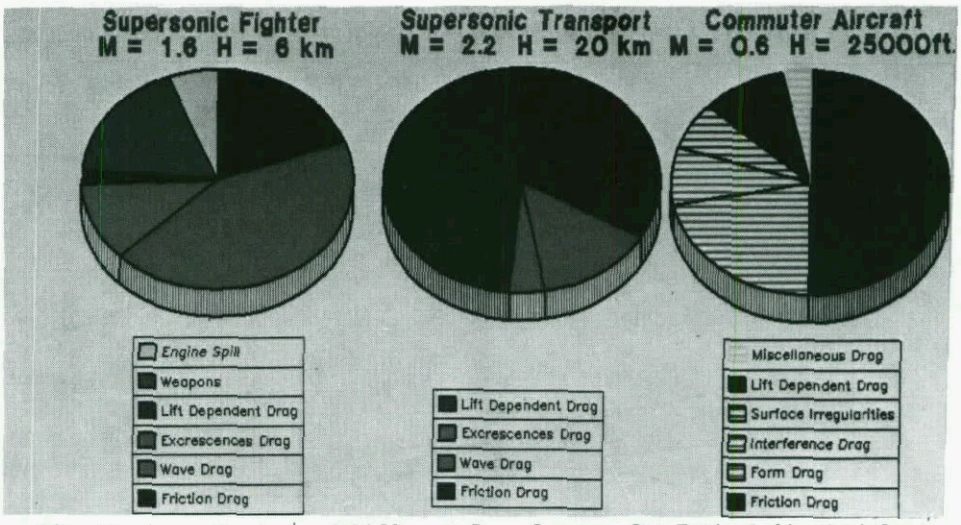

Fig. 2: Contributions of Different Drag Sources for Typical Air Vehicles

In order to obtain absolute drag values parasitic drag such as contributions from antennas, joints, steps, gaps, flap tracks, and other excresences have to be predicted. It is quite obvious, however, that such estimates are beyond the reach of CFD predictions. Even wind tunnel testing will not provide accurate information due to scaling problems.

DRAG IN COUNTS, 1 COUNT = 0.0001

CONTRIBUTION	ΔC_D
● ANTENNAE	.53
● WINDSHIELD WIPER	.16
● ANTI-COLLISION LIGHT	.01
● JOINTS/STEPS/GAPS	2.73
● EXPOSED FLAP TRACKS	1.60
● APU EXHAUST OUTLET	.02
● BUMPS/BLISTERS/PROTRUSIONS	1.05
● DOORS	.26
● VENTS/PRESSURIZATION LEAKS/AIR. COND. I/O	2.30
● WAVINESS/FAIRINGS/MISC.	.42
TOTAL	9.08 ≈ 3.5 % OF TOTAL DRAG

Fig. 3: Parasitic Drag, Escresences

These contributions from small scale elements can amount totally 3 - 4 % of total drag very easily. Aerodynamicists must rely upon past experience or semi-empirical information to account for this part. Limiting ourselves to component drag analysis, CFD still has to face a range of problems in order to be used by the design engineers:

- o CFD tools require more time and cost for drag analysis of complete vehicles than we can afford in predesign and even conceptual design.
- o Configuration Concept Studies require extremely fast predictions with reasonable accuracy.
- o Geometric complexity is limiting current mesh generation.
- o For Final Design fully validated methods along with representative geometry discretizations and physical modelling have to be used.

Since these problems can only be solved for a very limited number of simplified cases, applied aerodynamics should not forget semi-empirical methods, since a good configuration selection is mandatory for configuration optimization. However, it should be kept in mind, that data-base-type semi-empirical methods can be improved and extended by using CFD analysis.

To evaluate the current state-of-the-art in CFD drag prediction for Germany, items from the aircraft, missile, and space industry have been gathered. Aircraft applications concentrate primarily on problems related to transonic flow wave drag, vortex flow, and complex interference problems. For space applications hypersonic flow applications are increasing at a rapid pace.

2. TRANSPORT DRAG ANALYSIS

Transport Aircraft design requires optimum performance in take-off, climb, cruise (one or two cruise conditions) and landing. Competition between manufacturer leads to a race in performance improvements. To a large extend these improvements are due to better wing designs with lower drag, better engines, and better airframe-engine-installations. Since the manufacturers have to guarantee performance data prior to the first flight, very accurate and reliable performance prediction is required. CFD so far has problems in accurate prediction of even changes/modifications on complete aircraft. So far, only very reliable testing and scaling of W/T results versus flight test data can help improving. Fig. 4 - 6 taken from Ref. [1] are representative for an experimental status that in it's accuracy so far is beyond the reach of CFD.

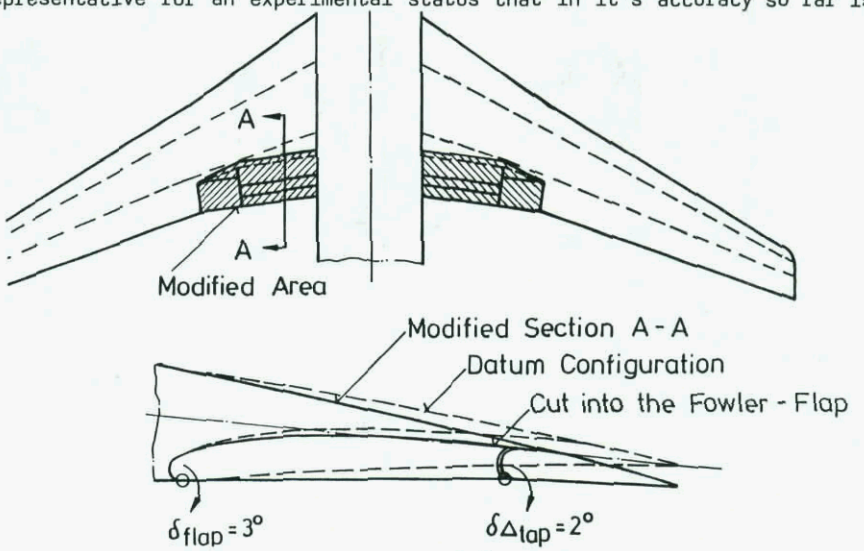

Fig. 4 Drag Analysis on A-300 Inboard Wing Modifications - A Challenge for CFD -

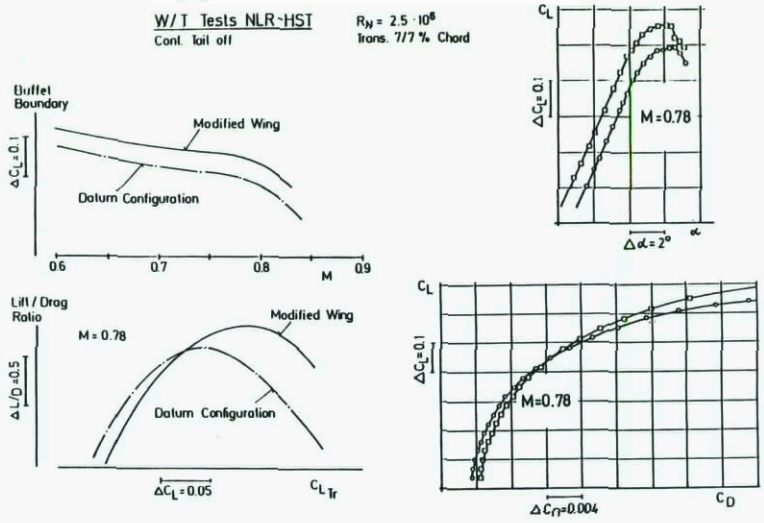

Fig. 5: Drag Analysis on A-300 Inboard Wing Modifications - A Challenge for CFD -

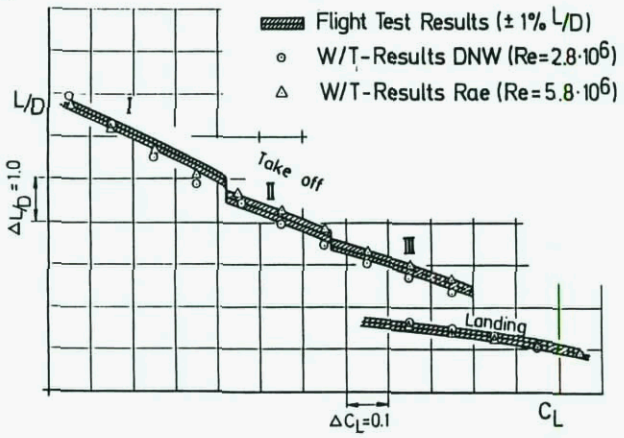

Fig. 6: A-310 Scaled W/T-Results Compared with F/T-Test Results

However, CFD can be an excellent tool for basic section studies, engine integration analysis, and overall wing design.

2.1 Section Drag

For two-dimensional airfoil design very efficient methods have been developed in the past for inviscid as well as viscous flows. The results of the AGARD FDP Working Group 07 published in Ref. [2] give an excellent overview over the capabilities of Euler methods predicting inviscid section flow and drag due to transonic flows with shocks. For viscous flows, however, in general the results look not as good, *Ref. [3]. The main reason* for problems in viscous flows is steeming from incomplete turbulence modelling and transition prediction if free transision is assumed.

As long as transition is prescribed and the flow over the airfoil remains attached, iterative inviscid/viscous methods such as potential flow/boundary layer or Euler/boundary layer can provide very fast and reliable answers. Fig. 7 represents a typical result of the full potential flow/boundary layer methods described in Ref. [4].

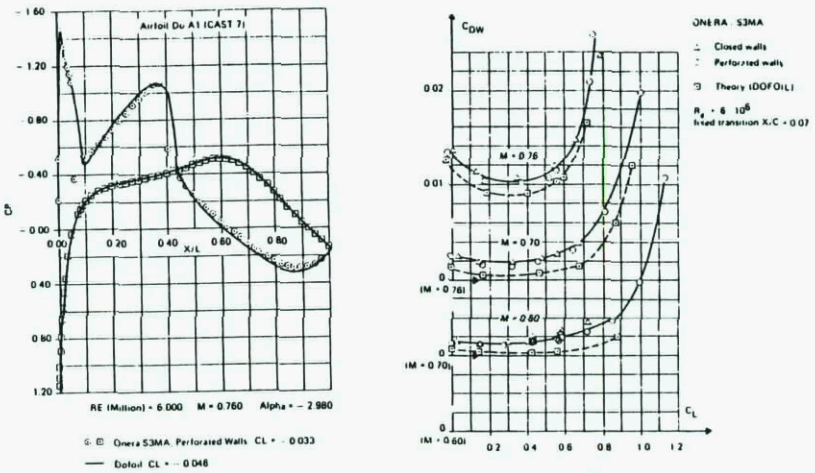

Fig. 7: Full Potential Airfoil Simulation with Boundary Layer Correction

For flows with separation Navier-Stokes Solutions with appropriate turbulence models can provide quite good solutions. Fig. 8 from Ref. [5] is showing some results compared with wind tunnel testing. It should be kept in mind that these tunnel results are not interference-free and that the better agreement between test data and DOFOIL for lift coefficients up to 0.55 might be misleading.

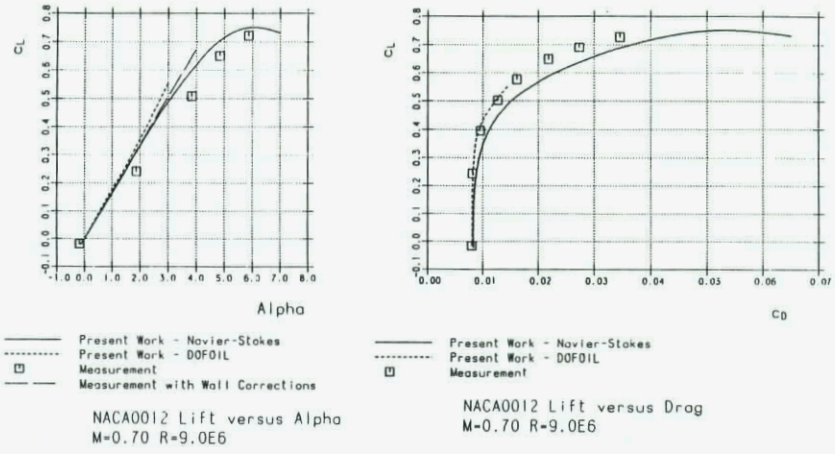

Fig. 8: Navier-Stokes Analysis for Airfoil Sections NACA 0012

A typical Navier-Stokes Solution for the VA7-00-0 transonic airfoil using the method described in Ref. [6] is presented in Fig. 9.

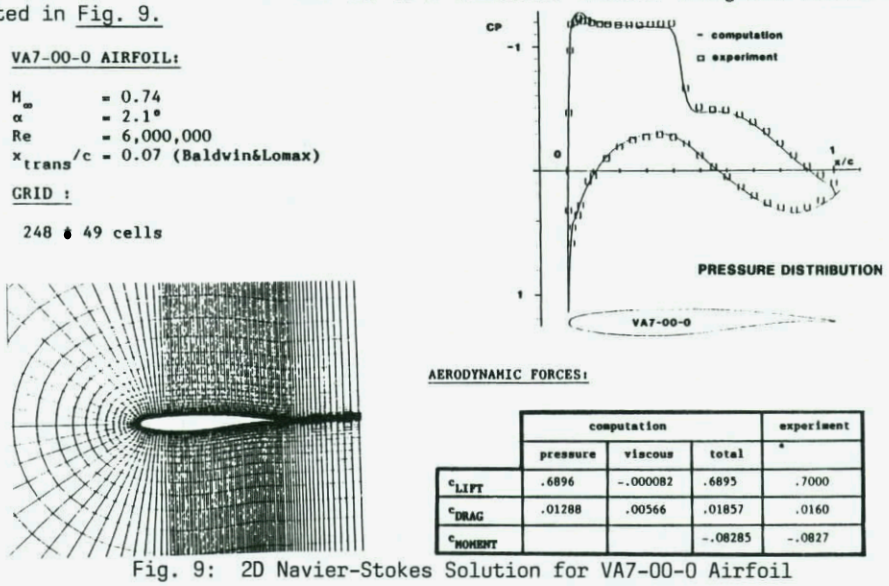

Fig. 9: 2D Navier-Stokes Solution for VA7-00-0 Airfoil

All total force data agree reasonably well, as well as the pressure distribution.

Since Navier-Stokes solutions in the complete domain require quite some compute power, zonal solutions might be attractive, where simplified equations are solved, whenever applicable. Fig. 10 presents such a result, described in detail in Ref. [7].

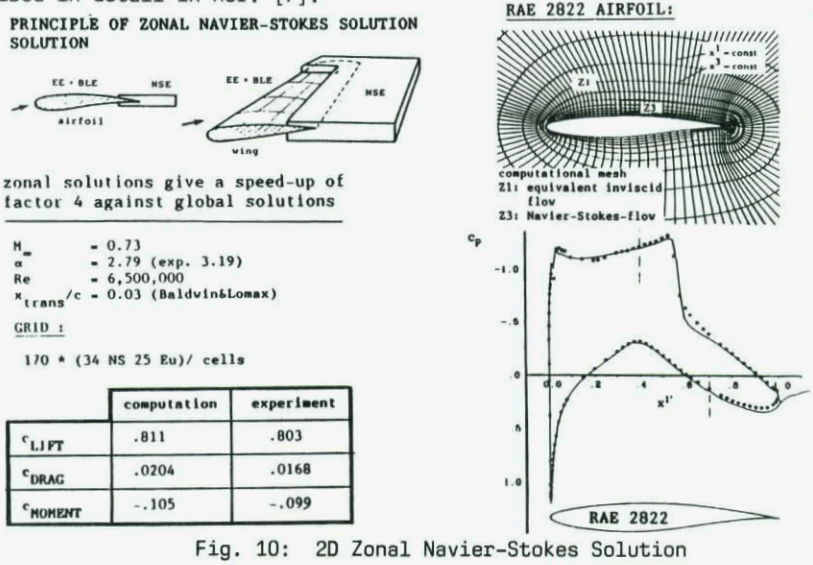

Fig. 10: 2D Zonal Navier-Stokes Solution

Although pressure distribution, lift and moment coefficients are predicted reasonably well, drag is off by 36 counts.

Most recent trends in drag reduction require CFD tools for the analysis of airfoils with extended laminar flow regions on upper as well as lower surface. Prescribing transition as occured in the wind tunnel or even calibrating the transition prediction method in one point against the test data, very good agreement in pressure distribution as well as drag data can be obtained between a Navier-Stokes Solution and the wind tunnel results. The results portrayed in Fig. 11 and 12 are described in detail in Ref. [8].

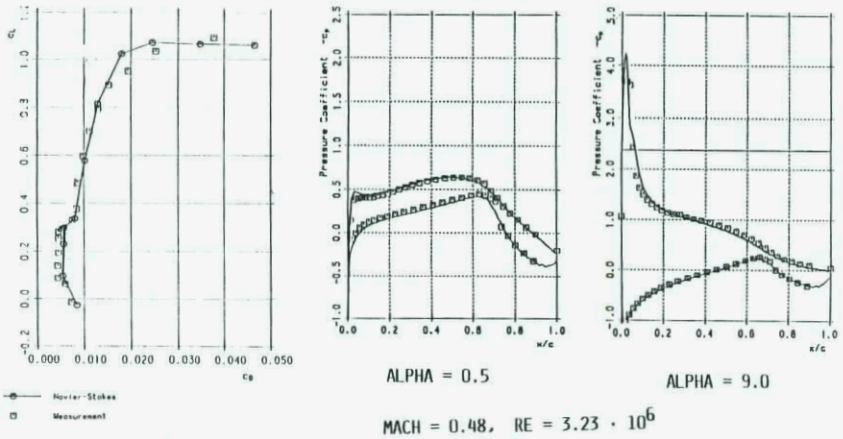

Fig. 11: Navier-Stokes Analysis for Laminar Airfoil Section Do-AL3

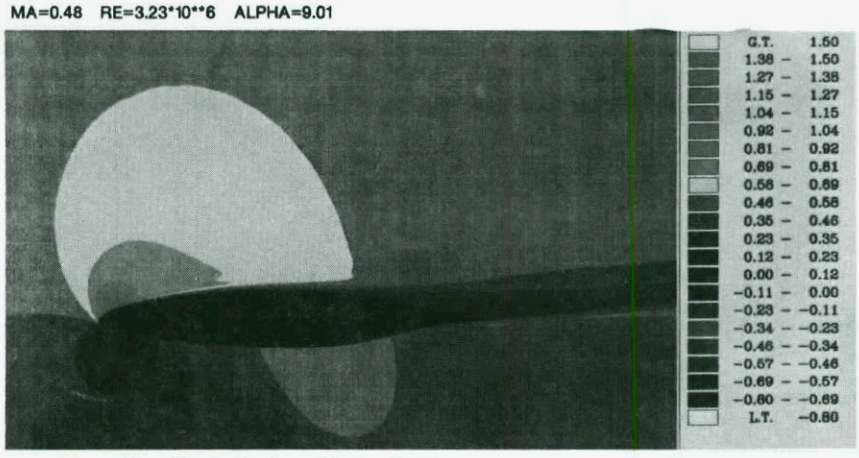

Fig. 12: Mach Number Distribution Do-AL3 Airfoil Section

It can be concluded that airfoil section analysis by using potential flow/boundary layer methods and more recently Navier-Stokes Methods is fairly advanced. Drag data can be as accurate and reliable as wind tunnel results or even better if tunnel interference or Reynolds number effects are out of range.

2.2 Wing Drag

Three-dimensional wing analysis and drag prediction is complicated by the trailing edge vortex sheet and its induced drag. While for two-dimensional flows or even nonlifting three-dimensional flows very accurate inviscid flow field solutions are possible, three-dimensional lifting wing analysis is still leading to different results depending on the type of model equation and/or numerical method used. Ref. [9] is summarizing a GARTEur activity out of which Fig. 13 shows a typical result for transonic flow on the left and subsonic flow on the right.

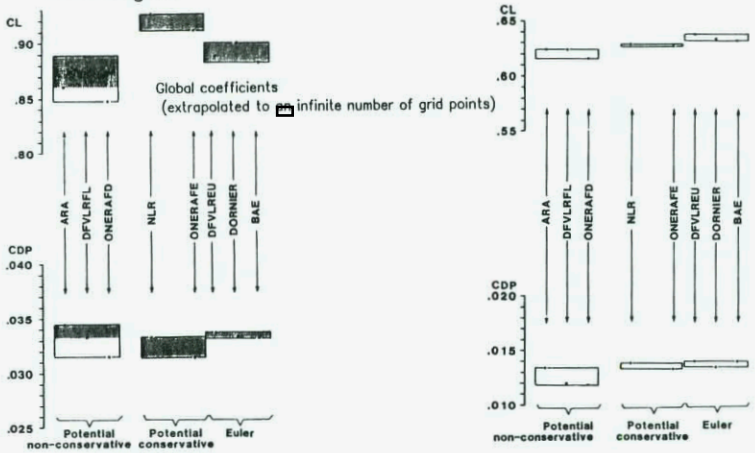

Fig. 13: Comparison of CFD Methods for Wing Analysis

These results indicate that Euler predictions are more reliable and it is hoped that consequently three-dimensional Navier-Stokes Solutions for wings will give similar results as for airfoils, but at a much higher expence in computer time.

2.3 Interference Drag due to Propulsion Systems

Advanced turboprop-engined regional airliner as well as jet-engined transport aircraft require wing design and high lift analysis taking into account the interference effects from the propulsion system. Euler methods are very attractive tools to analyse such effects on wing span loading and consequently drag.

Fig. 14 taken from Ref. [10] is giving an excellent example of the interference effects on the wing and loading an the nacelle drag.

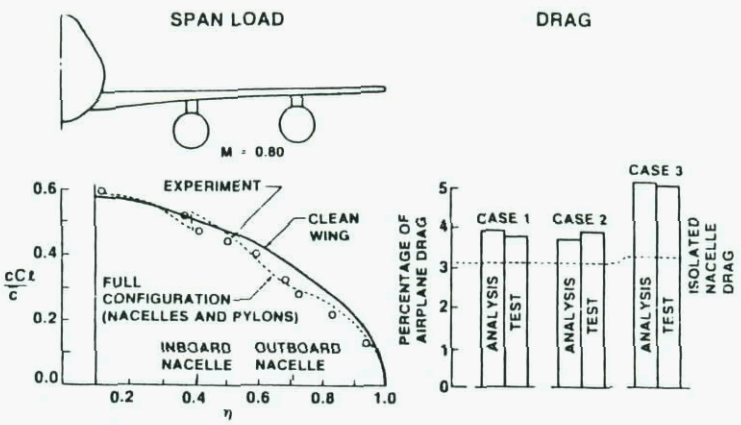

Fig. 14: Analysis of Wing Loading and Nacelle Drag

Consequently, nacelles and pylons can be optimized to reduce unfavourable interference drag effects by using such CFD tools.

For regional airliners with prop-engines and without hydraulic control systems flight conditions with high lift and large thrust require very careful designs. Propulsion integration effects can limit stall and minimum control speeds as well as increase drag at cruise. Large scale wind tunnel testing with TPS-driven propellers and CFD can help optimizing the configuration. Fig. 15 presents the interference effects on wing loading due to thrust and swirl.

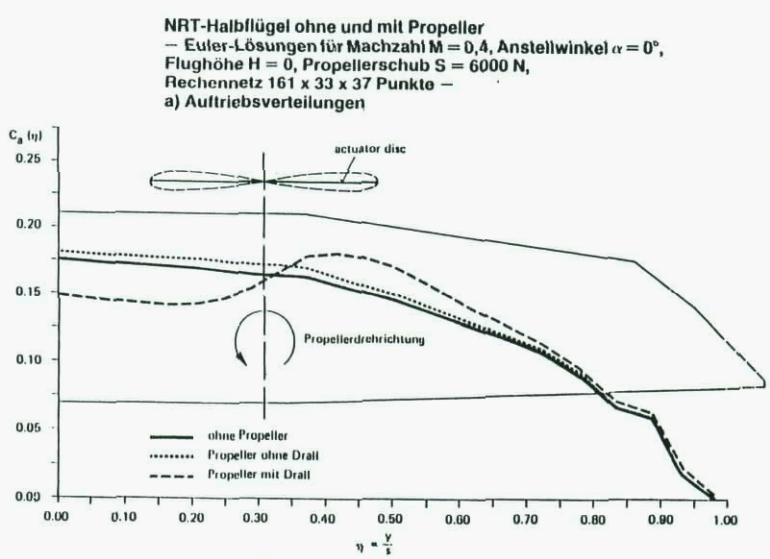

Fig. 15: Spanwise Load Distribution for Wing with Propeller

More detailed results in Ref. [11] also include nacelle interference effects as shown in Fig. 16.

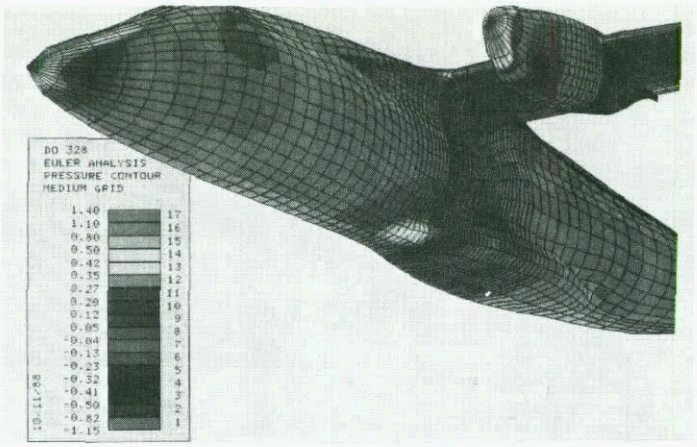

Fig. 16: Wing-Nacelle Analysis using Euler Methods

It is obvious that CFD can help improving such interference problems and will lead to better designs.

3. FIGHTER AIRCRAFT DRAG ANALYSIS

In contrast to transport aircraft, the design of fighters requires optimum performance in even more prescribed design conditions, in subsonic and supersonic manoeuvering and cruise. This may be expressed in terms of maximum attained and sustained turn-rates, maximum specific excess power, maximum manoeuverability and highest agility. According to Fig. 17, this means generally large thrust at low weight and high lift at low drag.

Performance	requires: *subsonic*	*supersonic*
• *Instantaneous Turn-Rate (ITR)*	- *large max. lift* - *low weight*	
• *Sustained Turn-Rate (STR)*	- *large thrust* - *low lift-dependent drag* - *low weight*	- *large thrust* - *low lift-dependent drag* - *low zero-lift drag* - *low weight*
• *Specifis Excess Power (SEP)*	- *large thrust* - *low weight*	- *large thrust* - *low zero-lift drag* - *low weight*
• *high Agility*	- *large control power*	- *large control power*

Fig. 17: Conflicting Goals in Fighter Design

This are conflicting requirements because large thrust normally leads to a large engine and therefore to large weightand drag. On the other side high lift is connected with a large amount of lift-dependent drag.

These conflicting design goals require complete by different geometric shapes, e. g. low zero-lift drag (including wave-drag) leads to small wing span, high sweep angles and slender fuselages, low lift-dependent drag on the other hand means large wing span and small leading edge sweep. High manoeuverability requires large wing area, highly twisted and cambered wing sections, maximum SEP's at supersonic Mach number minimize area, camber and twist. A compilation of "Conflicting Aircraft Design Parameters" is given in Fig. 18.

	requires:
• *low Zero-lift Drag*	- *small wing span* - *long and slender fuselage* - *small empennage*
• *low Lift-dependent Drag*	- *large wing span* - *low "span-specific" drag* *(e-Factor → unstable design)*
• *large max. Lift*	- *large wing area* - *large max. lift-coeff. → unstable design*
• *large Control Power*	- *large empennage* - *strong structure* - *not too unstable design*
• *large Thrust*	- *large engine*
• *low Mass*	- *small engine* - *small wing* - *small wing span* - *short and blunt fuselage* - *small empennage* - *weak structure*

Fig. 18: Conflicting Requirements for Geometry in Fighter Design

3.1 Induced Drag

One of the most important tasks of numerical analysis concerning drag computation is the prediction of dependent induced drag. At least for all cases with attached flow the prediction of lift-dependent drag using CFD has a long successful tradition. According to Fig. 19, the calculation of the drag-polar shows clearly the impact of twist (wing planform) and camber (wing profil) on wing efficiency (lift/drag).

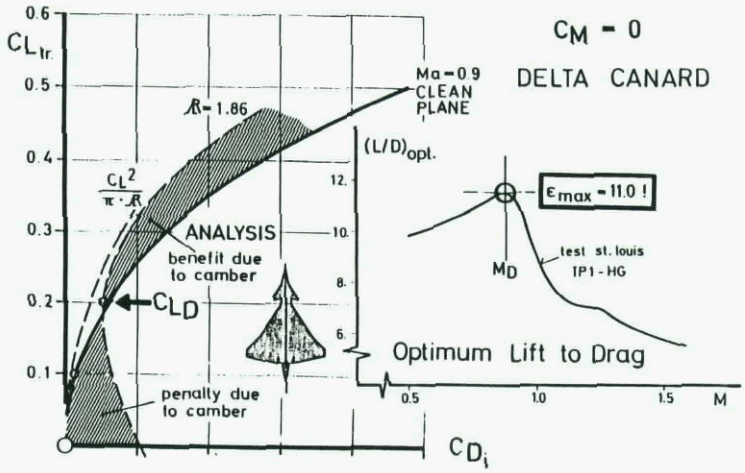

Fig. 19: Subsonic Design using Potential Theory for Minimization of Lift Dependent Drag

Improvements at c_L-design and at higher c_L have to be ballanced with penalties at lower lift. By carefully optimizing the wing planform and wing-section shapes, for an optimum L/D using computational tools, values near c_L/c_D = 11.0 have been achieved in more recently developed delta-canard fighter aircraft configurations [12]. The comparison with experiments in Fig. 20 does not show overall satisfactory agreement, but in most cases the differences do not exceed 10 %.

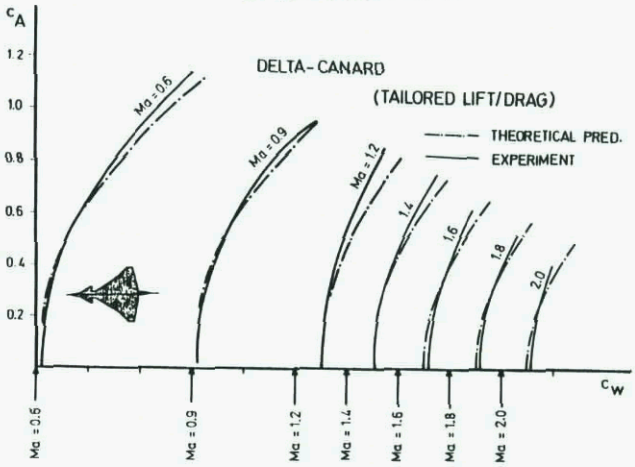

Fig. 20: Comparison of Experimental and Theoretical Trimmed Drag Polars

Especially for delta wings, the condition of fully attached flow could not be assumed any more at higher angles of attack and so the approach by linear theory has to be improved.

But even at lower angles of attack, potential flow methods do in general not predict correctly span loading in all regions of the wing planform, due to tip and/or leading edge vortices. This can be demonstrated drastically in the case of a slender configuration with small aspect ratio according to Fig. 21.

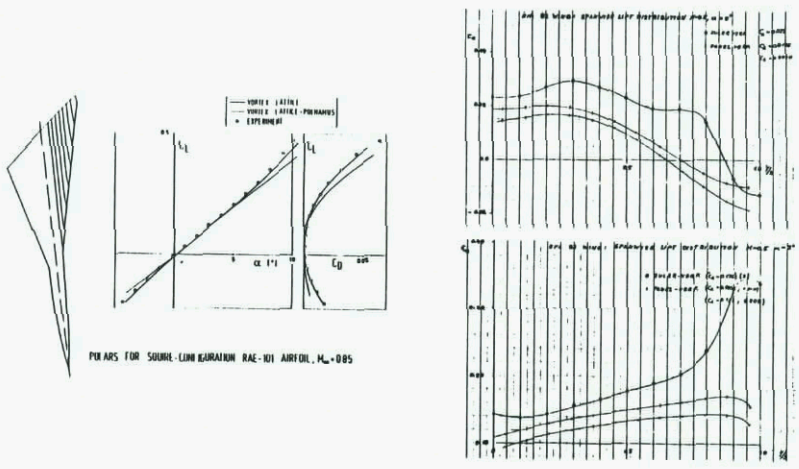

Fig. 21: Potential Flow Methods for Induced Drag Analysis

In spite of rather good agreement for the overall coefficients in comparison with the experiment in the left part, the distribution of local sectional lift versus wingspan at the right half shows some typical deviations of potential flow and Euler flow theory. Even at 3° angle of attack the Euler flow calculation shows impact of separated vortex flow at the outer part of the wing span. Therefore, do not use any more linear theory for design and analysis of slender wings with highly swept leading edges (even at low c_L)!

In order to validate the performance of Euler flow codes to predict fighter aircraft aerodynamic coefficients, a data base covering the whole range of speed and angle of attack has been established [13]. Fig. 23 shows the agreement which has been achieved in comparing computational results obtained by using a recently developed Euler flow code using different types of grids discretizing the outer flow field [14].

Mach 0.85 , Alpha 10 deg. **Total Derivatives**

Vortex Flow Model	cl	cd	cm
Experiment (NLR)	0.4377	0.0756	-0.0072
C-type grid	0.4567	0.0675	-0.0182
mod. C-type grid	0.4393	0.0633	-0.0115
H-type grid	0.4430	0.0679	-0.0100
H-type grid with 2 F.C.	0.4386	0.0633	-0.0128

Fig. 22: Comparison of Measured and Predicted Aerodynamic Coefficients using an Euler Flow Code

Even for the most sensitive drag coefficient, the agreement lies within 10 % for a case with transonic shock waves and fully separated leading edge vortex. This result seems to be extremely successful. A large amount of data has been obtained during this calculations but you must still have in mind that even in this complex calculations viscosity is still not physically modelled. Finally, the solution of the Navier-Stokes equations can give an answer to what extent differences may be interpreted as due to viscous effects. According to data in Fig. 23, an improvement has been achieved concerning the drag.

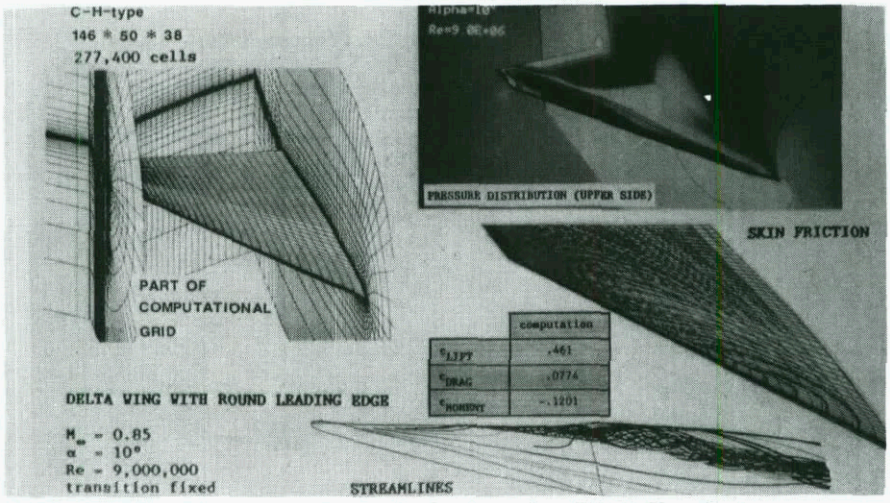

Fig. 23: Flow Field Analysis using EULER Flow Code including Leading Edge Flow Separation

This figure gives in addition an impression how complex the flowfield is. Data representation must make use of a series of postprocessing procedures as shown here. The results presented in this paper were obtained by [15].

3.2 Wave Drag

The second most important part of total drag is drag at zero lift, mainly pressure drag and friction drag. Numerical methods to predict friction drag have reached a highly sophisticated standard, they normally solve the boundary layer equations in two as well as in three dimensions. Also higher order boundary layer codes have been developed more recently, taking into account the effects of blunted bodies (or large curvature of any geometric shape) where the approximation of small disturbance is no longer valid. All these methods suffer from the lack of prediction criteria of transition from laminar to turbulent flow. Nevertheless boundary layer methods are widely spread in use throughout industry and they work satisfactorily for attached flow and fixed (or known) transition. So in this paper we have excluded examples for the prediction of viscous drag using B. L. codes.

The prediction of pressure drag, even at zero lift, however, still remains a hard exercise. This is due to the fact that all coefficients obtained by numerical methods have to be integrated from pressures. No experimentalist dares to integrate pressures to get the drag for a 3D configuration! In both cases there are not enough values available in regions where steep gradients exist (nose, trailing edges, base, etc.). The largest part of zero lift drag (up to 2/3!) is wave drag at supersonic speed. So we have tried to concentrate ourselves in this survey on the compilation of the state-of-the-art in Germany for the prediction of wave drag. More or less three classes of prediction methods are in use:

- o semi-empirical "Area-Rules"
- o potential flow codes
- o Euler flow codes

Results obtained by the use of different codes have shown significant discrepancies. So a special effort has been sponsored by the German MOD to provide an extensive data base for the validation of computer codes concerning the prediction of wave drag.

According to Fig. 24 a modular pilot model has been designed, built and measured in the supersonic wind tunnel of DFVLR in Göttingen [16].

Wave Drag Code Validation Program
1986-1988
(sponsored by German Ministry of Defense RüFo 4)

- **Systematic Variation of main Configuration Components**
  - **Body**
  - **Nose**
  - **Tail**
  - **Stores**
  - **Wing**

- **Code Hierarchy**
  - **Supersonic Area Rule (SAR)**
  - **Supersonic Higherorder Panel (HISSS)**
  - **Euler**
    (Marching,Time Dependent)

Fig. 24: Wave Drag - Code Validation Program 1986 - 1988

A systematic variation of all main configurational parameters of a fighter aircraft has been performed, followed by extensive calculations using all available flow codes. Fig. 25 and 26 give an impression of the complexity of the model and the variety of interchangeable components.

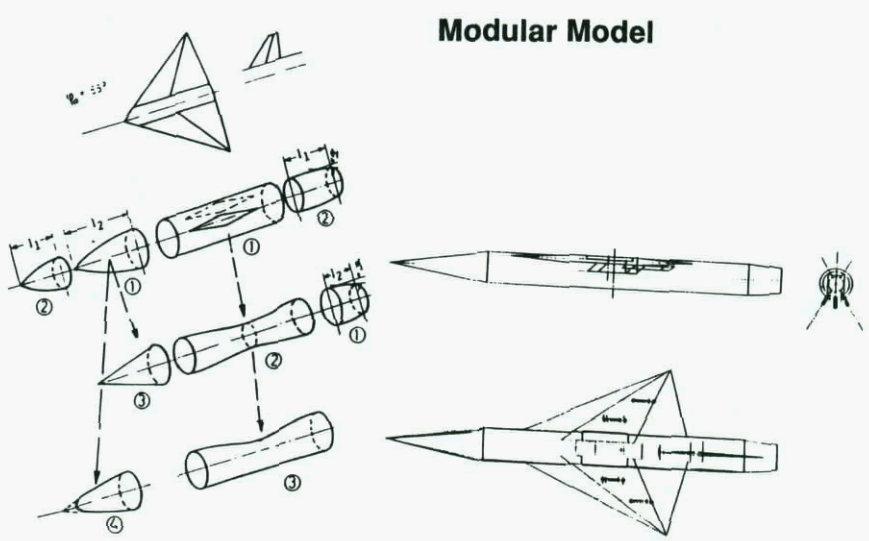

Fig. 25: Wave Drag Code Validation - Modular Model

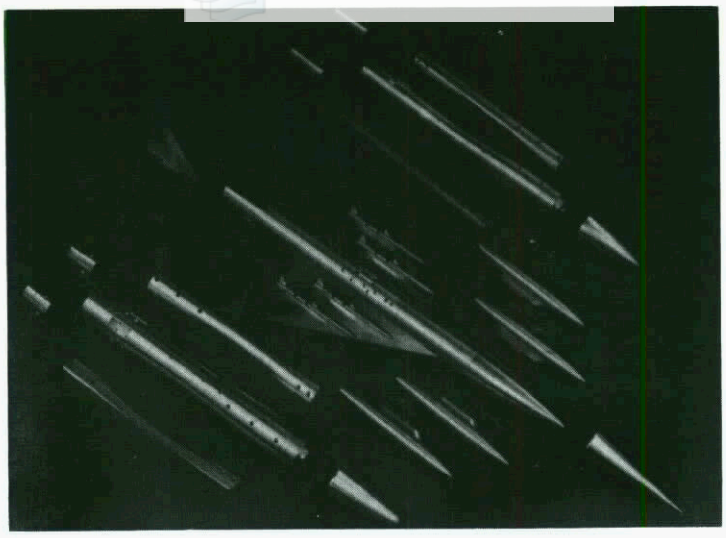

Fig. 26: Wave Drag Code Validation - Modular Model

A special effort was untertaken to investigate non-axisymmetric body shapes, wing position with respect to the body and unsymmetric store arrangements. The intention was to demonstrate the limits of the applicability of supersonic Area-Rules. In the next three figures typical examples are given for the comparison of theory and experiment on the clean wing body configuration. First in Fig. 27 the forebody shape of the fuselage has been changed.

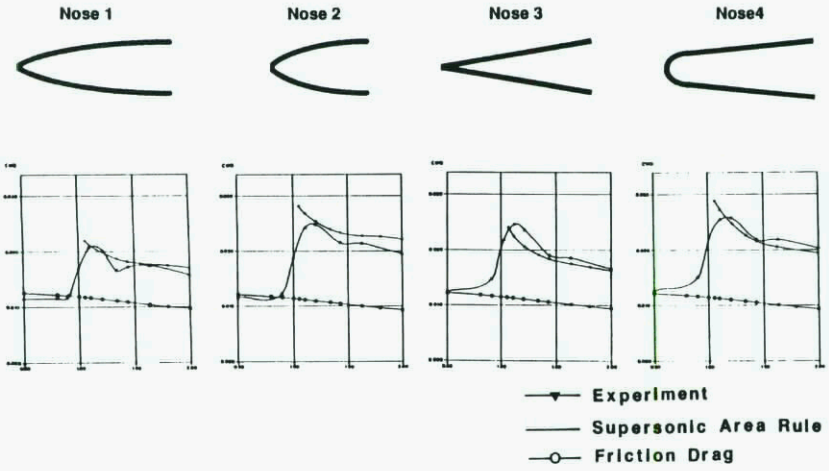

Fig. 27: Wave Drag Code Validation - Variation of Forebody Nose Shape

The lowest curve always gives the theoretical value for viscous drag obtained by simple DATCOM-Estimation. Fig. 28 shows the influence of mid-body shape and Fig. 29 demonstrates the effect of changing the afterbody.

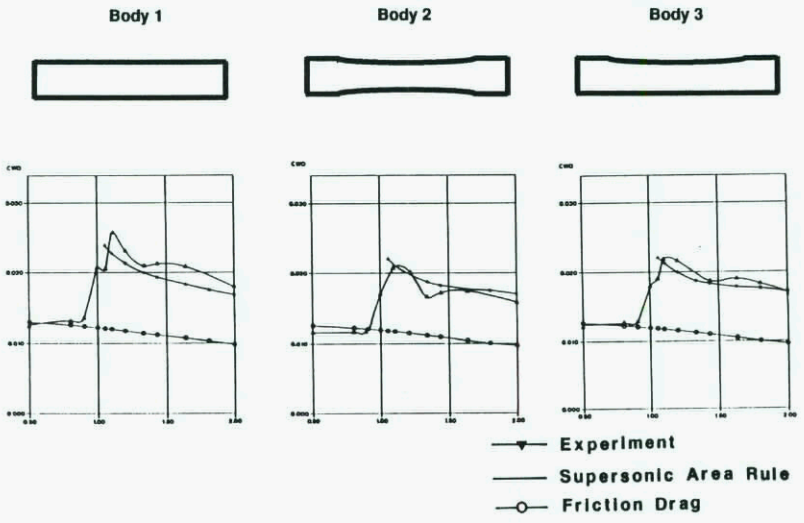

Fig. 28: Wave Drag Code Validation - Variation of Body Cross Section

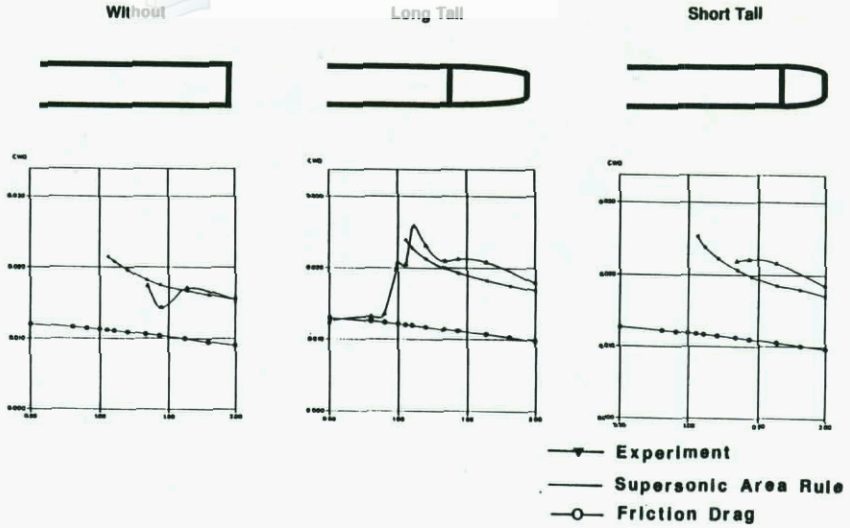

Fig. 29: Wave Drag Code Validation - Variation of Boat-Tail

In all three examples of variation of the body shape, the predicted values differ significantly from measured data, but unfortunately in some cases they fail also in prediction of the trend with Mach number.

It is quite obvious that local characteristics of the supersonic flow are not represented correctly in linear theory.

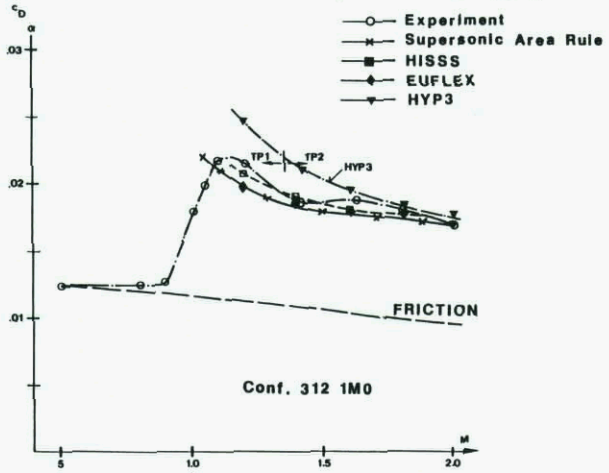

Fig. 30: Wave Drag Code Validation - Comparison of Different CFD Codes for Prediction of Drag

This situation can be improved, as Fig. 30 shows, by using more sophisticated methods like Higher Order Panel Code HISSS [17] or an Euler Code like EUFLEX [13]. For high supersonic Mach numbers the agreement with Newtonian theory is improved, see HYP3 [18].

Of great importance is the applicability of CFD to predict store installation effects.

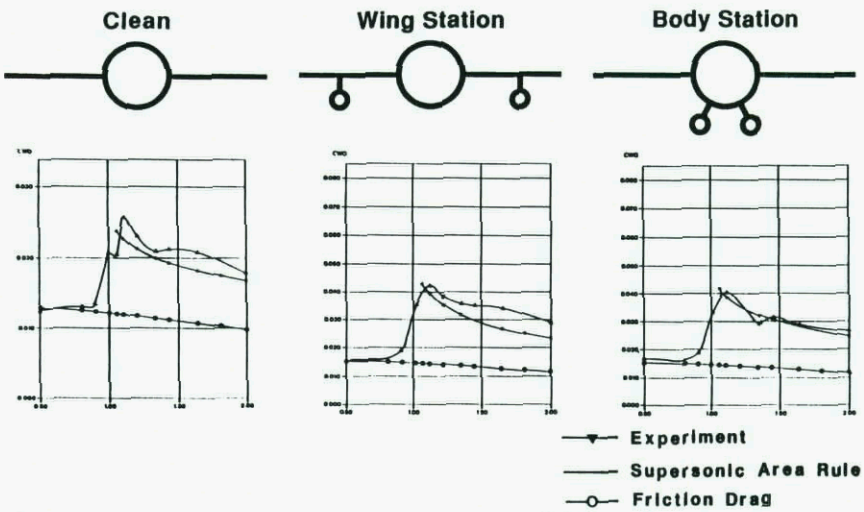

Fig. 31: Wave Drag Code Validation - Variation of Store Installation Location

As Fig. 31 demonstrates, the effect of store location (under wing or fuselage) is not represented correctly in the supersonic area rule, but the experiment shows typical changes of the slope of wave drag *versus Mach number*. (*Please note the different scale used for the clean configuration!*) How important the effects of weapon integration really is, shows Fig. 32.

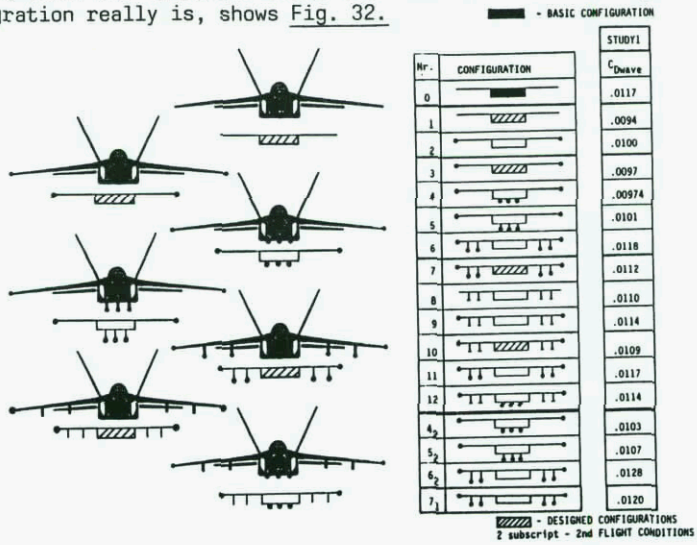

Fig. 32: Drag Optimization for Store Integration

In some cases wave drag is increased by about 30 %! By using numerical tools to optimize the geometry including stores this drag penalty can be reduced significantly. Progress which has been achieved by improving classical Area-Rules is shown in Fig. 33.

- **Classical SS area-rule is an adequate procedure for in-loop wave-drag calculations.**

Advantages:

- *Simple input: Possibility of quick reaction on permanent configuration changes in the design-phase*
- *Low-cost program: Possibility of many trend- and optimization studies in order to influence the development of the configuration.*

Disadvantages:

- *Classical SS area-rule codes sometimes give inconsistent results, because of:*
  - ** linearity*
  - ** assumption of smooth end of the configuration*

- **Improvements**

- *By introduction of nonlinear procedures (e.g. Characteristics, Euler-marching) the results are much more consistent, especially for more blunt configurations.*
- *Drag changes due to configuration variations in the front or aft part (e.g. fin) become consistent with Euler results.*

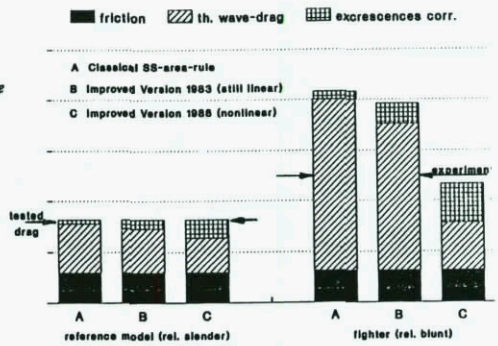

Fig. 33: Improved Wave-Drag Calculations for Advanced Fighter Design

The modification of the prediction code is based on additional nonlinear terms out of reference models (experiments) of from Euler calculations [19]. So in the next figures some typical representative examples for the application of more complicated CFD codes are given.

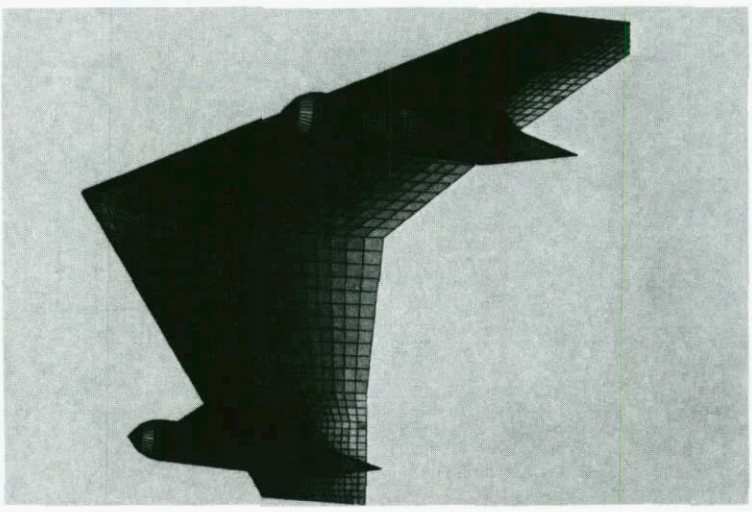

Fig. 34: Wing Pylon Interference Analysis

First in Fig. 34 the surface grid and calculated pressure distribution of a wing pylon interference analysis at transonic Mach number is shown. The colours represent different levels of pressure. Another more complex configuration is shown in Fig. 35.

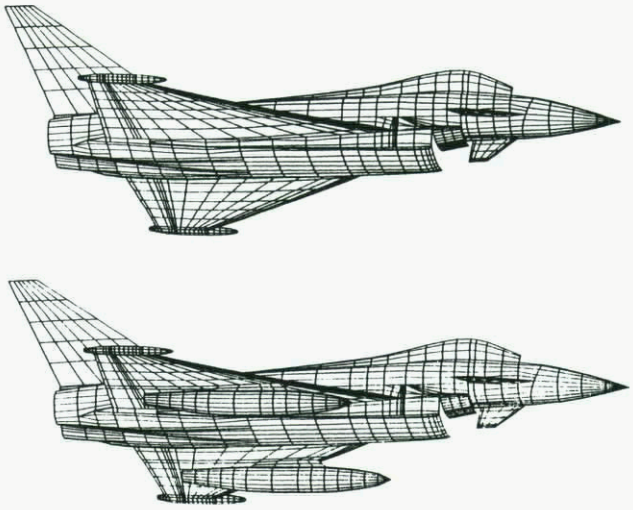

Fig. 35: Panel Model for HISSS to Predict Installation Effects of External Wing-Mounted Stores

This represents a fighter aircraft with and without external stores.

Isobars obtained by HISSS [17] in Fig. 36 show the impact of pylon-store installation on the clean aircraft wing at M = 1.2 and α = 3°. Of course this pressures have to be integrated to obtain drag and for α 0° the result is shown in Fig. 37.

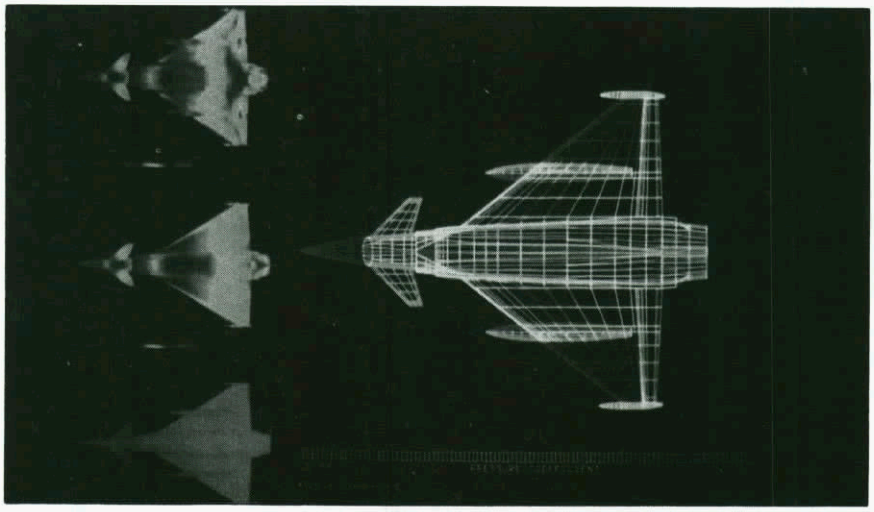

Fig. 36: Isobar-Patterns from Supersonic Panel Code Application to Predict Installation Effects of External Wing-Mounted Stores

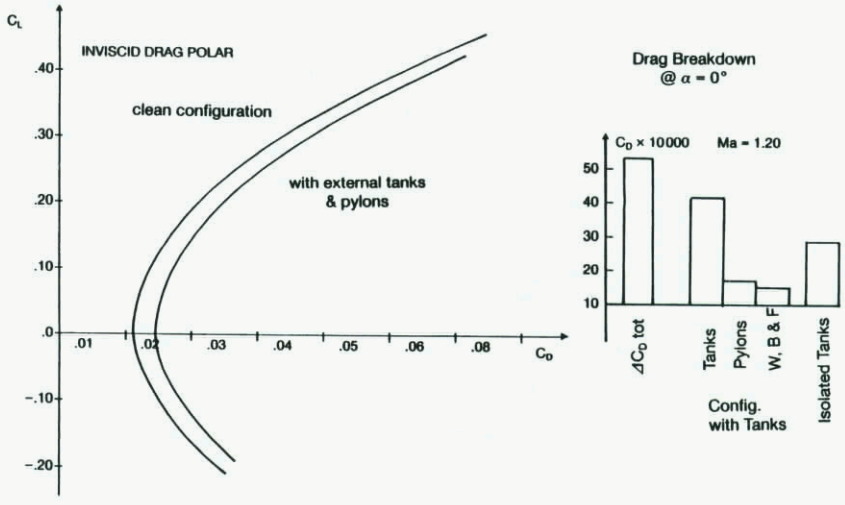

Fig. 37: Wave Drag Increment Analysis due to Store Installation

The detailed analysis reveales that the integration of the pressures on the isolated (free-flying) and the installed store results in completely different wave drag components. Due to the interference effects of pylon, wing, body and fuselage one obtains twice the pressure-drag value as for the isolated tank. Fig. 38 shows once more the impact of tank installation on the pressures at the wing lower side.

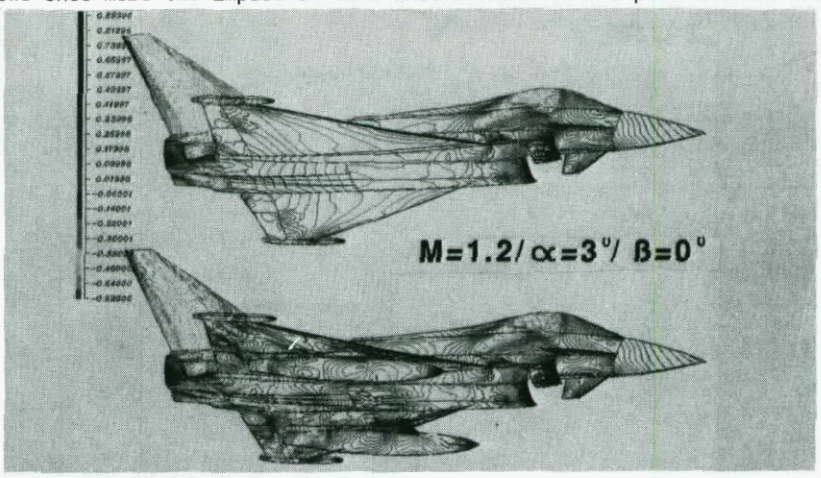

Fig. 38: Supersonic Panel Code Application to Predict Installation Effects of External Wing-Mounted Stores

So higher order PANEL methods and Euler flow codes represent powerful tools in predicting drag increments due to configurational modifications which are not taken into account in semi-empirical rules. In Fig. 39 a successful attempt has been made to improve for example the Sears-Haack body shape for different design Mach numbers using an optimization procedure and an Euler space marching code [20].

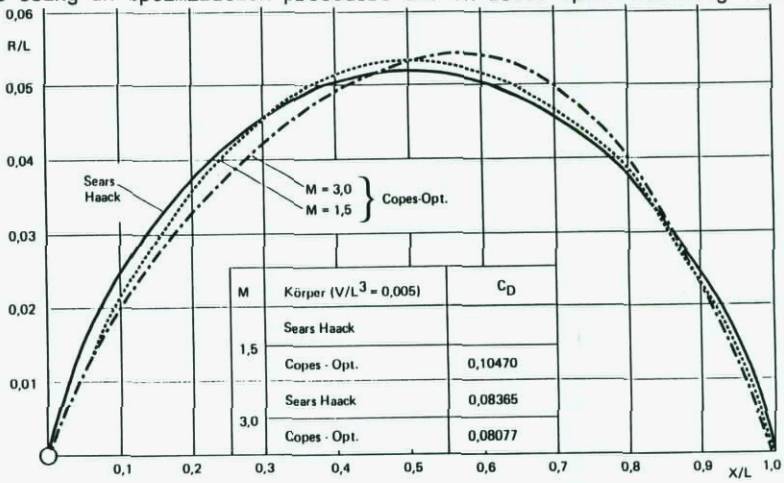

M	Körper ($V/L^3 = 0{,}005$)	C_D
1,5	Sears Haack	
	Copes - Opt.	0,10470
3,0	Sears Haack	0,08365
	Copes - Opt.	0,08077

Fig. 39: Body Design for Low Drag Using Space Marching Methods and Optimization

3.3 Afterbody Drag

After having stressed the methods for the prediction of drag at lifting and at zero-lift conditions due to the aerodynamics of the **airframe,** another cathegory of problems contributing to drag in fighter aircraft design has to be mentioned: configurational aspects of drag. The **engine integration** has to be performed very carefully concerning drag minimization. Especially afterbody drag may contribute up to 50 % of total drag at transonic Mach numbers according to examples shown in Fig. 40.

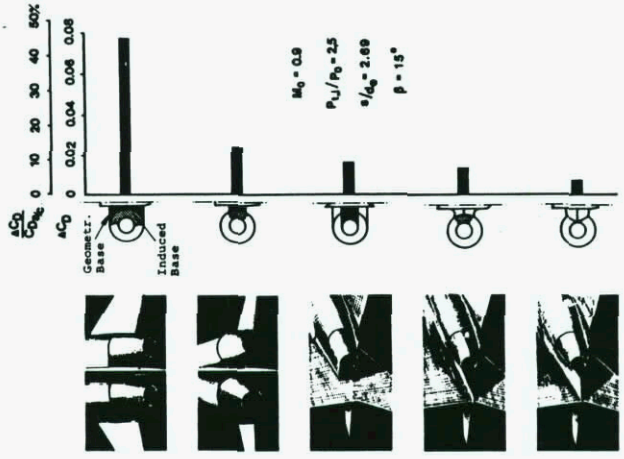

Fig. 40: Afterbody Drag Increment for Fighter Aircraft

The AGARD Working Group 08, 1982 - 1984, has reported extensively on the theoretical and experimental state-of-the-art in prediction of afterbody drag in the NATO countries [21]. Special emphasis was directed towards the prediction methods available in industry to predict the afterbody flow at transonic and supersonic speed. A series of (axisymmetric) test cases has been specified (Fig. 41) and three different classes of prediction codes have been compared.

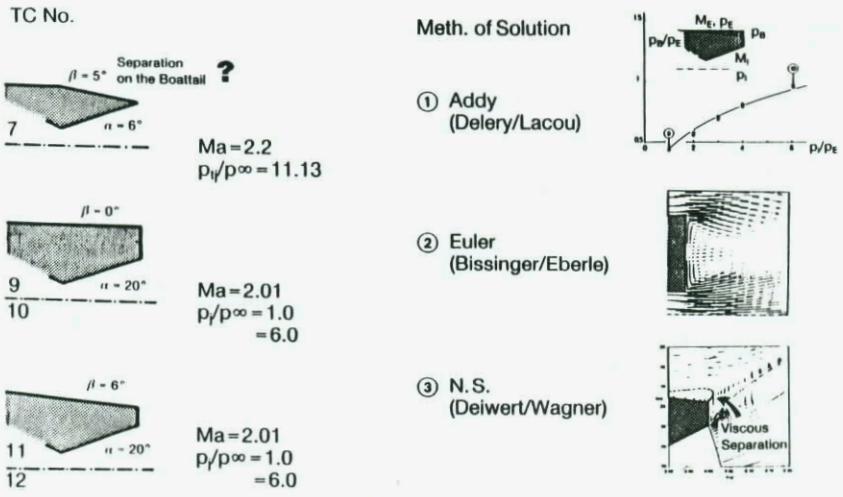

Fig. 41: AGARD FDP WG08 - Test Cases for Numerical Flow Calculations

Semi-empirical potential flow based codes (mean values for the base pressure), Euler flow codes (vortical type of flow separation) and Navier-Stokes Solutions (viscous flow separation). In conclusion of the results of the Working Group 08 one can state that even (or especially) for the most complex Navier-Stokes Solution, the computed results look not very satisfying in general. According to the left part of Fig. 42, the (simple?) problem of extrapolating the last pressure value to the base, in order to integrate the boattail contribution to drag dominates the numerical result.

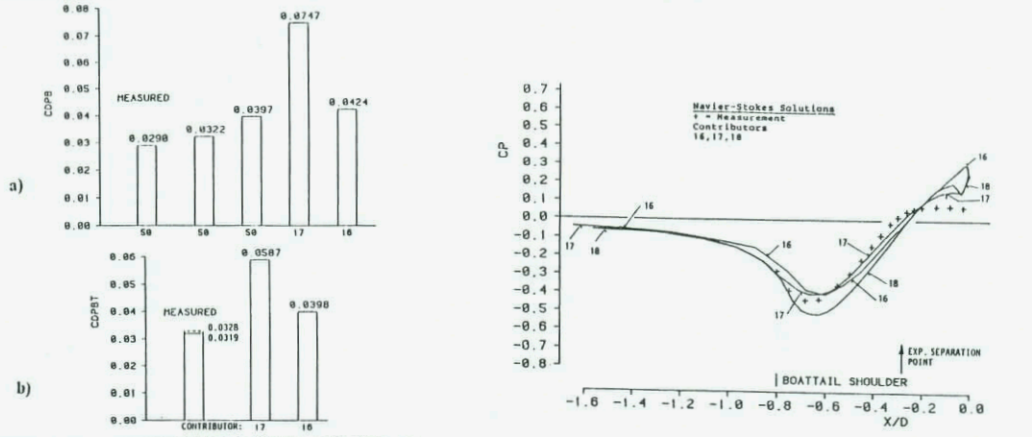

PRESSURE DRAG COMPONENT OF CONICAL BOATTAIL IN TRANSONIC FLOW. a) BASE-DRAG-COEFFICIENT b) BOAT-TAIL-DRAG

PRESSURE DISTRIBUTION ON CIRCULAR BOATTAIL WITH FLOW SEPARATION, (NAVIER-STOKES SOLUTIONS).

Fig. 42: AGARD WG 08: Integration of Boattail Drag

So far the remarkable discrepancies shown for boattail drag and base drag are not surprising. A compilation of all numerical results obtained by the Working Group is shown in Fig. 43 for the test cases with and without afterbody flow separation.

PRESSURE DRAG COEFFICIENT FOR CIRCULAR BOATTAIL WITHOUT SEPARATION

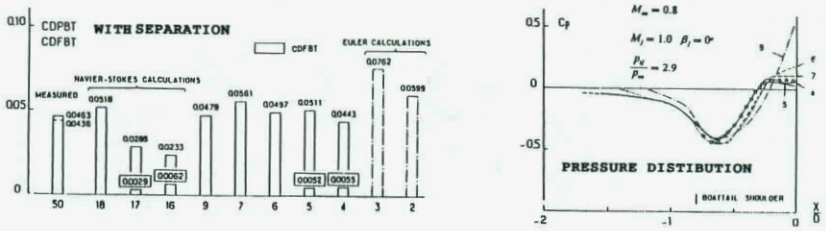

Fig. 43: AGARD WG 08: Compilation of Computational Results for Boattail Drag

There is a wide scatter with respect to the comparison with experiment as well as with results obtained by computer codes solving different classes of equations. But even worse, there is also the same scatter imparing results obtained within the same class of computer codes. At present the simple empirical prediction methods seem to work within the same level of agreement with experiment as the highly sophisticated CFD codes do, at least regarding integrated values for boattail and base drag.

3.4 Inlet Drag

In addition to boattail drag, inlet drag is the second important contribution of engine integration to drag. Total force in flight direction can be defined as the difference between installed propulsive thrust and the airframe system drag [22].

$$F_{N_{Prop.}} = F_{N_{Eng.}} + \Delta F_{N_{Inl.}} + \Delta F_{N_{Exh.}} + \Delta F_{N_{Trim.}}$$

$F_{N_{Prop.}}$ Installed propulsion thrust

$\Delta F_{N_{Inl.}}$ Throttle dependent external force increment due to inlet

$\Delta F_{N_{Exh.}}$ Throttle dependent external force increment due to exhaust system

$\Delta F_{N_{Trim.}}$ Changes in trim drag associated with operation or propulsion system

Some general remarks on the thrust/drag accounting system are made in Fig. 44.

- Important thing is that all forces are accounted for. Allocation between reference drag and propulsion system drags by mutual agreement.
- Selection of reference conditions for bookkeeping is somewhat arbitrary but must be consistent between airframer and engine companies.
- Intent of propulsion system drag breakout is to identify portion of aircraft drag which is throttle related and chargeable to engine.

Fig. 44: Thrust/Drag Accounting System: Overview

In detail this system is a rather complicated procedure ("book-keeping") which has to be agreed on between the airframe and the engine manufacturer. All the components mentioned above have to be based on reference conditions. Fig. 45 tries to explain schematically the drag/thrust accounting system agreed on at MBB.

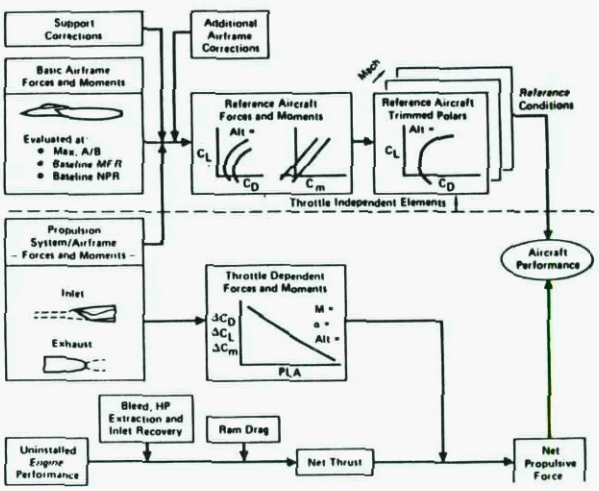

Fig. 45: Thrust/Drag Accounting System: Procedure, schematically

So far, the inlet drag component has to be provided either by experimental or theoretical approach. Fig. 46 shows the components which have to be determined by the aerodynamic engineer.

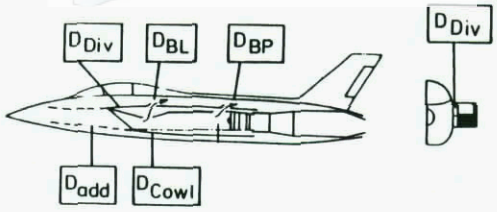

D_{add}	Additive Drag	Spillage Drag
D_{Cowl}	Cowl Drag	
D_{BL}	Boundary layer Bleed Drag	
D_{BP}	Drag due to Bypass	
D_{Div}	Diverter Drag	

Fig. 46: Thrust/Drag Accounting System: Inlet Drag Components

The knowledge of the 3D local flow distribution at the intake location is of fundamental importance. So numerical methods are predestinated to be used and again CFD plays an increasing role in intake design and the prediction of pressures. Fig. 47 demonstrates the power of CFD comparing the flow fields calculated using EUFLEX [12] around a fighter aircraft forebody with and without canard surface. These results are of significant importance to the optimization of intake (and diverter) geometry and location concerning minimum inlet drag.

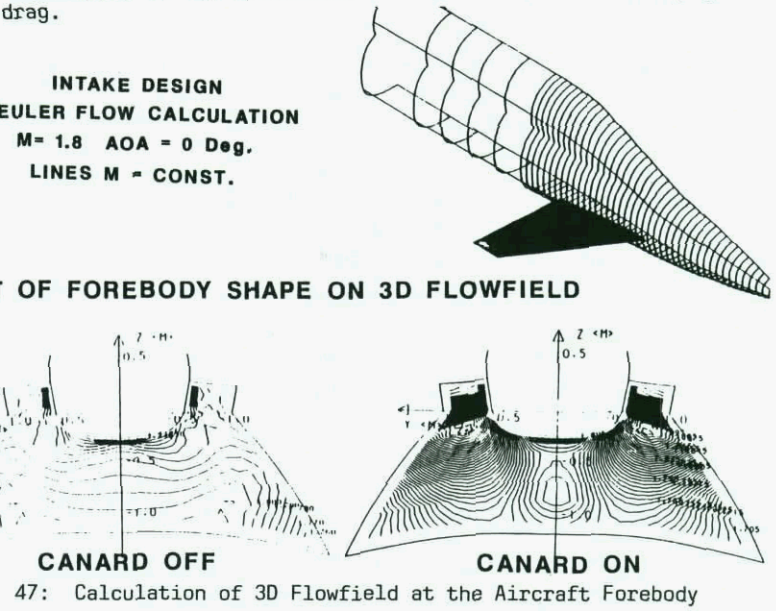

Fig. 47: Calculation of 3D Flowfield at the Aircraft Forebody

4. HYPERSONIC VEHICLE DRAG ANALYSIS

The new strong interest in efficient aerodynamic prediction methods for super- and hypersonic flows has been stimulated by some new European projects and advanced concept studies in the field of high speed missiles and aerospace transportation systems. Basically in the low supersonic flow regime important aerodynamic quantities can be predicted with some success by considering inviscid computational methods. However, in the high supersonic or even hypersonic region the flow field is influenced in an increasing manner by viscous and real gas effects as well as by non-equilibrium chemistry phenomena, so that the full conservation laws have to be taken as the starting point for the development of valuable numerical prediction tools. Especially from the theoretical simulation of flow fields around vehicles during reentry extremely reliable results are required concerning thermal and structural loads. On these answers the design of the necessary thermal protection systems and the vehicles payload will critically depend. Also these reentry vehicles will fly for most part of their reentry trajectory with high angle of attack so that strong streamwise vortex systems on the wing leeside will be generated which under some circumstances can interact with existing shock systems resulting in extreme local thermal loads.

Limits of current ground test facilities are expected to focus considerable attention on CFD as a means for designing hypersonic vehicles and weapons. Accurate drag prediction, however, and minimization will be critical for success. This problem is compounded by aero-propulsion concepts for which the examination of isolated components provides only a basis or foundation for building complete configuration analyses.

For sharp-nose type configurations of missiles or cruise vehicles Euler space marching methods or parabolized Navier-Stokes methods can provide excellent results for forebody analysis. Fig. 48 and 49 are portraying corresponding results taken from Ref. [24].

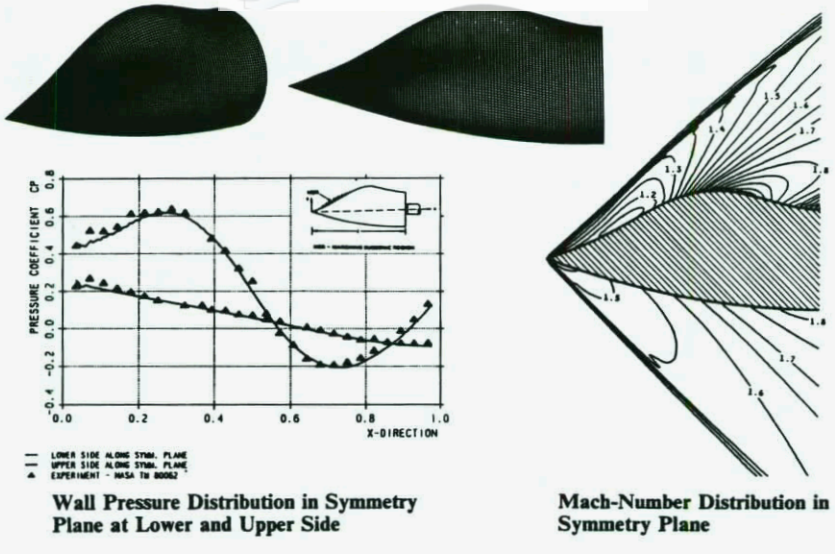

Wall Pressure Distribution in Symmetry Plane at Lower and Upper Side

Mach-Number Distribution in Symmetry Plane

Fig. 48: Euler Space Marching for Results for NASA-Forebody 4

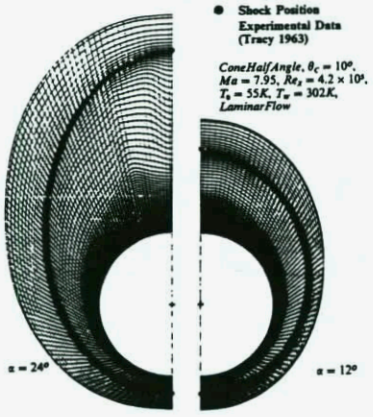

Solution-adaptive coordinate system for PNS space-marching scheme

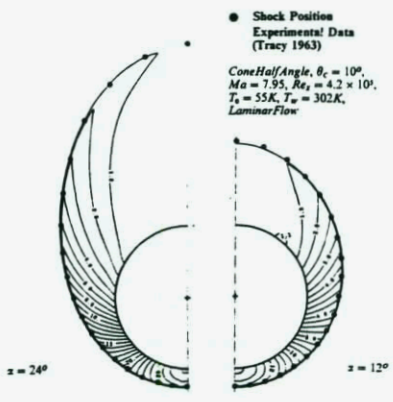

Static pressure distribution

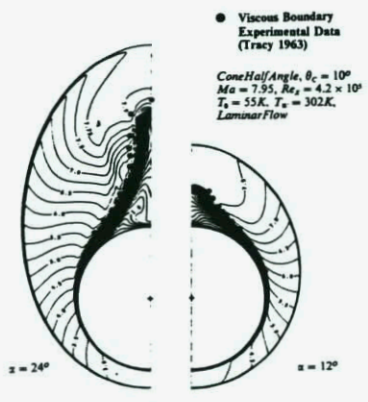

Mach-number distribution

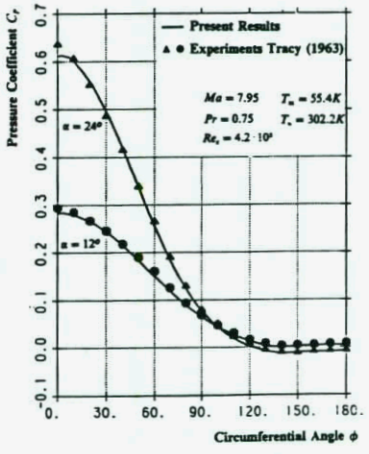

Circumferential wall pressure distribution

Fig. 49: PNS Selection for Cone at Incidence

For conceptual design applications also simplified methods based on Newton-type approaches can provide helpful tools, similar to the results in Fig. 30 and as discussed in Ref. [18].

More recent computations by Rieger [25] for the complete HERMES configuration provide insights into the difficulties which can be expected designing and analyzing such configurations. The comparison of Euler and laminar Navier-Stokes solutions as shown in Fig. 50 taken from Ref. [25] clearly indicate the sensitivity of the complex flowfield and the importance of viscous effects that are not confined to any thin layer close to the surface.

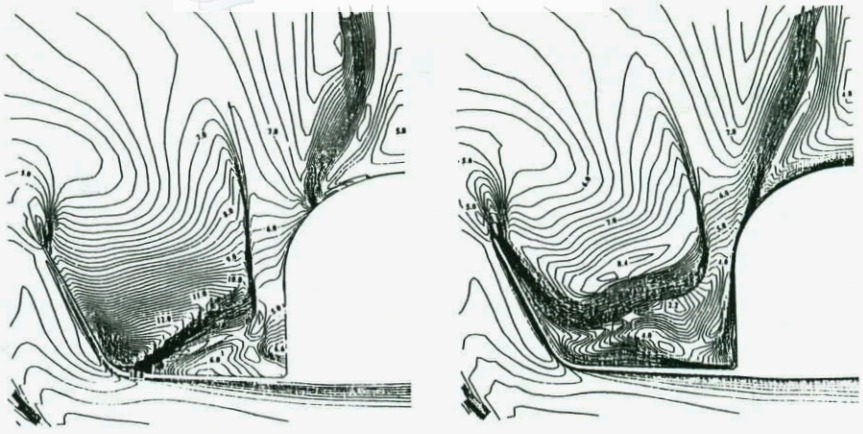

Inviscid Flow

Viscous Flow

MACH = 8.0, ALPHA = 30°, X = 15.4 m

Fig. 50: Comparison of Euler/Navier-Stokes for HERMES

The results for wall shear stresses in Fig. 51 are another indication for the complexity and also difficulty to obtain accurate results for drag as well as for heat transfer.

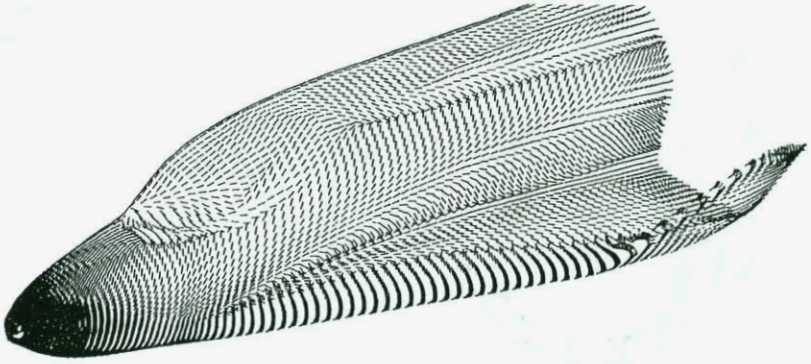

Viscous Flow

MACH = 8.0, ALPHA = 30°, RE = 10^6/m, LAMINAR

Fig. 51: Direction of Wall Stress Vector for HERMES

The integration of wall pressures and skin friction to obtain total drag requires extremely fine resolution of geometry as well as flow gradients.

The pressure distribution, portrayed as isobar-plot in Fig. 52, allows an important insight into the physics of the flowfield.

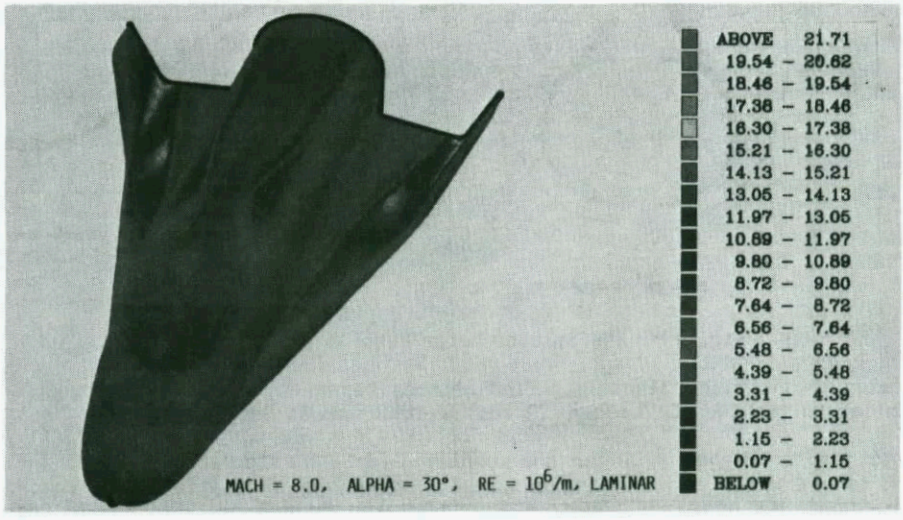

Fig. 52: HERMES Isobars as Navier-Stokes Solution

These results emphasize on the strength of CFD, namely resolving all details and giving information on all physical relevant quantities on the surface as well as in the field. But unfortunately, CFD has no build-in balance to obtain total forces.

5. CONCLUSIONS

Recent engineering and research advances in Germany addressing the CFD drag prediction problem have been reviewed. In addition, the impact of two-dimensional airfoil analysis accuracy level on wing design has been assessed. The most important conclusion to be drawn is that there are no simple answers to the CFD drag prediction problem. Accurate and consistent direct computation of absolute drag level for complete air vehicle configurations is currently beyond reach. Reasons for this come from many sources. Fig. 53 is summarizing the most important ones.

- o NO EFD PERSON WILL USE MEASURED PRESSURES TO INTEGRATE FOR DRAG
  - 2 - D: USE WAKE-RIGG
  - 3 - D: USE BALANCE
- o IN CFD EVERYBODY IS USING CP AND CF TO INTEGRATE FOR DRAG
  - 2 - D: WAKE - PREDICTION BY CFD IS QUITE DIFFICULT, SQUIRE AND YOUNG FORMULA CAN HELP
  - 3 - D: CFD HAS NO BUILD-IN BALANCE, 3 - D WAKE ANALYSIS IS VERY COMPLICABLE IF VORTEX-FLOW WITH LONGITUDINAL AXIS IS APPARENT
- o ABSOLUT DRAG VALUES SUFFER FROM RESOLUTION FOR INTEGRATION, RELATIV VALUES IN A COMPARATIVE SENSE CAN BE VERY ACCURATE

Fig. 53: Drag Prediction Techniques

Advances on many fronts can be identified. Most solutions, however, will involve added expense. It should be recognized that once a solution to the CFD drag prediction is found, the solution may not be affordable to industry, partially due to computer cost, but mainly due to the man power time and cost involved.

Despite these elements which limit direct CFD drag prediction applications, in closing the following items should be kept in mind:

- o Knowledge-based semi-empirical methods for drag prediction are work-horse for design-engineer
- o CFD is very useful for analysis of interference effects on drag
- o In 2-D airfoil flows CFD can be as accurate as EFD for drag
- o In 3-D flows, induced drag, wave drag, and some friction components can be predicted quite well
- o For performance guarantees there is no way but experiment for drag assessment
- o But: CFD is very strong on detailed flowfield surveys. Relative changes can be assessed

  - CFD is no drag polar machine -

6. REFERENCES

[1] G. Krenz: Accuracy Problems in Wind Tunnels during Transport Aircraft Development. AGARD-CP-429, pp 31-1, 31-9.

[2] H. Yoshihara; P. Sacher (editors): Test Cases for Inviscid Flow Field Methods. AGARD-AR-211, 1985.

[3] T. L. Holst: Viscous Transonic Airfoil Workshop Compendium of Results. AIAA-87-1460, 1987.

[4] J. Longo; W. Schmidt; A. Jameson: Viscous Transonic Airfoil Flow Simulation. ICAS Proceedings 1982, ICAS-82-6.1.2, 1982.

[5] W. Haase; H. Echtle: Computational Results for Viscous Transonic Flows Around Airfoils. AIAA-87-0422, 1987.

[6] M. A. Schmatz; A. Brenneis; A. Eberle: Verification of an Implicit Relaxation Method for Steady and Unsteady Viscous and Inviscid Flow Problems. AGARD-CP-437, pp 15-1, 15-32, 1988.

[7] M. A. Schmatz: Simulation of Viscous Flows by Zonal Solutions fo the Euler, Boundary Layer, and Navier-Stokes Equations. ZFW Vol. 11, 1987, pp 281-290.

[8] H. W. Stock; W. Haase, H. Echtle: Comparative Study of Calculation Procedures for Viscous Flows around Airfoils in the Transonic Regime. AGARD-CP-437, pp 7-1, 7-9, 1988.

[9] M. Carr (editor): Accuracy Study of Transonic Flow Computations for Three Dimensional Wings. GARTEur/TP-030, 1989.

[10] P. E. Rubbert: Use of CFD and Experimental Results in Transonic Aircraft Design. Symposium Transsonicum III, Göttingen, 1988.

[11] S. Leicher: Euler-Rechnungen für die Dornier 328. Dornier-AV BF30-43/89, 1989.

[12] W. Kraus; R. Kunz; P. Sacher: Computational Aerodynamic Design Tools and Techniques used at Fighter Development. AGARD-CP-280, 1979, Neubiberg.

[13] A. Elsenaar; L. Hjelmberg; K. Bütefisch; W. J. Bannink: The International Vortex Flow Experiment. AGARD-CP-437, 1988, Lisbon.

[14] A. Eberle: 3-D EULER Calculations using Characteristic Flux Extrapolation. AIAA-85-0119, 1985.

[15] M. A. Schmatz: Three-Dimensional Viscous Flow Simulations using an Implicit Relaxation Scheme. Nts. Num. Fl. Mech., Vieweg, Vol. 22, 1988, pp 226-243.

[16] W. Kraus: Minderung des Wellenwiderstandes. MBB-FE127/S/R/1615, 1988.

[17] L. Fornasier: A Higher Order Panel Method for Subsonic and Supersonic Flow about Arbitrary Configurations. Nts. Num. Fl. Mech., Vieweg, Vol. 21, 1987, pp 52-70.

[18] G. Cucinelli: HYP3 - Ein Hyperschall-Nachrechnungsverfahren nach der Impact-Methode. MBB-FE127-AERO-MT-811, 1988.

[19] S. Leicher, et al.: Aerodynamische Waffenintegration. Dornier-FB BF 36/85 B, 1985.

[20] K.-W. Bock: Aerodynamic Optimization. ICAS Proceedings 1988, ICAS-88-4.4.1, 1988.

[21] AGARD-AR-226: Report on the AGARD Working Group 08 on Aerodynamics of Aircraft Afterbody. 1986.

[22] K. Lotter: Air Inlet Design Considerations for Supersonic Fighter Airplanes. AGARD Lecture Series at Turkish Aircraft Industry, 1982.

[23] N. C. Bissinger: Berechnung der reibungsfreien Überschallströmung um einen Fighter-Vorderrumpf mit Canard. MBB-FE122-AERO-MT-779, 1987.

[24] H. Rieger: Solution of Some 3-D Viscous and Inviscid Supersonic Flow Problems by Finite Volume Space-Marching Schemes. AGARD-CP-428, pp 17.1, 17.17, 1987.

[25] H. Rieger; A. Jameson: Solution of Steady Three-Dimensional Compressible Euler and Navier-Stokes Equations by an Implicit LU Scheme. AIAA-88-0619, 1988.

[26] W. Schmidt: Computational Fluid Dynamics in West Germany. AIAA-87-1130-CP, 1987.

SOME RESULTS ON FLOW CALCULATIONS INVOLVING DRAG PREDICTION

By

PAPAILIOU,K.D., Professor

Lab. of Thermal Turbomachines,
National Technical University,
Athens, Greece.

ABSTRACT

Different calculation methods have been developed in the Thermal Turbomachinery Lab. of the Athens National Technical University concerning drag prediction.

A Navier-Stokes solver, based on a fractional step method, has been developed in order to solve viscous incompressible flow in ducts.

A second Navier-Stokes solver has been developed for transonic flow using, again, a fractional step method, but this time for quasi-three dimensional cascade flow.

Integral methods have been developed as well in order to predict secondary flows in compressors and shear layer development on blades. High speed laminar and turbulent flow is predicted, attached and separated. Viscous inviscid interaction techniques have been developed for the stabilization of the separated flow calculation.

Phenomena such as transitional flow, laminar separation bubbles and shock/shear layer interaction for turbulent flow are predicted with good accuracy. The general methods will be reviewed briefly and results will be presented.

1. INTRODUCTION

In recent years, computations tend to replace experiment in the field of Fluid Mechanics and its applications. The success of using the computer as a test bed depends largerly upon the success in predicting the behaviour of the viscous part of the flow.

Since the investigation of Thomson /1/ in 1962, where only Head's incompressible boundary layer calculation method was proved to give sufficiently accurate results, the 1968-Stanford Conference resulted in an assessment of some good calculation methods for simple boundary layer attached flows, while the corresponding 1981-Conference assessed the progress realized in the prediction of Complex Turbulent Flows.

During these years, the rapid advent of modern computing equipment helped in providing the means to obtain fast calculation results using equations and models of increasing complexity and, today, computations using the Navier-Stokes equations are possible for simple situations and plausible for complicated ones in the near future.

Of course, there are still some important draw backs, as, even if the dream of developing a unique turbulence model for all situations was declared unrealisting during the 1981-Stanford Conference, progress in turbulence modeling of complex flows is still very slow. On the other hand, even the faster computers cannot give sufficiently rapid results for industrial needs and the advance Navier-Stokes solvers are still very sensitive to run, so that they become unfriendly when in the hands of the average engineer.

This state of affairs reflects in the past and present development of codes predicting the viscous behaviour in any Laboratory. This holds, as well for the Lab. of Thermal Turbomachines (LTT) of the National Technical Univ. of Athens (NTUA) on which this presentation will focus, although a quick survey will be given about the work on viscous flows that is taking place in Greece, as well.

Fifteen engineers (post docs) work in the TTL supported by four administrative staff.

The LTT of NTUA has four sections dedicated to:
a) Computational Fluid Mechanics
b) Viscous Flows
c) Diagnostics on Turbomachinery Components
d) Design/Analysis of Turbomachinery Components

We shall describe below the past, current and future work of the first two sections. The first one covers computations solving the Euler and the Navier-Stokes equations, while the second one develops codes for practical (industrial) viscous flow calculations. Although, naturally, the interest of the Lab. is directed towards viscous flows as they appear in turbomachinery applications or internal aerodynamics flow problems, the same codes may be and are used for external aerodynamics applications.

2. ENGINEERING VISCOUS FLOW COMPUTATIONS USING INTEGRAL SHEAR LAYER CALCULATION METHODS

2.1 Past and Current Work

Two methods have been developed in the Lab., essentially. The first one is a quasi-two dimensional (converging/diverging, axisymmetric) one. It is used to calculate blade or airfoil shear layer development, is using the integral energy equation and its formulation follows Le Foll's method /2/. The second method is an integrodifferential one (integral in the meridional and differential in the peripheral direction) and deals with the calculation of the hub and tip shear layers of axial and radial compressors. Shock/secondary flow interaction is computed as well by the method.

Originally, the first method was developed as an inverse one /3/, with the ability to produced optimized decelerating velocity distributions (Fig.(1), refs /4/ to /12/) for attached flow. Then, curvature and Coriolis effects on turbulence were incorporated (Fig.2, refs /11/,/13/) and the equations were solved in the rotating system of coordinates, so that the method may be adapted to turbomachinery applications.

A first attempt to deal with detached flows demonstrated the ability of the method to predict separation accurately and to advance in the separated region without any difficulty (refs /14/,/15/). However, no viscous/inviscid interaction techniques were used, in order to stabilize the viscous flow calculation behaviour. During the development of the method, systematic comparisons against experiment demonstrated the excellent accuracy with which the method could reproduce physical situations. These comparisons can be found in the cited references.

During the past years, work on the method continued in the TTL. Recognizing that a boundary layer approximation cannot give adequate accuracy in separated flow regions, higher order terms were retained in the equations and the compressibility effects were introduced using Morkovin's hypothesis. At the same time a more accurate turbulence model was developed /16/ and introduced to the method, which is particularly adapted for separated flow. Finally, an approximate viscous inviscid interaction technique was built in the method, protecting it against excessive external flow decelerations and rendering it independent of the particular computational method used for the inviscid external flow calculation. The viscous/inviscid approximate interaction method has been developed in ref./17/ for axisymmetric three-dimensional flows, recognizing the importance of blockage in internal flows. A second one was used for viscous/inviscid interaction for the shock/boundary layer interaction problem, which is described in references /18/ and /19/.

In this form, the shear layer calculation method was applied to various kinds of flows. Fig.(2) presents comparisons with experimental results for the shock/boundary layer interaction case /23/, where separation and reattachement are present. Fig.(3) presents comparisons for channel flow, where Coriolis effects are responsible for separation at 50% of the channel length. There, a simultaneous shear layer calculation was performed on the two walls of the channel.

The same kind of computation was realized for an NACA compressor cascade. Fig.(4) presents comparisons between theory and experiment for the loss variation with incidence.

Recognizing the need to predict some important aspects of viscous flows in turbomachines, versions of the method were developed to compute transitional boundary layers and laminar separation bubbles. The first development was based on the work of Bario /20/, which was based itself on the work of Narashima /21/. Results (comparison with experiment) are presented in Fig.(5). The second development aimed in producing a good first approximation, from where an accurate viscous/inviscid calculation could rapidly converge. The method is described in ref./22/ and some results are presented in Fig.(6).

Lately, work on blade optimization has taken up again, including, now, compressibility and detached flow. Some results /24/ are presented in Fig.(7), concerning a wind turbine blade section. They demonstrate that there is still room for improvement, if optimized shear layers are employed.

The second method, which is adapted for hub and tip wall layer development computation, considers the two wall shear layers simultaneously. The same techniques /17/ as previously are used for the interaction of the shear layers with the external flow. Each wall shear layer is calculated using integral equations in the meridional direction and the meridional vorticity transport equation in the meridional, as well, direction. In the vorticity transport equation, viscous terms are included. Higher terms are conserved so that the level of approximation comes close to that of the parabolized Navier-Stokes equations.

The method of solution is well adapted to the existance of separated regions as well as to an external flow with varying properties in a direction normal to the wall. The method is the outcome of a long work on the two-zone model (separation of the flow into an inviscid and a viscous part), as it is applied to complex internal flow situations, where thick shear layers exist covering part or even all of the flow field and the external flow field properties are varying strongly inside the viscous flow regions in a direction normal to that of the main flow.

This work has started some years ago (see references /25/ to /37/) in Lyon and was continued in Athens (refs /38/ to /41/). During the investigation, it was demonstrated that it was possible to extent this usefull model to extreme situations. Such a situation was the one, where the external flow was physically non existent (see ref./37/), the viscous flow occupying the whole computational space. Calculation results for this situation are compared with experiment in Fig.(8). We can also mention the one, where the shear layer is rotating /11/, or even the one, where a shear layer is developing inside another, when, after a stationary part, a rotational part of a cylinder follows (ref./39/). Calculation results for this last case are compared with experiment in Fig.(9). These cases prove that the principle of superposition can be extended beyond expectation, when an appropriate reference flow is defined. At the same time they demonstrate how rotating flows have to be handled.

The most important fact, however, which has come out recently from this investigation, is the acknowledgement of the existance of a peripheral blockage along with the well known meridional one, expressed through the meridional displacement thickness (details are given in ref./40/). Consideration of both blockage effects (meridional and peripheral) implies that the interaction of the viscous and the external flow parts results in influencing both the level and the direction of the external flow velocity field. At the same time, the analysis of a given experiment becomes somewhat more complicated. Finally, things are simplified in that, through this analysis, not only the vorticity but, also, the velocity field of the shear layer is limited inside a distance δ from the solid wall, δ being the thickness of the shear layer. Consequently, induced velocities outside of the shear layer do not exist (neither s-shape velocity profiles) and the calculation is considerably simplified.

The calculation method, now, exists in the Lab. and shall be very soon rendered public (references /43/,/44/). Computational results compared to experiment are presented in Figures (10) and (11) for a compressor cascade and an axial transonic compressor stage.

2.2 Future work

Work on the first method continues and the following development is planned, for which funding already exists:

a) Integrate in one direct calculation code all the elements mentioned above.
b) Develop the same direct calculation method for the case of the assymetric wake.
c) Explore the general shear layer properties in the separated flow region and develop a complete inverse method for blade design, including an inverse inviscid calculation method

which is, actually, in the final stage of its development.

d) Develop an unsteady version of the already existing one, following work that has already been done in the Lab.

Work on the second method with continue, equally well, and, besides following up what is being done now, in order to assess better the capabilities of the new method, a new item will be developed: The strong interaction of the hub and tip wall shear layers, which is important in the high pressure part of the multistage axial compressor, as well as in the diffusor of the centrifugal compressor.

3. VISCOUS FLOW COMPUTATIONS USING THE FULL NAVIER-STOKES EQUATIONS

3.1 Past and Current Work

The advent of high speed computing equipment and the speed with which this equipment is developing, favors, in the long run, the use of the full Navier-Stokes equations for the calculation of, even, complex industrial situations. Recognizing this fact, the TTL has initiated, some years ago, work in three directions:

1. Overcoming the numerical problems associated with the solution of the full 3D Euler equations in subsonic and transonic flow. In this respect, efforts were made to reduce the numerical entropy production and diffusion in subsonic and transonic flow problems.
2. Develop codes applicable to complex geometries, in order to be able to tackle industrial problems.
3. Proceed in adding viscous terms in the equations in order to obtain solutions for the complete Navier-Stokes equations for laminar and turbulent flow.

This development started five years ago. Three issues were investigated and the corresponding methodologies were applied to various idealized and practical situations. All the work that has been done up to now makes use of finite differences/finite volume schemes, be they implicit or explicit, and body fitted coordinate systems.

3.1.1 The Fractional Step method for the Solution of the Incompressible Navier-Stokes Equations

This method was developed on the basis of work that has been done in the LNH of EDF /45/. It consists of three successive steps. The first one is a convection step, the second a diffusion one and the third one's goal is to satisfy the mass conservation, either in a form using the stream function or in the well known Poisson's equation form for the static pressure. The method uses an explicit scheme.

The convection step satisfies that part of the momentum equation, which contains merely the substantial derivative of the velocity. It is realized through a forth order Runge-Kutta scheme, which is used in order to "trace numerically" the trajectories of the flow field. Thereafter, the velocity field is updated using already computed values from the previous time step.

The treatment of the viscous terms is realized during the second ("diffusion") step. This leads to the solution of a set of elliptic partial differential equations, one for each velocity component. These equations are completed with an easily applicable set of boundary conditions, the corresponding values being derived from the known velocity field of the previous iteration step.

The third and final step considers all the remaining terms of the momentum equations. As said previously, a Poisson type equation is formulated for the static pressure. Some difficulties may be encountered, then, at the boundaries. Alternativelly, a classical stream function formulation is used, leading again to a Poisson type equation with boundary conditions easy to comply with. Practically, both formulations are used in the iterative scheme.

For the time being, this method is tested only for laminar flow problems but a turbulent model of any level can easily be incorporated due to the modular structure of the code.

Although convergence is seriously affected by stability criteria, which are common for all explicit methods, it can be considerably accelerated, if very fast elliptic solvers are used during the "diffusion" and the last step of the method.

Calculation results from this method are presented in Fig.(12). For the moment, only internal flow aerodynamic problems can be treated, including flow through cascades. Although very attractive, because of the physically clear picture it presents, this method was not developed further, because, at the time, the possibility to treat compressible flow was not evident. Now, this possibility seems real and future work on the method is planned which will be discussed below.

3.1.2 A 3D Finite Difference Solver Based on the Decomposition of the Mass Flux Field Through Helmholtz Theorem (refs. /46/ to /49/)

This method has been developed in the TTL in order to compute essentially subsonic 2D or 3D flows. However, it is capable to treat transonic flow problems under certain conditions. The final solution is obtained through a series of elliptic computations. In this present form, this method is able to treat only 3D strongly rotational, steady, inviscid flow problems. A fixed or a rotating coordinate system may be used.

The method makes use of the decomposition of the mass-flux vector field into a potential and a rotational part. The potential part is expressed as the gradient of a scalar potential (φ), while the rotational part is expressed as the rotation of a vector potential ($\vec{\Phi}$). The mass flux decomposition is proved to be unique, if appropriate boundary conditions are imposed on (φ) and ($\vec{\Phi}$). The resulting formulation requires the iterative solution of two elliptic type equations (a scalar and a vector one) and a procedure for handling the transport of vorticity.

A curvilinear body-fitted coordinate transformation is applied to map the physical domain, bounded by the geometry solid and fluid boundaries, into an orthogonal paralillepiped, where the physical boundaries are transformed on orthogonal planes. All equations are, then, transformed and solved in that computational domain. This technique increases the range of applications of the method and enables an efficient implicit treatment of the elliptic equations' boundary conditions.

All elliptic type equations are discretized by use of finite differences/finite volume schemes and the resulting linear sparce-diagonal systems are solved by fast elliptic solvers, based on a preconditioned "Generalized Minimal Residual Method" (GMRES). The vector potential equation is expressed in

terms of the covariant ($\vec{\psi}$)-components and this formulation enables the direct handling of the vector potential boundary conditions, a fact that makes the method quite robust. The vorticity transport equations are replaced by the total temperature and entropy conservation laws along with the ellicity equation, the last one expressing the velocity-wise vorticity component attribute. All transport type equations are integrated in their Lagrangean form on the current flow-field streamlines, in the transformed domain.

Since no artificial viscosity is necessary for the convergence of the method, the calculated energy and entropy field is very accurate compared with the corresponding results of the primitive variables time marching solvers. Another advantage is that this method is much less time-consuming than its time-marching "opponents", as far as very efficient elliptic solvers are in use.

Some calculation results for a 3D complex shaped subsonic duct are presented in Fig.(13). It can be seen that no numerical entropy diffusion is observed. Fig.(14) presents results for a 2D transonic duct. There, it can also be seen that the elliptic solver can treat transonic flow problems under certain conditions, as mentioned above.

During the development of the method experience was acquired in constructing body-fitted grids for complex geometrical shapes, as well as solving elliptic equations rapidly. In fact, using GMRES techniques, the computational cost amounts to about 0.4 secs/grid point in a VAX-II microcomputer.

On the other hand, the code has been developed for 3D orthogonal or circular shaped ducts, as well as turbomachinery blade rows. Corresponding versions for 2D flows exist using, as seems each time appropriate, H-type, O-type or C-type grids.

Recently, external flow aerodynamic problems have been considered and a version for the calculation of steady 3D-flow through a wind turbine has been developed /50/.

The state of development of the inviscid part being considered satisfactory, an unsteady viscous flow solver is currently under development This development, having just started, will be considered along with the future work described below.

3.1.3 The Fractional Step Method for the Solution of the Compressible Navier-Stokes Equations

The investigation carried out with the elliptic solver mentioned above, demonstrated that it was not possible to solve transonic flow problems with supersonic flow at the boundaries or purely supersonic flow. It was evident that, for this flow problems, a hyperbolic solver was necessary. Work on fractional step methods guided us to the one developed currently in the TTL, which solves the compressible 2D Navier-Stokes equations, using an explicit fractional step algorithm, which transofrms the procedure of finding a solution for the multi-dimensional system, into solving a sequence of one-dimensional ones.

This method is actually developed for internal flow problems, including cascades. The experience gained from the development of the previous method helped in obtaining relatively rapidely an Euler solver with good behaviour and, now, results have been already obtained for the Navier-Stokes version.

For this method, the Navier-Stokes equations in primary variable form are written in a general stationary or rotating curvilinear coordinate system. Then, a geometrical transformation is applied to map the physical domain, bounded by the geometry's solid and fluid boundaries, into a rectilinear computational domain, where the boundaries are located on straight orthogonal lines. A distinction is made between points belonging to solid boundaries and the ones located along periodic boundaries. There, additional grid points are considered outside of the computational domain, where the flow quantities are known from periodicity considerations.

Each fractional step is materialized by a predictor-corrector McCormack explicit scheme. After the solution of each one-dimensional problem is obtained, the characteristic equations are applied in order to update the solution on all boundaries.

Moreover, in order to avoid odd-even uncoupling and oscillations that might occur close to discontinuities, artificial viscosity is introduced. This is realized by performing an extra fractional step, when an integer time step is reached, this being equivalent to the addition of a second derivative of the vector of unknowns to the LHS of the equations.

Finally, a local time step is implemented during the computation. This allows the procedure to advance as fast as the local application of the CFL criterion allows it to do so and, thus, relax somewhat one of the most severe limitations of the explicit scheme.

Up to now, the code has been tested for inviscid and laminar viscous flow calculations. Fig.(15) presents calculation results. Linited storage requirements make the fractional step methodology attractive for solving Reynolds averaged Navier-Stokes equations using conventional computing facilities. The code has been developed in a modular form and current work is directed towards introducing a two-equation turbulence model, as well as, reducing the computing time which is still rather long in respect to the time needed by the previous method.

3.2 Future Work

Work on all three methods mentioned above continues and the following development are planned, for which funding already exists:

a) For the first Navier-Stokes solver it is planned to introduce the GMRES techniques mentioned above, which will render it more rapid. Additionally, the introduction of a more sophisticated turbulence modelling is planned. Finally, an attempt will be made to render the code applicable to compressible flow, which seems now possible.

b) For the second Navier-Stokes solver it is planned to continue, in order to obtain a solution for the unsteady, essentially subsonic (and slightly transonic) flow situations for internal and external aerodynamics flow. The final solution will still be obtained by successive elliptic computations.

c) For the third Navier-Stokes solver, it is planned to continue, in order to render the method industrially acceptable. It is not currently planned to obtain a 3D version of this code.

Generally speaking, the level of turbulence modelling aimed at, presently, for all methods, is the one using two equations. As the codes are developed for industrial applications, it is felt unnecessary to introduce a more complicated model. However, it is planned to develop more systematically, than it

is done today in the Lab., the subdomain approach, which gives, in our opinion, the flexibility to use different turbulence "constants", when this is required.

4. COMPUTATIONAL WORK ON VISCOUS FLOWS IN GREECE

This fourth section is intended to give, very briefly, computational work which is taking place on viscous flows in Greece. This account is not intended to be complete neither in respect to the research workers list nor in respect to the subjects treated. To our knowledge, development of computer codes for viscous flows is taking place in:

1) The Athens National Technical University, (Professors Bergeles, Zervos, Athanassiades and Markatos)
2) The Aristotelian University of Thessaloniki (Professor Goulas)
3) The Democretian University of Thrace (Professor Soulis)
4) The University of Crete (Professor Dougalis).
5) The University of Patras (Professor Papailiou)

5. ACKNOWLEDGEMENTS

We would like to express our thanks to the Stē SNECMA, Stē Dassault, Stē Bertin, G.E.C.-Turbomachinery Applications and The Commission of the European Communities for the financial support of the developments mentioned above.

REFERENCES

/1/ THOMSON, G.B., "A critical review of existing methods of calculating turbulent boundary layers", ARC 26109, FM 3492, 1964.

/2/ LE FOLL, J., "A theory of representation of the properties of boundary layers on a plane", Proc., Seminar on Advanced Problems in Turbomachinery, VKI, March 29-30, 1965.

/3/ PAPAILIOU,K.D., "Blade Optimization based on boundary layer concepts", VKI CN60, 1967.

/4/ PAPAILIOU,K.D., "Optimization d'aubage de compresseur à forte charge sur la base des théories de couches limites", Thèse de Doctorat en Sciences Appliquées, Univ. de Liège, 1969.

/5/ PAPAILIOU,K.D., "Boundary layer optimization for the design of high turbing axial flow compressor blades", ASME Transactions, Journal of Engineering for Power, pp 147-155, 1971.

/6/ PAPAILIOU,K.D.,"An Investigation on Le Foll's method used for blade optimization based on boundary layer concept", Proc. Congress of the Intern. Aeronautical Federation, Argentina, 1967.

/7/ HUO, S.,"Blade optimization based on boundary layer concept", AGARD AG 164, 1973.

/8/ HUO, S.,"Optimization based on the boundary layer concept for compressible decelerating flows", Thèse de Doctorat, Univ. de Bruxelles, 1973.

/9/ HUO, S.,"Optimization based on the boundary layer concept for compressible decelerating flows", ASME paper 74-GT-86.

/10/ PAPAILIOU,K.D.,"Le Foll's method and the calculation of Attached and Separated Two Dimensional Boundary Layers", VKI., Lecture Series on Separated Flows in Turbomachinery Components, VKI-LS-81-1, 1981.

/11/ PAPAILIOU,K.D., SATTA,A., NURZIA,F.,"On the Two-Dimensional Boundary Layer as they appear on turbomachines blades", AGARD AG 164, 1972.

/12/ PAPAILIOU,K.D.,"Viscous Flows in centrifugal compressors", VKI Lecture Series 95. Shorte Course on Industrial Centrifugal Compressors, 1977.

/13/ PAPAILIOU,K.D.,"The Coriolis Force Influence when we calculate Turbulent Boundary layers in Centrifugal Compressors", Presenté Israel Joint Gas-Turbine Congress, Haifa, July 9-11, 1979, "Turbo and Jet Engine Technology", Benjamin Gal-Or, Editor, Part II, 1980.

/14/ ASSASSA,G.M.,"Calcul par des methodes integrales de couches limites laminaires ou turbulentes incompressibles ou compressibles introduant des zones faiblement decollées", Thèse de Docteur ès Sciences Physiques, Univ. Claude Bernard, Lyon, 1976.

/15/ ASSASSA,G.M., PAPAILIOU,K.D.,"An integral method for the calculation of the separated turbulent boundary layer", Transactions of the ASME. Journal of Fluid Engineering, pp 110-116, 1979.

/16/ GEROLYMOS,G., KALLAS,Y., PAPAILIOU,K.D.,"The Behaviour of the Normal Fluctuation Terms in the Case of Attached or Detached turbulent boundary layers", ASME PAPER 84-GT-179, 1984.

/17/ PAPAILIOU,K.D.,"A contribution to the calculation of secondary flows in an axial compressor", Proc. "6th International Symposium of Air Breathing Engines (ISABE), Paris, June 1983.

/18/ MASON,W.H., INGER,G.R.,"Analytical study of transonic normal shock boundary layer interaction", AIAA paper 78-831, 1975.

/19/ PANARAS,A.G.,"Normal shock boundary layer interaction in transonic speed in the presence of streamwise pressure gradient", Ph.D. Thesis, Un. Libre de Bruxelles, May 1976.

/20/ BARIO,F.,"Contribution à l'étude du developpement des couches limites sur les aubages de turbomachines", Thèse de Doctorat 3ème cycle. Université Claude Bernard, Lyon 1978.

/21/ DHAWAN,S., NARASIMHA,R.,"Some properties of boundary layer flow during the transition from laminar to turbulent motion", JFM, Vol.3, p.418, 1958.

/22/ STAMATIS,A., KTENIDIS,P., PAPAILIOU,K.D.,"Viscous inviscid interaction in the case of a laminar separation bubble", Proc. 38th Congresso Nazionale ATI, Bari, 28-30/9/83. LA TERMOTECNICA, Sept. 1984.

/23/ KALLAS,Y., PAPAILIOU,K.D.,"A Method for the calculation of the interaction of a turbulent boundary layer with a shock wave", Presented in the 8th ISABE Int. Symposium, Cincinnati, Ohio, USA, 1987.

/24/ BOLETIS,E., CHAVIAROPOULOS,P., BONATAKI,E., BOURAS,B., PAPAILIOU,K.D.,"A complete inverse calculation procedure for the optimization of horizontal axis wind turbine airfoils". To be presented in the 1988 European Community Wind Energy Conference and Exhibition, Henning Congress Center, Denmark, 6-10 June 1988.

/25/ FLOT,R., PAPAILIOU,K.D.,"Ecoulements Secondaires dans les compresseurs axiaux", IIe Colloque d'Aerodynamique Appliquée, AAAF, 1974

/26/ PAPAILIOU,K.D.,"Secondary flows in axial compressors", VKI Short course on "Secondary flows in turbomachines", LS 72, 1975.

/27/ PAPAILIOU,K.D.,FLOT,R., MATHIEU,J.,"Secondary Flows in Compressor Blading", ASME PAPER 76-GT-57, 1976, ASME Trans., Journal of Engg. for Power, Vol.99, pp 211-229, 1977.

/28/ BOIS,G.,LEBOEUF,F.,COMTE,A., PAPAILIOU,K.D.,"Experimental study of the behaviour of secondary flows in a transonic compressor", AGARD CP-214, 1977.

/29/ LEBOEUF,A.,COMTE,A., PAPAILIOU,K.D.,"Calculation concerning the secondary flows in compressor bladings", AGARD CP-214, 1977.

/30/ BOIS,G., VOUILLARMET,A.,DUCHEMIN,J., PAPAILIOU,K.D.,"Analyse experimentale de l'écoulement dans un etage de machine centrifuge", presenté au "Centrifugal compressors, flow phenomena and performance", AGARD CONGRESS, 7-9 May, 1980, AGARD CP 282.

/31/ COMTE,A., OHAYON,G., PAPAILIOU,K.D.,"A method for the calculation of the wall layers inside the passage of a compressor cascade with and without tip clearence", ASME Trans., Journal of Engg. for Power, Vol.103/3, 1981

/32/ BARIO,F.,LEBOEUF,F., PAPAILIOU,K.D.,"Study of secondary flows in blade cascades of turbomachines", ASME Trans. Journal of Engg. for Power, pp 497-503, 1982.

/33/ VOUILLARMET,A.,PAPAILIOU,K.D.,BOIS,G.,"Experimental Analysis and Theoretical Approach for the three-dimensional viscous flow in a centrifugal compressor" presented in Symposium on Energy and the Environment", Patras University, 1981.

/34/ BOIS,G.,LEBOEUF,F.,COMTE,A.,PAPAILIOU,K.D.,"Measurements of secondary flows in a transonic axial flow compressor: Measuring techniques in transonic and supersonic cascades and turbomachines. Editors A.Bölcs and T. Fransson, Proc. of the Symposium held in Lausanne on Nov. 18-19, 1976.

/35/ LEBOEUF,F.,BARIO,F.,BOIS,G.,PAPAILIOU,K.D.,"Experimental study and theoretical prediction of secondary flows in a transonic axial flow compressor", ASME paper 82-GT-14.

/36/ BOIS G.,PAPAILIOU,K.D.,"A contribution to the study of the design of an industrial centrifugal compressor", ASME PAPER 84-GT-60, 1984.

/37/ HARLAFTIS,S.,LEBOEUF,F.,PAPAILIOU,K.D.,"Experimental and theoretical investigation of turbulent asymmetric shear-layer interaction in a two-dimensional smooth-wall passage", 1985 ASME, Winter annual meeting, Miami, Fl.

/38/ KOTIDIS,P.,CHAVIAROPOULOS,P.,PAPAILIOU,K.D.,"An investigation of the transverse velocity profile in the case of internal viscous aerodynamic problems", ASME PAPER 84-GT-218,1984.

/39/ PAVIS,S.,KTENIDIS,P.,PAPAILIOU,K.D.,"Boundary layer development passing from a stationary to a rotating axisymmetric surface", presented in the 8th ISABE Int. Symposium, Cincinnati, Ohio, 1987.

/40/ DOUVIKAS,D.,KALDELLIS,J.,PAPAILIOU,K.D.,"The circumferential velocity profile for secondary flow calculations" ASME PAPER 87-GT-255.

/41/ LAMBROPOULOS,L.,KTENIDIS,P., PAPAILIOU,K.D.,"Boundary layer development on rotating bodies of revolution", Proc., Symposium AGARD sur "Les Effets Visqueux dans les Turbomachines", Copenhagen, June 1983, AGARD CP 351.

/42/ KALDELLIS,J.,DOUVIKAS,D.,PAPAILIOU,K.D.,"A secondary flow calculation method based on the meridional vorticity transport equation", paper to be presented in 33rd ASME Intern. Gas Turbine Conference, Amsterdam, 1988.

/43/ KALDELLIS,J.,"Shock/secondary flow interaction in modern axial flow compressors", Doctorat Thesis (In preparation).

/44/ DOUVIKAS,D.,"Secondary flows in radial compressors", Doctorat Thesis (In preparation).

/45/ GOUSSEBAILE,J.,"Modélisation d'écoulements et de transferts de chaleur par une méthode de différences finies en mailles curvilignes non orthogonales", Rapport EDF-DER HE41/81/27.

/46/ GIANNAKOGLOU,K., "Contribution to the Calculation of a Two-Dimensional Inviscid, Transonic, Rotational flowfield", Ph.D. Thesis, NTUA, 1987.

/47/ CHAVIAROPOULOS,P.,"Contribution to the Calculation of 3D inviscid, rotational, compressible, subsonic flowfield", Ph.D. Thesis, NTUA, 1987.

/48/ GIANNAKOGLOU,K.,CHAVIAROPOULOS,P., PAPAILIOU,K.D.,"Numerical Computation of Two-Dimensional rotational inviscid transonic flows, using the decomposition of the flow field into a potential and a rotational part", Proceedings of the 7th Conf. of Intern.Society of Air Breathing Engines (ISABE), Beijing 1985. Accepted for publication in the Journal of AIAA.

/49/ CHAVIAROPOULOS,P.,GIANNAKOGLOU,K., PAPAILIOU,K.D.,"Numerical Computation of Three-Dimensional Rotational Inviscid Subsonic Flows, Using the decomposition of the flow into a potential and a rotational part", ASME PAPER 86-GT-169, 1986.

/50/ CHAVIAROPOULOS,P., PAPAILIOU,K.D.,"A full potential prediction of a HAWT rotor performance", 1988 European Community Wind Energy Conference and Exhibition, June 1988, Denmark.

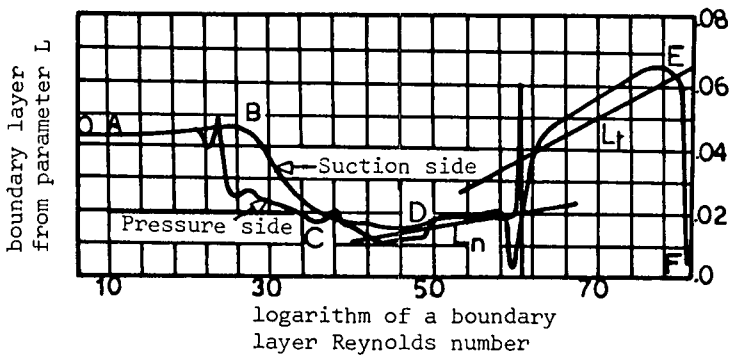

The image curve corresponding to the velocity distributions of the calculated blade.

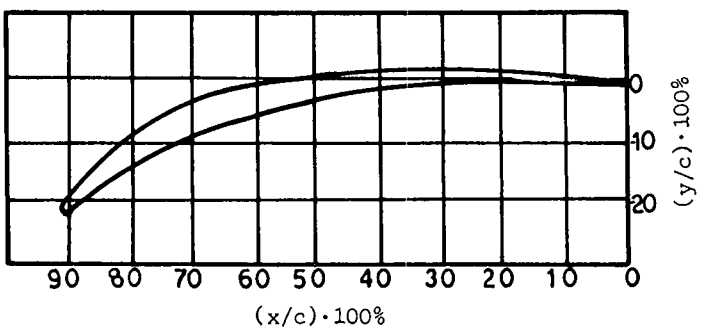

The calculated blade

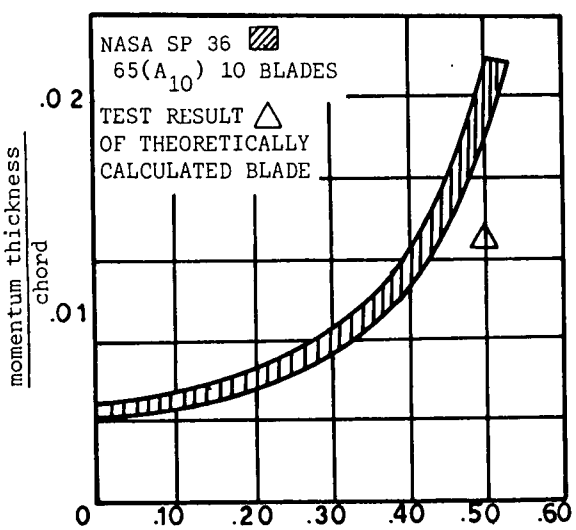

Test results for the blade designed

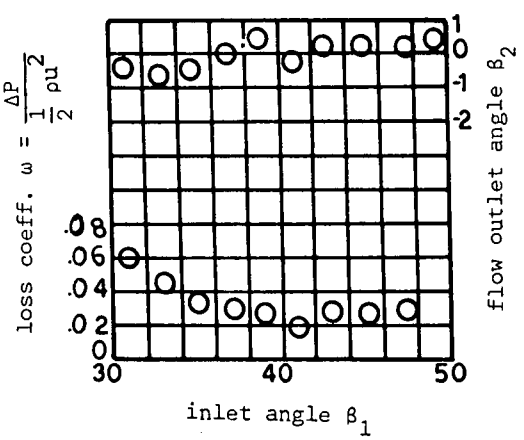

The experimental results of the test carried out at Pradd and Whitney Co

FIG. 1 Results of the optimization procedure applied to the design of a compressor cascade for incompressible flow.

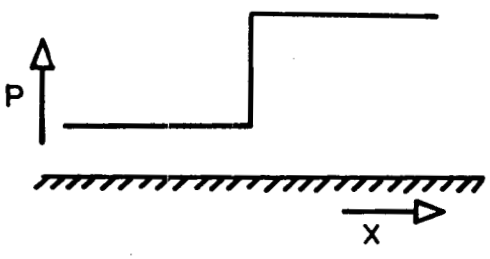

Initial external static pressure field

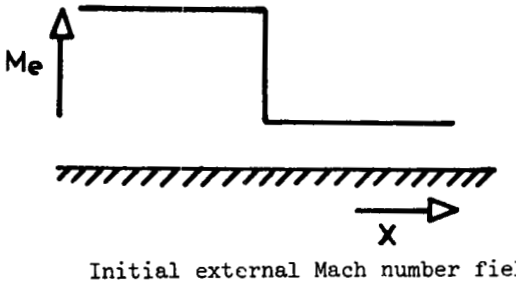

Initial external Mach number field

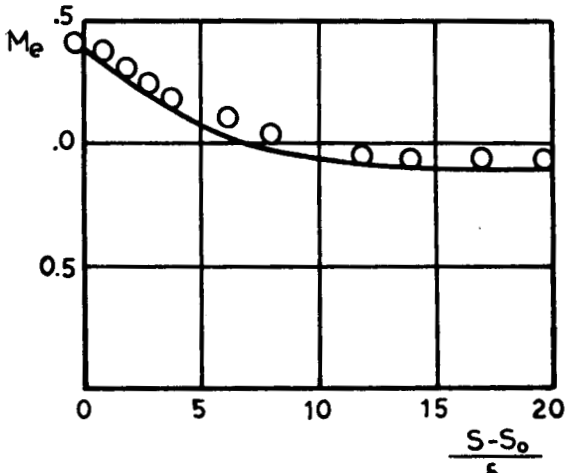

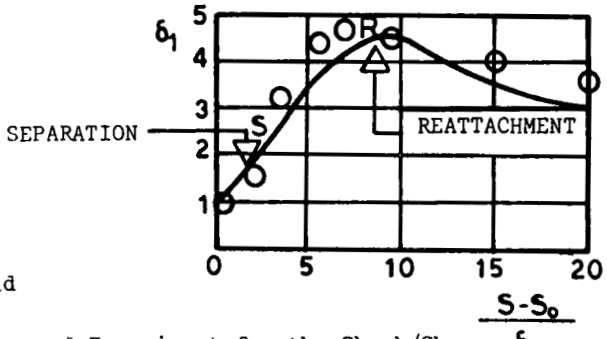

FIG. 2 Comparison of theory and Experiment for the Shock/Shear Layer Interaction Case.

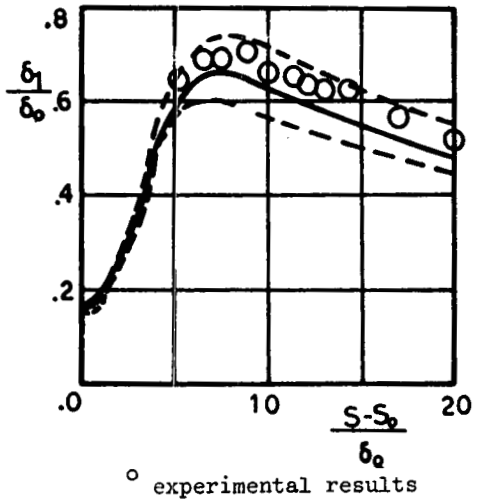

° experimental results

--- calculation results of Edwards Carter, Hafez for different models of turbulence

—— Present calculation results

Comparison between the present calculation and others

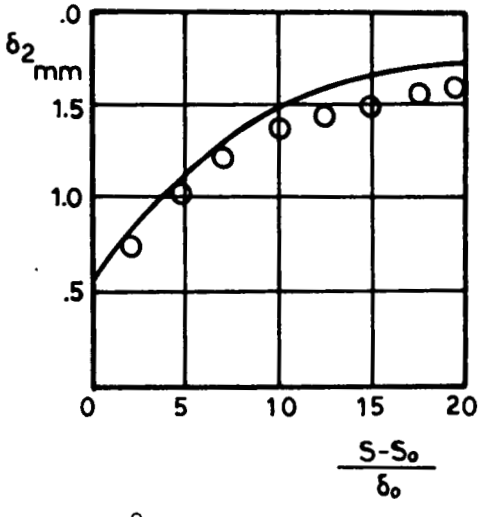

° Experimental results

--- Calculation results

Comparison between present calculation and experimental results
Experiment of KOOI

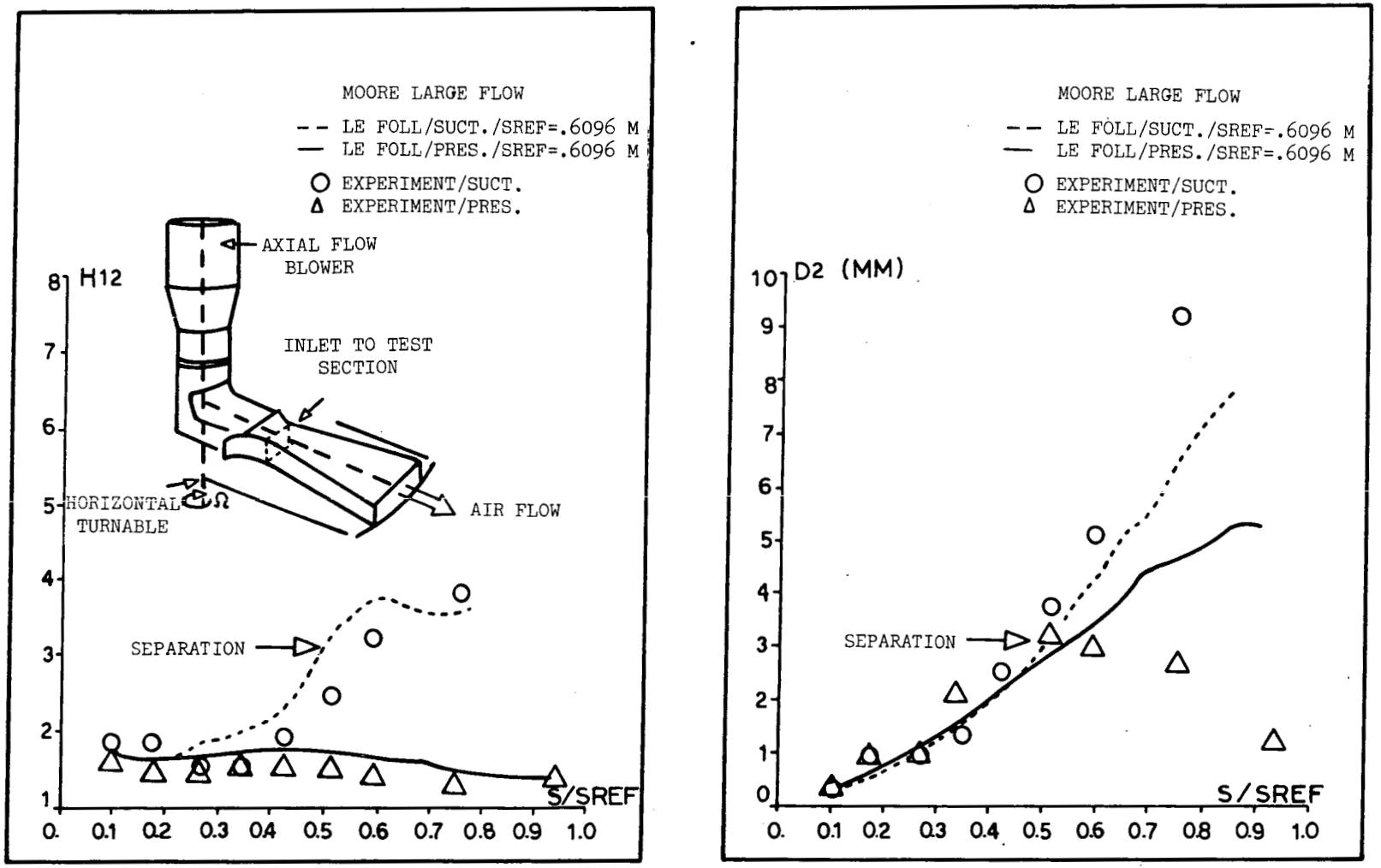

FIG. 3 Comparison of theory and Moore's Experiment.
Separated flow and Coriolis effects on turbulence.

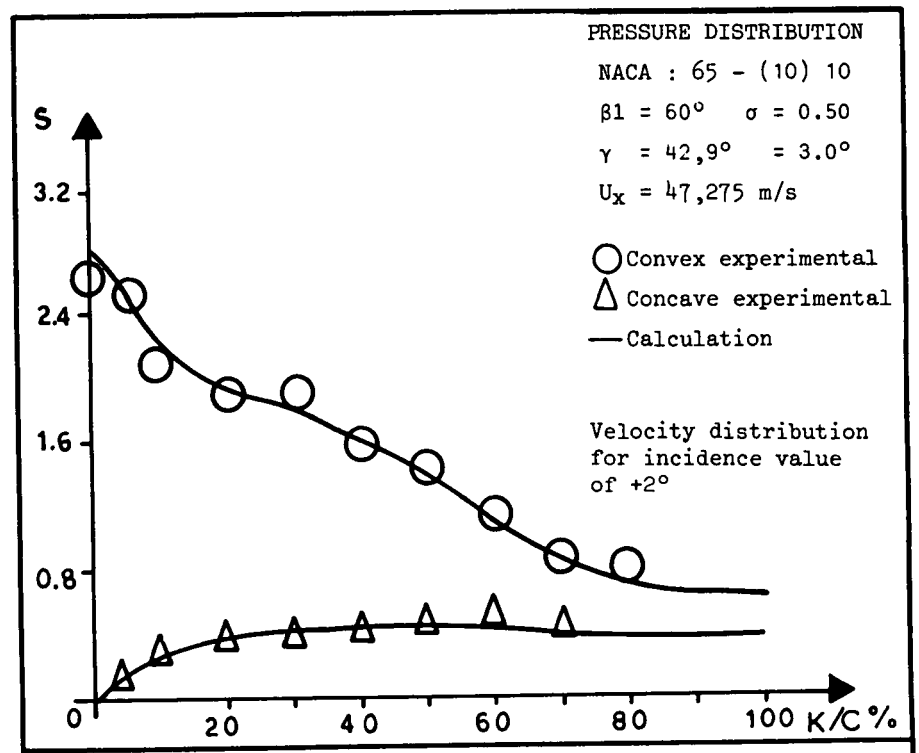

FIG. 4 Comparison of theory and Experiment. Cascade flow.

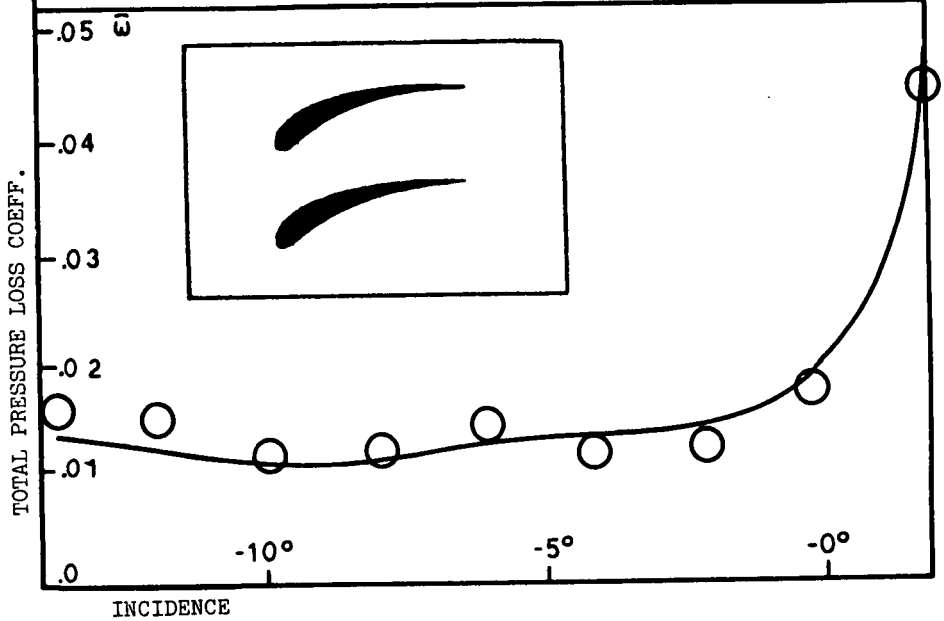

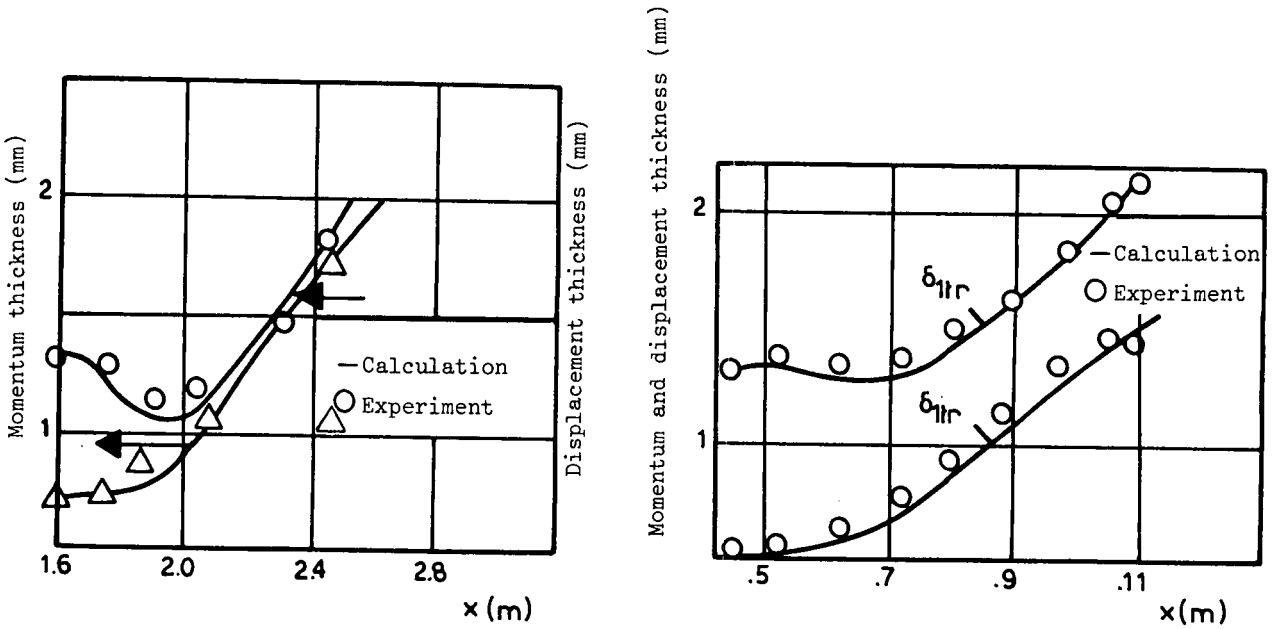

Displacement and momentum thicknesses.

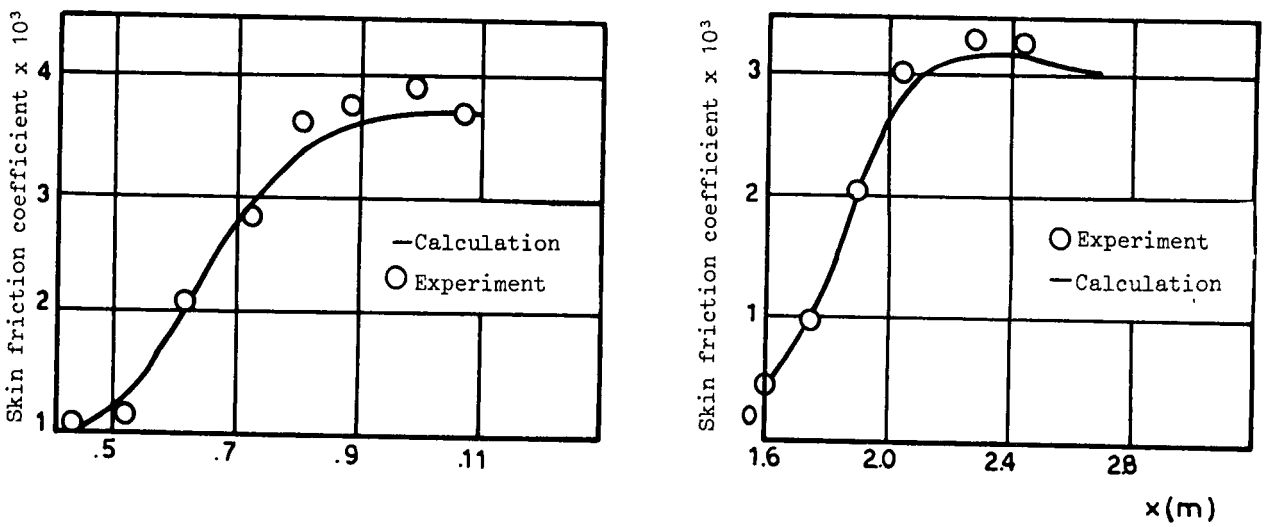

Skin friction coefficient

FIG. 5 Comparison between calculation and experimental results for two transitional boundary layers.

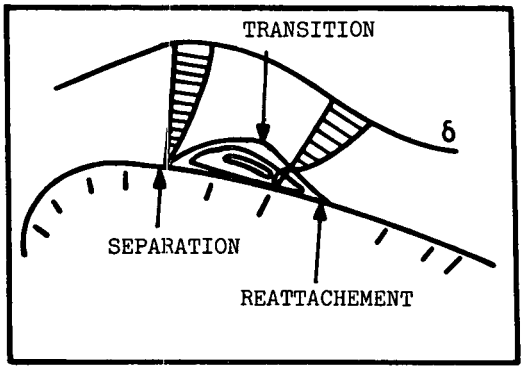

Schematic description of the flow region of a laminar separation dubble

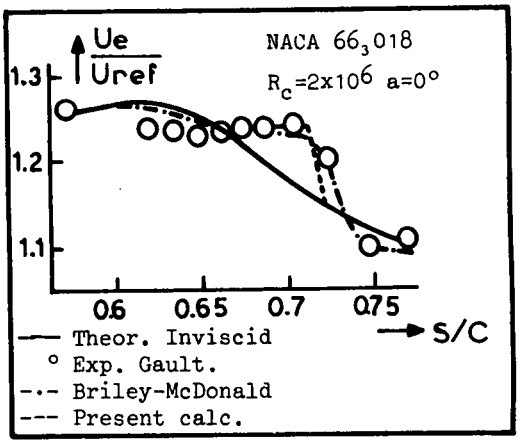

Comparison between theoretical calculation and experiment results. Gault´s experimental data.

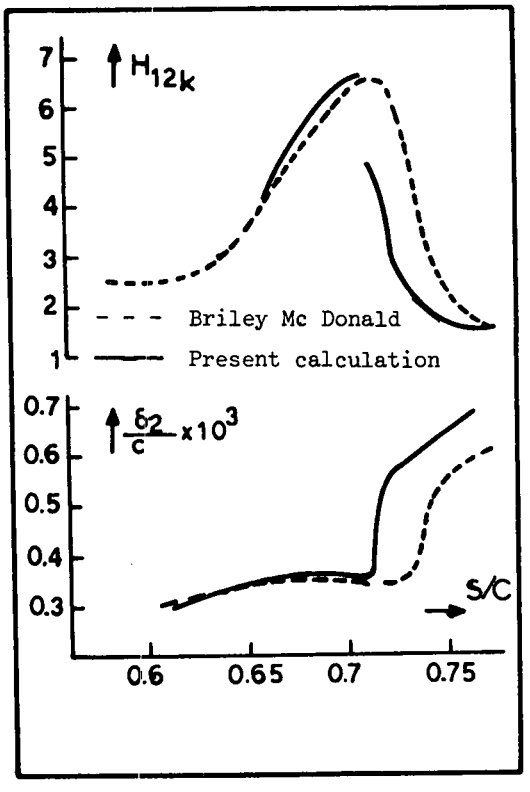

Comparison between theoretical calculations for the various boundary layer quantities. Gault´s experimental data.

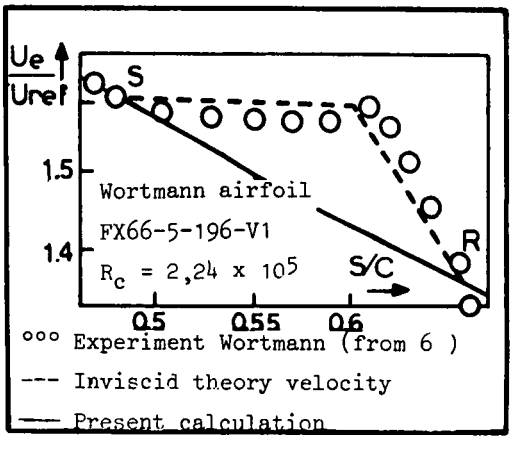

Comparison between theoretical calculations and experimental results. Wordmann´s experimental data-Case2.

FIG. 6 Comparison between calculation and experiment for transitional flow.

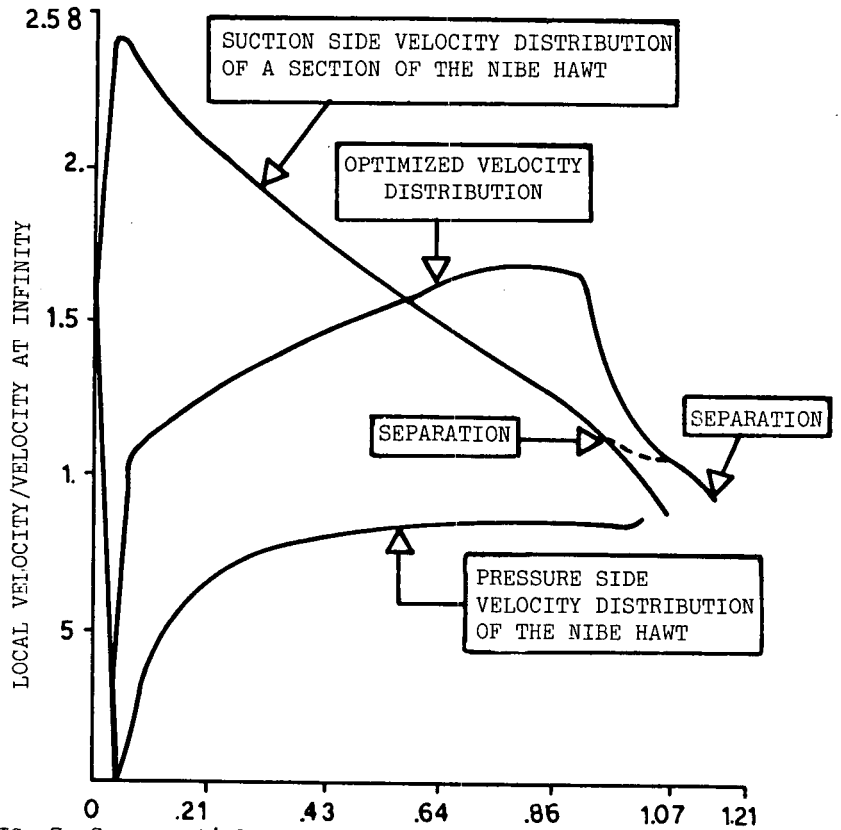

FIG. 7 Some partial results from applying the optimization procedure to the design of a HAWT (NIBE B) blade section. Comparison of the two suction side velocity distributions (actual and optimized), which give the same contribution to the blade circulation, reviels that losses may be divided by a factor of four.

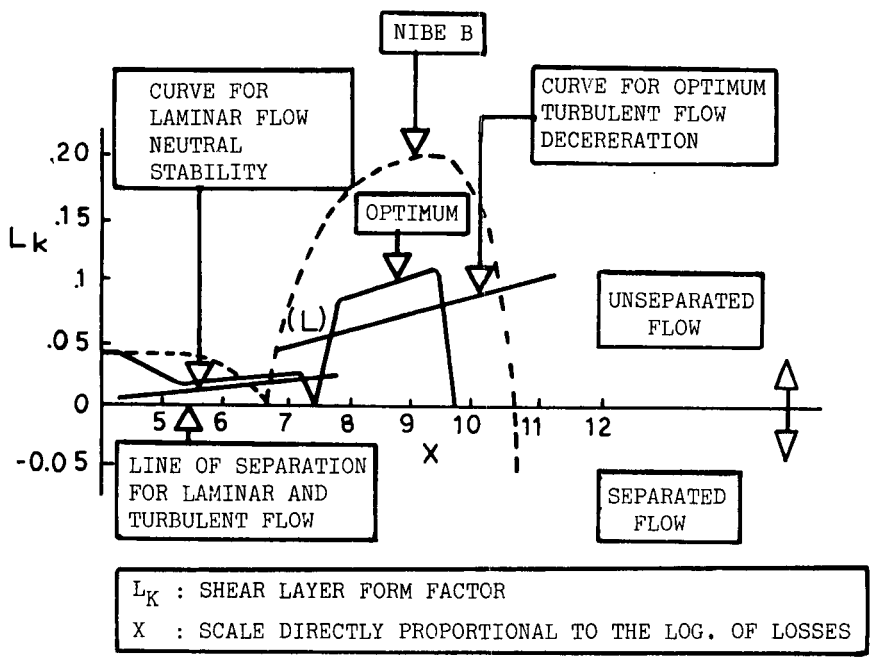

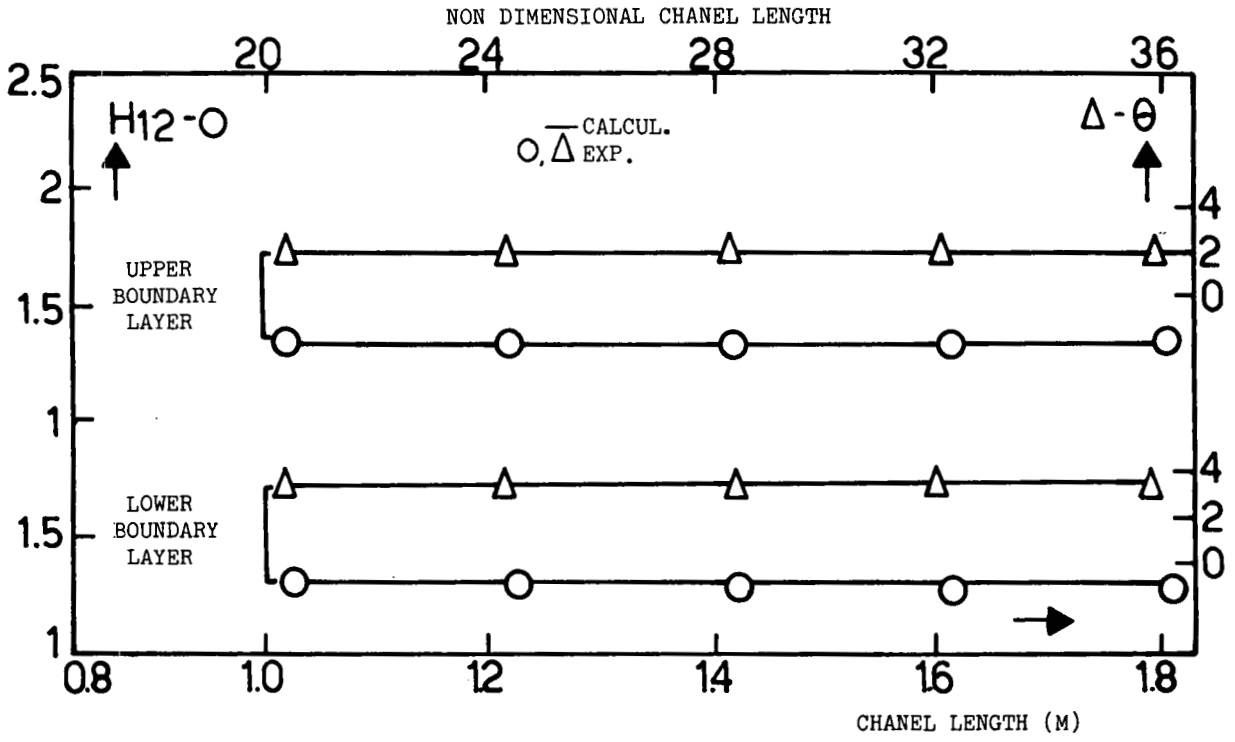

Comparison between calculation of integral quantities and experimental results.

FIG. 8 Comparison between calculation ans experiment. Fully developed channel flow.

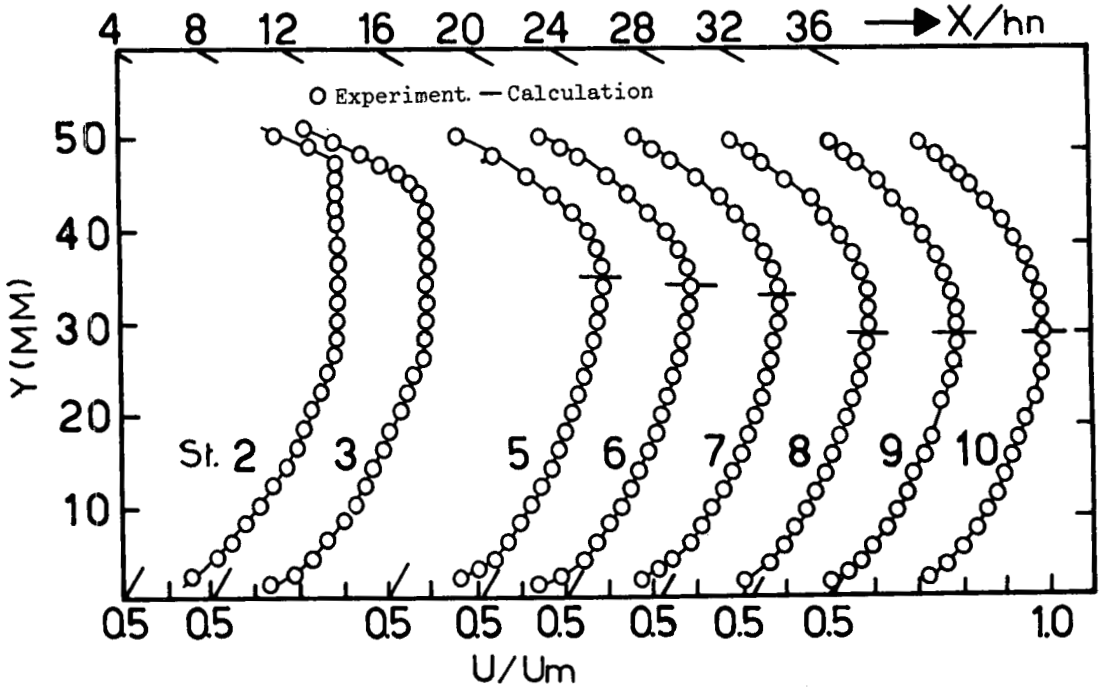

Experimental and calculated mean velocity profiles at various measuring stations.

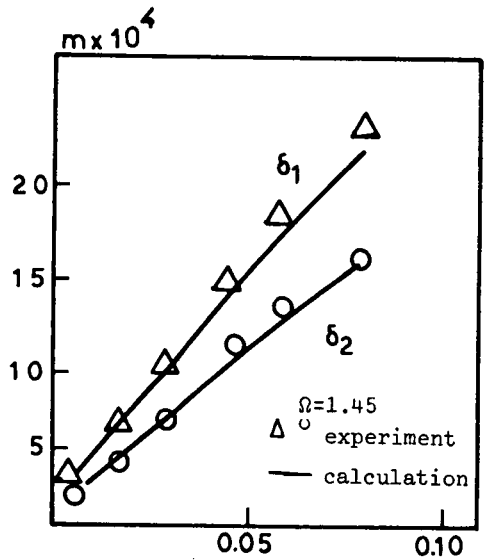

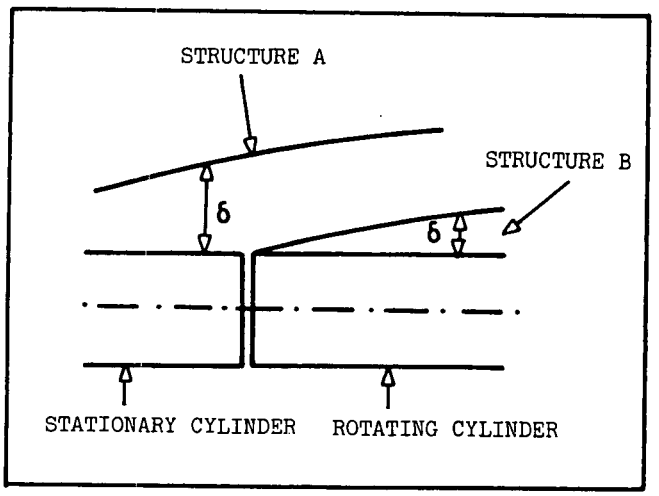

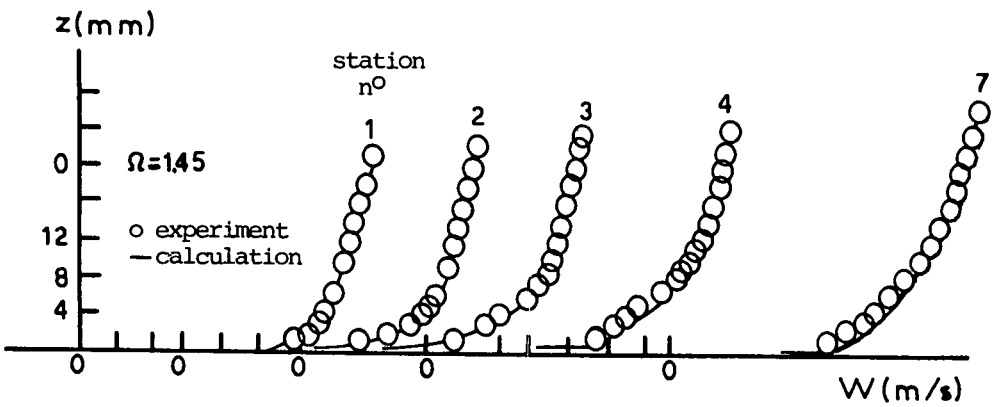

Velocity distribution in relative coordinates along the rotating part of the cylinder.

FIG. 9 Comparison between calculation and the experiment of Lohmann. Stationnary cylinder followed by a rotating part.

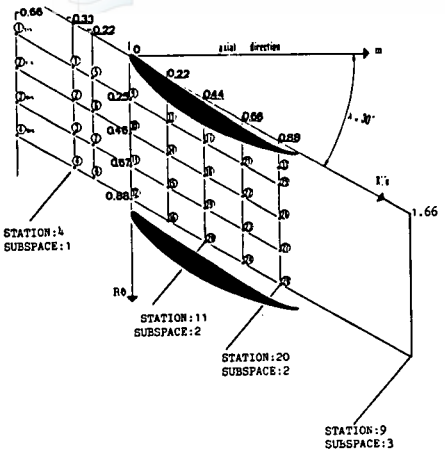

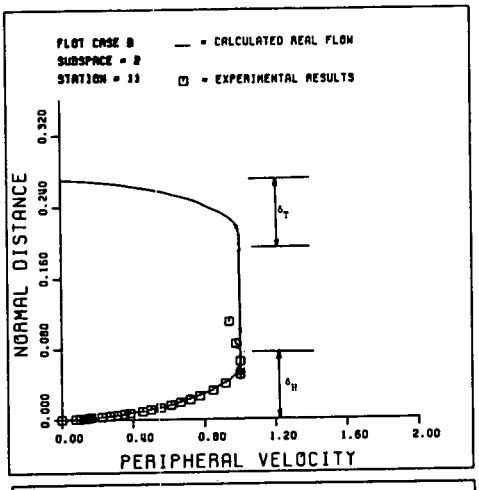

STATION:11
SUBSPACE:2

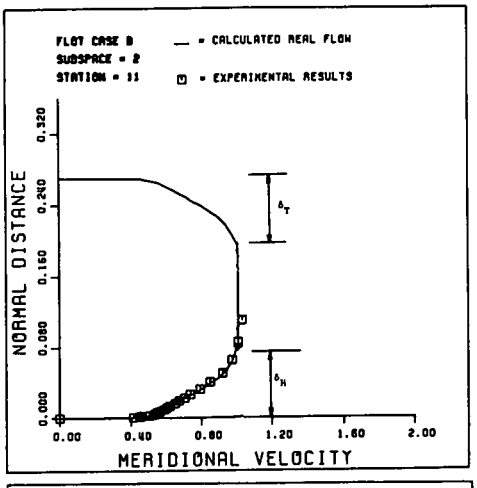

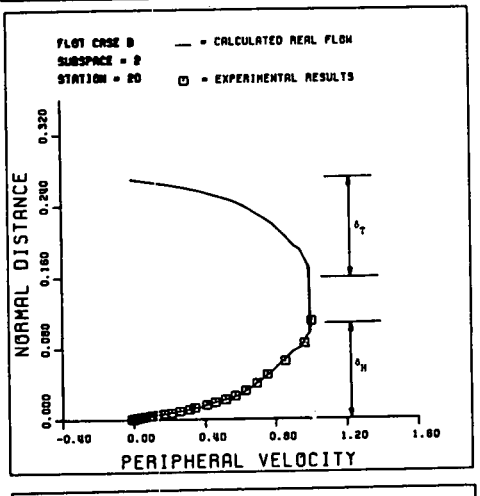

STATION:20
SUBSPACE:2

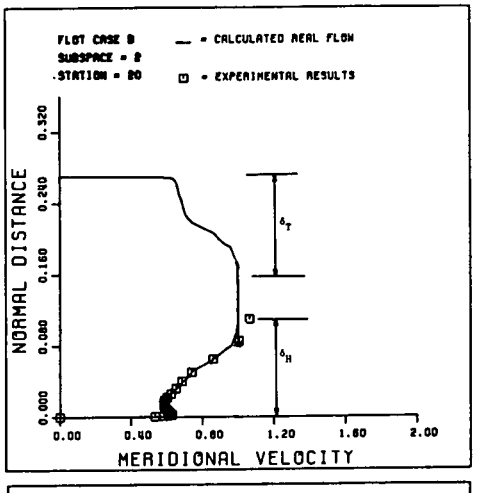

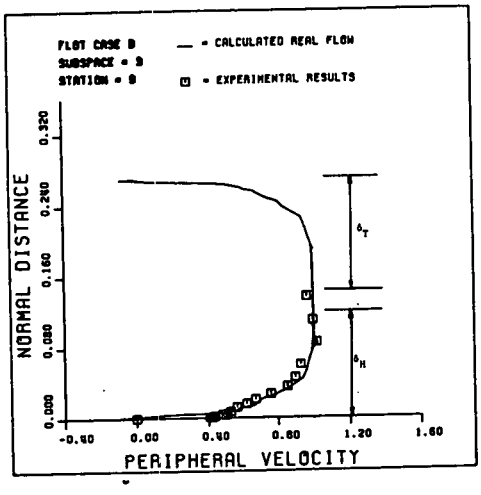

STATION:9
SUBSPACE:3

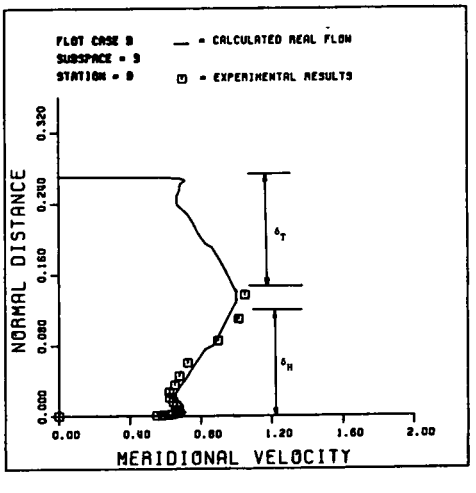

FIGURE 10 Comparison between theory and experiment. Peripherally averaged secondary flow through a highly loaded compressor cascade (Experimental results of Flot-Case B).

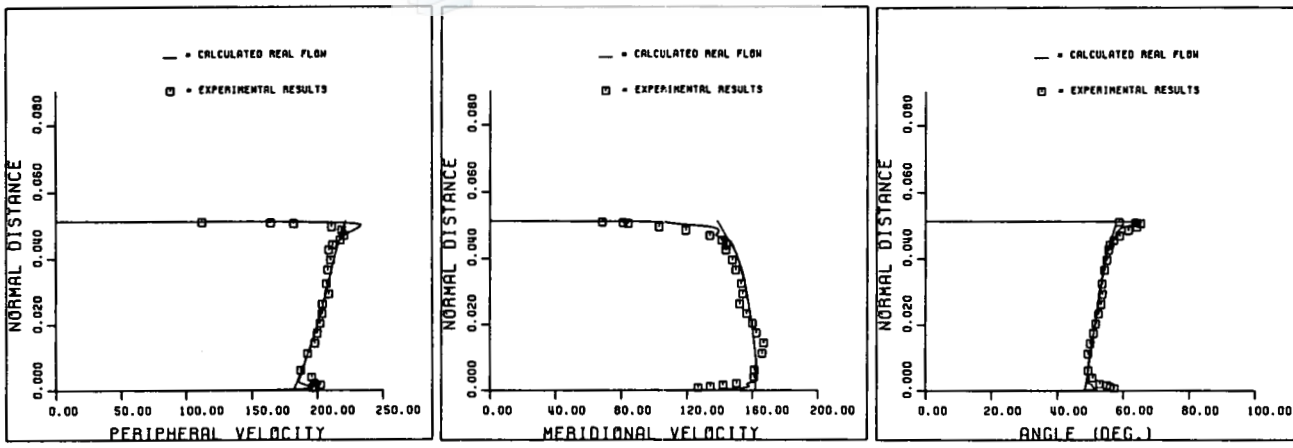

a) Rotor exit (Station 2)

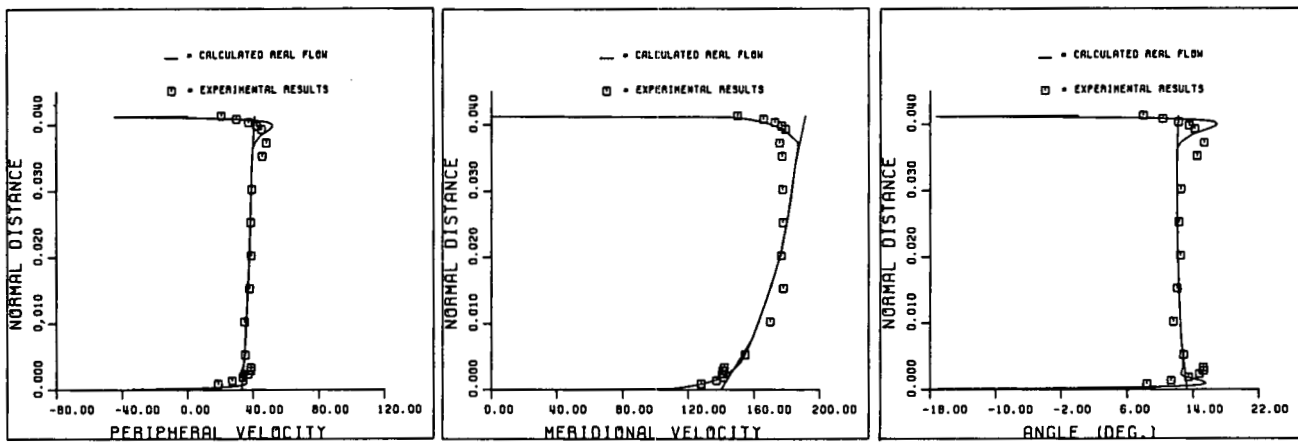

b) Stator exit (Station 3)

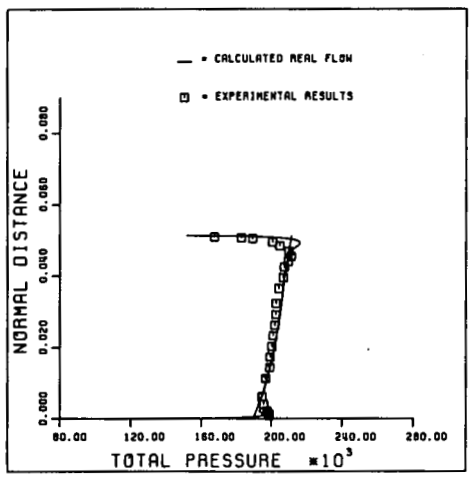

c) Rotor exit (Station 2)

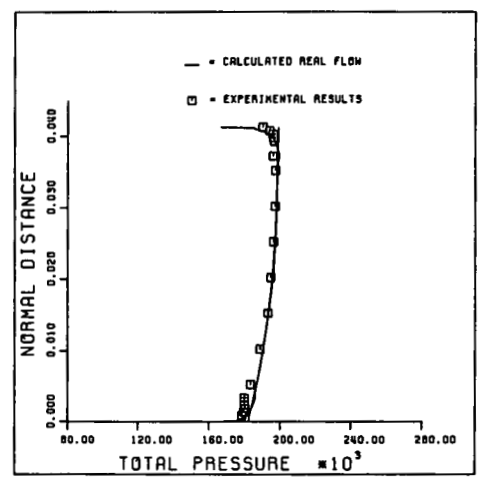

d) Stator exit (Station 3)

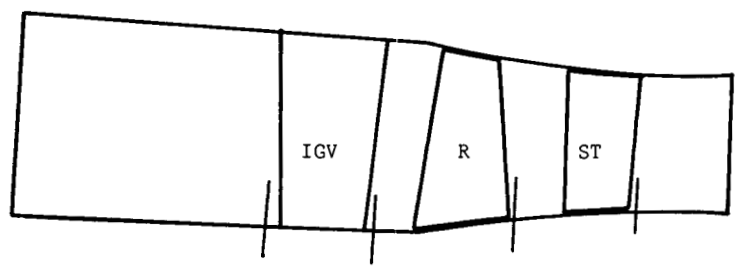

FIGURE 11 Comparison between theory and experiment. Circumferentially averaged secondary flow through a transonic single stage compressor.

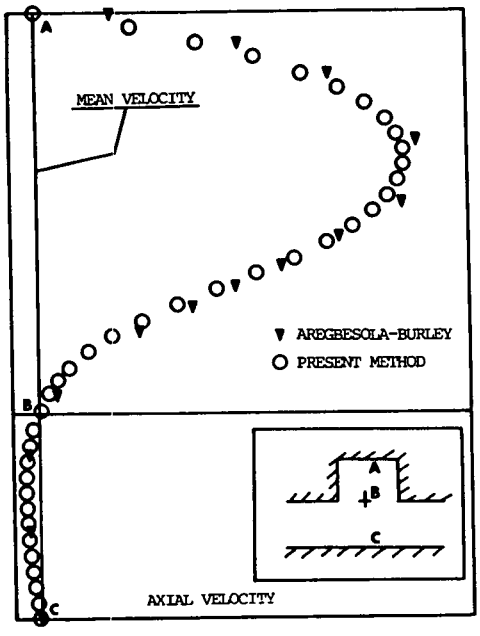

(a) velocity profile in the plane groove

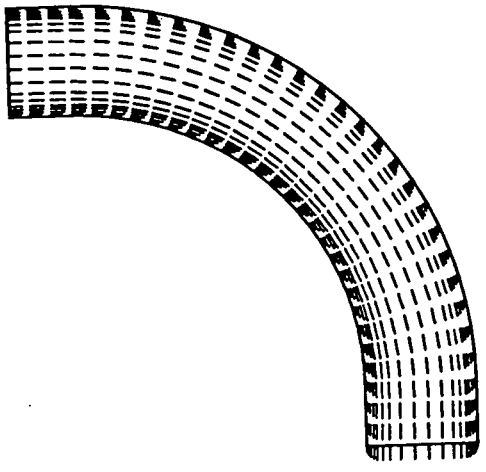

(b) the plane elbow duct

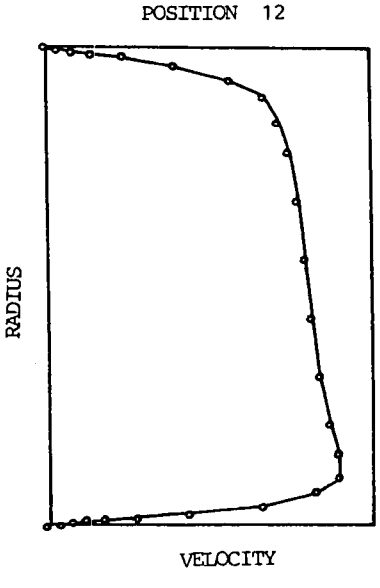

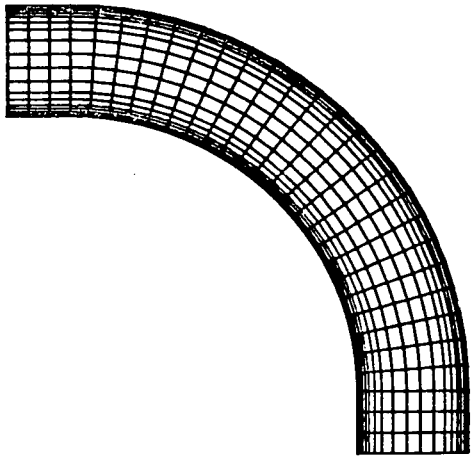

FIGURE 12 Application of the incompressible Navier-Stokes solver to the solution of flow problems (a) in a plane groove, Re 50 and (b) in a plane elbow with constant cross-section.

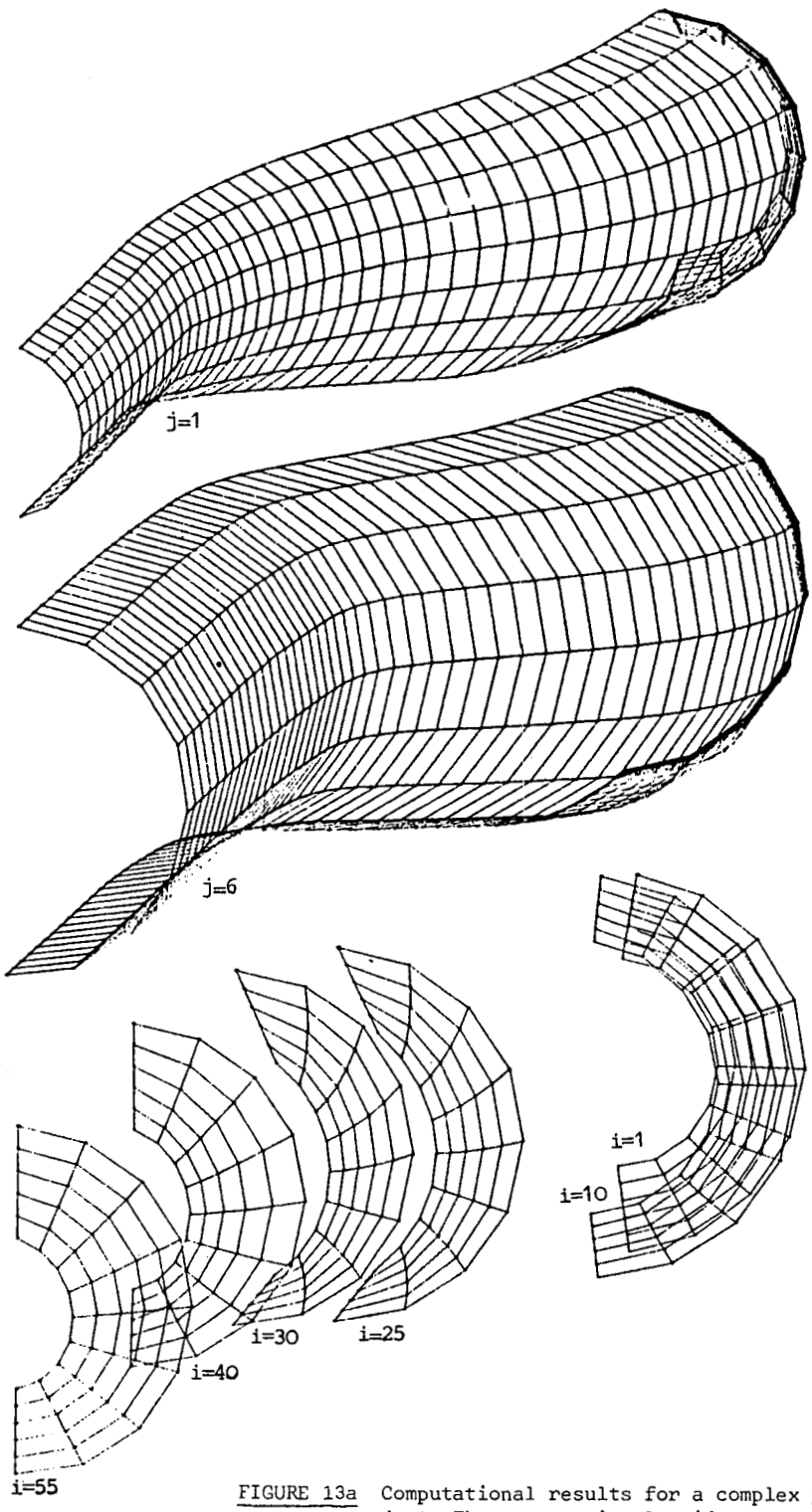

FIGURE 13a Computational results for a complex geometry duct. The computational grid.

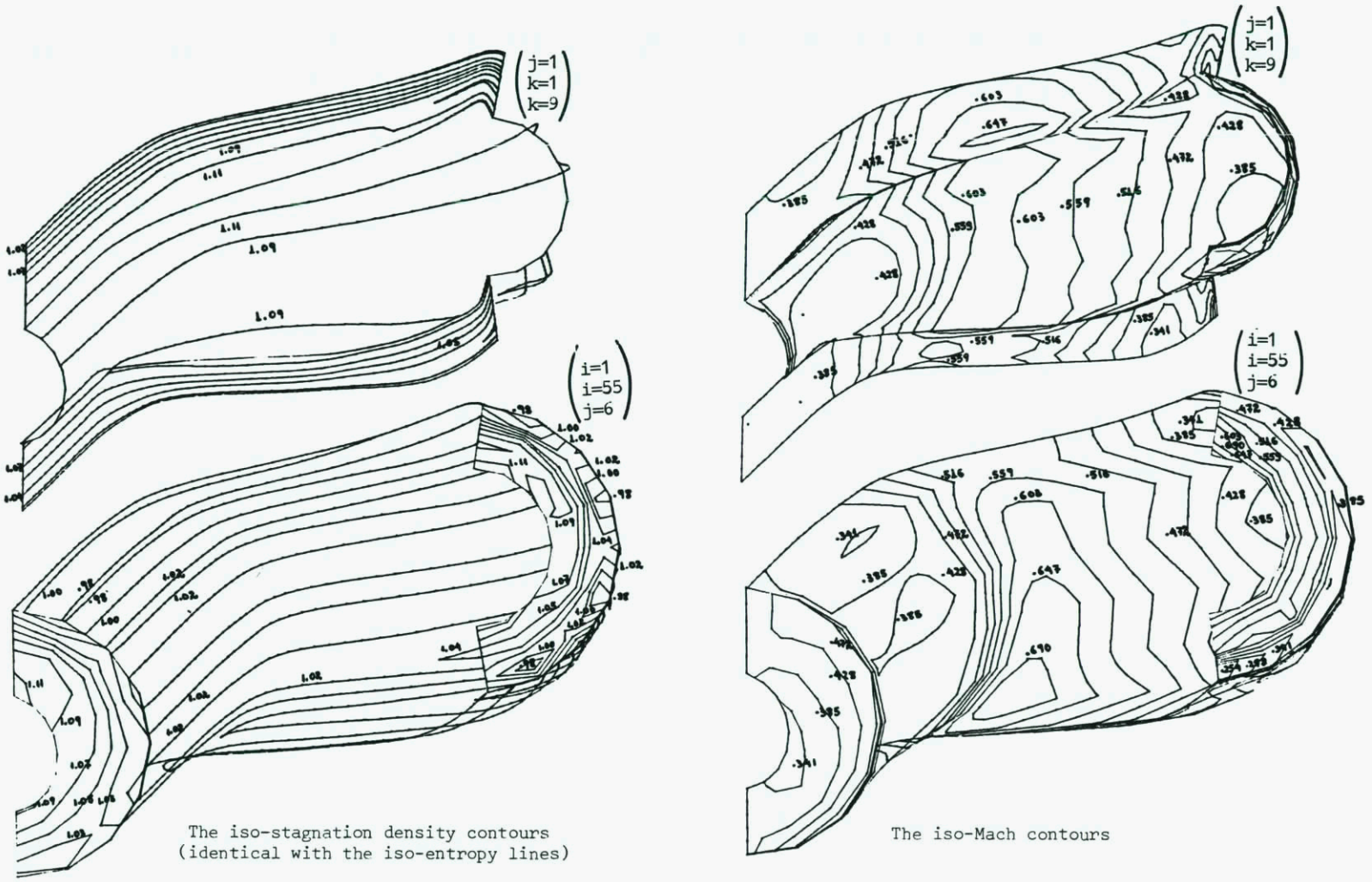

FIGURE 13b Computational results for a complex geometry duct. The iso-Mach contours and the iso-stagnation density contours, which are identical with the iso-entropy ones.

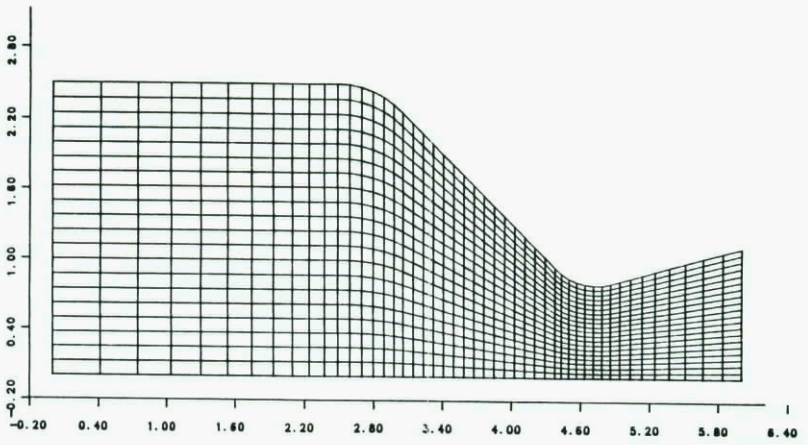

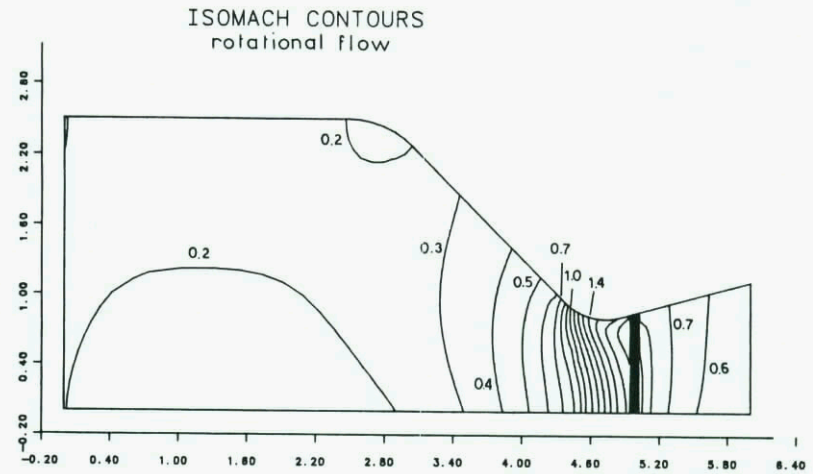

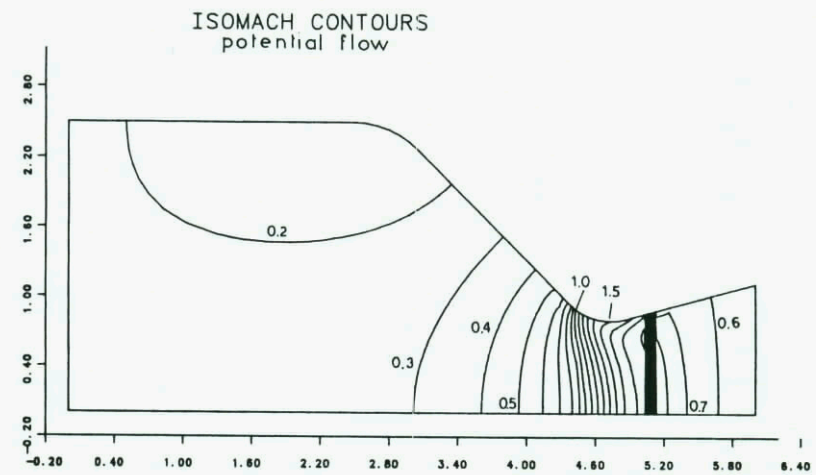

FIGURE 14 Calculation results for the JPL Nozzle

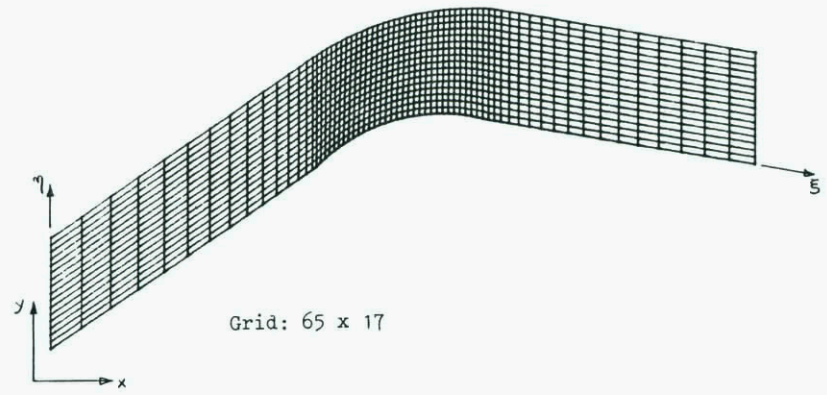

Grid: 65 x 17

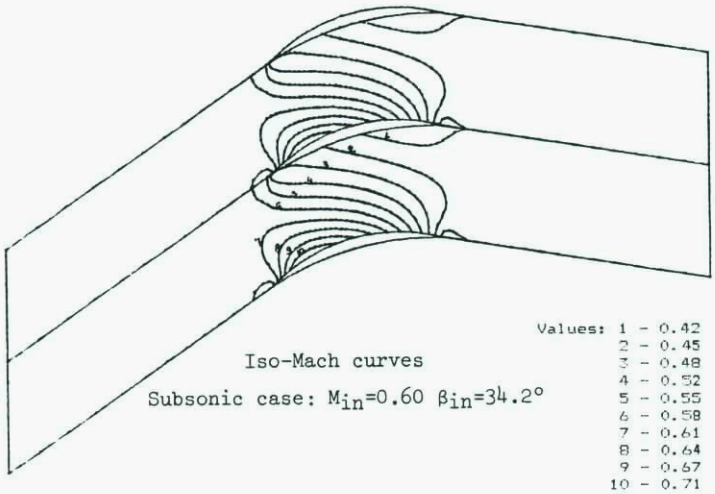

Iso-Mach curves

Subsonic case: M_{in}=0.60 β_{in}=34.2°

Values: 1 - 0.42
2 - 0.45
3 - 0.48
4 - 0.52
5 - 0.55
6 - 0.58
7 - 0.61
8 - 0.64
9 - 0.67
10 - 0.71

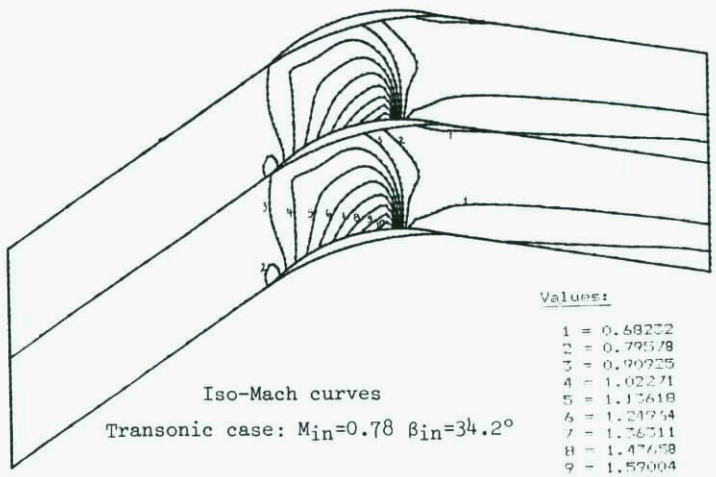

Iso-Mach curves

Transonic case: M_{in}=0.78 β_{in}=34.2°

Values:

1 = 0.68232
2 = 0.79578
3 = 0.90925
4 = 1.02271
5 = 1.13618
6 = 1.24964
7 = 1.36311
8 = 1.47658
9 = 1.59004
10 = 1.70351

Figure 15a. Non-viscous calculation results
DCA Cascade

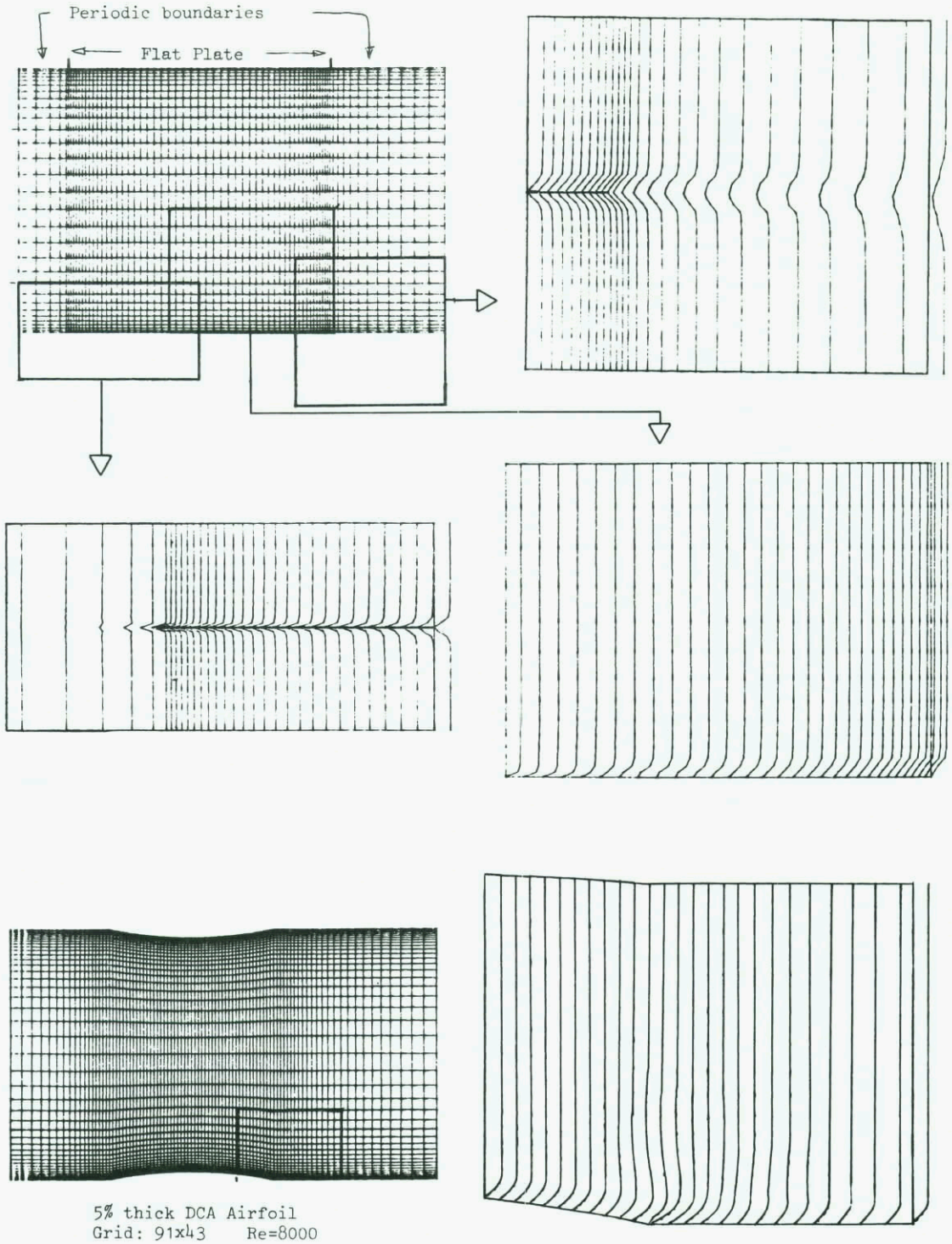

Figure 15 b. Viscous laminar flow calculation results

Velocity profiles

STATE OF THE ART OF AIRCRAFT DRAG PREDICTION IN ITALY BY MEANS OF THEORETICAL METHODS

G. Bucciantini, and M. Borsi
AERITALIA - Società Aerospaziale Italiana
Combat Aircraft Group
10146 Torino, Corso Marche 41 - ITALY

SUMMARY

The state-of-the-art in Italy on the aerodynamic drag prediction, based on theoretical methods, is presented and discussed.

A brief description of the methods used is given, with examples of application for typical aircraft configurations.

A survey of critical areas is provided, together with present research activities to improve the drag prediction capabilities and accuracy.

1. INTRODUCTION

Drag estimations of an aircraft configuration are needed during the whole design cycle to evaluate the current performance level and identify critical areas open to aerodynamic design improvements.

Typical industry goals, such as costs reduction and time savings in defining new configurations, have dramatically increased the demand of methods able to predict accurately the aerodynamic characteristics, including drag, of very complex 3D configurations even at an early design phase.

To give an answer to this problem great effort has been put in research and development of accurate and reliable numerical methods.
On the other hand the introduction of high speed, large storage computers, together with CAD systems, allow to define, and quickly analyze, highly detailed geometries whenever during the project life.

In fact existing theoretical tools are able to predict accurately the lift characteristics for a wide range of configuration layouts, while obtaining the same accuracy in total drag computation is a formidable task that cannot yet be completely carried out by current state-of-the-art CFD methods.

However CFD models are currently employed during the evolution of the project for drag estimations and local flow characteristics assessment to pursue the optimum design.

2. COMPUTATIONAL TOOLS

Various numerical methods are currently used to calculate subsonic, transonic and supersonic flows around aircraft configurations. In many cases the inviscid calculations are followed by a boundary layer analysis to get informations about flow separation and friction drag. In some cases a weak viscous-inviscid coupling procedure is also included to enhance the level of accuracy of predicted aerodynamic data. By using these methodologies, lift-induced drag, pressure drag and friction drag can be computed for attached or slightly separated flows.

The subsonic flow analysis is presently based on various versions of 3D panel methods. References (1) to (9) provide the basis of both low and high order approach that have been implemented in Italy. By these methods only the induced drag can be predicted with an acceptable level of accuracy. In the case of Low Order Panel Method a viscous-inviscid procedure has been introduced allowing the estimation of viscous effects on lift and drag. The adopted method is based on the "transpiration technique" approach, i.e. the viscous displacement thickness is transported into the inviscid solution by replacing the usual flow-tangency boundary condition by a non-zero-velocity-normal-to-the-surface one. The transpiration velocities are computed from boundary layer quantities in attached flow regions while linear extrapolation is performed beyond separation. The whole procedure has been applied to realistic 3D configurations obtaining encouraging results as shown in the following chapter.

The viscous flow, up to the separation, is computed by 3D Boundary Layer codes. One of these is the finite differences, 3D viscous code of J.P.E. Lindhout, E. De Boer, B. Van Den Berg (10-12), that has been updated by introducing a general mesh generation system and an interface with inviscid solvers. Moreover both surface Cf integration to estimate friction drag, and the computation of the transpiration velocities from boundary layer data to allow the coupling with inviscid methods, have been added.
Reference (13) to (21) provide the basis of the followed approach. The code has been successfully applied to attached subsonic and transonic flows giving interesting results.

Transonic aerodynamic design requires the evaluation of the wave drag besides the induced and friction drag. Varous codes, based both on full potential equations and Euler equations, are currently employed to investigate the transonic regime. One of the widely used is XFL022AIT (22, 23). The program is based both on the XFL022 program, developed at NLR from the Jameson's FL022 (24) code, and the afore-mentioned Subsonic Panel Method. The code is able to handle wing alone configurations with the inclusion of body effects by means of non-zero crossflow velocity in the symmetry plane.

A viscous flow analysis, usually based on 3D boundary layer codes such as the one described above, can be successively performed to identify possible flow separations and evaluate the friction drag. In this case the inviscid solution is not actively coupled with the boundary layer solution, so the viscous effects on both induced drag and wave drag are not modeled, but an empirical correction, based on 2D calculations, is applied to the wave drag.

Other full potential codes, such as the Eberle Wing Alone, Finite Volume Method (25) for transonic flows, have been used in the past during the design cycle, to evaluate the wing pressure distribution and, by means of 2D boundary layers, the flow separation. The main advantage of such an approach with respect to Finite Differences is the ability to work on non-orthogonal meshes that, in principle, allows the calculation of flow fields with complex solid boundaries. A straight consequence of this is the ability to compute thin delta wings with sharp and cranked leading edge naturally within the potential flow theory.

The standard full potential models show their limitations when the entropy generation, associated with shock computation, becomes important. In this case the rotational Euler equations model has proven to be more realistic and accurate and has demonstrated the ability to capture the generated vorticity without any special modeling.

The experiences made in Italy by developing and using Euler codes have shown that an improvement in wave and lift induced drag computation can be effectively achieved, but some topics, as for example the sensitivity to mesh size and topology, need further investigation. In view of this an intensive research is presently in progress to improve solution quality and robustness and reduce computation costs and geometric limitations.

Two similar approaches, based on finite volume techniques, and a third one based on the finite element method, are pursued. The finite volume solvers take FL057 (26) as starting point, but one version has multiblock structure, multistage (4th order) Runge-Kutta time stepping scheme, complete configuration capabilities, while the other version is single-block, 3-stage Runge-Kutta type in time integration (Rizzi scheme (27-30)), wing alone code. Both of them have 2nd and 4th order artificial dissipative models.

The finite element scheme is explicit, conservative and take into account the characteristic directions of the problem. For one-dimensional flows, it is equivalent to Van Leer's Q-scheme (31-32). The numerical viscosity introduced by the scheme is controlled by the characteristics speed. This dissipative effect is built up by using an algebraic procedure introduced by Roe (33) which has the computational advantage of perfectly resolving stationary discontinuities. The extention to multidimensional problems is performed on finite element unstructured triangulation (tetrahedrization in 3D) using a finite volume formulation (34-35). The scheme has been found very robust at all Mach numbers, first-order accurate and free of any viscosity parameter to be tuned.

The participation to EAP and EFA programs has led the Italian Industries to deal with supersonic design problems. The Italian version of the low order subsonic/supersonic panel method NLRAERO (9) has been used to carry out the aerodynamic analysis. Preliminary body plus interference wave drag data were computed by means of the Transfer Rule method (36); DATCOM formulas supplied an estimate of skin friction drag.

A higher order 3D subsonic/supersonic Panel Method has been recently implemented at starting from an MBB pilot code and it is expected to be the future standard in linearized supersonic calculations.

Finally it must be mentioned that 3D analyses are generally integrated by 2D ones in case of more complicated aerodynamic problems. Typical examples are transonic maneuver configurations studies, preliminary high-lift systems design, low speed CLmax predictions, buffet analyses, airfoil design, etc.. In these cases drag evaluation is not the main goal, but the computed aerodynamic characteristics serve as a guideline for design changes proposals needed to meet the required performance levels.

References (37) to (41) provide some indications about available 2D numerical methods.

3. EXAMPLES AND APPLICATIONS

The analysis of a 3D configuration, representative of a combat aircraft in subsonic and transonic flow by using potential methods and boundary layer investigations, has been chosen as an example of CFD drag prediction techniques.

As a first step a subcritical analysis has been done by using the subsonic Panel Method with the weak viscous-inviscid coupling procedure briefly described in the previous chapter 2.

The surface of the wing-body-pylons configuration was described by about 1700 flat panels as shown in fig. 1. The complete velocity distribution was computed by the Panel Method and then transferred to the boundary layer code by means of a proper interface. Inviscid lift and induced drag coefficients are shown in figs. 2, 3 compared with experimental data. As a consequence of lift overestimation, an error in induced drag is also exhibited. Figs. 4-7 show the comparison in terms of sectional pressure distributions and an overview of pressure levels on the configuration.

The 3D boundary layer survey was performed on aircraft components, starting from the nose of the aircraft and continuing on the next surface by properly transferring the computed quantities. A summary of collected data, in terms of displacement thickness distribution and surface streamlines, is presented in figs. 8-11. As a result of this analysis a transpiration velocity distribution on the configuration was generated and returned to the Panel Method and a new inviscid calculation with modified boundary conditions was performed.

By this way viscous effects were included in pressure computation and finally resulted in lift and induced drag as shown in fig. 12. The friction drag was also included to obtain the total drag evaluation as shown in fig. 13.

The second step in aerodynamic analysis was a transonic calculation performed by means of XFL022AIT method. In this case the configuration was simplified, by removing the pylons, to meet the geometric restrictions of the full potential solver. The cross-flow velocity distribution in a plane near the body was computed by the Panel Method and fitted into the XFL022 system. The results were completed by a 3D boundary layer investigation.

In figs. 14, 15 the comparison in terms of measured and computed pressures for two incidences is presented. A good agreement is shown on the upper surface while a velocity underestimation is visible on the lower one. The influence of the body seems to be also correctly simulated. It must be noted that in the first case the flow is attached and in the second one it exhibits a separation bubble on sections toward the tip.

A comparison in terms of forces and moments is also shown in figs. 16-18. Fuselage plug wing root contributions were obtained by the Panel Method and have been included in lift and pitching moment, while drag coefficient includes also the friction term. The agreement between numerical predictions and measured quantities is good up to flow separation.

In figs. 19-20 the qualitative comparison between computed wall streamlines and oil flow visualizations for two incidences is presented. The agreement is satisfactory in both cases. The shock position is correctly computed in the attached region even at the higher critical incidence, while at separation it is overestimated due to the lack of viscous-inviscid interaction.

Figure 21 shows the flow evolution locally around the critical incidence. The computed isobars at the separation have been plotted for three incidences showing that a shock induced separation occours in the tip region as confirmed by experimental oil flow.

4. CRITICAL AREAS AND FUTURE ACTIVITIES

In previous chapters it was shown which methods are currently used in Italy to evaluate the aerodynamic drag and which level of accuracy can be obtained with them.

There are some problems, such as for instance the drag estimation of afterbody-jet configurations, that are treated only by statistical correlation methods or by direct scaling techniques. Other limitations in CFD drag prediction come from the presence of large separated regions. In these cases the complexity of both the flow physics and the configuration geometry and the lack of appropriate numerical models prevents reliable CFD applications. On the other hand this class of problems should be addressed by the solution of 3D, Navier-Stokes equations subject of future developments.

It has been emphasized the effort presently put in hand to improve Euler codes, but it must be pointed out that major attention is presently focused on computational aspects rather than on engineering applications.

Last but not least some considerations on computer hardware and software. Increasing in mathematical models complexity and size of problems require the availability of suitable hardware together with a strong effort from the codes developers to produce good software, easy to be used, integrated within the design environment, possibly free from tuning parameters.

Failure to meet these requirements will result in limited application of that method for industrial purposes.

Since pure theoretical drag computation seems, at present, unrealistic, an improvement in current capabilities must be pursued.

Possible areas for future improvements should include:

- development of methods able to deal with separated flows,
- drag prediction procedure, including friction terms, in supersonic flow,

- development of models for jet-aircraft interaction,
- identification of CFD validation procedures to assess the accuracy level of the prediction,
- intensive application of available methods to realistic configurations in transonic and supersonic flows.

Many of these activities are in progress in Italian Aerospace Industries together with research on Euler and Navier-Stokes equations to pursue an effective advance in design applications of CFD methods.

5. CONCLUSIONS

Theoretical drag estimation, even with the difficulties and limitations presented in the paper, is an ordinary activity in the whole design cycle of an aerospace product, expecially in the early phases of the projects, and the aeronautical engineer must continuously answer specific and general drag questions at the best level of accuracy.

The present capabilities in terms of computer hardware and software provide reliable CFD drag estimations for a certain class of problems. For the applications where the available CFD methods are not able to provide reliable results, a great effort is in hand at the Universities, the Aerospace Industries and Research Centers, to improve the physics modelization and the capabilities of computer codes.

6. REFERENCES

1. Kraus, W.: "Panel Methods in Aerodynamics", VKI Lecture Series 87 on "Computational Fluid Dynamics", March, 1976, Rhode-Saint-Genese, Belgium.

2. Fornasier, L.: "HISSS - A Higher-Order Subsonic/Supersonic Method for Calculating Linearized Potential Flow", AIAA Paper No. 84-1646, June 1984.

3. Fornasier, L.: "Linearized Potential Flow Analysis of Complex Aircraft Configurations by HISSS, a Higher-Order Panel Method", AIAA Paper No. 85-0281, January 1985.

4. Bertolone, G. and Fornasier, L.: "Subsonic Military Aircraft Engine Intake: an Integrated Theoretical-Experimental Design" - Agard CP 301.

5. Fornasier, L.: "Wing Design Process by Inverse Potential Flow Computer Programs" - Agard CP 280.

6. Magnus, A.E., Ehlers, F.E., and Epton, M.A.: "Pan Air - A Computer Program for Predicting Subsonic or Supersonic Linear Potential Flow About Arbitrary Configurations Using a Higher-Order Panel Method", NASA CR-3251, Parts 1 and 2, April 1980.

7. Woodward, F.A.: "An Improved Method for the Aerodynamic Analysis of Wing-Body-Tail Configurations in Subsonic and Supersonic Flow - Part I, II", NASA CR-2228, May 1973.

8. Woodward, F.A.: "USSAERO Computer Program Development, Versions B and C", NASA CR 3227, 1980.

9. Hoeijmakers, H.W.M.: "A Panel Method for the Determination of the Aerodynamic Characteristics of Complex Configurations in Linearized Subsonic or Supersonic Flow, Part I-III", NLR TR80124 U Part I-III, 1980.

10. Lindhout, J.P.F., Moek, G., De Boer E.: "A Method for the Calculation of 3D Boundary Layers", Trans. ASME, Vol. 103, 1981.

11. Lindhout, J.P.F., De Boer E., van den Berg, B.: "Three Dimensional Boundary Layer Calculations on Wings, starting from Fuselage", NLR MP82060U, 1982.

12. Lindhout, J.P.F., van den Berg, B., Elsenaar, A.: "Comparison of Boundary Layer Calculations for the Root Section of a Wing", NLR MP80028, 1981

13. Borsi, M. and Ceresola, N.: "Calcolo dello strato limite tridimensionale con interazione tra flussi viscosi ad una configurazione complessa", IX Congresso Naz. AIDAA, Oct. 1987.

14. Cousteix, J.: "Integral Methods and Turbulence Models Applied to Three-Dimensional Boundary Layers", Proc. IUTAM Symposium on 3D Boundary Layers. Springer Verlag, 1982.

15. Cousteix, J.: "Three Dimensional Boundary Layers. Introduction to Calculation Methods.", VKI LS 07-1986.

16. Cebeci, T.: "An Approach to Practical Aerodynamic Calculations", VKI LS 07-1986.

17. Hirschel, E.H.: "Computation of Three Dimensional Boundary Layers on Fuselages", J. Aircraft, Vol. 21, Jan. 1984.

18. Hirschel, E.H.: "Evaluation of Results of Boundary Layers Calculations with Regard to Design Aerodynamics", VKI LS 07-1986.

19. Hirschel, E.H.: "Boundary Layers Coordinates on General Wings and Bodies", ZFW, Vol. 6, 1982.

20. Mc Lean, J.D. and Randall, J.L.: "Computer Program to Calculate 3D Boundary Layer Flows", NASA CR 3123, 1979.

21. Le Balleur, J.C.: "Interactive Boundary Layer Calculations", VKI LS 07-1986.

22. J. van der Vooren, J.W. Sloof, J. Th. van der Kolk: "A System for the Numerical Simulation of Sub- and Transonic Viscous Attached Flows around Wing-Body Configurations", AIAA paper No. 82-0935, 1982.

23. Van der Kolk, J. Th.: "XFL022 Version 1.0, A System for Calculating Transonic Flow around a Wing including Body Influence. Reference Manual and System Description", NLR AT-83-002 U, 1983.

24. Jameson A., Caughey, D.A.: "Numerical Calculation of the Transonic Flow Past a Swept Wing", ERDA-C00-3077-140.

25. Eberle, A.: "Transonic Potential Flow Computations by Finite Elements: Airfoil and Wing Analysis, Airfoil Optimization", DGLR/GARTEur 6 Symposium on Transonic Configurations. Bad Harzburg, June 1978.

26. Jameson, A., Schmidt, W., and Turkel, A.: "Numerical Solution of the Euler Equations by Finite Volume Methods using Runge-Kutta Time Stepping Schemes", AIAA Paper 81-1259, June 1981.

27. Rizzi, A., and Eriksson, L.E.: "Explicit Multistage Finite Volume Procedure to solve the Euler Equations for Transonic Flow", VKI LS-04, 1983.

28. Eriksson, L.E.: "Three-Dimensional Spline-Generated Coordinate Transformations for Grids around Wing-Body Configurations", NASA CP 2166.

29. Rizzi, A. private communications.

30. Rizzi, A., and Eriksson, L.E., Schmidt, W., and Hitzel, S.: "Numerical Solution of the Euler-Equations simulating Vortex Flows around Wings", Agard CP 342, 1983.

31. Vijayasundaram, G.: "Résolution numérique des équations d'Euler pour des écoulements transoniques avec un schème de Godunov en Element Finis;" Thèse 3e cycle Paris VI, 1983.

32. Van Leer, B.: "Towards the Ultimate Conservative Difference Scheme III."; Journal of Computational Physics 23, 263-275, 1977.

33. Roe, P.L.: "Approximate Riemann Solvers, Parameter Vectors and Difference Schemes"; Journal of Computational Physics 43, 357-372, 1981.

34. Fezoui, F.: "Résolution des équations d'Euler par un schème de Van Leer en élements finis", INRIA Report 358, 1985.

35. Fezoui, F. and Stoufflet, B.: "A Class of Implicit Upwind Schemes for Euler Simulations with Unstructured Meshes", INRIA Report 517, 1986.

36. Whitcomb, R.T., Sevier, J.R.: "A Supersonic Area Rule and an Application to the Design of a Wing-Body Combination with High Lift-Drag Ratios", NASA TR R.72.

37. Bauer, F., Garabedian, P., Korn, D. and Jameson, A.: "Supercritical Wing Sections I, II, III", Berlin, Springer Verlag, Lecture Notes in Economics and Mathematical Systems, Voll. 66, 108, 150.

38. Zannetti, L., Colasurdo, G., Fornasier, L., Borsi, M.: "Numerical Computation of Transonic Flow About Two Dimensional, Two Elements Airfoils", AIT-GVC internal report T827/83060, Feb. 1983.

39. Russo, V.: "Programma bidimensionale MEFN-10. Confronto risultati con dati sperimentali", AIT-GVT internal report PAEN/80001, Jan 1980.

40. Lippolis, A. and Moretti, G.: "Shock Fitting Calculations on Airfoils and Intakes", Paper presented at the GAMM workshop on Numerical Simulations of Compressible Euler Flows-Paris, June 1986.

41. Ceresola, N.: "Development of a Numerical Code for the Solution of the Navier-Stokes Equations for 2D Steady Transonic Flows", AIT-GVC internal report T827/88103, Feb. 1988.

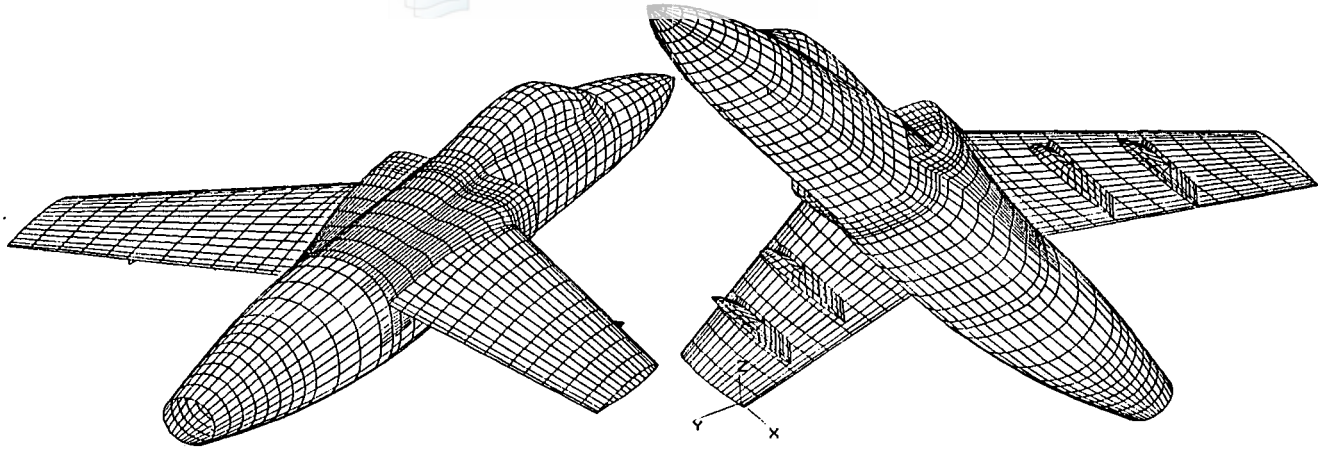

Fig. 1 - Panel Layout

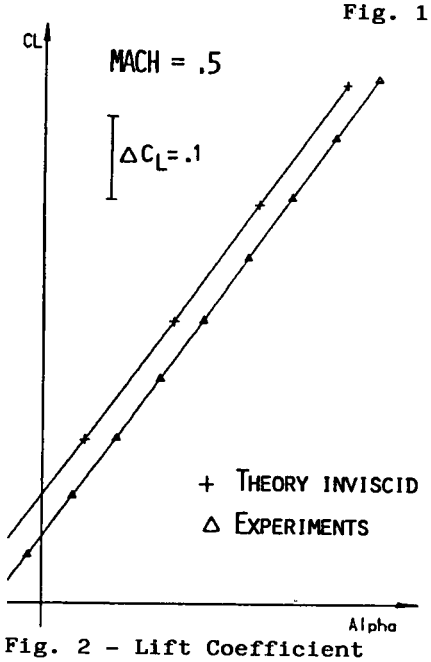

Fig. 2 - Lift Coefficient

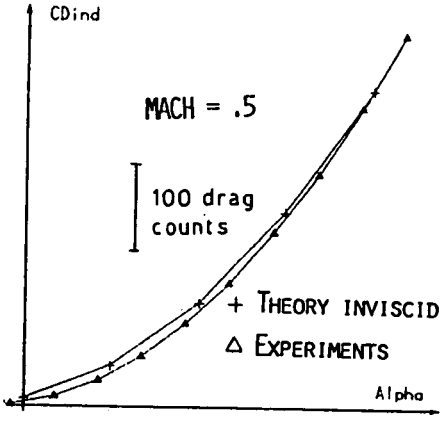

Fig. 3 - Induced Drag Coefficient

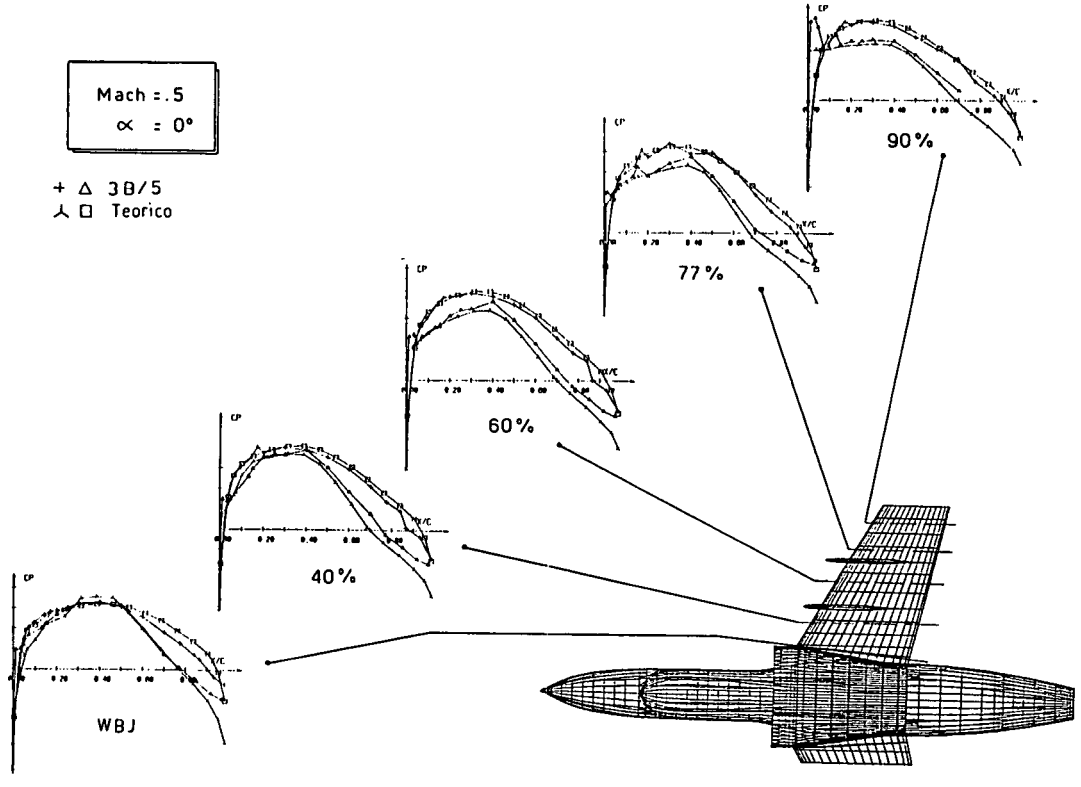

Fig. 4 - Theoretical - Experimental Pressure Distributions

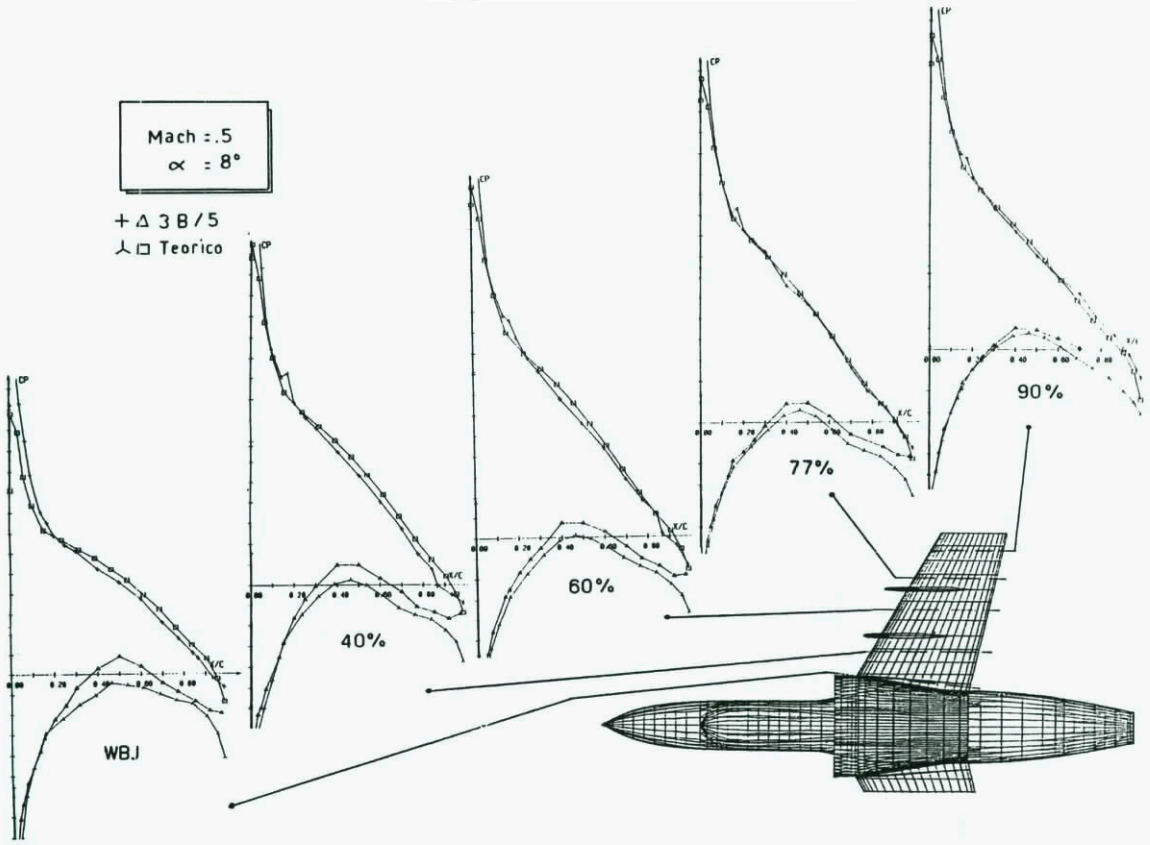

Fig. 5 - Theoretical-Experimental Pressure Distributions
$\alpha = 8°$

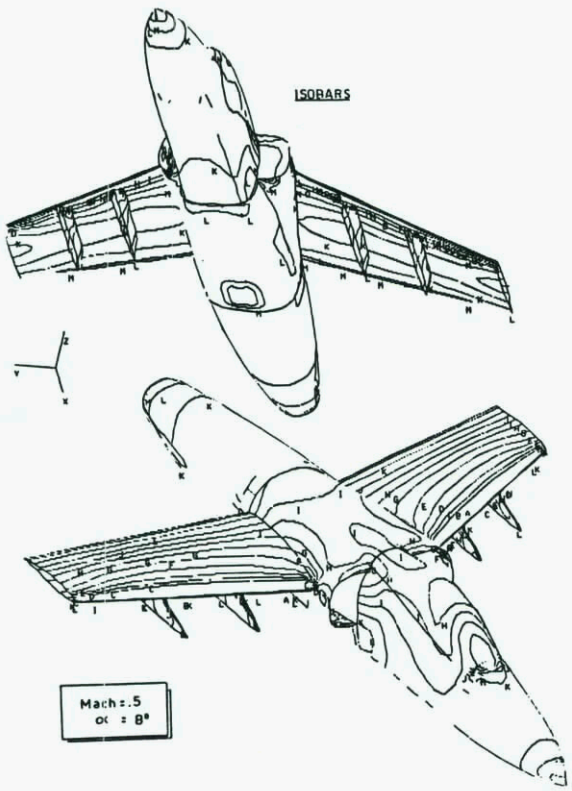

Fig. 6 - Theoretical Pressures

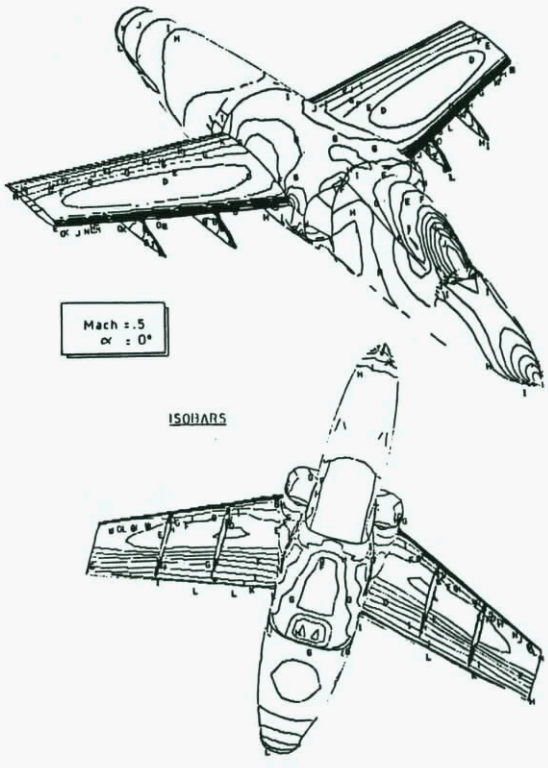

Fig. 7 - Computed Pressures

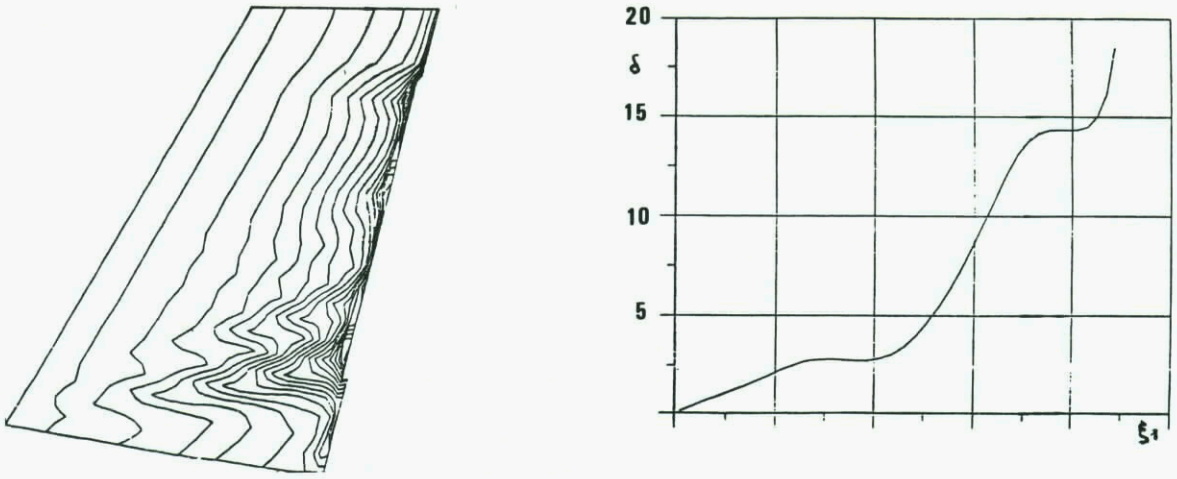

Fig. 8 - Delta Distribution Over Wing Upper Surface

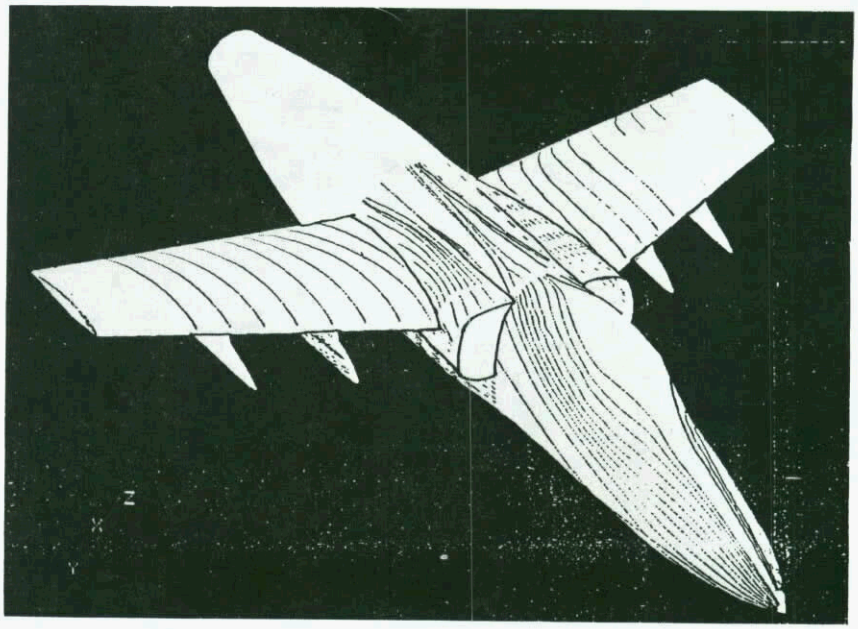

Fig. 9 - Computed Wall Streamlines

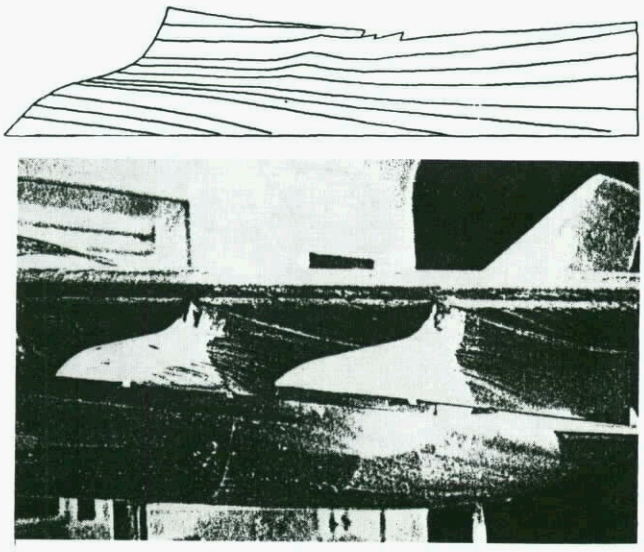

Fig.10 - Experimental and Computed Wall Streamlines on Inboard Pylon

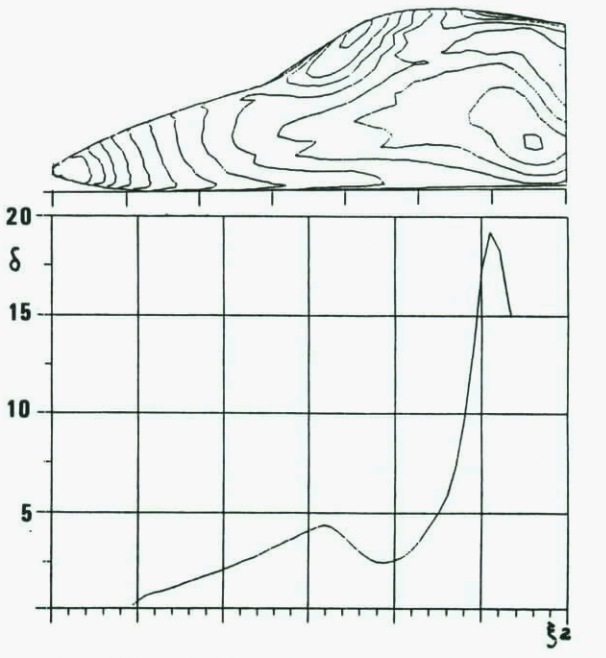

Fig. 11 - Delta Over Aircraft Forebody

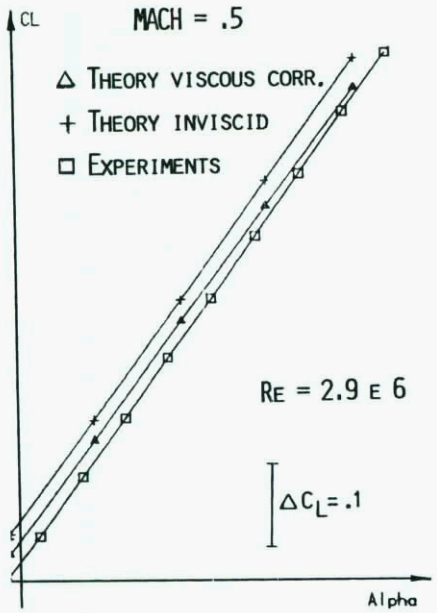

Fig. 12.a - Lift Coefficient

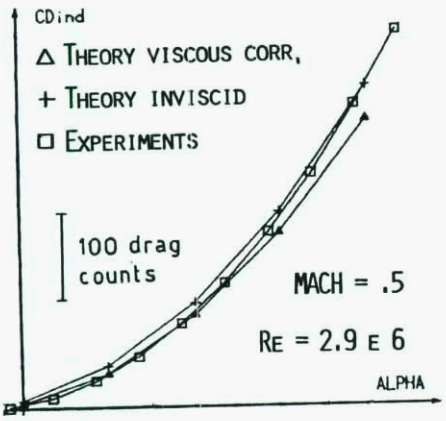

Fig. 12.b - Induced Drag Coefficient

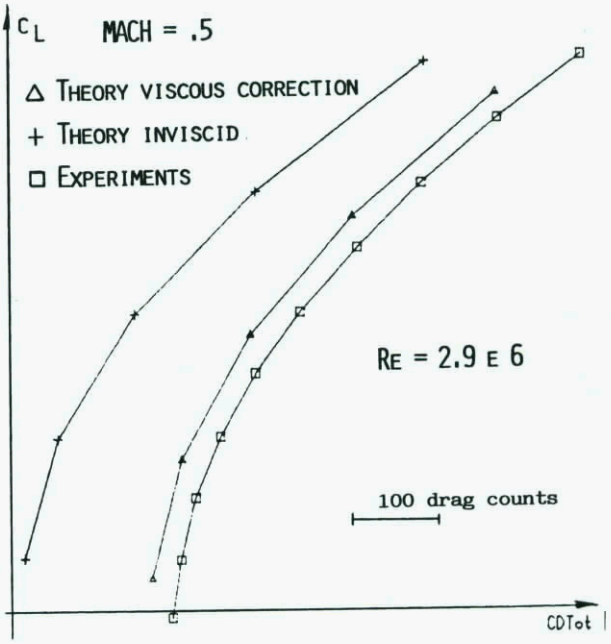

Fig. 13 - Total Drag Coefficient

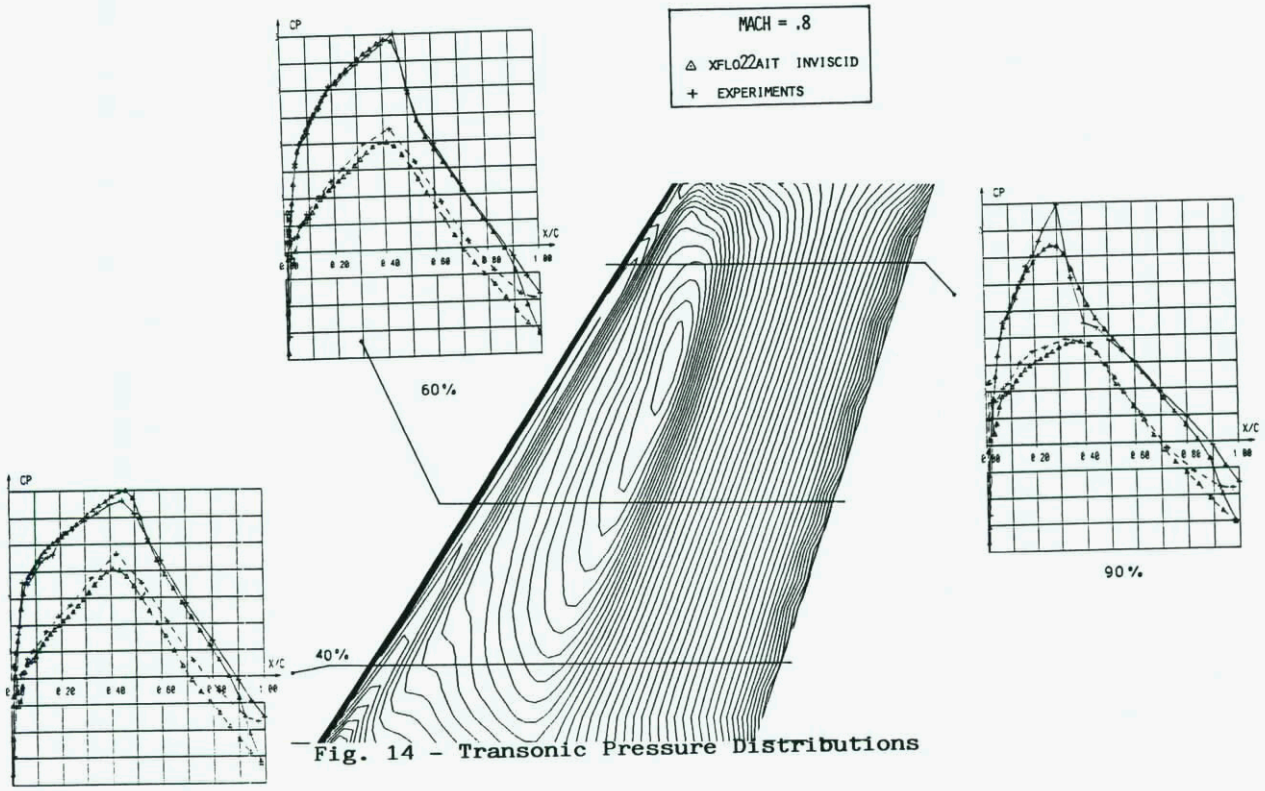

Fig. 14 - Transonic Pressure Distributions

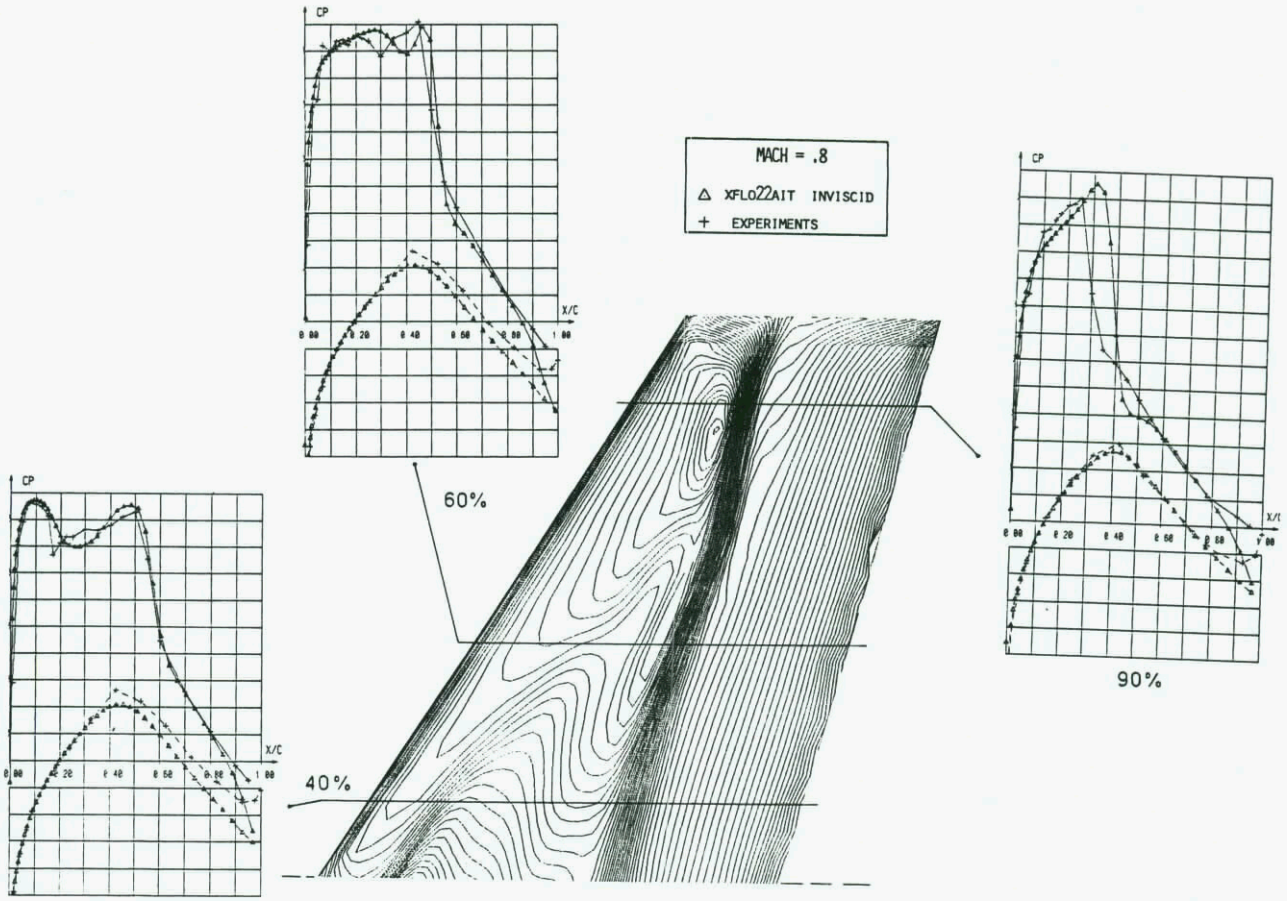

Fig. 15 - Comparison Between Transonic Wind Tunnel and Numerical Pressure Distributions.
Isobars From XFLO22AIT - Case α=5°

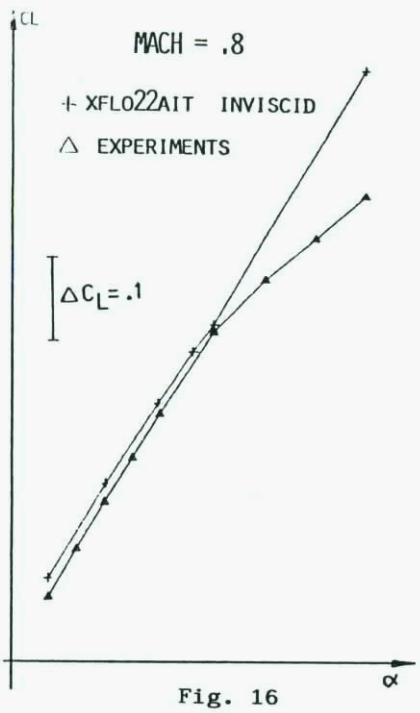

Fig. 16

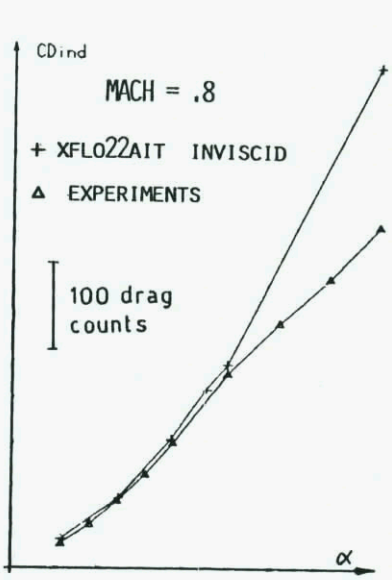

Fig. 17.a

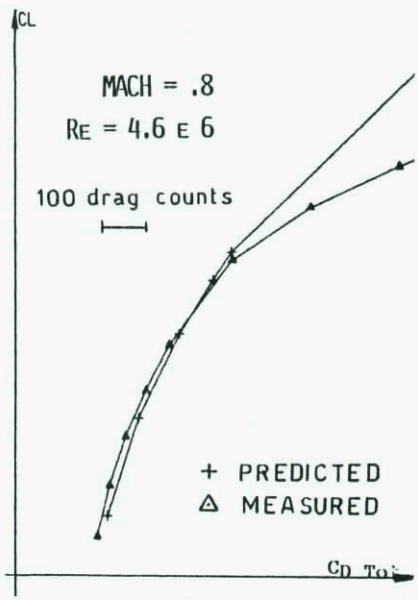

Fig. 17.b

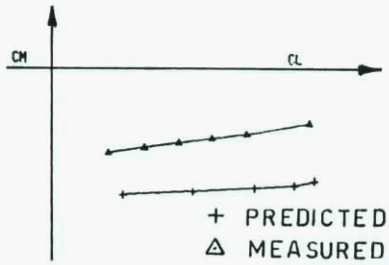

Fig. 18

Fig. 16 - Computed and Measured Lift Coefficient
Fig. 17 - a) Induced Drag Coefficient Vs. α
b) Numerical and Experimental Polars
Fig. 18 - Comparison Between Computed and Measured Pitching Moment

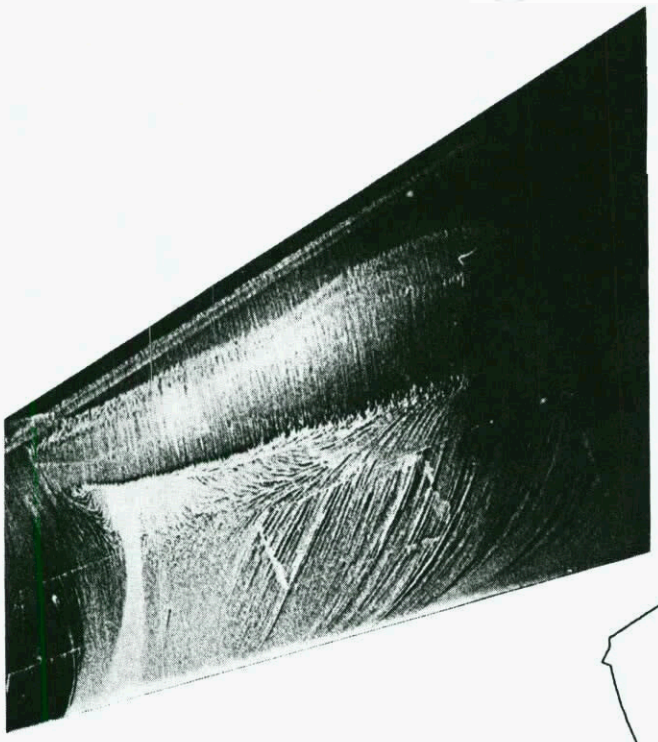

MACH = .8
ALPHA =3.7°
RE =4.6 E 6
SHOCK TRACE — — —

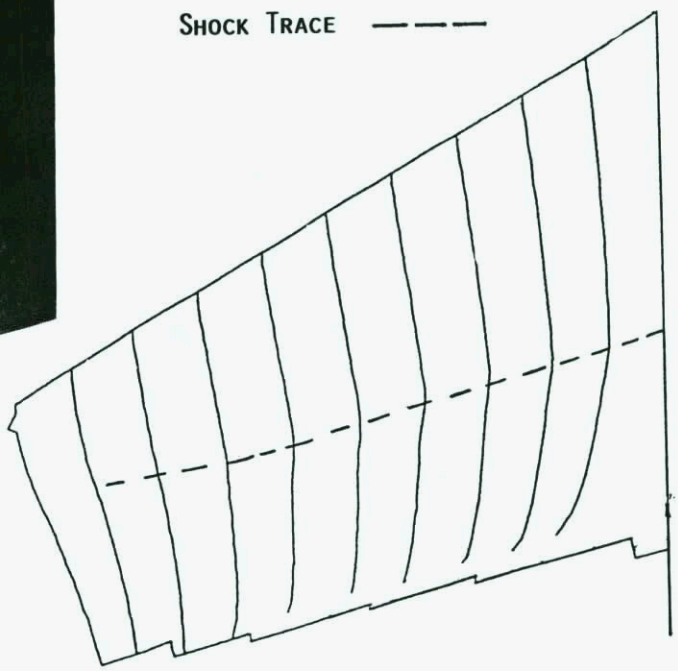

Fig. 19 - Experimental and Numerical Oil Flow. Attached Flow

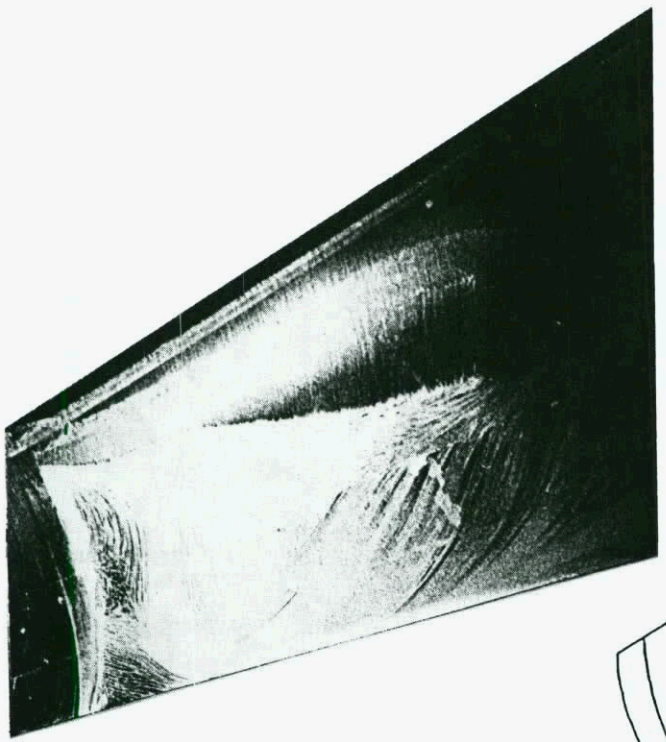

MACH = .8
ALPHA = 5°
RE =4.6 E 6
SHOCK TRACE — — —

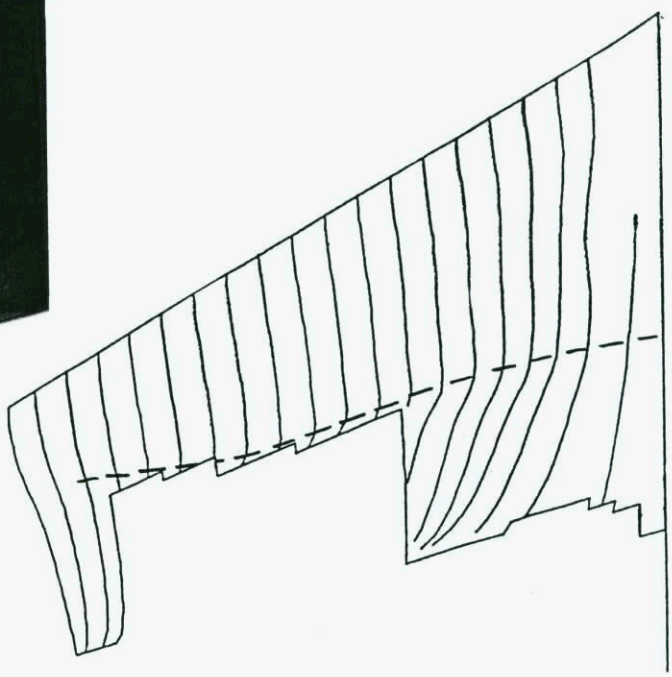

Fig. 20 - Experimental and Numerical Oil Flow. Separated Flow

Fig. 21 - Theoretical Pressure and Separation Evolution Near Critical Incidence.

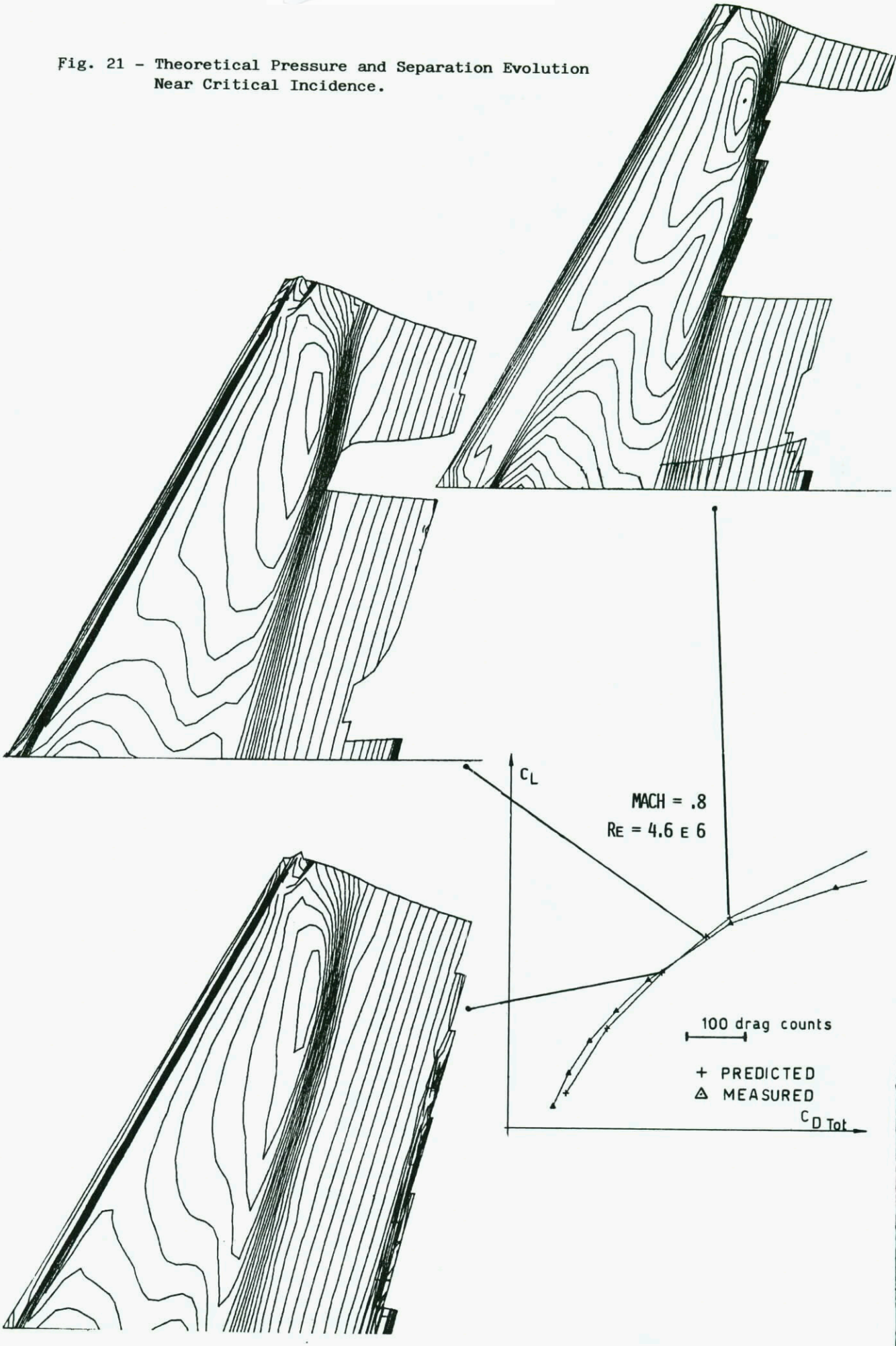

AIRCRAFT DRAG PREDICTION FOR TRANSONIC POTENTIAL FLOW*

by
J. van der Vooren**
National Aerospace Laboratory NLR, Informatics Division
P.O. Box 90502, 1006 BM Amsterdam, The Netherlands

SUMMARY

The state-of-the-art on computational drag prediction and diagnostics in The Netherlands for transport aircraft in the transonic flight regime is described. Subsequently, a method is discussed that is currently being developed at NLR to calculate wave drag in transonic potential flow. The method is a generalization and extension of Garabedian's and McFadden's idea of determining wave drag by volume-integration of the artificial viscosity. The generalization involves the introduction of a reference artificial viscosity which provides a solid theoretical basis. At the same time this ensures that calculated wave drag is to a certain extent independent of the specific details of the artificial viscosity in different codes. The extension accounts for the fact that artificial viscosity does not smear out supersonic/subsonic shock waves completely, but leaves room for a truly discontinuous sonic/subsonic 'shock remainder' that contributes substantially to the wave drag. A number of first results that illustrate the potential of the method are presented and discussed.

1. INTRODUCTION

The reduction of aircraft drag is an important objective in aerodynamic design. However, a successful drag reduction strategy requires that the various sources of aircraft drag are not only identified but also reliably quantified. The three major physical phenomena responsible for aircraft drag are boundary layers and wakes, vortex shedding and shock wave formation. The associated components of aircraft drag are respectively viscous drag, induced drag (drag due to lift) and wave drag. Computational aerodynamics should serve the purpose of quantifying each of these components.

Accurate prediction of aircraft total drag and its various components on the basis of computational aerodynamics is generally recognized as being difficult and therefore represents a continuing challenge to computational aerodynamics research. The difficulties are in three categories, viz. the modelling of the physics, the identification of the various drag components, and numerical accuracy. With drag prediction from inviscid codes, the limitations of the various flow models (Prandtl-Glauert, full-potential, Euler) are clear, the identification of the various drag components (static pressure drag, induced drag, wave drag) is reasonably well understood, and the quest for numerical accuracy prevails. The prediction of viscous drag from boundary layer codes seems to hinge at present on the limitations of the physics modelling (e.g. integral or field method, transition and turbulence models, attached or separated flow), rather than on numerical accuracy. Drag prediction from the upcoming Reynolds-averaged Navier-Stokes codes, however, is likely to be confronted with difficulties in all three categories. Though such codes, at least in principle, can provide all necessary information, the identification and therefore also the quantification of certain drag components of interest is as yet unclear, and might even be impossible.

At present, the situation on drag prediction from computational aerodynamics codes can roughly be assessed as follows. Accurate determination of the static pressure drag by surface-integration from inviscid codes is almost impossible for the mesh densities and convergence levels that are currently being used in engineering environments (Ref. 1). Much finer meshes and much better convergence levels are mandatory, and this really requires the power of modern supercomputers like the CRAY-XMP, CRAY-2, NEC SX-2, ETA 10. With respect to induced drag, acceptable numerical accuracy can be obtained with inviscid potential codes (Prandtl-Glauert as well as full-potential) using Trefftz-plane type integration (Ref. 1). Calculating wave drag from a full-potential code, however, is at present far from sufficiently accurate. A step in the right direction is indicated by the work of Garabedian and McFadden (Refs. 2, 3, 4), who calculate wave drag by volume-integration of the artificial viscosity. But even then, much finer meshes and much better convergence levels are likely to be needed. With inviscid Euler codes, the situation is still more difficult, because both the induced drag and the wave drag are represented in the Trefftz-plane, and can be separated only under simplifying assumptions (Refs. 5, 6). In particular, the prediction of wave drag is bound to suffer from the well known phenomenon of spurious entropy production in todays Euler codes. Since this latter phenomenon is of a numerical nature, again the need for much finer meshes and much better convergence levels than are currently being used in engineering environments is indicated. Concerning the prediction of viscous drag from boundary layer codes, the absolute errors seem to be in the order of 5 to 15 counts for attached flows, and possibly larger for separated flows (Ref. 1).

The above discussions seem to indicate that, notwithstanding current problems with wave drag in particular, the prediction of drag from invicid codes (static pressure drag, induced drag, wave drag) has today the best prospects in view of the rapidly increasing computing power. With the prediction of viscous drag from boundary layer codes, current problems seem of more fundamental character. Naturally, this situation will reflect in the prediction of drag from Reynolds-averaged Navier-Stokes codes.

If absolute drag values are required, the proper interaction of the viscous dominated and nominally inviscid regions of the flow is mandatory. This, of course, is guaranteed with Reynolds-averaged Navier-Stokes codes, but is also offered in an approximate sense with viscous/inviscid interaction codes where

---

* Part of this research has been performed under contract with the Netherlands Agency for Aerospace Programs (NIVR)
** Senior research scientist

boundary layer equations and inviscid equations modelling the outer flow are coupled. Given the fact that viscous/inviscid interaction codes are, say, between one and two orders of magnitude faster than Reynolds-averaged Navier-Stokes codes, it seems not unrealistic to expect that aerodynamic designers will use viscous/inviscid interaction codes for e.g. wing design for some time to come. On an increment/decrement basis, this seems at present a viable approach towards drag prediction and diagnostics during the aircraft aerodynamic design cycle.

In The Netherlands, research on the prediction and diagnostics of aircraft drag on the basis of computational aerodynamics codes concentrates on the subsonic and transonic flow about transport aircraft. The paper discusses first the state-of-the-art for the transonic flight regime. In particular, the determination of wave drag using an engineering approach based on potential flow will be described. Subsequently, NLR work on the development of a more direct and robust method for calculating wave drag from full-potential codes will be discussed. This involves a generalization and extension of Garabedian's and McFadden's work (Refs. 2, 3, 4). The method aims at handling fully-conservative and non-conservative shock waves, as well as quasi Rankine-Hugoniot shock waves (compare Ref. 7).

2. STATE-OF-THE-ART

Drag prediction and diagnostics in the aircraft industry in The Netherlands for transport aircraft in the transonic flight regime is currently still being done using a system developed by NLR before 1982 (Ref. 8), involving the transonic full-potential code XFLO22 (Ref. 8) for wing/body combinations, the subsonic PANEL METHOD (Ref. 9) and the fully three-dimensional laminar/turbulent finite-difference boundary layer code BOLA (Ref. 10). In XFLO22 the body is actually modelled approximately by prescribing the proper 'crosswind', calculated by the PANEL METHOD for the full wing/body combination, in a vertical plane through the wing root (Fig. 1 and Ref. 8).

XFLO22 is a first generation non-conservative finite-difference code, whence interactive coupling with a boundary layer code to account for viscous effects cannot be justified. However, mesh-tuning and directing the vortex sheet to leave the trailing edge tangent to the wing lower surface were found to be adequate measures to obtain pressure distributions that are representative for full-scale Reynolds numbers. A recent example is shown in reference 11, where XFLO22-calculated pressure distributions are compared with in-flight measured pressure distributions for two wing stations of the Fokker 100, flying at transonic speed. The above argument suggests that the static pressure drag as obtained from the inviscid XFLO22 code, and therefore also its components induced drag and wave drag, are fairly representative for full-scale Reynolds numbers.

The following engineering approach is used in XFLO22 to estimate the wave drag (Refs. 1, 8). Consider the static pressure drag of the wing (CDp,wing) as obtained from surface-integration of the static pressure for the subsonic case where shockwaves are absent (subcritical). The value of CDp,wing is usually inaccurate due to insufficient mesh density and too low convergence levels. A far more accurate value (denoted as CDi,wing) can be obtained from momentum considerations and Trefftz-plane integration utilizing the spanwise circulation distribution of the wing. Theoretically, CDp,wing and CDi,wing (the contribution of the wing-alone to the induced drag) are equal in the subcritical case. Computationally, however, there holds in this case

$$CDp,wing = CDi,wing - \Delta CDp,wing, \tag{2.1}$$

where ΔCDp,wing is a correction to the calculated static pressure drag. It is then assumed, that this correction is a function of wing lift and freestream Mach number as follows,

$$\Delta CDp,wing = C_0 + C_2\,(CLwing + C_1)^2 + C_3 M_\infty^2 + C_4 (1-M_\infty^2)^{-\frac{1}{2}} + C_5 M_\infty^2 (CLwing)^2. \tag{2.2}$$

The quadratic CLwing-term is suggested by the fact that induced drag (and hence, in subcritical flow, also the static pressure drag) is a quadratic function of the lift. The terms with M_∞^2 and $(1-M_\infty^2)^{-\frac{1}{2}}$ are respectively suggested by the Rayleigh-Janzen M_∞^2-expansion theory and the Prandtl-Glauert theory. The cross-term with $M_\infty^2(CLwing)^2$ is merely empirical. The constants C_0 to C_5 are determined by applying equation (2.1) for six subcritical flow conditions. The experience is, that in this way the corrected static pressure drag can be determined in the whole subcritical flow regime with an accuracy of only a few drag counts. With the constants C_0 to C_5 known, equation (2.2) is assumed to be also valid for supercritical flow. Then the wave drag (CDw) can be determined from

$$CDw = CDp,wing + \Delta CDp,wing\,(M_\infty, CLwing) - CDi,wing. \tag{2.3}$$

Note, that this procedure assumes that wave drag is generated by the wing only.

The induced drag (CDi) of the full wing/body combination can be calculated from Trefftz-plane integration, utilising the spanwise circulation distribution of the wing, and the principle of left carry-over to account for the body. Note that this principle implies that no vorticity is being shed by the body. It follows that the static pressure drag (CDp) of the full wing/body combination can be estimated from

$$CDp = CDi + CDw\ . \tag{2.4}$$

It remains to estimate the viscous drag (CDv) of the full wing/body combination. The contribution of the wing (CDv,wing) is estimated by first calculating the boundary layer on the wing using the BOLA code with the static pressure distribution as obtained by XFLO22 as input, and subsequently estimating the

viscous drag from the momentum thickness using an extended form of the Squire and Young method (Refs. 1, 8). The contribution of the body (CDv,body) must be estimated using empirical means or windtunnel data. The total drag (CD) of the full wing/body combination can then finally be estimated from

$$CD = CDp + CDv, \tag{2.5}$$

where

$$CDv = CDv,wing + CDv,body. \tag{2.6}$$

Figure 2 shows a comparison of measured and computed total drag for a narrow body transport combination, obtained using the above described prediction procedure, illustrating its usefulness. Further examples can be found in reference 8. The procedure played a role in predicting the aircraft drag for the Fokker 100 (Ref. 11). Finally, figure 3 shows a comparison of the calculated viscous drag distribution for a transport type wing, using the extended Squire and Young method, with experimental (wake rake) data (Ref. 12).

3. WAVE DRAG IN POTENTIAL FLOW

Wave drag in mass-conserving potential flow is known to be the consequence of momentum production across the shock waves in the direction normal to these shock waves. Wave drag can therefore, at least in principle, be calculated directly from the flow conditions either upstream or downstream of the shock waves, the orientation of the shock surfaces, and the relevant shock jump conditions. However, this is a difficult and not very accurate procedure with the shock capturing full-potential codes that are currently being used. On the other hand, the possibility exists to try to solve this difficulty by applying the momentum theorem for the freestream direction to (narrow) control surfaces enveloping each captured smeared out shock wave. Work along this line by Yu et al. (Ref. 13) has made it very clear, however, that the mesh density used today in routine applications and the convergence levels achieved are insufficient for an accurate prediction of the wave drag (see also Ref. 1). Unpublished work along the same line at NLR using XFL022 (Ref 8) has confirmed this. It seems therefore, that a very fine mesh and very high levels of convergence are mandatory for success. As discussed in the previous chapter, wave drag in XFL022 is calculated indirectly, namely by subtracting (in principle) the induced drag from the (corrected) static pressure drag. This procedure can work satisfactorily in cases of practical significance. Yet, dificiencies are always to be feared, and hence a robust procedure that works under all circumstances is still required.

At present, work is in progress at NLR to develop and validate a method to determine wave drag from full-potential codes directly. The method is based on a generalization and extension of Garabedian's and McFadden's work (Refs. 2, 3, 4), where wave drag is determined by volume-integration of the artificial viscosity. The advantage is mainly, that an important part of the wave drag can be calculated by summing up only positive contributions, as opposed to surface-integration of the static pressure where a large positive contribution, and an almost equally large negative contribution, tend to cancel. The method aims at handling eventually fully-conservative shock waves, non-conservative shock waves, and quasi Rankine-Hugoniot shock waves (compare Ref. 7), and is being implemented in the full-potential MATRICS code (Ref. 14) that is continuously being extended further at NLR. At present, MATRICS can handle a wing/body combination on a CH-topology grid. Here the fully-conservative option is to be used when MATRICS is extended with an interactively coupled boundary layer. The non-conservative option is to be used in cases where mesh-density, and the direction in which the vortex sheet leaves the trailing edge of the wing, are tuned to match the pressure distributions for full-scale Reynolds numbers (see Ref. 11 for a comparison of thus obtained MATRICS results and in-flight measurements on two wing sections of the Fokker 100). The quasi Rankine-Hugoniot shock wave is in practise a fair approximation of a true Euler code result, and as such is also useful in combination with an interactively coupled boundary layer, especially if the upstream normal Mach number at the shock wave exceeds, say, Mnormal = 1.3, and potential theory is no longer a good approximation.

3.1 Wave drag formulas

MATRICS is based on a fully-conservative finite-volume scheme of the full-potential equation in strong conservation form. The scheme is second order accurate in the mesh size in subsonic parts of the flow, and first order accurate in supersonic parts of the flow. For the capture of supersonic/subsonic shock waves a Godunov type shock operator is used. The modified equation of the scheme is

$$(\rho u + P)_x + (\rho v + Q)_y + (\rho w + R)_z = 0 \ . \tag{3.1}$$

Here ρ is the density,

$$\rho = [1 + \frac{\gamma-1}{2} M_\infty^2 \ (1 - q^2)]^{\frac{1}{\gamma-1}} \ , \tag{3.2}$$

with

$$q^2 = u^2 + v^2 + w^2. \tag{3.3}$$

The velocity components u, v, w derive from the velocity potential φ as follows,

$$u = \varphi_x \ , \ v = \varphi_y \ , \ w = \varphi_z \ . \tag{3.4}$$

Artificial viscosity is introduced through the artificial viscous fluxes P, Q, R, which are of the order of the mesh size in supersonic parts of the flow.

Assume for the sake of analysis, that the artificial viscous fluxes satisfy the requirement,

$$P \sim u, \quad Q \sim v, \quad R \sim w. \tag{3.5}$$

As will be shown later, this can indeed be realized if the mass flux ρq in the supersonic parts is retarded precisely against the flow direction.

The finite-volume discretization of equation (3.1) can be described in terms of discrete operators for the different situations of subsonic, supersonic and sonic flow, and of supersonic/subsonic shock waves. In particular, the shock operators for the supersonic/subsonic shock waves guarantee the mass conservation across such shock waves if the fully-conservative option in MATRICS is used.

The non-conservative option in MATRICS is obtained by replacing all shock operators by subsonic operators. Hence, only across supersonic/subsonic shock waves, mass is no longer conserved. Mass conservation is therefore retained in all other flow situations, including supersonic/supersonic shock waves.

Away from shock waves, the modified full-potential equation (3.1) can be written in the alternative form

$$(\rho u)_x + (\rho v)_y + (\rho w)_z = m \ , \tag{3.6}$$

where

$$m = -(P_x + Q_y + R_z) \tag{3.7}$$

can be interpreted as a distributed mass-source per unit volume.

If the upstream direction is the x-direction, then the corresponding x-momentum equation is

$$(\rho u^2 + p)_x + (\rho v u)_y + (\rho w u)_z = m\, u, \tag{3.8}$$

if p is the static pressure.

The effect of the artificial viscosity, which is of first order in the mesh size, is to smear out the shock waves (true discontinuities in potential flow) to narrow zones of steep gradients. However, the artificial viscosity is only non-zero in supersonic parts of the flow. Hence, only supersonic/supersonic shock waves smear out <u>completely</u>. A supersonic/subsonic shock wave smears out only <u>partly</u> and reduces in fact to a narrow zone of steep gradients with sonic conditions on its downstream side, immediately followed by a true discontinuity with sonic conditions on its upstream side. This discontinuity is of course considerably weaker than the full shock wave, and will be referred to as the 'shock remainder' .

In view of equation (3.6), which is a second order accurate representation of the finite-volume scheme in the mesh size, the total amount of mass created in the supersonic region of the flow is

$$\int_{V_{M>1}} m \, dV,$$

if V is the infinite physical space surrounding the aircraft. Similarly, in view of equation (3.8), the total amount of x-momentum created in the supersonic region of the flow is

$$X1 = \int_{V_{M>1}} m\, u \, dV. \tag{3.9}$$

Further x-momentum is created in the shock remainders, viz.

$$X2 = \int_{S_s} \{(p_d - p_u^*) n_x + \rho_d \, q_{n,d} \, u_d - \rho_u^* \, q_{n,u}^* \, u_u^*\} \, d\,S. \tag{3.10}$$

Here n is the downstream pointing normal on the shock remainder surfaces S_s, the indices u and d refer to upstream and downstream of the shock remainder respectively, and * refers to sonic conditions.

If the discretization is <u>fully-conservative</u>, no mass flows into the downstream far-field, and the mass created in the supersonic parts of the flow must obviously be destroyed again. The only way this can happen is by concentrated mass-sinks $\bar{M}$ per unit area interior the shock remainders. Then there holds evidently

$$\int_{V_{M>1}} m dV = \int_{S_s} \bar{M} dS, \tag{3.11}$$

while the jump relation across shock remainders satisfies

$$\rho_d q_{n,d} - \rho_u^* q_{n,u}^* = -\bar{M} < 0. \tag{3.12}$$

Using this relation in equation (3.10), the expression for X2 reduces to

$$X2 = \int_{S_s} \{(p_d - \overset{*}{p}_u)\, n_x + \rho_d q_{n,d}\,(u_d - \overset{*}{u}_u)\}\, dS - \int_{S_s} \overset{*}{\bar{M}} \overset{*}{u}_u \; dS. \tag{3.13}$$

Then the total gain in x-momemtum associated with shock wave formation is X1 + X2, and this must be balanced by the wave drag D_w. Hence, it follows that

$$Dw = X1 + X2 = \int_{S_s} \{(p_d - \overset{*}{p}_u)\, n_x + \rho_d\, q_{n,d}\,(u_d - \overset{*}{u}_u)\}\, dS - \int_{S_s} \overset{*}{\bar{M}} \overset{*}{u}_u dS + \int_{V_{M>1}} mudV. \tag{3.14}$$

Using equation (3.7) in equation (3.11), the following result can be obtained,

$$\begin{aligned} \int_{V_{M>1}} mdV &= -\int_{V_{M>1}} (P_x + Q_y + R_z)dV = \\ &= -\int_{\partial V_{M>1}} (Pn_x + Qn_y + Rn_z)dS = \\ &= -\int_{S_s} (Pn_x + Qn_y + Rn_z)dS = \int_{S_s} \bar{M} dS. \end{aligned} \tag{3.15}$$

Here use is made of the following facts. The boundary $\partial V_{M>1}$ of $V_{M>1}$ is made up of the shock remainder surfaces S_s, sonic surfaces and parts of the aircraft surface. On sonic surfaces P = Q = R = 0. On the aircraft surface $Pn_x + Qn_y + Rn_z = 0$ in view of equation (3.5). On the shock remainder surfaces S_s the quantity $Pn_x + Qn_y + Rn_z$ is finite. This can easily be understood by considering equation (3.12) for a normal shock. Then indeed $\rho_d q_d - \overset{**}{\rho} \overset{**}{q}_u = -\bar{M} < 0$, because $\overset{**}{\rho}\overset{**}{q}$ is the maximum value that ρq can assume.

Similarly, there holds

$$\begin{aligned} \int_{V_{M>1}} mudV &= -\int_{V_{M>1}} (P_x + Q_y + R_z)\, udV = \\ &= -\int_{V_{M>1}} (Pn_x + Qn_y + Rn_z)\, udS + \int_{V_{M>1}} (Pu_x + Qu_y + Ru_z)dV = \\ &= -\int_{S_s} (Pn_x + Qn_y + Rn_z)udS + \int_{V_{M>1}} (Pu_n + Qu_y + Ru_z)dV = \\ &= \int_{S_s} \overset{*}{\bar{M}} \overset{*}{u}_u \; dS + \int_{V_{M>1}} (Pu_x + Qu_y + Ru_z)\, dV. \end{aligned} \tag{3.16}$$

Substitution of equation (3.16) into equation (3.14) then gives for the wave drag,

$$\begin{aligned} Dw = &\int_{S_s} \{(p_d - \overset{*}{p}_u)\, n_x + \rho_d q_{n,d}\,(u_d - \overset{*}{u}_u)\}\, dS - \int_{S_s} \overset{*}{\bar{M}} \overset{*}{u}_u \, dS + \int_{S_s} \overset{*}{\bar{M}} \overset{*}{u}_u \, dS \; + \\ &+ \int_{V_{M>1}} (Pu_x + Qu_y + Ru_z)dV. \end{aligned} \tag{3.17}$$

Here the fourth term is a generalization of Garabedian's and McFadden's work (Refs. 2, 3, 4). The third term is the x-momentum associated with the excess mass created in the supersonic parts of the flow as a consequence of the artificial viscosity. The second term is the x-momentum associated with destroying the excess mass in the shock remainders. In fact, the third and second terms are both spurious contributions to the wave drag, which, however, cancel as a consequence of the fully-conservativeness of the finite-volume scheme. Finally, the first term is the x-momentum produced across the shock remainders. Cancelling of the second and third term in equation (3.17) consequently gives as the final expression for the wave drag,

$$Dw = \int_{S_s} \{(p_d - \overset{*}{p}_u)\, n_x + \rho_d q_{n,d}\,(u_d - \overset{*}{u}_u)\}\, dS + \int_{V_{M>1}} (Pu_x + Qu_y + Ru_z)dV. \tag{3.18}$$

In confirmation of equation (3.18), the following considerations are useful. Consider the exact mathematical solution of full-potential theory where shock waves are true discontinuities. Then

$$Dw = \int_{S_s} \{(p_d - p_u)\, n_x + \rho_d q_{n,d} u_d - \rho_u q_{n,u}\, u_u\}\, dS, \tag{3.19}$$

the right-hand side being the x-momentum production of the full shock waves. In view of mass-conservation there holds across each shock wave in this case,

$$\rho_d q_{n,d} = \rho_u\, q_{n,u}\,. \tag{3.20}$$

Using equation (3.20), the wave drag according to equation (3.19) can be rewritten as follows in case of supersonic/subsonic shock waves,

$$Dw = \int_{S_s} \{(p_d - \overset{*}{p}_u)n_x + \rho_d q_{n,d}\,(u_d - \overset{*}{u}_u)\}dS + \int_{S_s} \{(\overset{*}{p}_u - p_u)n_x + \rho_u q_{n,u}\,(\overset{*}{u}_u - u_u)\}dS. \tag{3.21}$$

In the limit of vanishing mesh size (i.e. if the artificial viscosity approaches zero), the first term in the right-hand side of equation (3.18) approaches the corresponding term in equation (3.21). Consequently, the second term in the right-hand side of equation (3.18) replaces the corresponding term in equation (3.21) in case artificial viscosity smears out part of the supersonic/subsonic shock waves.

If the discretization is non-conservative, the excess mass, created in the supersonic parts of the flow as a consequence of the artificial viscoisty, is not destroyed interior the shock remainders, but instead flows into the downstream far-field. This then corresponds to an amount of x-momentum, compare equation (3.11),

$$X3 = u_\infty \int_{V_{M>1}} \rho dV = \int_{S_s} \bar{M}u_\infty dS \tag{3.22}$$

being destroyed in the downstream far-field. It follows also, that the jump relation across shock remainders satisfies in this case,

$$\rho_d q_{n,d} - \overset{**}{\rho} q_{n,u} = 0\ , \tag{3.23}$$

whence the expression for X2 in equation (3.10) becomes

$$X2 = \int_{S_s} \{(p_d - \overset{*}{p}_u)n_x + \rho_d q_{n,d}\,(u_d - \overset{*}{u}_u)\}dS. \tag{3.24}$$

So in this case, the total gain in x-momentum associated with shock wave formation is X1 + X2 - X3, and this must be balanced by a force Dx on the aircraft, satisfying

$$Dx = X1 + X2 - X3 = \int_{S_s} \{(p_d - \overset{*}{p}_u)n_x + \rho_d q_{n,d}\,(u_d - \overset{*}{u}_u)\}dS - \int_{S_s} \bar{M}u_\infty\, dS + \int_{V_{M>1}} \rho u dV\ . \tag{3.25}$$

The question then is, whether this force equals the wave drag, or not. Using again equation (3.16), the expression for Dx in equation (3.25) can be rewritten as follows,

$$Dx = \int_{S_s} \{(p_d - \overset{*}{p}_u)n_x + \rho_d q_{n,d}\,(u_d - \overset{*}{u}_u)\}dS - \int_{S_s} \bar{M}u_\infty dS + \int_{S_s} \bar{M}\overset{*}{u}_u dS + \int_{V_{M>1}} (Pu_x + Qu_y + Ru_z)dV. \tag{3.26}$$

This equation is similar to equation (3.17). The difference is, that the two spurious terms associated with the excess mass cancel in equation (3.17), whereas they do not cancel in equation (3.26). Since the creation of mass through artificial viscosity is by itself a spurious effect of the finite-volume discretization, the conclusion can be no other than that the spurious terms in equation (3.26) must be disregarded when it comes to wave drag. Hence, compare equation (3.18), also in the non-concervative case, the wave drag is

$$Dw = \int_{S_s} \{(p_d - \overset{*}{p}_u)n_x + \rho_d q_{n,d}\,(u_d - \overset{*}{u}_u)\}dS + \int_{V_{M>1}} (Pu_x + Qu_y + Ru_z)dV. \tag{3.27}$$

The necessity to neglect the spurious terms in equation (3.26) has already been observed by Garabedian in 1976 (Ref. 2). More recently, in 1987, this observation was repeated by Ross (Ref. 15). The way of presenting the above derivations has benifited from Ross's presentation in reference 15. A graphical presentation of the above derivations is given in figures 4, 5. For a more elaborate mathematical analysis, see reference 16.

3.2 Reference artificial viscosity

Define reference artificial viscous fluxes $\bar{P}$, $\bar{Q}$, $\bar{R}$ by retarding the mass flux ρq in the supersonic parts precisely against the flow direction. Then

$$(\rho q)_{\text{retarded}} = \rho q - (\rho q)_s \Delta s = \rho q - \rho(1 - M^2)q_s\ \Delta s. \tag{3.28}$$

Here s is the streamwise coordinate and Δs is of the order of the local mesh size. In this case,

$$\left.\begin{aligned} \bar{P} &= -\varepsilon \frac{u}{q}\,\rho(1 - M^2)q_s\ \Delta s\ , \\ \bar{Q} &= -\varepsilon \frac{v}{q}\,\rho(1 - M^2)q_s\ \Delta s\ , \\ \bar{R} &= -\varepsilon \frac{w}{q}\,\rho(1 - M^2)q_s\ \Delta s\ , \end{aligned}\right| \tag{3.29}$$

with ϵ being a positive constant of order one in supersonic flow ($M>1$), and zero in subsonic flow ($M<1$). Note that the artificial viscous fluxes $\bar{P}$, $\bar{Q}$, $\bar{R}$ according to equation (3.29) satisfy the requirement (3.5), are zero on sonic surfaces, and can indeed approach finite values at the upstream side of shock remainders where $q_s \to \infty$.

In analogy with equations (3.18), (3.27), consider the quantity $\bar{P}q_x + \bar{Q}q_y + \bar{R}q_z$. Using equation (3.29) and the definition of q_s, viz.

$$q_s = \frac{u}{q} q_x + \frac{v}{q} q_y + \frac{w}{q} q_z \ , \tag{3.30}$$

it can easily be shown, that

$$(\bar{P}q_x + \bar{Q}q_y + \bar{R}q_z) = -\epsilon\rho(1 - M^2)\, q_s^2\, \Delta s > 0 \tag{3.31}$$

in supersonic parts of the flow. This inequality in fact replaces the entropy inequality in Euler flow, and is the mechanism that ensures the occurrence of compression shock waves only. The following may serve to illustrate the point further.

Introduce the retarded density $\bar{\rho}$ satisfying

$$\bar{\rho}q = (\rho q)_{\text{retarded}}. \tag{3.32}$$

Then, in view of equations (3.28), (3.29),

$$\bar{\rho} = \rho - \frac{1}{q}(1 - M^2) q_s \Delta s, \tag{3.33}$$

and the modified full-potentital equation (3.1) or (3.6) can be given the form,

$$(\bar{\rho}u)_x + (\bar{\rho}v)_y + (\bar{\rho}w)_z = 0 \ . \tag{3.34}$$

Similarly, using equation (3.7), the corresponding x-momentum equation can be rewritten as

$$(\bar{\rho}u^2 + p)_x + (\bar{\rho}vu)_y + (\bar{\rho}wu)_z = \bar{P}u_x + \bar{Q}u_y + \bar{R}u_z = k_x = -\epsilon\rho(1 - M^2) u_s q_s \Delta s. \tag{3.35}$$

Equations (3.34), (3.35) show that the solution of a finite-volume code using artificial viscous fluxes $\bar{P}$, $\bar{Q}$, $\bar{R}$ can be interpreted as a fictitious real flow with velocities u, v, w, pressure p, and density $\bar{\rho}$, under the action of distributed forces $\vec{k}$ per unit volume,

$$\vec{k} = -\epsilon\rho(1 - M^2)\vec{q}_s\, q_s\, \Delta s. \tag{3.36}$$

Note in particular, that it is precisely the force term in the right-hand side of equation (3.35) which is responsible for the Garabedian type contribution to the wave drag, compare equations (3.18), (3.27). Note also, that $|\vec{k}|$ is precisely the amount of streamwise momentum that is being created in the fictitious flow per unit volume. In supersonic parts of the fictitious flow, indeed

$$|\vec{k}| = -\epsilon\rho(1 - M^2) q_s^2 \Delta s > 0, \tag{3.37}$$

compare equation (3.31). Hence the streamwise momentum increases along a streamline in supersonic parts of the fictitious flow, and this is in agreement with the fact that (compression) shock waves in mass-conserving full-potential theory are associated with an increment of shock-normal momentum if the shock-normal points in the downstream direction and the shock is traversed from upstream to downstream. Outside smeared out shock waves in the fictitious flow, $q_s = O[1]$ and therefore $|\vec{k}| = O[\Delta s]$. Inside smeared out shock waves, $q_s = O[\Delta s^{-1}]$ and therefore also $|\vec{k}| = O[\Delta s^{-1}]$. Since the 'thickness' of a smeared out shock wave is of $O[\Delta s]$, it follows that the gain in streamwise momentum over the smeared out shock wave is of $O[1]$ as indeed it should.

3.3 Implementation

In MATRICS, the artificial viscous fluxes are defined as

$$\left.\begin{aligned} P &= -\epsilon_x \ \text{sign}\ [u]\ \frac{u}{q}\ \rho\ (1 - M^2) q_x \Delta x \ , \\ Q &= -\epsilon_y \ \text{sign}\ [v]\ \frac{v}{q}\ \rho\ (1 - M^2) q_y \Delta y \ , \\ R &= -\epsilon_z \ \text{sign}\ [w]\ \frac{w}{q}\ \rho\ (1 - M^2) q_z \Delta z \ . \end{aligned}\right| \tag{3.38}$$

Here ϵ_x, ϵ_y, ϵ_z are positive and of order $O[1]$ in supersonic flow parts, and zero in subsonic flow parts. Though P, Q, R can easily be seen to satisfy an entropy inequality of the form (3.31), it is also obvious that the requirement (3.5) is not satisfied, whence the analysis in section 3.1 is not exact for MATRICS.

If s, m, n is a local orthogonal coordinate system, then

$$\begin{bmatrix} \partial/\partial x \\ \partial/\partial y \\ \partial/\partial z \end{bmatrix} = \begin{bmatrix} \frac{u}{q} & c_{12} & c_{13} \\ \frac{v}{q} & c_{22} & c_{23} \\ \frac{w}{q} & c_{32} & c_{33} \end{bmatrix} \begin{bmatrix} \partial/\partial s \\ \partial/\partial m \\ \partial/\partial n \end{bmatrix} , \tag{3.39}$$

and the following result can be obtained, compare equation (3.11),

$$Pq_x + Qq_y + Rq_z = -\rho\,(1 - M^2)\,\{\varepsilon_x \frac{|u|}{q} q_x^2 \Delta x + \varepsilon_y \frac{|v|}{q} q_y^2 \Delta y + \varepsilon_z \frac{|w|}{q} q_z^2 \Delta z\} =$$

$$= -\varepsilon\rho(1 - M^2)q_s^2 \Delta s + \text{deviation term} = \bar{P}q_x + \bar{Q}q_y + \bar{R}q_z + \text{deviation term}, \tag{3.40}$$

if

$$\varepsilon\Delta s = \varepsilon_x (\frac{|u|}{q})^3 \Delta x + \varepsilon_y (\frac{|v|}{q})^3 \Delta y + \varepsilon_z (\frac{|w|}{q})^3 \Delta z. \tag{3.41}$$

The sign of the 'deviation term' in equation (3.40), which contains terms with $q_s q_m$, $q_s q_n$, q_m^2, q_n^2, is in fact uncertain and will be disregarded in the determination of the wave drag. Consequently, the Garabedian type contribution to the wave drag, i.e. the second term in the right-hand side of equations (3.18), (3.27), will be evaluated using equation (3.41) to determine Δs for the reference artificial viscosity. This has the advantage, that this contribution is to a certain extent independent of the specific details of the artificial viscosity in different codes.

It was shown in section 3.2 that streamwise momentum is being produced in supersonic flow parts as a consequence of artificial viscosity. Here it makes no difference whether the flow accelerates or decelerates. However, since a smeared out shock wave is always in decelerating flow, all contributions to the wave drag stemming from accelerating supersonic flow parts can be disregarded. This observation has already been made before by Garabedian and McFadden (Ref. 3). Hence the wave drag formulas (3.18), (3.27) are implemented in the adapted form, see equations (3.29), (3.30),

$$Dw = \int_{S_s} \{(p_d - \overset{*}{p}_u)n_x + \rho_d q_{n,d}\,(u_d - \overset{*}{u}_u)\}dS - \int_{V_{M>1, q_s<0}} \varepsilon\rho(1 - M^2)u_s q_s \;\Delta s\; dV. \tag{3.42}$$

Note that the disregarded 'acceleration contributions' are of order $O[\Delta s]$, compare section 3.2, and therefore vanish anyway in the limit of vanishing mesh size. Note also, that

$$u_s = \frac{u}{q} q_s + (\frac{u}{q})_s q, \tag{3.43}$$

whence u_s and q_s are likely to have the same sign in the supersonic parts of the flow where streamlines are approximately in the freestream (x-) direction and only weakly curved. This then illustrates the strong point of Garabedian's and McFadden's work, viz. that an important contribution to the wave drag can be determined by summing up (at least in many cases) only positive numbers, compare equation (3.31).

It remains to discuss the implementation of the first term in the right-hand side of equation (3.42) i.e. the momentum production in the x-direction across shock remainders. For the capture of supersonic/subsonic shock waves, MATRICS uses a Godunov type shock operator acting on mass-fluxes in primary cell centres. Then the situation in the vicinity of the shock wave is as shown in figure 6. Here the cell centre $(i + \frac{1}{2}, j + \frac{1}{2}, k + \frac{1}{2})$ is the subsonic point downstream of the shock. The cell centres $(i - \frac{1}{2}, j + \frac{1}{2}, k + \frac{1}{2})$, $(i + \frac{1}{2}, j + \frac{1}{2}, k - \frac{1}{2})$, $(i + \frac{1}{2}, j - \frac{1}{2}, k + \frac{1}{2})$ are approximately sonic and are therefore approximately located on the upstream side of the shock remainder. However, calculated flow quantities at these latter cell centres are very inaccurate and sensitive due to 'differencing through the shock wave'. Consequently, flow quantities on the upstream side of the shock remainder are calculated e.g. as follows,

$$\overset{*}{u}_{u_{i-\frac{1}{2},\, j+\frac{1}{2},\, k+\frac{1}{2}}} = \tfrac{1}{2}\,\{(\frac{u}{q})_{i+\frac{1}{2},\, j+\frac{1}{2},\, k+\frac{1}{2}} + (\frac{u}{q})_{i-1\frac{1}{2},\, j+\frac{1}{2},\, k+\frac{1}{2}}\}\,\overset{*}{q}. \tag{3.44}$$

The implementation of the x-momentum production across shock remainders then becomes

$$\int_{S_s} \{(p_d - \overset{*}{p}_u)n_x + \rho_d q_{n,d}\,(u_d - \overset{*}{u}_u)\}dS =$$

$$= \Sigma\,[\{(p_{i+\frac{1}{2},\, j+\frac{1}{2},\, k+\frac{1}{2}} - \overset{*}{p}) + (\rho q)_{i+\frac{1}{2},\, j+\frac{1}{2},\, k+\frac{1}{2}}\,(u_{i+\frac{1}{2},\, j+\frac{1}{2},\, k+\frac{1}{2}} - \overset{*}{u}_{u_{i-\frac{1}{2},\, j+\frac{1}{2},\, k+\frac{1}{2}}})\}\,\Delta S_x +$$

$$+ (\rho q)_{i+\frac{1}{2},\, j+\frac{1}{2},\, k+\frac{1}{2}}\,(u_{i+\frac{1}{2},\, j+\frac{1}{2},\, k+\frac{1}{2}} - \overset{*}{u}_{u_{i+\frac{1}{2},\, j-\frac{1}{2},\, k+\frac{1}{2}}})\;\Delta S_y +$$

$$+ (\rho q)_{i+\frac{1}{2},\, j+\frac{1}{2},\, k+\frac{1}{2}}\,(u_{i+\frac{1}{2},\, j+\frac{1}{2},\, k+\frac{1}{2}} - \overset{*}{u}_{u_{i+\frac{1}{2},\, j+\frac{1}{2},\, k-\frac{1}{2}}})\;\Delta S_z\;], \tag{3.45}$$

where the summation extends over all subsonic points downstream of supersonic/subsonic shock waves. In equation (3.45), there is taken

$$\left.\begin{aligned} \Delta S_x &= (\Delta y\, \Delta z)_{i+\frac{1}{2},\, j+\frac{1}{2},\, k+\frac{1}{2}} , \\ \Delta S_y &= (\Delta z\, \Delta x)_{i+\frac{1}{2},\, j+\frac{1}{2},\, k+\frac{1}{2}} , \\ \Delta S_z &= (\Delta x\, \Delta y)_{i+\frac{1}{2},\, j+\frac{1}{2},\, k+\frac{1}{2}} . \end{aligned}\right| \qquad (3.46)$$

3.4 First results

In order to illustrate a number of characteristic features of the above discussed method to predict wave drag in potential flow, and to inspire confidence in its results, a number of experiments has been carried out for a simple non-swept wing of constant chord and constant section profile. The semi-wing planform is shown in figure 7. The aspect ratio of the full wing is approximately AR ≅ 5; the upstream Mach number is M_∞ = .77; the angle of attack is α=6°. The section profile of the wing is the same symmetric profile as is used in the 'ONERA M6 wing' wind tunnel model, and consequently this wing will be referred to as the 'M6 test wing'. Calculations are made using MATRICS in the fully-conservative as well as in the non-conservative mode. For the fully-conservative case, the isobar pattern on the wing upper surface is also shown in figure 7. As can be expected, the pressure distribution is almost two-dimensional in the vicinity of the mid-span section. The pressure distribution for the mid-span section is shown in figure 8 for the fully-conservative as well as for the non-conservative solution. It can be observed from figure 8 that the mid-span section carries only one supersonic/subsonic shock wave with approximately the same pressure (and consequently also approximately the same upstream Mach number) for both the fully-conservative and the non-conservative solution. Hence the situation is locally particularly well suited to check numerical results against what must theoretically be expected. Evidently, the supersonic/subsonic shock wave at the mid-span section is much stronger for the fully-conservative solution, and this should reflect in the local contribution to the wave drag. An additional advantage at the mid-span section is, that there the down wash is no doubt smallest whereas the strong shock wave is at its strongest. It can then be expected that the local static pressure drag is only slightly higher than the local wave drag. All calculations shown in figures 7, 8 were carried out on a computational grid involving 176 * 32 * 32 primary cells and are well converged. Since MATRICS is a multigrid code, the results for the corresponding 88 * 16 * 16 and 44 * 8 * 8 grids are also available. Note that the 176 * 32 * 32 grid is a normal production grid for engineering applications.

The results obtained for the wave drag on the 'M6 test wing' can best be discussed in terms of a number of specified contributions. These are, compare equations (3.18), (3.26), (3.27), (3.42) and figures 4, 5,

$$Dw_{SR} = \int_{S_s} \{(p_d - \overset{*}{p}_u)n_x + \rho_d q_{n,d}(n_d - \overset{*}{u}_u)\}dS \quad , \qquad \text{(SR: Shock Remainder)} \qquad (3.47)$$

$$Dw_G = -\int_{V_{M>1, q_s<0}} \varepsilon\rho(1 - M^2)\, u_s\, q_s\, \Delta s\, dV \quad , \qquad \text{(G: Garabedian)} \qquad (3.48)$$

$$Dw_{G,\,spur} = -\int_{V_{M>1, q_s>0}} \varepsilon\rho(1 - M^2) u_s\, q_s\, \Delta s\, dV \quad , \qquad \text{(G,spur: Garabedian, spurious)} \qquad (3.49)$$

$$Dx_{mass} = \int_{S_s} \bar{M}(\overset{*}{u}_u - u_\infty)\, dS \quad . \qquad \text{(mass: excess mass in the non-conservative case)} \qquad (3.50)$$

Then

$$Dw = Dw_{SR} + Dw_G . \qquad (3.51)$$

$Dw_{G,spur}$ is a spurious contribution that tends to zero with vanishing mesh size. Dx_{mass} is a spurious contribution that shows up in the static pressure drag Dp as calculated from surface-integration in the non-conservative case, as a consequence of the excess mass created by the non-conservative finite-volume scheme. Dx_{mass} does not tend to zero with vanishing mesh size, but approaches a constant value. Quantification of Dx_{mass} is straightforward. $\bar{M}$ can be measured by simply substituting the non-conservative solution in the fully-conservative shock operators. Since $\bar{M}$ is in fact created at approximately sonic grid points (e.g. the grid points $(i-\frac{1}{2}, j+\frac{1}{2}, k+\frac{1}{2})$, $(i+\frac{1}{2}, j+\frac{1}{2}, k-\frac{1}{2})$, $(i+\frac{1}{2}, j-\frac{1}{2}, k+\frac{1}{2})$ in the example of Fig. 6), it suffices to multiply the mass created at each such grid point with the local value of $u - u_\infty$ and sum up the resulting x-momenta.

The results obtained for the 'M6 test wing' for the full wing as well as for the mid-span section are summarized in table 1. First consider the results for the mid-span section in relation with the pressure distributions of figure 8. On the 176 * 32 * 32 grid, the Garabidean type contribution to the wave drag is slightly higher in the fully-conservative case (cdw_G = 367 counts) than in the non-conservative case (cdw_G = 320 counts), as suggested by the slightly higher upstream pressure in the fully-conservative case. However, the contribution of the shock remainder is much stronger in the fully-conservative case (cdw_{SR} = 434 counts) than in the non-conservative case (cdw_{SR} = 126 counts), as indeed it should. In the fully-conservative case, the total wave drag (cdw = cdw_{SR} + cdw_G = 801 counts) is indeed slightly lower than the static pressure drag (cdp = 821 counts) as was expected before. In the non- conservative case, the total wave drag (cdw = 446 counts), however, is considerably lower than the static pressure drag (cdp = 641 counts); the reason is that the static pressure drag contains a spurious contribution (cdx_{mass} = 173 counts) due to the excess mass created by the non-conservative shock capture; therefore the static pressure drag should be compared instead with cdw + cdx_{mass} = 619 counts, after which the same tendency as with the fully-conservative case is indeed observed. Both in the fully-conservative and in the non-con-

servative case the spurious Garabedian type contribution ($CDw_{G,spur}$, corresponding to acceleration, and being of the order of the mesh size) can be observed to diminish as the grid gets finer. However, the point where it halves upon mesh-halving is evidently not yet reached. This illustrates very clearly that finer grids are required for really accurate results. How much finer the grids should be cannot be estimated from the available results, and requires more elaborate convergence experiments. The situation could be improved by introducing a second order accurate finite-volume scheme in supersonic parts of the flow, away from smeared out shock waves. In particular, this would reduce the spurious Garabedian type contribution.

Next consider the results for the full wing. The only difference with the above discussion on the results for the mid-span section is in fact, that now the static pressure drag must be compared with the total drag, being estimated here as the sum of the wave drag and the induced drag ($CD_{tot} \cong CDw + CDi$). Remarkably, it can be observed that the difference between the static pressure drag (CDp) and the total drag (CD_{tot}) in the fully-conservative case, respectively the sum of the total drag and the spurious drag due to the excess mass (CDx_{mass}) in the non-conservative case, increases upon grid refinement. A possible explanation is that true convergence upon grid refinement is not possible in the tip regions for a CH-topology grid, while this tip region has comparatively much influence with the present constant chord wing of only aspect ratio AR ≅ 5.

As an illustration of a more realistic application, the wave drag has also been calculated for the 'DFVLR-F4 wing' which is representative for a transonic transport wing. The flow conditions are $M_\infty = .75$, $\alpha = .84°$. The wing planform and the upper surface isobar pattern are shown in figure 9. The same case has been the subject of an extensive accuracy study in the GARTEUR framework (compare Ref. 17). Calculations have been made using MATRICS in the fully-conservative as well as in the non-conservative mode on a 176 * 32 * 32 grid, which is typical for engineering applications. As the flow is particularly three-dimensional in character on the inner portion of the wing (compare Fig. 9), the fully-conservative calculation was repeated on a 176 * 56 * 32 grid with improved spanwise resolution. The results are summarized in table 2. Note that the wave drag in the non-conservative case (CDw = 27.5 counts) is slightly lower than in the fully-conservative case (CDw = 29.0 counts) on the same 176 * 32 * 32 grid. This can indeed be expected, because the dominating supersonic/subsonic shock wave on the outer portion of the wing (Fig. 9) moves upstream and becomes weaker when going from a fully-conservative to a non- conservative scheme (compare Ref. 17). However, if the spanwise resolution is improved on the 176 * 56 * 32 grid, the wave drag in the fully-conservative case drops from CDw = 29.0 counts to CDw = 26.4 counts, which is even slightly lower than the non-conservative value obtained on the 176 * 32 * 32 grid (CDw = 27.5 counts). Note also, that in all three cases calculated, the spurious Garabedian type contribution to the wave drag ($CDw_{G,spur}$, corresponding to acceleration) is about 50 % of the wave drag CDw. Like with the 'M6 test wing' it is obvious from the results obtained, that further grid refinement is mandatory for accurate drag prediction. Again, second order accurate schemes in supersonic parts of the flow, away from smeared out shock waves, would improve the situation. Nevertheless, it is encouraging that the theoretical drag balances $CDw + CDi + CDw_{G,spur} \cong CDp$ in the fully-conservative case, and $CDw + CDi + CDx_{mass} + CDw_{G,spur} \cong CDp$ in the non-conservative case, are satisfied within 3 % of the total drag value CD_{tot}. A final comment in view of the results obtained is the following. If in the non-conservative case on the 176 * 32 * 32 grid, the spurious drag due to the excess mass (CDx_{mass}) which appears as part of the surface-integrated static pressure drag (CDp) would be counted as wave drag, this would lead to an (erroneous) wave drag of $CDw + CDx_{mass} = 27.5 + 15.6 = 43.1$ counts well in excess of the corresponding 29.0 counts in the fully-conservative case. This would be in total disagreement with the pressure distributions in both cases which indicate that the fully-conservative solution with the stronger shock waves has the largest wave drag (compare Ref. 17). This also underlines the correctness of Garabedian's point of view, that the spurious drag due to the excess mass (CDx_{mass}) created with non-conservative schemes must be disregarded (compare Ref. 2 and also section 3.1).

In completion of this section on first results, it seems appropriate to pay attention to the usefulness of the method described for predicting wave drag from potential theory to visualize where wave drag originates in the flow field. A good illustration is the well known 'ONERA M6 wing' at $M_\infty = .84$, $\alpha = 6°$ (Fig. 10) where a strong supersonic/subsonic rear shock and a much weaker supersonic/supersonic forward shock appear on the wing upper surface. For the sections at 13 % and 39 % span the wave drag is visualized in figure 11 by plotting iso-lines of the wave drag contributions in each grid point expressed per unit volume. The rear and the forward shock are clearly distinghuised. Note that the outer iso-line enveloping each smeared out shock is taken to be the iso-line of zero wave drag contribution, signifying the boundary between decelerating and accelerating flow. Note also, that in particular the iso-lines at the rear shock show a typical zigzag behaviour which is apparently due to misalignment of the shock and the gridplanes. Upon grid refinement this visualization technique might also be helpful in distinguishing between shocks and isentropic recompressions.

3.5 Conclusions

A method has been developed to calculate wave drag in transonic potential flow. The method is based on a generalization and extension of Garabedian's and McFadden's work (Refs. 2, 3, 4) where wave drag is determined by volume-integration of the artificial viscosity. The generalization utilizes the concept of a reference artificial viscosity which can be quantified for a particular full-potential code provided that the structure of the artificial viscosity used for that code is known. This has the advantage that calculated wave drag is to a certain extent independent of the specific details of the artificial viscosity used in that particular code. Because artificial viscosity in full-potential codes is used only in supersonic parts of the flow, it was observed that supersonic/subsonic shock waves are not smeared out completely under the action of artificial viscosity. Rather, there exists a sonic/subsonic 'shock remainder' that appears as a true discontinuity in the solution of the modified full-potential equation representing the discretization. This shock remainder constitutes a substantial contribution to the wave drag that must be added to the Garabedian/McFadden type contribution. The implementation of this extension and the above mentioned generalization to a reference artificial viscosity were discussed for the NLR full-potential code MATRICS.

The method was demonstrated for fully-conservative as well as non-conservative capture of supersonic/subsonic shock waves. Numerical examples for a simple non-swept constant chord wing and a wing representative for transonic transport aircraft show the correct tendencies in comparing the wave drag for fully-conservative and non-conservative solutions. Also, the wave drag counts obtained have the proper order of magnitude. Furthermore, it became clear, however, that finer grids than are currently being used in MATRICS for engineering applications are mandatory for sufficient accuracy of the wave drag prediction; this will require the computing power of modern super-computers. Second order accurate schemes in supersonic parts of the flow, away from smeared out shock waves, would improve this situation.

The method is useful to visualize where wave drag originates in the flow field and can be used to distinghuish between shock waves and isentropic recompressions through a process of grid refinement.

The method can be extended to handle also quasi Rankine-Hugoniot supersonic/subsonic shock waves (compare Ref. 7) where the creation of excess mass in the shock wave is prescribed rather than spontaneous as with non-conservative shock capture.

4. REFERENCES

1. J.W. Slooff, Computational Drag Analysis and Minimization, Mission Impossible?, NLR MP 85080 U, 1985.

2. P.R. Garabedian, Computation of Wave Drag for Transonic Flow, Journal d'Analyse Mathématique, Vol. 30, pp. 164-171, 1976.

3. P. Garabedian and G. McFadden, Computational Fluid Dynamics of Airfoils and Wings, Proceedings of Symposium on Transonic, Shock and Multidimensional Flows, University of Wisconsin, Madison, 1981. Academic Press Inc., 1982.

4. P. Garabedian and G. McFadden, Design of Supercritical Swept Wings, AIAA Journal, Vol. 20, No. 3, March 1982. AIAA paper 82-4058, 1982.

5. R.C. Lock, Prediction of the Drag of Wings at Subsonic Speeds by Viscous/Invicid Interaction Techniques, AGARD Lecture Series on 'Drag Prediction and Reduction', 1985.

6. R.C. Lock, The Prediction of the Drag of Aerofoils and Wings at High Subsonic Speeds, Aeronautical Journal, June/July, 1986.

7. M. Hafez and D. Lovell, Entropy and Vorticity Corrections for Transonic Flows. AIAA paper 83-1926, 1983.

8. J. van der Vooren, J. Th. van der Kolk and J.W. Slooff, A System for the Numerical Simulation of Sub- and Transonic Viscous Attached Flows around Wing-Body Configurations, AIAA paper 82-0935, 1982. Also NLR MP 82019 U, 1982.

9. Th. E. Labrujere, W. Loeve and J.W. Slooff, An Approximate Method for the Calculation of the Pressure Distribution on Wing-Body Combinations at Sub-Critical Speed, AGARD CP. No. 71, paper 11, 1970.

10. J.P.F. Lindhout, G. Moek, E. de Boer and B. van den Berg, A method of the Calculation of 3-D Boundary Layers on Practical Wing Configurations, Paper presented at the joint ASME/CSME Applied Mechanics, Fluids Engineering and Bio-engineering Conference, Niagara Falls, NY, June 1979, Transactions of the ASME, March 1981. Also NLR MP 79003 U, 1979.

11. N. Voogt, W.J.A. Mol, J. Stout and D.F. Volkers, CFD Applications in Design and Analysis of the Fokker 50 and 100, Paper presented at the AGARD 62nd FDP Symposium on Validation of Computational Fluid Dynamics, Lisbon, Portugal, 2-5 May, 1988.

12. A.C. de Bruin, Private Communication.

13. N.J. Yu, H.C. Chen, S.S. Samant and P.E. Rubbert, Inviscid Drag Calculations for Transonic Flows, AIAA paper 83-1928, 1983.

14. J. van der Vooren, A. J. van der Wees and J.H. Meelker, MATRICS, Transonic Potential Flow Calculations about Transport Aircraft, AGARD Conference Proceedings No. 412, 1986.

15. D.S. Ross, Redesign of a Supercritical Wing in the Presence of an Engine Nacelle, Journal of Computational Physics 73, pp. 233-243, 1987.

16. J. van der Vooren and A.J. van der Wees, Wave Drag Determination in the Transonic Full Potential Flow Code MATRICS, NLR Technical Report to be published.

17. M.P. Carr, Accuracy Study of Transonic Flow Computations for 3-D Wings, Paper presented at the AGARD 62nd FDP Symposium on Validation of Computational Fluid Dynamics, Lisbon, Portugal, 2-5 May, 1988.

5. ACKNOWLEDGEMENT

The author wishes to express his thanks to A.J. van der Wees, for his substantial contributions and endeavours during the development and implementation of the method to predict wave drag from potential flow.

SCHEME	NON–CONSERVATIVE			FULLY–CONSERVATIVE		
GRID	COARSE	MEDIUM	FINE	COARSE	MEDIUM	FINE
cdw_{SR}, SHOCK REMAINDER	72	94	126	135	348	434
cdw_G, GARABEDIAN	146	269	320	64	254	367
$cdw_{G,spur}$, GARAB. SPURIOUS	81	68	42	84	76	46
cdx_{mass}, EXCESS MASS	76	145	173			
$cdw = cdw_{SR} + cdw_G$, WAVE	218	363	446	199	602	801
cdp, STATIC PRESSURE	419	584	641	443	699	821
$cdw + cdx_{mass}$	294	508	619			

SCHEME	NON–CONSERVATIVE			FULLY–CONSERVATIVE		
GRID	COARSE	MEDIUM	FINE	COARSE	MEDIUM	FINE
CDw_{SR}	40	47	65	63	165	205
CDw_G	69	144	180	57	140	189
$CDw_{G,spur}$	62	54	35	66	60	39
CDx_{mass}	42	89	104			
$CDw = CDw_{SR} + CDw_G$	109	191	245	120	305	394
CDi	193	230	251	210	283	327
$CDtot \cong CDw + CDi$	302	421	496	330	588	721
CDp	313	465	528	325	530	637
$CDtot = CDw + CDx_{mass}$	344	510	600			

COARSE 44 * 8 * 8 MEDIUM 88 * 16 * 16 FINE 176 * 32 * 32

Table 1. Drag counts for the 'M6 test wing' at $M_\infty = .77$, $\alpha = 6^\circ$

NON–CONSERVATIVE BALANCE:
$CDp \cong CDw + CDi + CDw_{G,spur} + CDx_{mass}$

FULLY –CONSERVATIVE BALANCE:
$CDp \cong CDw + CDi + CDw_{G,spur}$

WITHIN 3% CDtot

SCHEME	NON–CONS.	FULLY–CONSERVATIVE	
GRID	176*32*32	176*32*32	176*56*32
CDw_{SR}, SHOCK REMAINDER	7.7	10.3	8.0
CDw_G, GARABEDIAN	19.8	18.7	18.4
$CDw_{G,spur}$, GARAB. SPURIOUS	14.4	15.7	13.1
CDx_{mass}, EXCESS MASS	15.6		
$CDw = CDw_{SR} + CDw_G$, WAVE	27.5	29.0	26.4
CDi, INDUCED	257.6	274.1	279.1
$CDtot \cong CDw + CDi$, TOTAL	285.1	303.1	305.5
CDp, STATIC PRESSURE	316.6	327.3	327.8
$CDtot + CDx_{mass}$	300.7		

Table 2. Drag counts for the 'DFVLR-F4-wing' at $M_\infty = .75$, $\alpha = .84^\circ$

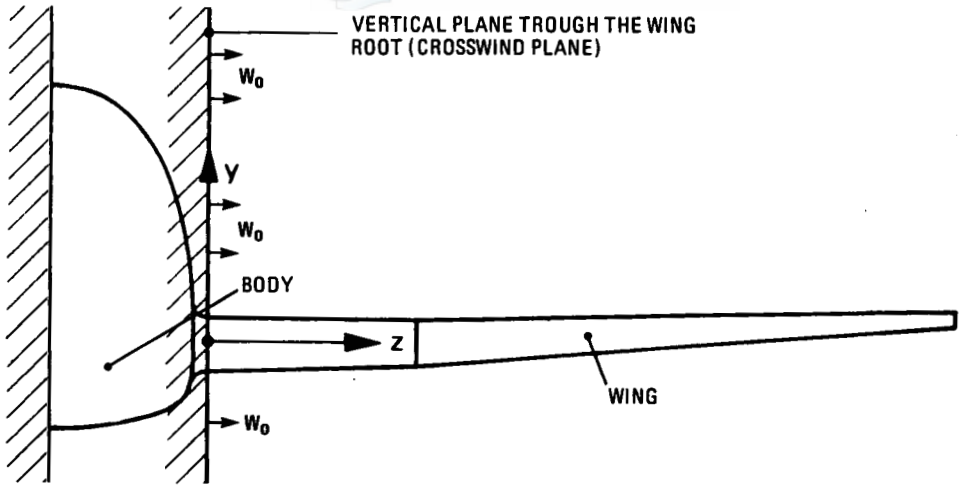

Fig. 1 The 'X-wind' concept in XFLO22

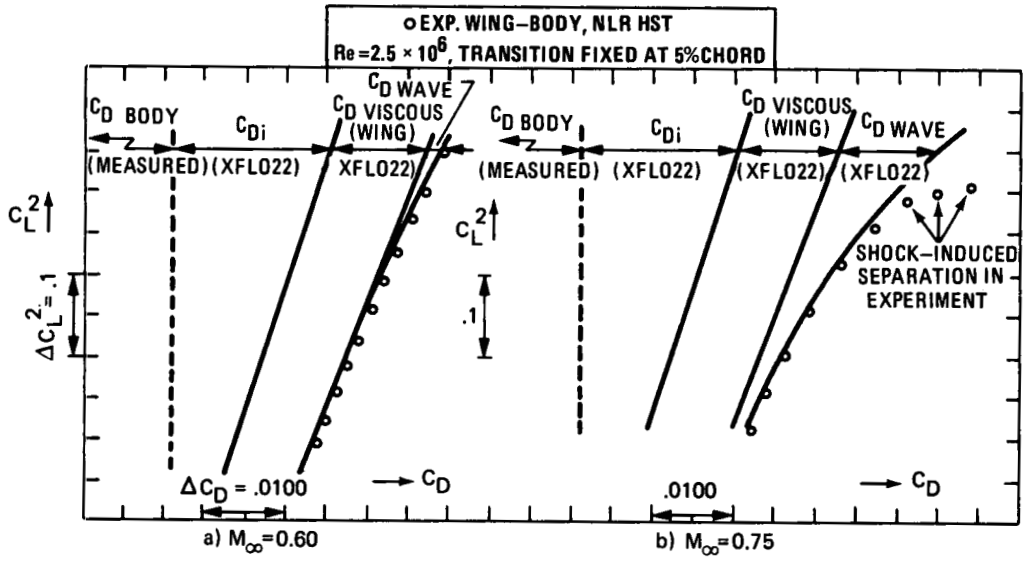

a) DRAG CORRELATION AT CONSTANT MACH NUMBER

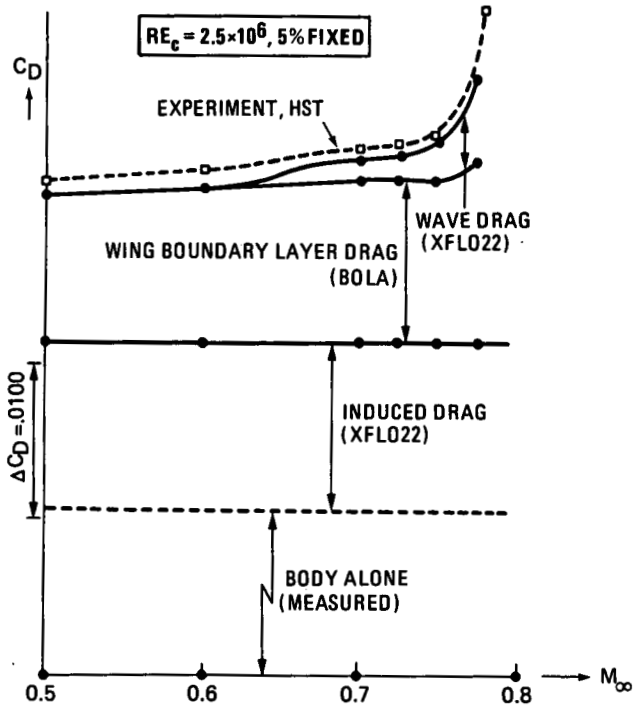

b) DRAG CORRELATION AT CONSTANT LIFT

Fig. 2 NLR XFLO22 drag analyses for narrow-body transport configuration

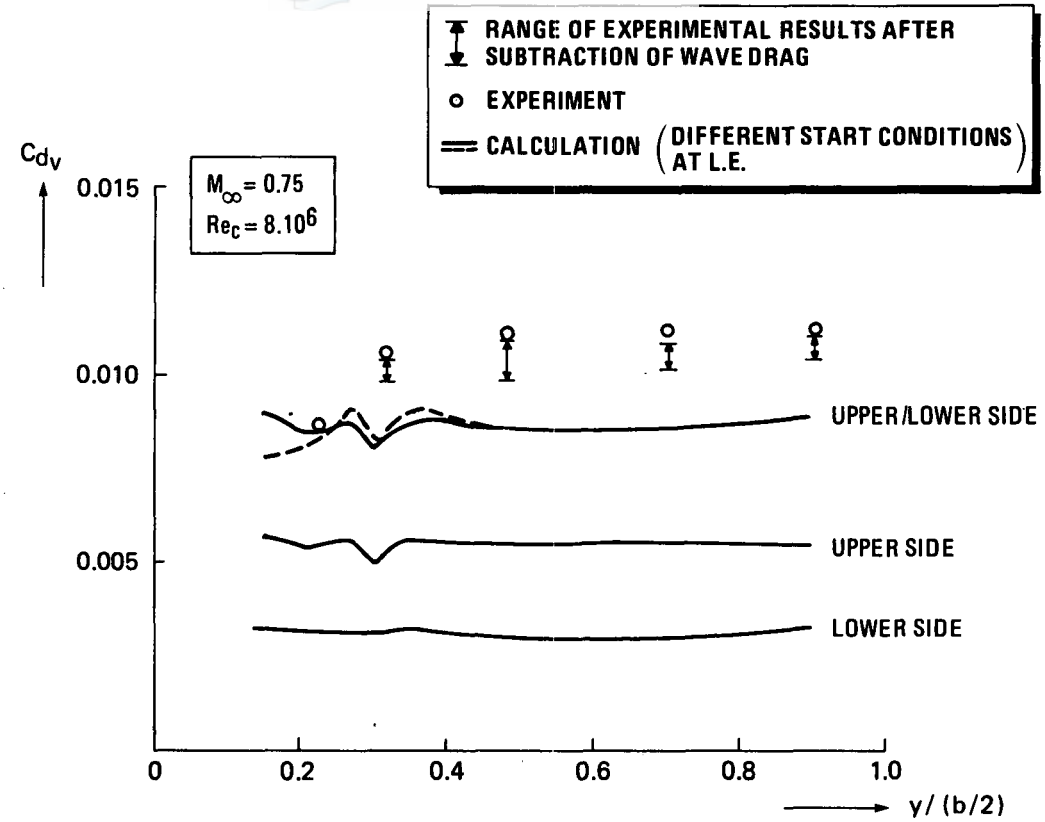

Fig. 3 Comparison of experimental (wake rake) and calculated viscous drag distribution for transport type wing

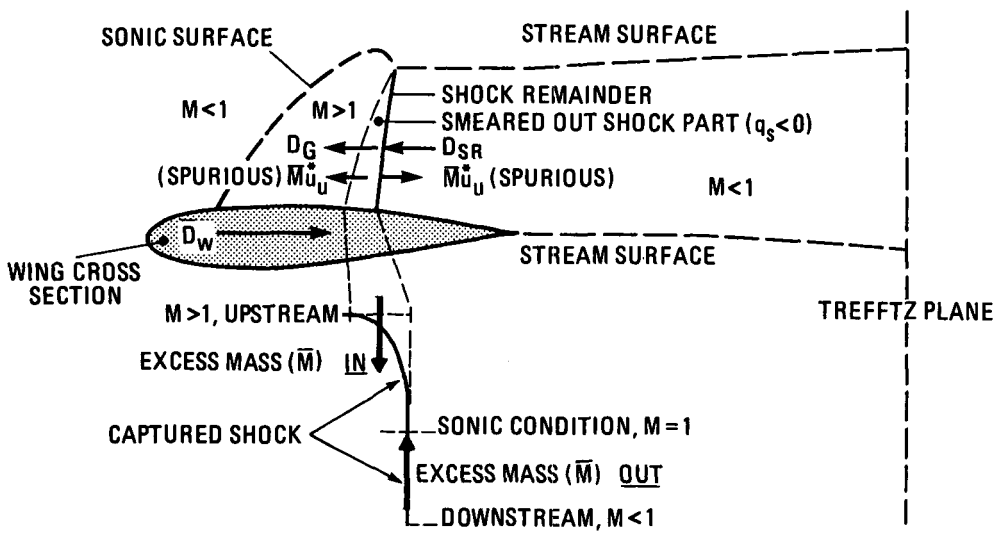

CANCELLING 'SPURIOUS' CONTRIBUTIONS !

$$\text{WAVE DRAG: } D_W = D_G + \overbrace{\int_{S_s} \bar{M}u^* dS - \int_{S_s} \bar{M}u^* dS} + D_{SR}$$

$$\text{GARABEDIAN DRAG: } D_G = \int_{V_{M>1,\, q_s<0}} (Pu_x + Qu_y + Ru_z)\, dV, \begin{pmatrix} P \\ Q \\ R \end{pmatrix} - \text{ARTIFICIAL VISCOUS FLUXES}$$

$$\text{SHOCK REMAINDER DRAG: } D_{SR} = \int_{S_s} \{(p_d - p_u^*) + \rho_d q_{n,d} (u_d - u_u^*)\} dS$$

Fig. 4 Wave drag build-up; fully-conservative

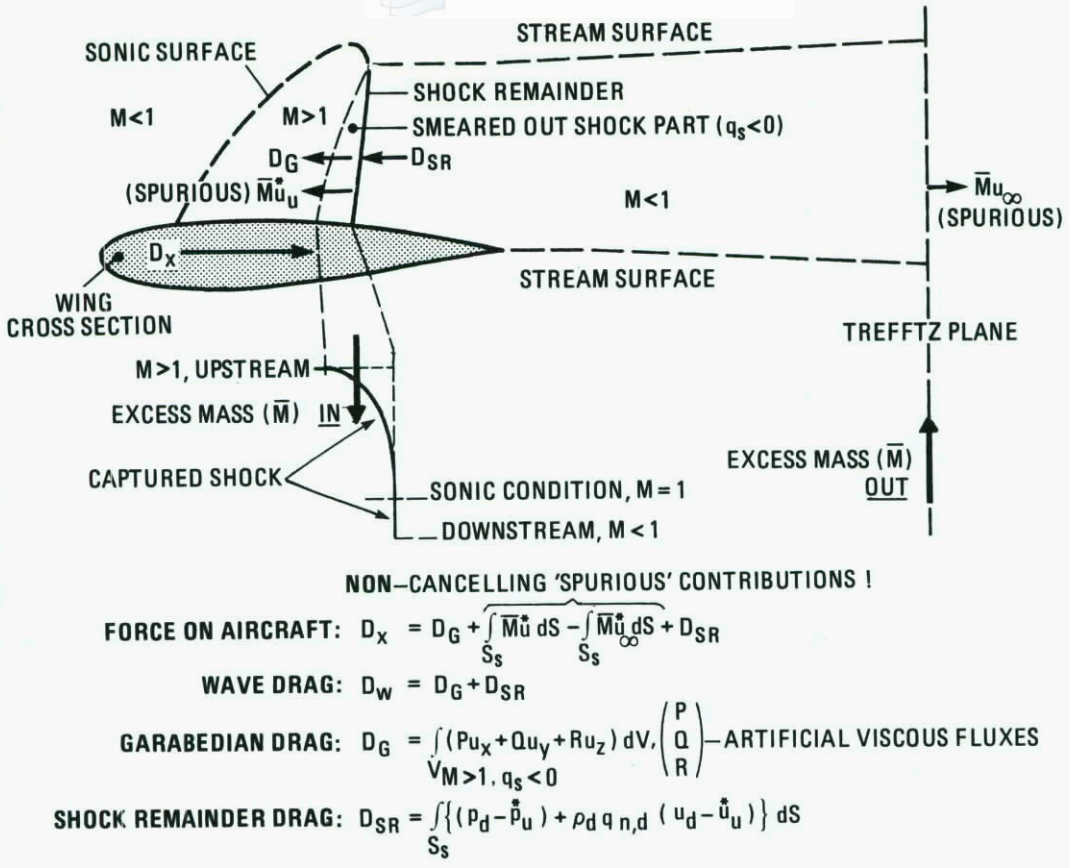

NON–CANCELLING 'SPURIOUS' CONTRIBUTIONS !

FORCE ON AIRCRAFT: $D_X = D_G + \overbrace{\int_{S_s} \bar{M}u^* \, dS - \int_{S_s} \bar{M}u_\infty^* \, dS} + D_{SR}$

WAVE DRAG: $D_W = D_G + D_{SR}$

GARABEDIAN DRAG: $D_G = \int_{V_{M>1,\, q_s<0}} (Pu_x + Qu_y + Ru_z) \, dV, \begin{pmatrix} P \\ Q \\ R \end{pmatrix}$ – ARTIFICIAL VISCOUS FLUXES

SHOCK REMAINDER DRAG: $D_{SR} = \int_{S_s} \{ (p_d - p_u^*) + \rho_d q_{n,d} (u_d - u_u^*) \} \, dS$

Fig. 5 Wave drag build-up; non-conservative

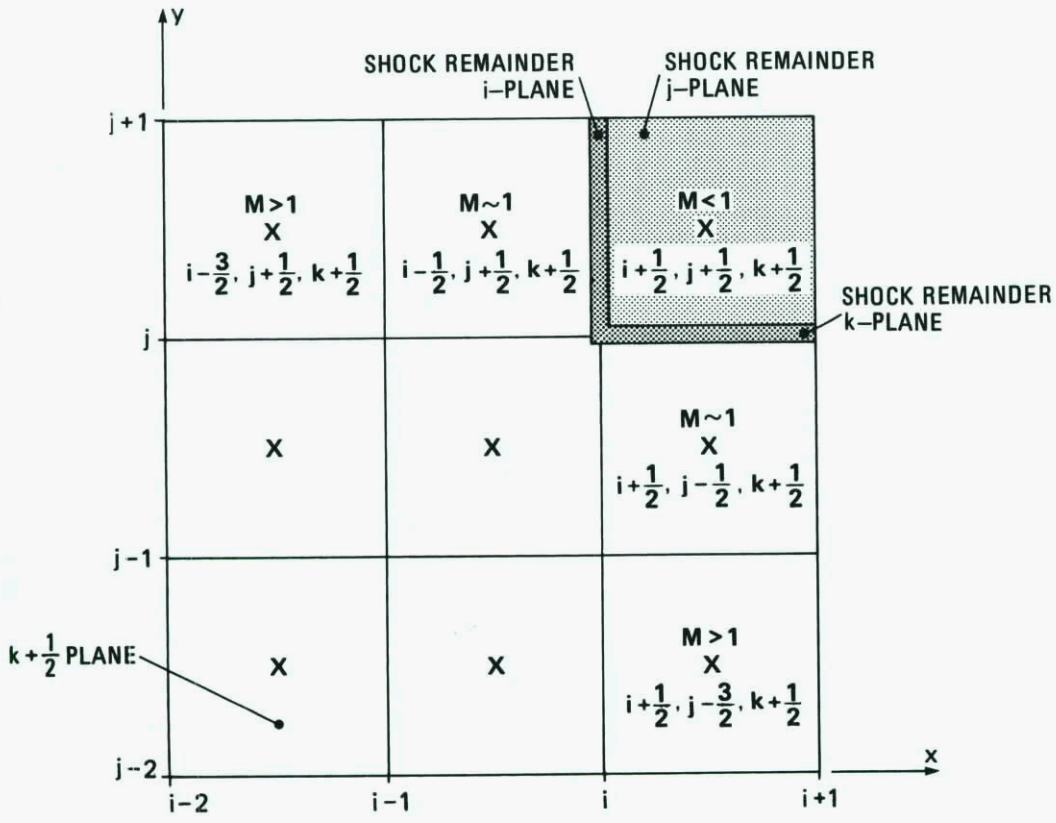

Fig. 6 Capture of shock remainders in MATRICS

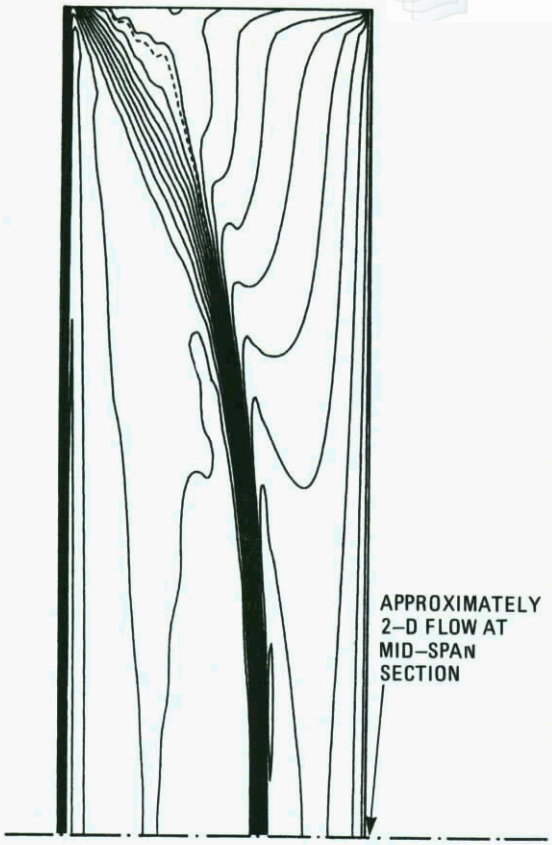

Fig. 7 Simple non-swept constant chord wing with M6 section profile (M6 test wing), showing the upper surface isobars at M_∞=.77, $\alpha = 6^o$

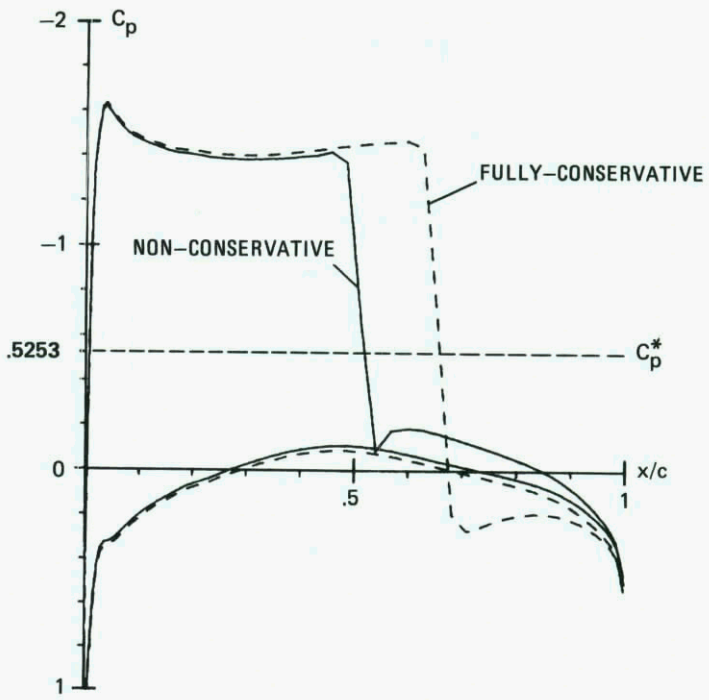

Fig. 8 Pressure distributions for the mid-span section of the 'M6 test wing at M_∞=.77, $\alpha = 6^o$

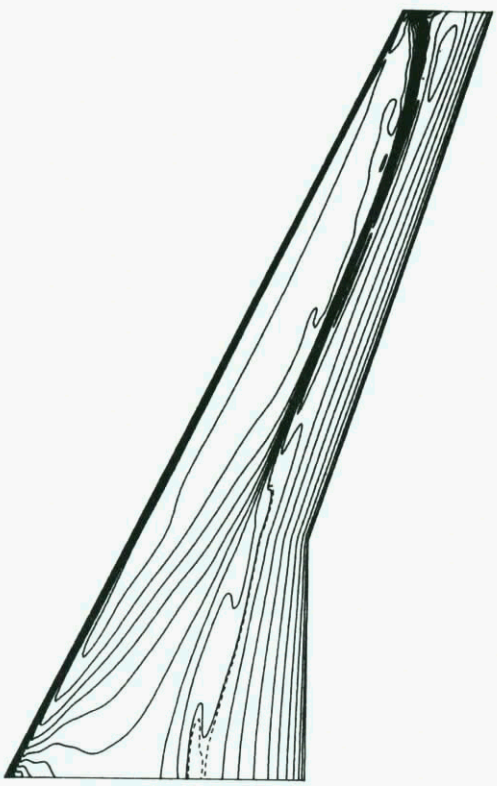

Fig. 9 Planform of the 'DFVLR-F4-wing', and upper surface isobars for the transonic condition M_∞=.75, α =.84°

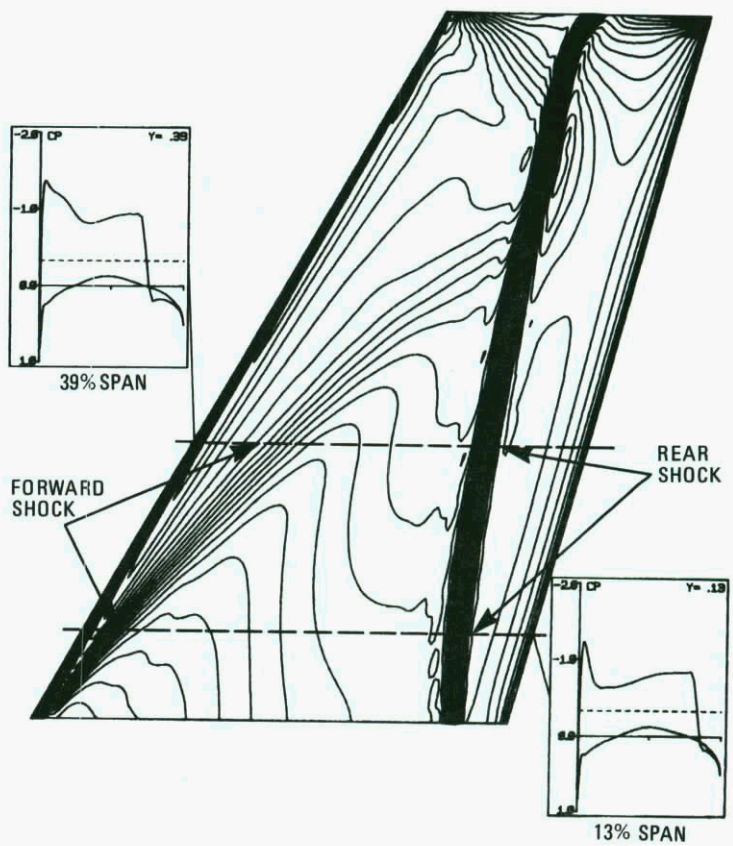

Fig. 10 Upper surface isobars on the 'ONERA M6 wing' at M_∞=.84, $\alpha = 6^o$

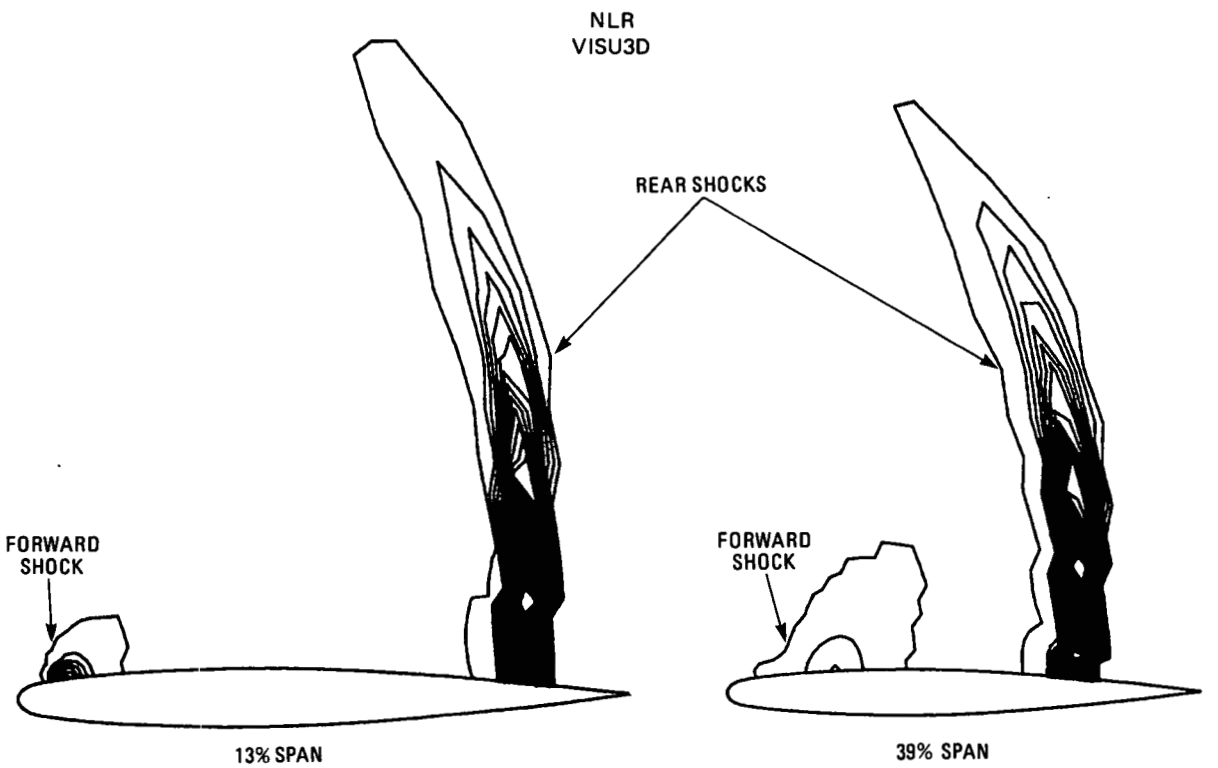

Fig. 11 Visualization of wave drag on two sections of the 'ONERA M6 wing' at M_∞=.84, α = 6°

CFD METHODS FOR DRAG PREDICTION AND ANALYSIS CURRENTLY IN USE IN UK

by

P.R. Ashill
Procurement Executive,
Ministry of Defence
Royal Aircraft Establishment
Bedford MK41 6AE
England

SUMMARY

Computational methods developed in UK for the prediction of the drag of aircraft components at subsonic and supersonic speeds are critically reviewed. In many cases, the flow modelling is found to be lacking in certain respects. Despite this, however, the review suggests that these methods have a useful function both in the early stages of aircraft design, when they may be used to study differences in the drag of various shapes, and later in support of wind-tunnel tests as a diagnostic tool and also to 'extrapolate' the data to 'full scale'.

LIST OF SYMBOLS

AR	wing aspect ratio
$c(\eta)$	local streamwise chord
C_D	drag coefficient based on wing planform area
$C_D(\eta)$	local drag coefficient based on local chord
C_{D_A}	drag coefficient based on surface area
$C_{D_{cowl}}$	cowl pressure drag coefficient (Fig 24)
C_{D_S}	notional drag coefficient per surface = $C_D/2$
C_{D_F}	drag coefficient based on frontal area
C_f	skin friction coefficient based on free stream dynamic pressure
C_L	lift coefficient based on wing planform area
C_M	pitching moment coefficient based on wing planform area and mean chord, nose up positive
C_p	pressure coefficient
D	drag
M	free stream Mach number
M_N	Mach number of the flow component normal to and just upstream of the shock
R	Reynolds number based on streamwise chord
S	wing planform area
T	plane normal to free-stream vector and downstream of aircraft
z	distance normal to the wing surface
α	angle of incidence
Δ	incremental part of
η	non-dimensional spanwise distance

SUFFIXES

BAL	balance measured
B	body alone
f	skin-friction component
p	normal-pressure component
TV	trailing-vortex component
V	viscous or boundary-layer component
W	wave component
WA	notional wing alone
∞	far upstream

1 INTRODUCTION

In the Technical Evaluation Report of the AGARD Conference on 'Aerodynamic Drag' held at Izmir, Turkey in April 1973, it was concluded that 'a comprehensive drag prediction method, valid for the main classes of aircraft and based entirely on theory, is not likely to be possible for a long time to come'. Fifteen years later, the wholly theoretical prediction of aircraft drag to a satisfactory standard of accuracy is still not possible. However, this period has seen considerable progress in the development of flow algorithms, notably for transonic flows, and a reduction in the cost of computations of at least two orders of magnitude[2].

These developments have encouraged the increasing use of CFD in the design of aircraft from the preliminary stages, through the development phase, to pre-production. In the early stages, approximate CFD methods (eg inviscid methods) provide the project engineer with simple tools for selecting suitable designs. Later, during the development phase, increased reliance is placed on more complex CFD methods, including, for example, viscous effects. Combined with data from carefully-conducted wind-tunnel tests, these methods enable the designer to diagnose sources of excess drag and to predict the drag of modified shapes. Used in this way, the methods need only be reliable in their predictions of small drag differences and thus it is not necessary for the flow modelling to be precise so long as the main features of the flow are represented. At this stage CFD also has an important supporting role in the wind-tunnel tests for

(i) Establishing a basis for simulating full-scale flows in the wind tunnel and, where necessary, extrapolating the tunnel data to full scale;

(ii) Calculating tunnel wall and model support interference.

Although the second application is important it is indirect and is not considered further in this paper.

Finally, before production, it is necessary to guarantee performance predictions from prototype flight-test data, and, in this phase, CFD has a possible role in the interpretation of the flight test data. Again, however, this aspect is not discussed in the paper.

This paper reviews current UK CFD methods for drag prediction. Where possible, the predictions are compared with measurement; otherwise results of calculations are included to illustrate the use of the methods in aircraft design. Because of limitations on the length of the paper the review is not exhaustive but it is hoped that the paper gives the flavour of UK activities in this field.

Following a discussion of general aspects of drag prediction in section 2, the paper reviews methods for subsonic aircraft in section 3 and for supersonic aircraft in section 4.

2 GENERAL CONSIDERATIONS

Two alternative procedures are available for obtaining drag from CFD predictions, as shown in Fig 1; the first or 'local' method involves integration of the streamwise contributions of the forces due to normal pressure and skin friction; the second is a 'field' method requiring an integration over a plane normal to the free stream and downstream of the aircraft, 'T'.

The susceptibility of the 'local' method to truncation errors is well known and results obtained by this technique should always be checked for the effect of grid spacing. The 'field' method may also be sensitive to grid density but, as yet, there is little experience on which to base a judgement of this procedure.

Investigating the drag of an aerofoil inferred from calculations by an inviscid Euler code, Yu et al[3] showed that both the 'local' and 'field' methods incorrectly gave non-zero drag for a subcritical flow. Lock[4] attributed this problem to the generation of spurious entropy near the leading edge. Thus it would appear that further development of flow algorithms is needed before the 'field' method can be used with confidence. On the other hand, with possible enhancements in mind, it may be noted that the 'field' method, unlike the 'local' method, does not depend directly on details of the aircraft geometry and may thus find an application to the prediction of the drag of complex configurations.

With the plane 'T' taken sufficiently far downstream, the various terms in the 'field' integral may be expanded in powers of the perturbation velocities (non-dimensionalised with respect to free-stream speed). Lock[4] showed that, to an order of approximation that is adequate for subsonic transport aircraft at cruise conditions, this expression reduces to the classical 'far field' integral which can be divided into three components as shown in Fig 2.

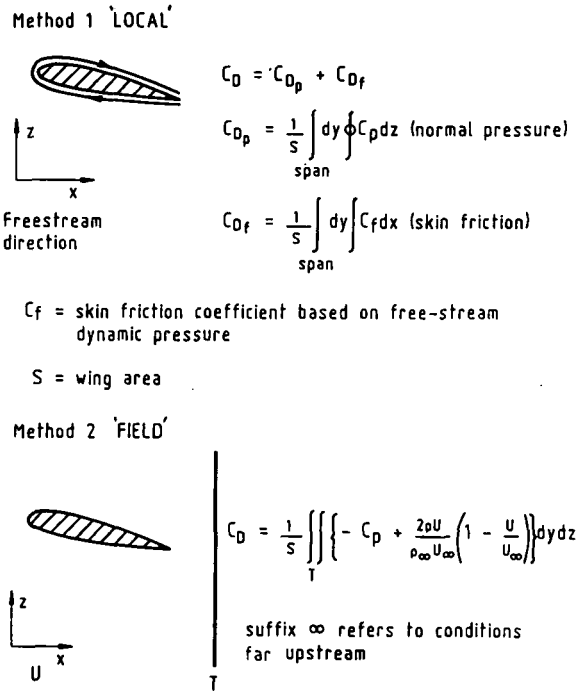

Fig.1 Two methods of determining drag

Lock4 observed that the drag components of wings could be determined most conveniently and accurately by relating flow conditions at 'T' to those on or near the wing. The three drag components are treated as follows:

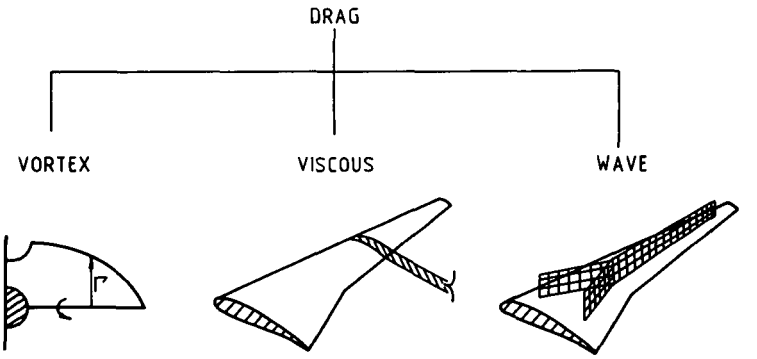

Fig.2 Far field analysis of drag of wings at subsonic speeds

(a) Wave

On the reasonable assumption that the flow downstream of all the shocks is isentropic and adiabatic, wave drag is determined by the reduction in total pressure across each element of the shock system. This statement has no meaning for potential flows but methods have been developed in UK for inferring wave drag from potential-flow solutions. A method for aerofoils at subsonic free-stream speeds due to Billing and Bocci5, which has led to the development of the computer program known as MACHCONT, relates each element of the shock to a Rankine-Hugoniot shock of the same strength, ie having the same Mach number normal to and just upstream of the shock, M_N . Billing and Bocci also assumed that the local flow is normal to the shock. This assumption is reasonable for inviscid flows at high subsonic speeds but, in viscous flows, where the interaction beween the shock and the boundary layer causes the shock to be oblique near the aerofoil surface, the method probably overestimates wave drag.

This approach has been generalised to wing flows by Allwright6 except that, in his method, no assumptions are made about the direction of the flow just upstream of the shock.

In cases where details of the flow field are not known or a rapid indication of wave drag is needed, a simple method due to Lock4 is useful. In its two dimensional form, Lock's approach is similar to that of Billing and Bocci except that it uses the assumption that the shock wave lies along the normal to the aerofoil section contour. With this assumption and by retaining only the first term in the Maclaurin expansion with respect to distance from the aerofoil contour for the gradient of shock-upstream Mach number M_N normal to the aerofoil contour, Lock obtained the following expression for wave drag

$$\frac{D_W}{q} = C_{D_W}c = \frac{0.243}{k_w}\left(\frac{1 + 0.2M^2}{M}\right)^3 \frac{(M_{NO} - 1)^4(2 - M_{NO})}{M_{NO}(1 + 0.2M_{NO}^2)} \qquad (1)$$

Here M is free-stream Mach number, k_w is the local curvature of the aerofoil section at the foot of the shock, defined by the suffix O , and q is free-stream dynamic pressure.

Equation (1) implies that, for a given value of M_{NO} , section wave drag in Lock's approximation depends only on the local radius of curvature $1/k_w$. This is an appropriate length scale so long as either (a) the aerofoil curvature changes slowly upstream of the shock or (b) the height of the shock penetration into the field is small compared with $1/k_w$. Thus for wings with both a surface curvature that changes rapidly with streamwise distance and a strong shock, Lock's method may be expected to give inaccurate predictions of wave drag (see section 3.2).

Since Lock's method utilizes the assumption that the shock is normal to the aerofoil contour and is based on wing surface curvature, it does not include the effect of the viscous/inviscid interaction between the boundary layer and the shock.

Lock modified equation (1) to allow for wing sweep by using the assumption that, at each wing section, the flow is identical to that over an infinite yawed wing having the same sweep as the shock.

The determination of wave drag from solutions of the Euler equations is less straightforward than it first appears. As noted above, spurious entropy is invariably produced upstream of the shock from areas such as the wing leading edge where there are rapid changes in shape along the wing chord. Thus wave drag calculations based on the field method can be significantly in error. Attempts to infer the wave drag from the entropy rise across the shock are complicated by numerical errors in the region of the shock. Methods of dealing with this problem have been discussed by Sells7 and Lock4.

(b) Vortex

In order to have any reasonable prospect of calculating this component directly, it is necessary to ignore the rolling up of the trailing-vortex sheet. Considerable

simplification is also possible if the downward inclination of the sheet is ignored, the resulting expression being the classical contour integral around the vortex trace in the Trefftz plane. This approach is probably adequate for high aspect-ratio wings at low to moderate lift[4] (C_L < 0.5) but for low aspect-ratio wings at high lift it must be of questionable accuracy.

(c) Viscous

In two-dimensional flows, viscous drag may be inferred from the solution for the viscous wake far downstream but this would not seem possible for flows over finite wings because of complications arising from wake-edge conditions[4]. Therefore, for wings, or if an accurate solution is not available for the viscous wake in two-dimensional flow, an extended version of the Squire/Young formula allowing for compressibility and wing sweep[4,8] may be used.

Unless otherwise stated, the 'far-field' method is used in drag predictions discussed later. As shown in section 3.2, this simple framework for analysis appears to be justified for subsonic transport aircraft at cruise conditions. For flows with powerful interactions between the viscous shear layers, the shock waves and the trailing vortices, a decomposition of this kind is no longer valid and the scope for diagnostic studies accordingly limited. Furthermore, overall drag would then have to be calculated using either the 'local' or 'field' methods with all the difficulties that implies.

3 METHODS FOR SUBSONIC AIRCRAFT

3.1 Aerofoils

Methods for aerofoils are viewed in UK as a first step towards the development of satisfactory flow algorithms for wings and, as such, have been used to test ideas on various aspects of flow modelling. However, aerofoil methods have progressed to the point of being powerful design tools in their own right and are currently used for tasks such as:

(i) selection of wing sections;

(ii) design of flaps and slats; and

(iii) extrapolation of tunnel data to 'full scale'.

The majority of the methods currently in use in UK (Fig 3) are of the viscous/inviscid interaction type in which calculation of the two parts of the flow is performed interactively and iteratively to numerical convergence. A number of numerical schemes are used, namely Direct (which is only suitable for attached flow), Semi-Inverse (SI) (which may be used for separated flows) and Quasi-Simultaneous (QS) (which is equally effective for both separated and attached flows). Full details of these schemes are given in the review by Lock and Williams[9].

In the remainder of section 3.1, the methods summarised in Fig 3 are reviewed, methods for low speed (and high lift) being considered in section 3.1.1 and techniques for high subsonic speeds in section 3.1.2.

3.1.1 Low speed

UK methods for calculating drag and maximum lift of aerofoils at low free-stream speeds may be summarised as follows:

(i) SIVP (Semi-Inverse Viscous Program)

This method[10] is restricted to single aerofoils, and, as its name suggests, utilises an SI scheme, with a surface-singularity technique for the inviscid flow and integral methods for the shear layers. The turbulent boundary-layers are calculated by the lag-entrainment method[11] while the laminar layers are computed using a compressible version of Thwaites' method[12].

Further allowance is made in the turbulent boundary-layer calculation for the effect on skin friction of low Reynolds-number (ie a local value of momentum-thickness Reynolds number, R_θ, less than about 1000). However, R_θ is not allowed to fall below 320 just downstream of transition, since this a natural limit for a fully-developed turbulent boundary-layer. In addition, the secondary influence of flow curvature on turbulence structure is included in the 'lag' equation.

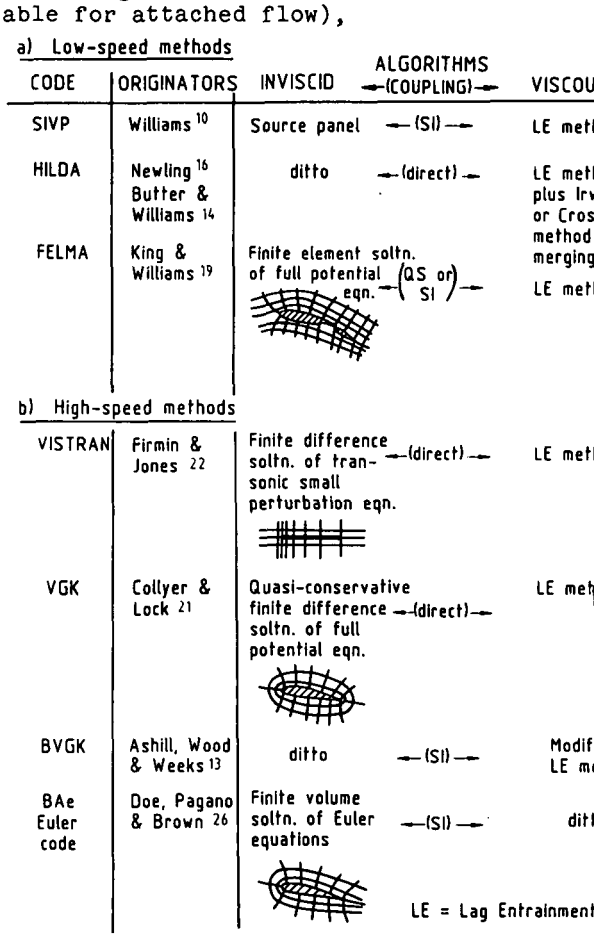

Fig.3 U.K. CFD methods for aerofoil drag prediction

Finally, the standard shape-parameter relationship[11] is replaced by one that is more suitable for separated flows[9]. No allowance is made for the 'higher-order' effects in the streamwise momentum equation due to normal pressure gradients and Reynolds normal stresses. The latter 'higher-order' effect, which is the more important of the two, is not included because correlations of it[13] are of doubtful validity for flows with extensive regions of separation.

While the method gives close predictions of maximum lift, as illustrated for two different aerofoils in Fig 4, it predicts much lower drag than that measured on the aerofoil GA(W)-2 (Fig 5). This discrepancy might be explained by results of calculations which suggest that the transition trips used in this experiment were not adequate over the entire range of incidences tested[9]. The neglect of the Reynolds normal-stress term mentioned above may also be significant.

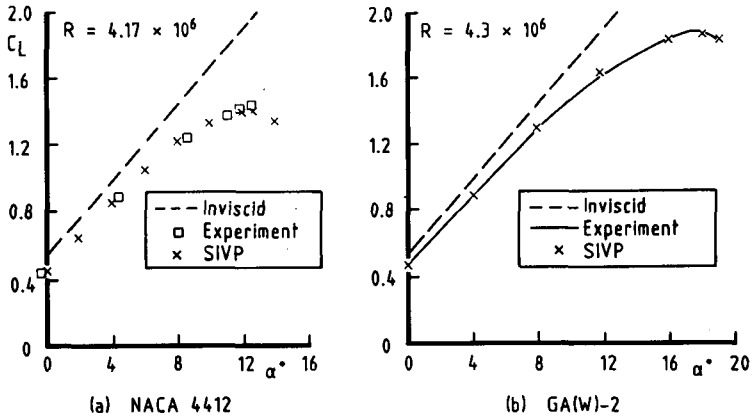

Fig.4 Variation of lift coefficient, C_L, with angle of incidence, α, for two aerofoils

The viscous 'package' in this program has been written so that it can readily be coupled with other inviscid methods, and it has also been used in the FELMA and British Aerospace (BAe) Euler codes described later.

(ii) HILDA (High Lift Design and Analysis)

Developed to calculate flows over multi-element aerofoils, this method[14] uses the Direct coupling scheme of the earlier MAVIS[15] (Multiple Aerofoil Viscous Iterative System) program but has an improved surface-singularity method for the (incompressible) inviscid flow[16]. As in SIVP, the turbulent boundary-layers and isolated wakes are calculated by the lag-entrainment method. No allowance is made for 'higher-order' effects in the streamwise momentum equation but a correction for the influence of low Reynolds number on turbulent skin-friction is included.

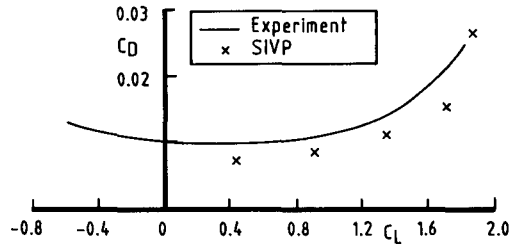

Fig.5 Variation of C_D with C_L for GA(W)-2 aerofoil, R = 4.3 × 10⁶

Merging of the wakes from upstream elements with boundary layers is calculated by the integral method of Irwin[17] and more recently by a method due to Cross[18].

Since the Direct scheme is used, the method fails where separation occurs and thus bubble separations occurring in re-entrant or 'cove' regions are empirically modelled.

Predictions of lift and drag for a three-element aerofoil are shown in Fig 6. The viscous-induced loss in lift is well predicted for angles of incidence, α, up to 20° but, at higher angles, the flow separates on the main aerofoil and consequently the method fails. In Ref 9 it is argued that the good agreement between calculations and measurement at α ≈ 20° is to some extent fortuitous, the lift on the main aerofoil being overestimated while the lift on the other two elements is underestimated.

The estimates of drag are far less satisfactory especially as the stall is approached. As well as the omission of 'higher order' effects referred to above, possible reasons include the lack of compressibility effects in the calculation of the inviscid flow and the inadequacy of the modelling of the aerofoil wake in the region of high flow-curvature above the flap.

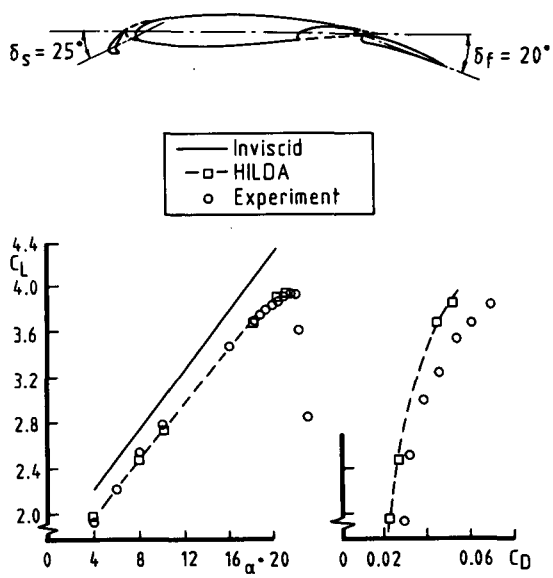

Fig.6 Variation of lift with angle of incidence and drag for a multi-element aerofoil

(iii) FELMA (Finite Element Multiple Aerofoil)

As implied above, compressibility can exert a significant influence on low speed flows over multiple-element aerofoils at high lift particularly where the flow accelerates to high speeds locally, eg at the leading-edge slat. FELMA[19] represents compressibility in the inviscid flow by solving the exact potential equation

numerically by a finite-element technique. As noted previously, the viscous shear layers are calculated by the method used in SIVP but, in contrast to HILDA or MAVIS, FELMA does not represent the merging between wakes and boundary layers. The option is provided to use either SI or QS couplings, allowing flows with separation to be calculated. Of the two schemes, QS is the more efficient, being faster than SI and not requiring a switch from Direct coupling for the attached portion of the flow to SI coupling in regions of separation.

Comparisons of predictions by FELMA and measurements of lift and drag are shown in Fig 7 for the NLR 7301 aerofoil/flap configurations 1 and 2, having, respectively, flap gaps of 2.6% and 1.3% basic aerofoil chord. The calculation of maximum lift is in reasonable accord with measurement for the larger of the two flap gaps but for the smaller gap the maximum lift is overestimated, possibly because an observed interaction between the aerofoil wake and the flap boundary layer is not represented in FELMA.

While some encouragement can be drawn from the drag predictions in Fig 7, it should be noted that the NLR configurations are somewhat idealised in that they do not represent a 'cove' on the main aerofoil. It remains to be seen if FELMA offers improved accuracy over that of HILDA for more practical configurations where the merging of wakes from upstream elements and boundary layers may be an important feature of the flow.

Overall, the present situation in UK as regards the prediction of drag of high-lift aerofoils is not altogether satisfactory. There are reasons to believe that this arises because of defects in the modelling of the wake of the main aerofoil in the region of high flow-curvature above the flap. In this region both streamwise and crosswise pressure gradients are large and hence the flow there is highly elliptic in character. Thus, in order to achieve the required accuracy, it may be necessary to use one of the new generation of methods for solving the Reynolds-averged, Naviers-Stokes equation[20]. However, these methods will only be able to provide the necessary accuracy if turbulence models are found which are suitable for highly-curved wakes[19].

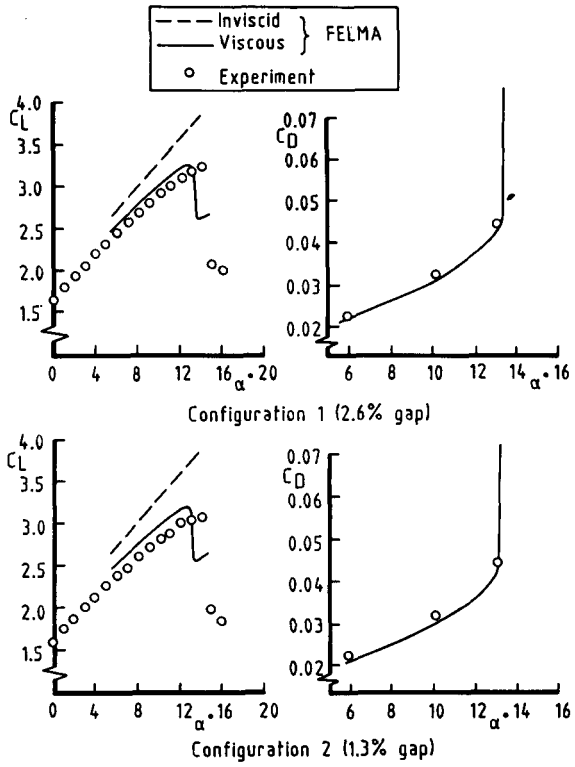

Fig.7 Lift and drag versus incidence, NLR two element (aerofoil/flap) configurations, R = 2.5 × 10^6, M = 0.185

3.1.2 High speed

Because of the importance of being able to estimate accurately section drag for transport-type wings, emphasis has been placed in UK on the development and validation of transonic-flow codes (Fig 3). Methods currently favoured include those based on the assumption that the inviscid flow is potential and others in which the Euler equations are used to simulate the 'outer' flow.

(i) Methods using potential-flow approximation

The code VGK[21] has been the mainstay of wing section design and analysis in UK for over ten years, having superseded the transonic small-perturbation code VISTRAN[22]. VGK couples, in the Direct way, a numerical solution of the full-potential equation with integral methods for the shear layers, the laminar and turbulent layers being calculated, respectively, by Thwaites method[12], extended to allow for compressibility, and the lag-entrainment method[11].

In general, VGK gives satisfactory predictions of drag for attached flows but, where flow separation is approached, the method underestimates drag by a significant margin as shown later. The cause can be traced, in part, to the neglect of 'higher order' effects in the streamwise momentum equation and in the matching between the viscous and inviscid flows. A revised version of the program, known as BVGK, has therefore been developed[13] including these effects together with corrections to the lag-entrainment method similar to those in SIVP described previously. (A slightly different shape-parameter relationship from that of SIVP is used which is considered to be suitable for flows with trailing-edge separation).

Drag is calculated in BVGK by both the 'local' and 'far-field' methods. However, for reasons given in section 2, the 'far-field' method is generally preferred, and predictions of drag by BVGK and VGK shown later have been obtained in this way, using MACHCONT as the subroutine for wave drag.

Examples of predictions by VGK and BVGK of overall forces and pitching moment are shown in Fig 8 for a series of 14% thick aerofoils with relatively-large rear loading. This figure is taken from Ref 23 where details are given of the aerofoils and the wind

tunnel measurements used in the assessment of CFD methods. Here it suffices to note that, at the lower of the two chord Reynolds numbers, $R = 6 \times 10^6$, flow separation is calculated by BVGK to occur on the upper surface of three of the aerofoils, RAE 5225, 5230 and 5234, the chordwise positions of the separation point being at 99%, 95% and 98%, respectively, for $C_L = 0.4$. Hence these flows present a challenge to CFD methods for predicting drag.

Fig 8 reveals that the predictions of drag by BVGK are in good agreement with measurement for flows with weak shocks at both Reynolds numbers. Therefore, by implication, BVGK predicts accurately the differences in drag between sections at a given Reynolds numbers and between Reynolds numbers for a given section. The improvement in agreement with measurement compared with the predictions by VGK is especially evident at $R = 6 \times 10^6$, where, as noted before, separation is calculated to occur on the upper surface of three of the aerofoils. However, the drag estimates by BVGK are less satisfactory where there is significant wave drag ($\Delta C_{DW} > 0.001$). Two possible explanations are given in Ref 23, one related to the fact that MACHCONT assumes that the local flow is normal to the shock wave and the other to the tendency for BVGK to underestimate the rear loading for flows with significant rear separation (notably RAE 5230). A study of possible causes for the latter effect suggests that the correction to turbulence structure for flow curvature is of doubtful validity for separated flows and is probably best ignored in such cases. The result of neglecting this correction is shown in Fig 8 for RAE 5230, the modified calculation being referred to as -CURV. The improved predictions of rear loading with -CURV lead to estimates of pitching moment and drag at the 'drag rise' condition in better agreement with measurement.

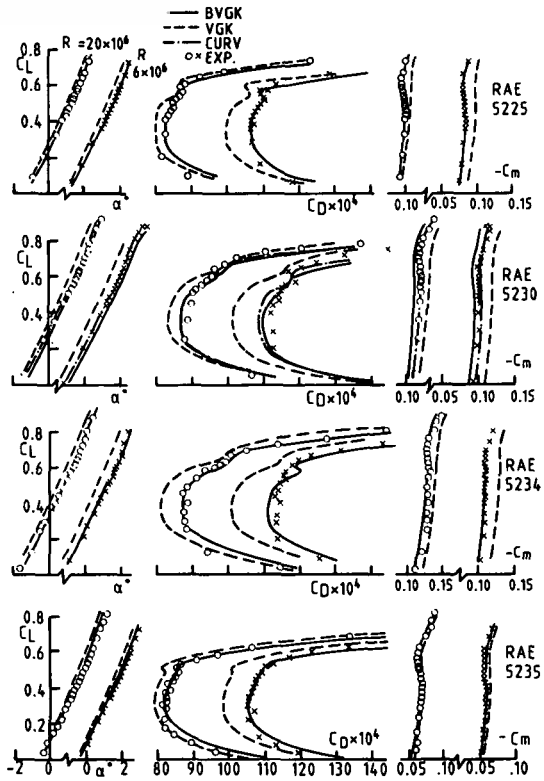

Fig.8 Lift, drag and pitching moment curves, $M \triangleq 0.735$ $R = 6 \times 10^6$ & 20×10^6 (17.7×10^6 RAE 5230)

A version of VGK is available with allowance for wing sweep. Known as SWVGK, this method[24] represents the influence of cross flow on the shear layers but does not include effects allowed for in BVGK, which are known to become important for unswept aerofoils as separation is approached.

The accuracy of the predictions by this method and also by VGK and BVGK of drag differences between sections and between Reynolds numbers have been studied by comparison with data from a panel wing swept at 25°. In this assessment, the effect of sweep on drag in VGK and BVGK is allowed in a simple way as discussed in Ref 23 which also describes the aerofoil sections and the wind-tunnel tests. Here it may be noted that (a) section drag was determined by the wake-rake technique and (b) the wing was cylindrical, of symmetrical section and was tested at zero lift.

Comparisons are shown in Fig 9 between predictions and measurement for the difference in the notional drag-coefficient per surface $C_{DS} = C_D/2$ between the two sections RAE 5237 and 5238 over a range of Mach numbers. These sections are related through calculated boundary-layer characteristics close to the trailing edge to the unswept aerofoil sections RAE 5225 and 5230 (see Fig 8). Of the three methods, the best agreement with measurement is obtained with BVGK, suggesting that the effects shown to be important for unswept aerofoils as separation is approached have a similar significance for wings of moderate sweep.

The effect on the variation with Mach number of the drag coefficient C_{DS} of changing chord Reynolds number from 6.5×10^6 to 14×10^6 is shown in Fig 10. Again, the closest estimates of this change are obtained with BVGK and this figure taken together with Fig 8 shows that BVGK has a potentially-useful role in the extrapolation of wind-tunnel data to 'full scale', at least for wings of moderate sweep and high aspect ratio.

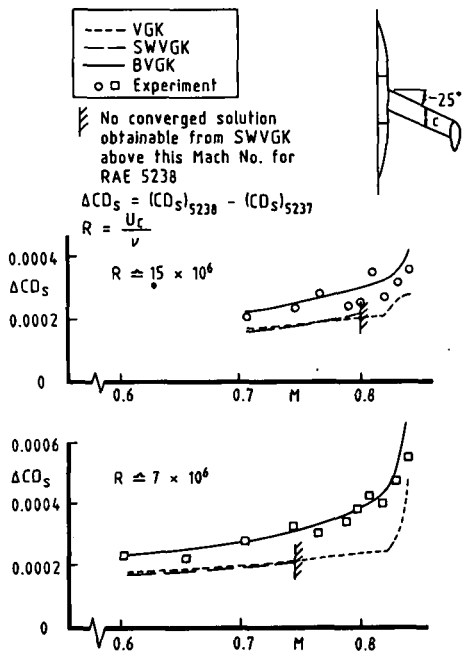

Fig.9 Notional drag per surface of RAE 5238 relative to that of RAE 5237, swept panel model

(ii) Methods based on the Euler equations

A code for the numerical solution of the Euler equations based on the finite-volume method

of Jameson et al[25] has been written at BAe Filton[26]. To permit detailed comparison with experiment, allowance has been made for viscous effects via the method due to Williams[10] ie, using an SI coupling and including certain 'higher-order' effects. Drag is computed using the 'far-field' method, the wave drag being inferred from the loss in total pressure across the shock in the way suggested by Sells[7].

Only limited comparisons with measurement have been published but these indicate that the method gives accurate predictions of drag for the sections RAE 5225 and 5230 at high Reynolds number (Fig 11).

Recently, Hall[27] has developed a multi-grid scheme for solving the Euler equations which, when combined with techniques similar to those mentioned above for solving the shear-flow equations, promises a method for calculating viscous transonic flows over aerofoils that can represent shock waves accurately while being no more costly to run that BVGK.

Johnston[28] has described a method for solving the Reynolds-averaged, Navier-Stokes equations for the transonic flow around aerofoils which is based on the work of Weatherill et al[20] for multiple aerofoils. In this method, Reynolds stresses are modelled using the eddy-viscosity hypothesis combined with an algebraic turbulence-model. Thus the method is probably not reliable for predicting drag for cases with regions of separation near the trailing edge such as those considered previously.

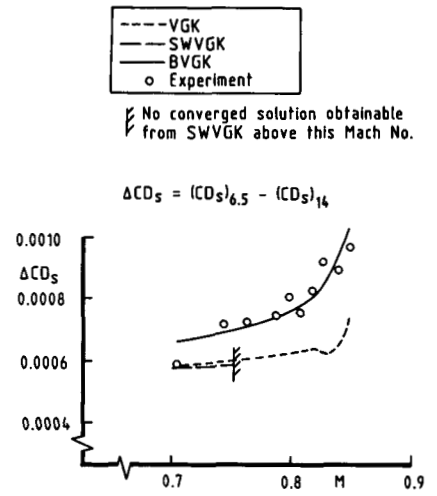

Fig.10 Differences between notional drag per surface at two unit Reynolds numbers, $R = 6.5 \times 10^6$ and $R = 14 \times 10^6$, RAE 5238

3.2 Wings

UK methods for wings are either inviscid or are of the viscous/inviscid interaction type. The viscous versions of these methods are not as advanced as those for aerofoils in the treatment of effects which are significant for flows that are close to separation and consequently cannot yet predict the drag of modern wings with the accuracy demonstrated in Figs 8 to 11. Generally, the viscous versions use Direct coupling, although SI coupling is employed in an approximate way in one method (see later). Despite lacking the accuracy of the aerofoil methods, wing techniques, used with caution and experience, are invaluable aids to design, providing the facility to identify and minimise three-dimensional sources of excess drag.

Fig 12 tabulates the methods. Of the panel methods,[29,30,31,32] that due to Petrie[32] (SPARV) appears to be the most used and is the subject of continuing development. Allowance is included in this method for the effect of wing boundary layers[33]. The inviscid transonic, small-perturbation method of Albone et al[34], with viscous effects incorporated by Firmin[35], is now largely superseded by the more accurate full-potential and Euler methods. The full-potential method of Forsey and Carr[36] (FP) has been used for several years and is generally regarded as a good example of a method of this type. A version of the method, due to Arthur,[37] is available with allowance for viscous effects (VFP). Finally, BAe Filton have programmed a three-dimensional version of the Euler method referred to in section 3.1.2; in this method[26], the shear layers are calculated on the assumption of planar flow at each streamwise section with the solution coupled to the inviscid-flow solver by an SI scheme.

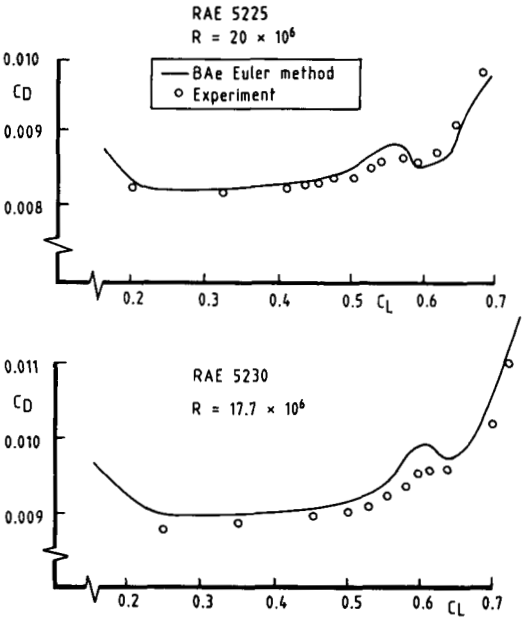

Fig.11 Variation of drag coefficient with lift coefficient, $M \simeq 0.735$

Few results of comparisons of drag predictions by these methods with wind-tunnel experiment are available for publication, and consequently the remainder of the section is concerned with methods of analysing the drag of wings from information provided by the

codes based on the classical 'far-field' approach described in section 2. Results of analysis are presented to illustrate the power of this approach in identifying sources of excess drag.

An analysis of drag is shown for a wing/body suitable for a transport aircraft comprising a wing of aspect ratio 8, with a leading-edge sweep of 28° and a trailing edge sweep outboard of the trailing-edge crank of 14° (Fig 13). In addition, a study of wave drag is presented for a wing representative of that of a subsonic combat-aircraft having leading and trailing edge sweeps 39° and 15° and an aspect ratio 3.3.

(i) Transport aircraft configuration

Comprehensive CFD calculations are not available for this configuration and so the analysis is performed using wing surface pressures measured on a complete model[8]. Limited calculations of wing pressures for this configuration by both the BAe[26] and VFP[37] codes have been found to be in reasonable agreement with measurement (made in the latter case on a related half model).

The form of analysis is illustrated in Fig 14. The body-drag coefficient C_{DB} is determined from tests on the body alone, thereby avoiding the difficulty of determining sting interference. Note that, in choosing the ordinate for this figure, use is made of the fact that the vortex drag is close to the minimum value for a planar wing by subtracting from the drag coefficient $C_{LBAL}^2/\pi AR$, where AR is wing aspect ratio and suffix BAL refers to force-balance measurement. The small excess vortex-drag coefficient.

$$\Delta C_{DTV} = C_{DTV} - C_L^2/\pi AR$$

is determined from the measured span loadings using the classical Treffz-plane method referred to in section 2. Two alternative vortex-trace models have been considered, one allowing for the body in a simple way and the other representing the trace as a planar slit of the same span as the wing. The latter model was chosen for the analysis on the basis that it yields values of overall lift in closer agreement with the balance-measured values than those of the other model. However, the excess vortex drags given by the two models do not differ by much ($\Delta C_D < 0.0002$) suggesting that, where overall lift is known accurately from some other source (in this case the force balance), the drag analysis is not sensitive to the shape of the vortex trace.

Calculated values of ΔC_{DTV} are shown in Fig 15 plotted against lift coefficient for various Mach numbers. Except where there is a rapid increase in vortex drag with lift, the excess vortex drag varies slowly with both lift and Mach number, the sudden increase being attributed to the loss in lift on part of the outer wing following flow breakdown.

Except in special cases, the integrand of the vortex-drag integral or 'local' vortex drag cannot be related to sectional drag; however there is a direct relationship between 'local' vortex drag and span loading, and, in the present case, the cause of the non-zero excess vortex-drag is that the outer wing is relatively lightly loaded compared with the ideal elliptic loading.

a) Panel methods

ORIGINATORS	INVISCID ALGORITHM	VISCOUS ALGORITHM
Roberts & Rundle[29,30]	Bi-cubic spline panels and source distributions 	P.D. Smith, 3D integral entrainment boundary layers only[40]
Hunt & Semple[31]	Source panel vortex surface	—
Petrie[32]	Source patch and ring vortex (SPARV)	Cross[33]

b) Field methods

Albone, Hall & Joyce[34] Firmin[35]	Transonic small perturbation 	P.D. Smith, turbulent boundary layers and wake
Forsey & Carr[36] Arthur[37]	Full potential 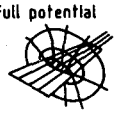	ditto
Doe,[26] Pagano & Brown	Euler 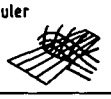	Strip treatment using B.R. Williams[10] 2D viscous package with 'higher-order' effects

Fig.12 U.K CFD methods for wings

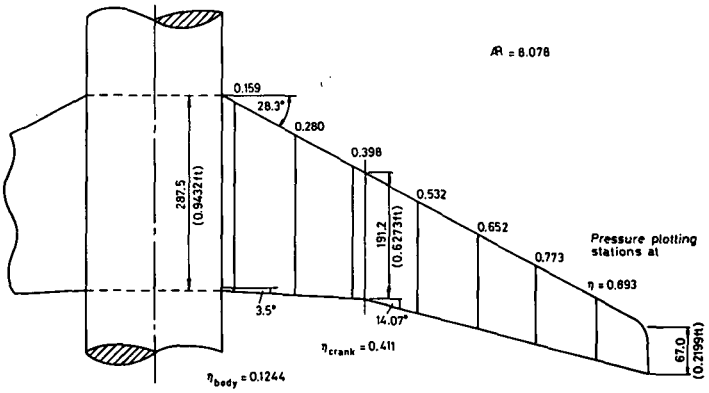

Fig.13 Planform of wing W4 showing pressure-plotting stations

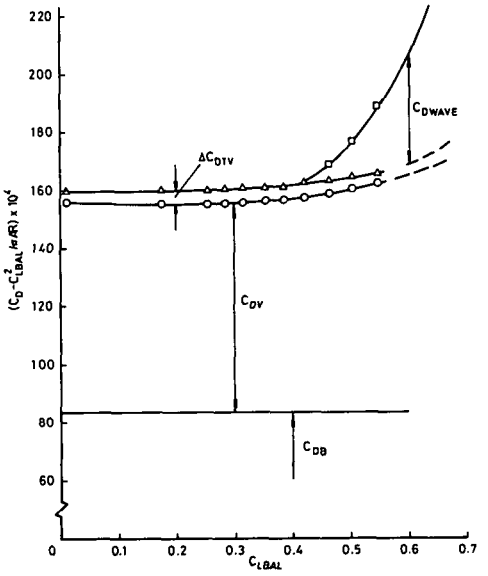

Fig.14 Analysis of drag, M = 0.78

As is well known, the vortex drag of wings with non-planar vortex traces (eg wing/winglet configurations) can be below the minimum for planar wings of the same span, and a technique for calculating the minimum vortex drag of non-planar configuration has been programmed by Isaacs[38].

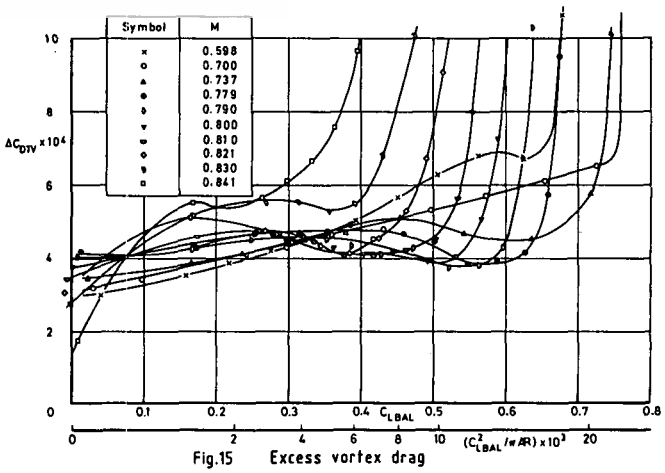

Fig.15 Excess vortex drag

As noted in section 2, viscous drag is inferred from boundary-layer quantities at the trailing edge using an extended version of the Squire-Young formula[8]. The turbulent boundary-layers are calculated using the measured pressure distributions and an 'infinite tapered wing' version[39] of the lag-entrainment method. Comparisons with the potentially, more-accurate, three-dimensional of Smith[40] suggests that the 'infinite tapered-wing' method simulates adequately three-dimensional effects in the present case except close to the tip and the root.

Typical spanwise distributions of local viscous-drag coefficient $C_{DV}(\eta)$ are illustrated in Fig 16, for M = 0.78. The relatively-large increase in local viscous-drag coefficient on the outer wing as lift coefficient increases from 0.42 to 0.55 is consistent with the growth in shock strength with lift and the consequent thickening of the boundary layer downstream of the shock on this part of the wing. The magnitudes of the local contributions to overall viscous drag are indicated in Fig 16 by $C_{DV}(\eta)c(\eta)/\bar{c}$, where $\frac{c}{\bar{c}}$ is local streamwise chord and $\bar{c}$ is geometric mean chord.

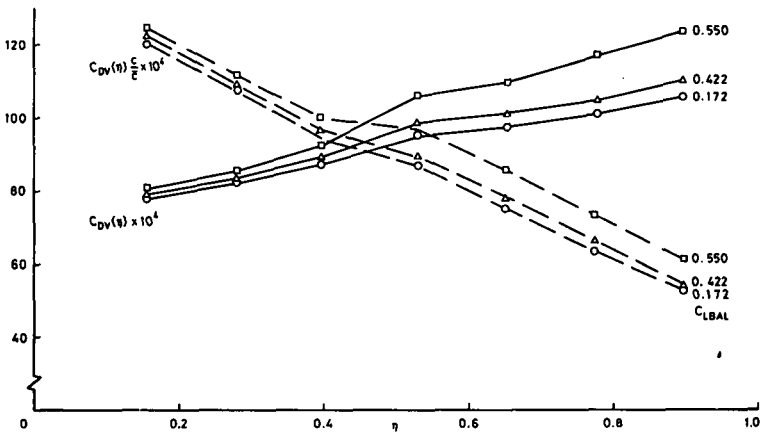

Fig.16 Spanwise variation of viscous drag, M = 0.78

In the absence of flowfield information, wave drag has been calculated by Lock's method[41]. It will be recalled from section 2, that, in this method, the variation of shock strength with distance normal to the wing surface is determined by wing streamwise curvature and static pressure at a point just upstream of the shock. This is equivalent to ignoring the effect on flow curvature of the boundary layer and assuming that the strength of the shock in the field is unaffected by the variation of surface curvature along the chord upstream of the shock. These aspects are considered again in the second example in which there is a rapid variation of streamwise curvature ahead of the shock on part of the wing. However, in the present case, the curvature of each wing section is close to a minimum in the region of the shock.

Spanwise variations of the local wave-drag coefficient $C_{DW}(\eta)$ calculated by Lock's method are shown in Fig 17 together with the local contribution to wave drag $C_{DW}(\eta)c(\eta)/\bar{c}$ for M = 0.78. The contribution to wave drag of the part of the wing inboard of the trailing-edge crank is seen to be relatively small, with most of the wave drag originating from a region just outboard of the crank.

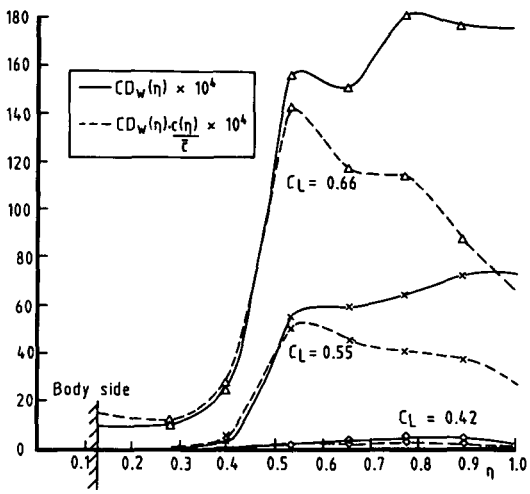

Fig.17 Spanwise distribution of normalised local wave drag coefficient, M = 0.78

Both local viscous and wave drags have been integrated across the wing span and have then been combined with vortex drag and body drag as shown in Fig 14 to give overall drag. Comparisons between 'calculated' and measured overall drags are shown in Fig 18 and indicate that, for subcritical flows or in the region of minimum drag, the 'calculated' drag coefficient is lower than the measured value by an amount which varies between 0.0004 at M = 0.6 and 0.0008 at M = 0.8. Although in less good agreement with measurement than BVGK is found to be for a series of aerofoils (Fig 8), these estimates are encouragingly close to measurement and show that the 'far-field' method has a useful role to play in the analysis of drag of wing/body configurations suitable for transport aircraft. A study of the sources of the

discrepancies[8] suggests that the errors can be largely explained by flow features not represented completely in the analysis including:

(a) wing/body, boundary-layer interference;

(b) flow curvature and Reynolds normal stresses in the turbulent shear layers; and

(c) transition-trip drag.

Fig 18 reveals that the differences between 'calculated' and measured drags decrease as wave drag increases for Mach numbers in the range 0.7 to 0.81. The most likely explanation for this is that Lock's method overestimates wave drag, since it is unlikely that the estimates of the other two drag components become more accurate as shock strength increases. On the evidence of studies of inviscid, two dimensional flows it is stated in Ref 40 that estimates by Lock's method are probably within -10 to 30% of the correct value except at low values of C_{DW} (< 0.0015) when it could be up to 0.0005 too high. No direct evidence is available on the effects of the boundary layer or three-dimensionalities in the flow. However, some comparisons have been made between predictions by Lock's method and those of Allwright's field method[6], in each case based on calculations by the FP method of Forsey and Carr[36] for the present configuration. These comparisons reveal that three-dimensional effects are significant only in the near vicinity of the tip (ie within about one or two chords) and thus, overall, their influence on wave drag may be ignored.

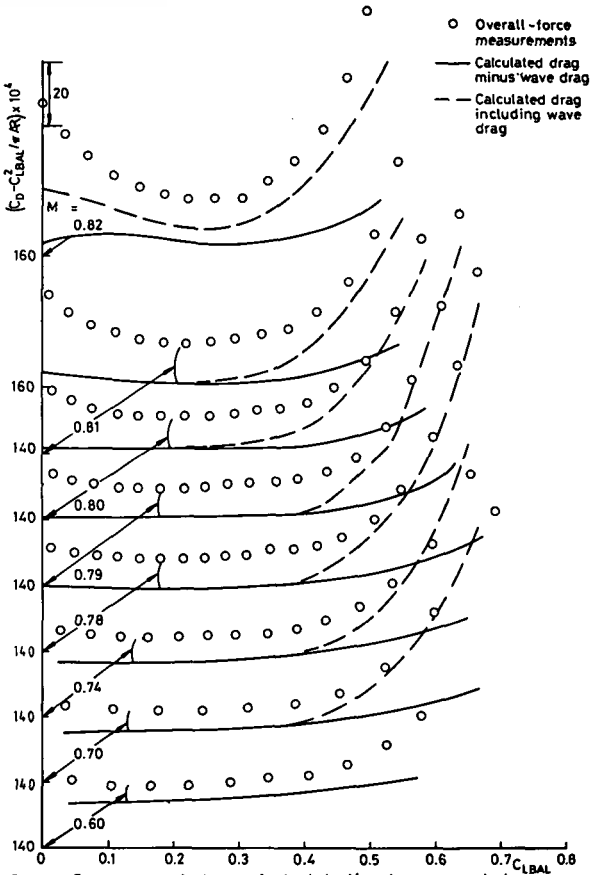

Fig.18 Comparison between 'calculated' and measured drags

(ii) Combat aircraft wing

The second configuration is an example of a wing design for which Lock's method - at least in its present form - is less reliable. The wing has been tested as a half model with the aim of providing fluid-dynamic data for the validation of CFD methods. Comparisons of predictions by VFP and measurements of wing pressure distributions are discussed in Ref 9. As part of this study, M. C. P. Firmin (RAE) has performed some calculations of wave drag using both Lock's and Allwright's techniques. Results for local wave-drag are shown in Fig 19. Outboard of the shock bifurcation at $\eta \approx 0.45$, Lock's method is seen to give much larger values of local wave-drag than those of Allwright while, further inboard, Lock's predictions for the rear shock are slightly lower on average than Allwright's values. An explanation for the former discrepancy is given in Fig 20 which shows the variation with distance from and normal to the wing surface of shock-upstream Mach number.

At $\eta = 0.604$, ie outboard of the bifurcation, Lock's method predicts that the shock penetrates much further into the field than is indicated by the more-accurate field method of Allwright. The reason for this is that the curvature of the wing upper-surface increases markedly with distance upstream of the shock on this part of the wing. Thus the flow curvature at the shock in the field is affected (via the outgoing Mach characteristics from the wing surface) and consequently the rate at which M_N changes with distance normal to the wing is modified.

Fig 20 also shows that, close to the wing surface, where the flow is strongly influenced by conditions at the foot of the shock, there is a marked difference in the two predictions of the variation of M_N with distance from the wing. This discrepancy arises from the neglect of the effect of the boundary layer on (a) the local flow curvature and (b) the inclination of the shock relative to the wing surface.

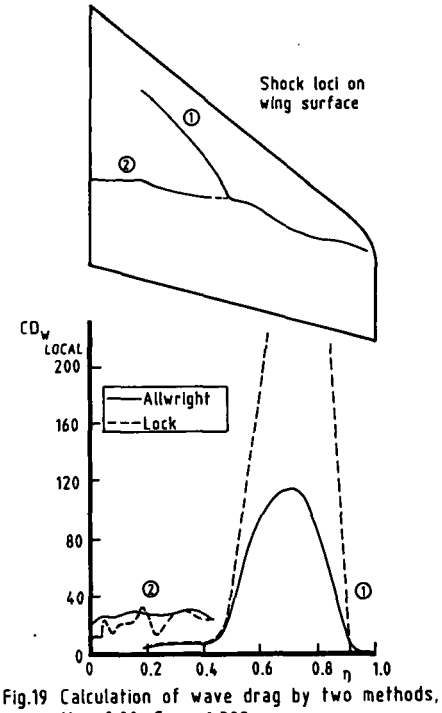

Fig.19 Calculation of wave drag by two methods, M = 0.88, C_L = 0.392

Despite these deficiencies, Lock's method is useful in providing a rapid indication of sources of excess drag both in the early stages of the wing design and later on as a diagnostic tool following wind-tunnel tests.

3.3 Bodies

Perhaps the first UK attempt to use CFD for the prediction of body drag was by Myring[42] who employed a viscous/inviscid interaction technique to calculate the subcritical flow over axisymmetric bodies at zero incidence. He represented the inviscid flow over the displacement surface of the body and the shear layer by a source-ring method and calculated the viscous shear-layers by integral methods, coupling the two solutions by a Direct procedure.

Using his method, Myring was able to design a 'low-drag' body, as illustrated in Fig 21, where it is distinguished from a conventional body of the same thickness ratio in having no pronounced suction peaks. Also shown in this figure is the variation with thickness ratio of drag-coefficient based on surface area, C_{DA}, for both types of body, clearly illustrating the superiority of the 'low drag' design, albeit at the expense of a lower body-volume. On the other hand, the 'low-drag' body has somewhat higher suctions or local velocities than those of the conventional shape in the region where the wings of an aircraft might be mounted, showing the danger of optimising aircraft components in isolation.

A number of methods have been developed in UK for calculating transonic flows over bodies, including the full-potential method of Baker and Ogle[43] for axisymmetric bodies and two methods of solving the Euler equations for the flow over forebodies.

Baker's method has been used[44] to calculate the variation of drag with Mach number of spherically-blunted forebodies at zero incidence for Mach numbers up to the limit of validity of the method, ie approximately unity. An example[44] of the reasonable agreement between predictions by this method of pressure distributions and drag is provided by Fig 22. Drag is inferred from the calculation by the 'local' method and a small tare correction to allow for discretisation errors in the method and skin-friction drag is applied to the theory to align prediction and measurement at M = 0.7.

Corresponding calculations of drag by the first of the Euler methods[45] are also shown in Fig 22. Based on the BAe algorithm for solving the Euler equations, this technique is applicable to axisymmetric forebodies[26]. Again the predicted variation of drag (by the 'local' method) with Mach number in the subsonic range is in fair agreement with measurement. This method has been generalised by BAe[26] to include forebodies of general shape at incidence, and a further generalisation has been performed by Aircraft Research Association, (ARA) Bedford[46] who have applied their multiblock technique to enable sideslip to be considered. Pressure distributions on the upper and lower sides of the body calculated by the latter method are compared with measurement for the forebody of the BAe Hawk at incidence and sideslip angle β in Fig 23. No comparisons of drag are available but the agreement between calculated and measured pressure distributions is reasonably good, suggesting that the method may be used to calculate the variation of drag with Mach number for such shapes.

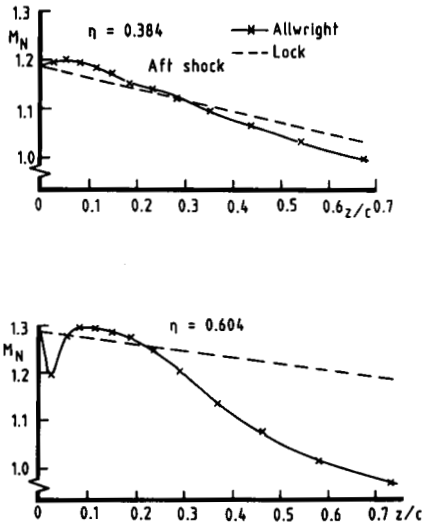

Fig.20 Calculation of Mach number normal to shock at two stations on wing

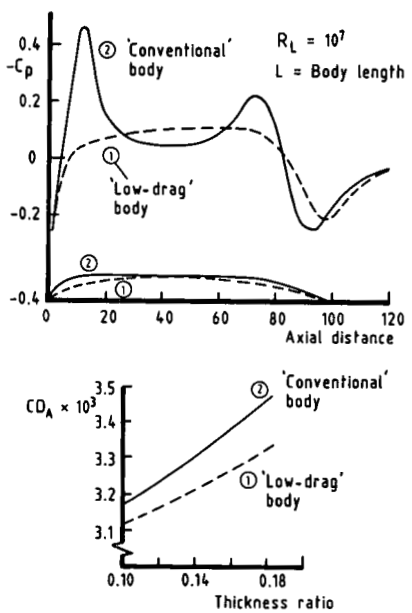

Fig.21 Pressure distributions and drag versus thickness ratio for axisymmetric bodies calculated by Myrings method

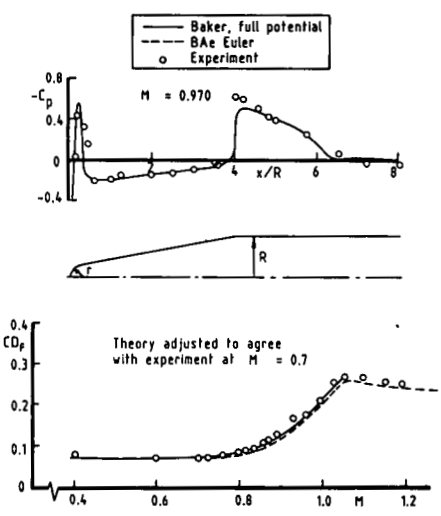

Fig.22 Pressure distributions and drag for a conical forebody with a spherical nose blunting ratio r/R = 0.3

Techniques such as the last one have yet to be combined interactively with boundary-layer calculation methods to predict the drag of general bodies. Of particular interest in this connection are fuselages with upswept afterbodies.

3.4 Cowls and nozzles

The accurate calculation of turbofan cowl drag is an important consideration in the design and the performance prediction of modern transport-aircraft. To be fully representative, the calculation method should simulate the interaction between the engine, the pylon and the wing. This cannot be done, at present, although progress is being made in the modelling of complex configurations (section 3.5) but, as a preliminary to obtaining solution to the complete problem, two methods have been programmed for isolated cowls. These methods have a similar function to that of aerofoil methods in providing a simple basis for checking flow algorithms. The first method, due to Peace[47], uses a Direct coupling of a full-potential solution of the inviscid flow with the lag-entrainment method for the turbulent boundary layers. The second procedure replaces Peace's potential-flow scheme by the BAe method for solving the Euler equations[26].

Goldsmith[48] has made comparisons between predictions by these methods and measurements of cowl pressure drag for a number of NACA-1 cowls aligned with the free stream. Comparisons for the cowl geometry sketched in Fig 24 are shown in Fig 25 where cowl pressure-drag coefficient is plotted against the relative-flow ratio A_∞/A_c as defined in Fig 24. Peace's method is limited to Mach numbers below about of unity, and in this Mach-number range it gives good agreement with measurement for relative-flow ratios above those for which cowl-lip separation occurs. For low relative-flow ratios, the agreement is less satisfactory, as might be expected for a method using a first-order treatment of the shear layers.

The Euler method has only been used for calculations at supersonic speeds and so a discussion of these comparisons is deferred until section 4 where methods for supersonic flows are discussed.

A number of methods have been produced in UK to calculate the drag of afterbodies with propulsive jets. Hodges[49] has considered the case of an axisymmetric afterbody with a single jet and simulates the external flow by a panel method, the jet by the method of characteristics and the boundary layer with the lag-entrainment method. Thus the method is restricted to uniformly-subsonic external flows and jet flows which are entirely supersonic. The solutions to the various parts of the flowfield are patched and empirical relationships are used to define the separation and reattachment points and also the entrainment in the mixing region. Comparisons of prediction by two methods[50], including Hodges' method, and measurements of afterbody pressure drag for a series of nozzles, at various jet-pressure ratios and for M = 0.6 and 0.8, reveal that Hodges' method is in reasonable agreement with measurement for subcritical external flows.

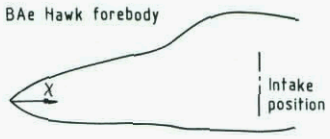

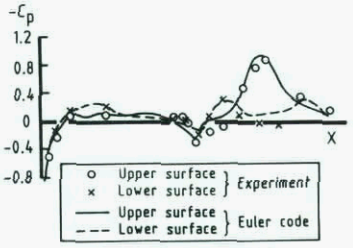

Fig.23 Upper and lower body pressure distributions, BAe Hawk forebody, M = 0.8, α = 3.72° β = 9.14°

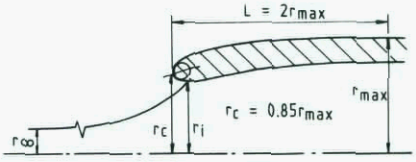

A_∞ = Streamtube cross-sectional area far upstream,
$= \pi r_\infty^2$

A_c = Cowl highlight or capture area,
$= \pi r_c^2$ (= 0.73 A_{max})

$A_{max} = \pi r_{max}^2$

$$C_{D_{cowl}} = \frac{2\pi}{A_{max}} \int_{r_i}^{r_{max}} C_p r dr$$

Fig.24 Cowl geometry and definitions

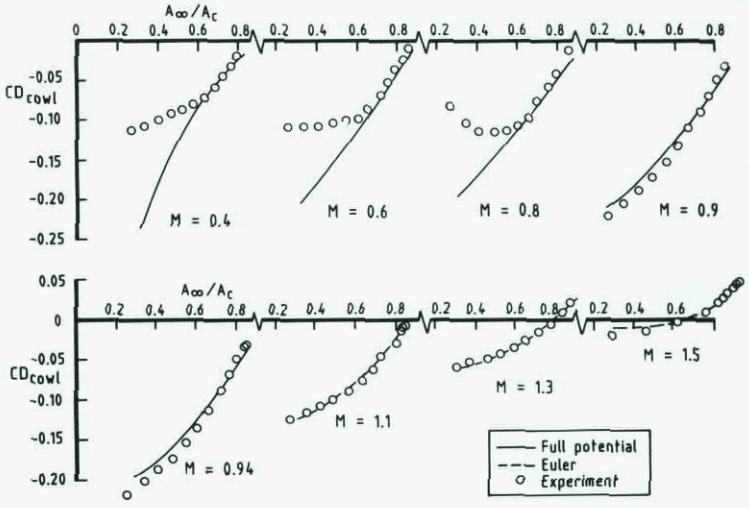

Fig.25 Cowl pressure drag as a function of capture ratio and free-stream Mach number

Peace[51] has developed a method based on solutions of the Euler equations in both the external flow and the jet which is not restricted to subcritical flows outside the jet. As in Hodges' procedure, the boundary layer is calculated by the lag-entrainment method[11] but replaces the Direct coupling and empirical separation prediction of Hodges' technique by an SI coupling. On the other hand, the entrainment in the jet mixing region is determined by a simple empirical correlation.

Fig 26 shows plots of afterbody pressure-drag coefficient against free-stream Mach number for an afterbody nozzle configuration tested by Reubush and Runckel[52]. The predictions by the method of Peace are seen to be in good agreement with measurement except close to M = 1.

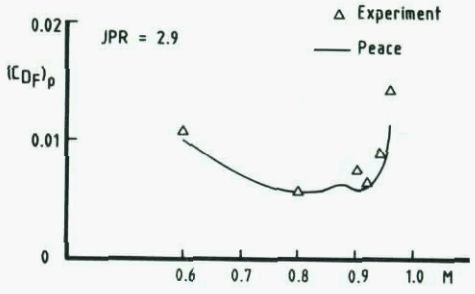

Fig.26 Pressure drag coefficient against M on Reubush and Runckel afterbody nozzle configuration 3

3.5 Complex configurations

The requirement to be able to calculate transonic flows around complex configurations, such as those shown in Fig 27, has led to the development at ARA, Bedford[53,54] and at BAe of multiblock grid generation schemes. Combined with the BAe technique for solving the Euler equations, these methods have been used for the calculation of the flow over a wide variety of configurations, an example being given in section 4. However, assessment of drag predictions by the method is still at an early stage, and, as noted in section 2, the production of spurious entropy by the current generation of Euler solvers makes the accurate determination of drag difficult; nevertheless it is envisaged that possible applications of the method in the future include:

(i) determination of the installed drag of pylon/cowl or weapon arrangements;

(ii) calculation of trimmed drag of closely-coupled configurations; and

(iii) calculation of drag of wing/winglet combinations.

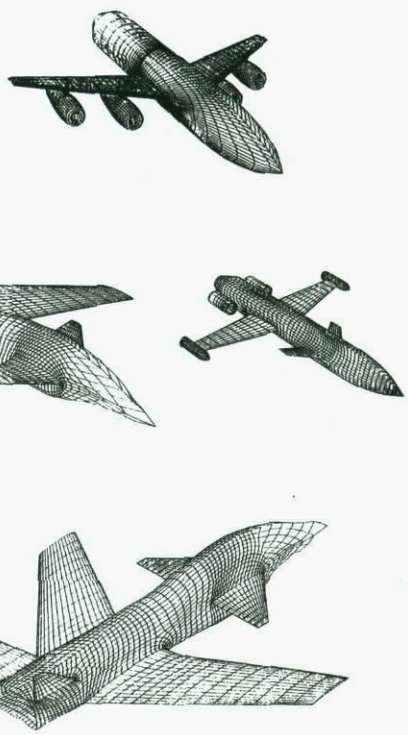

Fig.27 Surface grids for a variety of aircraft configurations

4 METHODS FOR SUPERSONIC AIRCRAFT

The airframe components of supersonic aircraft are generally integrated closely and hence the aerodynamic interference between them can be considerable. Consequently this section is different from the preceding section in that no distinction is made between components and the methods are considered under separate headings in chronological order of development.

4.1 Generalised near field wave drag program

The discovery that methods based on 'area transfer' rules do not give reliable predictions of zero-lift wave drag led BAe (Warton) to produce a code based on a simplified panel method for linearised supersonic-flow known as the Generalised Near Field Wave Drag (GNFWD) program[55]. Sufficient confidence has been established in the accuracy of the method for a range of military combat-aircraft configurations for it to be used in a routine way on project design. An application is illustrated in Fig 28; the design exercise involved changing the fuselage geometry and estimating drag using the procedure. The particular design alteration shown in Fig 28 increased fuselage volume while reducing zero-lift drag by 1½%. A combination of changes, such as straightening the

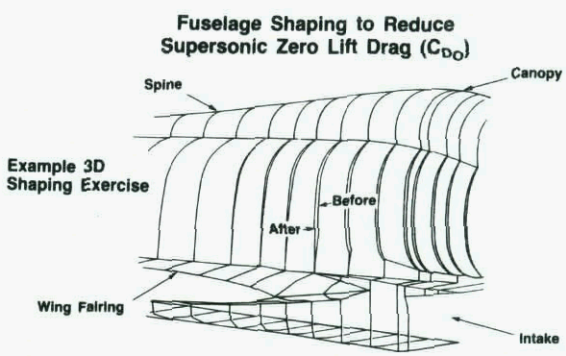

Fig.28 Full Shaping – Reduced C_{D_0} by 5%
Exercise Increased Volume by 400 Litres

spine, waisting the fuselage sides, and increasing centre-fuselage volume, reduced zero lift drag by 5% and increased internal fuselage volume for fuel system etc by 400 litres.

Although largely superseded by recent developments in methods for solving the Euler equations, techniques such as GNFWD currently retain an important function in the design of supersonic combat-aircraft because they are

(a) economical in terms of computer time and

(b) simple to use and to understand.

4.2 Euler/panel program for wing/body configurations

While giving reasonable predictions for the flow over bodies, panel methods are not satisfactory for lifting surfaces, in general. Thus a hybrid procedure has been programmed by BAe (Warton) using an Euler code for the wing and a panel method for the body[55]. The method has been used to predict incremental drags and pitching moments (from surface pressure integrations) for a combat aircraft configuration due to wing camber and twist. Fig 29 shows that the procedure gives accurate predictions of the changes between two different wings over a relevant range of lift coefficients.

Trim drag is an important consideration in the design of combat aircraft for both subsonic and supersonic manoeuvres. Consequently a version of the hybrid method has been specifically developed at BAe to estimate the variation of zero-lift pitching moment with Mach number. This technique has been used in a design process to reduce the trim drag of a combat aircraft configuration, yielding a 6% reduction in lift-dependent drag at the critical subsonic and supersonic design points.

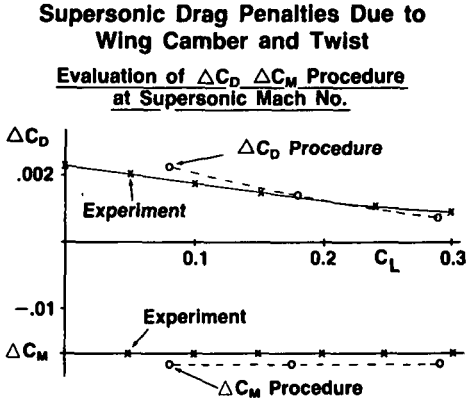

Fig.29 **Increments Due to Wing Camber Changes on BAe Wind Tunnel Model**

4.3 Euler methods for forebodies and pitot-intake cowls

The BAe Euler code for axisymmetric forebodies[26] has been used to calculate the variation of drag with Mach number at low supersonic speeds for the forebody of Fig 22 at zero incidence. Fig 22 shows that the method provides a reasonably faithful representation of the variation for Mach numbers between 1 and 1.2.

As noted in section 4, calculations have been made of cowl pressure drag by a version of the BAe Euler code[26] for pitot cowls (Fig 24) at supersonic speeds. Fig 25 shows that predictions by this method are in good agreement with measurement.

4.4 Euler/Multiblock method

Although methods such as those described in section 4.1 and 4.2 have demonstrated their usefulness as engineering tools, increasing use will be made in the future of methods such as the ARA/BAe Euler/Multiblock code, as noted in section 3.5. The application of this method to wing/body configurations representative of supersonic combat aircraft is described and assessed in Ref 56. In this study, drag is determined by the 'local' method and thus needs to be regarded with caution because of the sensitivity of the method to discretisation errors. A study has been made of the effect on drag of grid structure and density but this was not conclusive[56]. Therefore the assessment of the method has been based mainly upon comparisons with measurements of wing pressure distributions and overall forces made on two half models. In order that the comparison is not affected by extraneous effects, such as these due to the interaction between the half body and the sidewall boundary layer, overall force measurements on the body alone are subtracted from those of the wing/body configuration at each angle of incidence and an analogous procedure is used in the calculation by the CFD method. Comparisons are shown in Fig 30 for M = 1.6 and for one of the wings studied, the calculated value of drag coefficient having been increased by 0.0054 to allow for skin friction (assumed to be unaffected by wing incidence, thickness and camber). The agreement between calculation and measurement is, on the whole, fair. Differences between prediction and measurement of lift at angles of incidence above about 6° can be explained by the effects of shock-induced separation not simulated in the calculation method. The obvious discrepancies between calculation and measurement of drag at low lift is believed to be due mainly to inaccurate predictions of suction near the leading-edge.

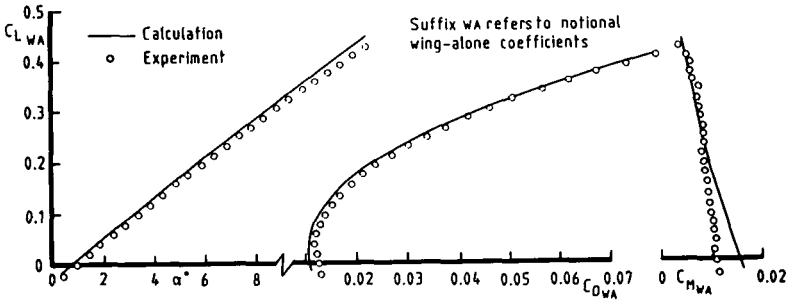

Fig.30 Overall lift, drag and pitching moment comparison between theory and experiment, M = 1.6, Wing A

4.5 Hall's multigrid method

Woodward[57] has used Hall's multigrid method[27] for solving the Euler equation, previously mentioned in section 3.1, to study the wave drag of aerofoils with rounded leading-edges at supersonic free stream speeds. This method is particularly suitable for studying flows of this kind since it has an unusually large number of grid points in the leading-edge region and is thus able to represent accurately the strong detached shock and the rapid spatial changes in the flow near the leading edge.

Fig 31 illustrates some of the results obtained by Woodward for wave drag by the 'local' method and shows the effect on the variation of wave drag with lift of changing nose radius. At zero lift an optimum nose radius of about 1½% chord is obtained but, as lift increases, the optimum value becomes smaller. This interesting result illustrates well the ability of CFD to provide relatively rapid assessments of drag differences due to changes in shape and the means of determining drag optima.

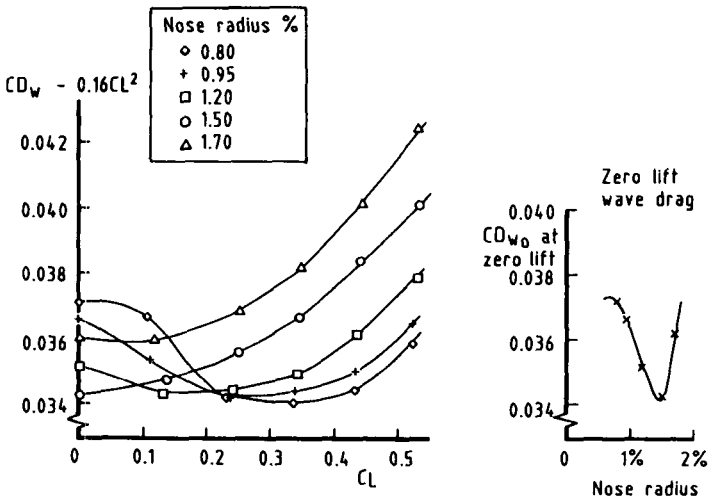

Fig.31 Calculated variation of wave drag with lift for varying nose - radius aerofoils, M = 1.1

5 CONCLUDING REMARKS

This paper has shown that, while the wholly theoretical prediction of aircraft drag is not yet possible, CFD methods exist in UK for drag prediction which are of considerable value to the aircraft designer in the following tasks:

- selection of the shape of aircraft components at the preliminary stages of the design;
- analysis of drag and diagnosis of sources of unwanted drag;
- 'extrapolation' of wind-tunnel drag data to 'full scale'.

Further refinements are needed to numerical methods for solving the Euler equation to reduce the sensitivity of drag predictions by these methods to grid density. Such developments would allow multiblock schemes to be exploited to calculate the drag of complex configurations, and, as such, would be a step in the direction away from the current dependence on wind-tunnel tests.

UK methods of solving the Reynolds-averaged, Navier-Stokes equation have yet to make a significant impact as techniques for drag prediction. Future developments in this area depend mainly on improvements being made to the turbulence models used, and the prospects of these being effected in the near term are uncertain. Thus viscous/inviscid inter-action techniques are expected to continue to feature prominently in UK drag prediction methods for some time to come.

REFERENCES

1 S. F. J. Butler. Technical evaluation report. AGARD-CP-124, Aerodynamic drag 1973.

2 F. R. Bailey, W. F. Ballhaus Jr. A large-scale computer facility for computational aerodynamics. IEEE Transactions on Nuclear Science Vol NS-32 No 1 February 1985.

3 N. J. Yu, H. C. Chen, S. S. Samant, P. E. Rubbert. Inviscid drag calculations for transonic flows. AIAA Paper 83-1928 (1983).

4 R. C. Lock. Prediction of the drag of wings at subsonic speeds by viscous/inviscid interaction techniques Paper 10 AGARD-R-723 1985.

5 C. M. Billing, A. J. Bocci. The MACHCONT method for calculating the wave drag of a 2D aerofoil. ARA Memorandum 272 (1986).

6 S. E. Allwright. Calculation of wave drag by analysis of 3D transonic flow field solutions. BAe unpublished Report.

7 C. C. L. Sells. Solution of the Euler equations for transonic flow past a lifting aerofoil. RAE Technical Report 80065 (1980).

8 P. R. Ashill, J. L. Fulker. Calculation of the viscous and vortex drag components of wing/body configurations. RAE Technical Report 87028 (1987).

9 R. C. Lock, B. R. Williams. Viscous/inviscid interactions in external aerodynamics. Prog Aerospace Sci Vol 24 pp 51-171. Pergamon Journals Ltd (1987).

10 B. R. Williams. The prediction of separated flow of using a viscous-inviscid interaction method. ICAS Paper 84-2.3.3 (1984).

11 J. E. Green, D. J. Weeks, J. W. F. Brooman. Prediction of turbulent boundary layers and wakes in compressible flow by a lag-entrainment method. ARC R&M 3791 (1977).

12 B. Thwaites. Approximate calculation of the laminar boundary layer. Aero, Qu., 1, 245 (1949).

13 P. R. Ashill, R. F. Wood, D. J. Weeks. An improved, semi-inverse version of the viscous Garabedian and Korn method VGK. RAE Technical Report 87002 (1987).

14 D. J. Butter, B. R. Williams. The development and application of a method for calculating the viscous flow about high-lift aerofoils. AGARD-CP-291. Paper No 25 (1980).

15 B. R. Williams, D. S. Woodward. Multiple Aerofoil Viscous Iterative System (MAVIS), the initial structure and possible extensions. RAE Technical Memorandum Aero 1632 (1975).

16 J. C. Newling. An improved two-dimensional multi-aerofoil program. HSA-MAE-R-FDM-0007 (1977).

17 H. P. A. H. Irwin. A calculation method for the two-dimensional turbulent flow over a slotted flap. ARC CP-1267 (1974).

18 A. G. T. Cross. BAe unpublished work.

19 D. A. King, B. R. Williams. Developments in computational methods for high-lift aerodynamics. Paper presented at Royal Aeronautical Society symposium 'High Lift Aerodynamics', Churchill College, Cambridge, 15-16 December 1986.

20 N. P. Weatherill, L. J. Johnston, A. J. Peace, J. A. Shaw. A method for the solution of the Reynolds-averaged Navier-Stokes equations on triangular grids. Paper presented at 7th GAMM Conference on Numerical Methods in Fluid Mechanics, Louvais-La-Neuve, Belgium September 9-11 1987.

21 M. R. Collyer, R. C. Lock. Prediction of viscous effects in steady transonic flow past an aerofoil. Aero, Qu., 30, 485 (1975).

22 A. F. Jones, M. C. P. Firmin. RAE unpublished Report.

23 P. R. Ashill, D. J. Weeks, J. L. Fulker. Wind Tunnel experiments on aerofoil models for the assessment of computational flow methods. To be presented at AGARD FDP Conference 'Validation of computational fluid dynamics' Lisbon May 1988.

24 P. R. Ashill. RAE unpublished work.

25 A. Jameson, W. Schmidt, E. Turkel. Numerical solutions of the Euler equations by finite volume methods using Runge-Kutta time stepping schemes. AIAA Paper 81-1259, 1981.

26 R. H. Doe, A. Pagano, T. W. Brown. The development of practical Euler methods for aerodynamics design. ICAS 86 5.5 (1986).

27 M. G. Hall. Cell vertex multigrid schemes for solution of the Euler equations. RAE Technical Memorandum Aero 2029 (1985).

28 L. J. Johnston. Some preliminary results from a prediction method for the viscous flow around aerofoil sections. ARA Memo 281 (1987).

29 A. Roberts, K. Rundle. Computation of incompressible flow about bodies and thick wings using the spline mode system. BAC (Weybridge) Report Aero MA19, 1972, ARC 33775.

30 A. Roberts, K. Rundle. The computation of first order compressible flow about wing/body combinations. BAC (Weybridge) Report Aero MA20, 1973.

31 B. Hunt. The panel method for subsonic aerodynamic flows. A survey of mathematical formulations and numerical models, and an outline of the new British Aerospace scheme. VKI LS 1978-4, Brussels, March 13-17, 1978.

32 J. A. H. Petrie. A surface source and vorticity panel method. Aero. Qu., 29 251 (1978).

33 A. G. T. Cross. Calculation of compressible three-dimensional turbulent boundary layers with particular reference to wings and bodies. British Aerospace (Brough) Report YAD 3379 (1979).

34 C. M. Albone, M. G. Hall, G. Joyce. Numerical solutions for transonic flows past wing-body combinations. RAE TM Aero 1645 (1975).

35 M. C. P. Firmin. Calculation of transonic flow over wing-body combinations with an allowance for viscous effects. AGARD-CP-291, Paper 8 (1981).

36 C. R. Forsey, M. P. Carr. The calculation of transonic flow over three-dimensional swept wings using the exact potential equation. DGLR Symposium on 'Transonic Configurations', DGLR Paper 78-064 (1978).

37 M. T. Arthur. A method for calculating subsonic and transonic flow over wings and wing-fuselage combinations with an allowance for viscous effects. AIAA-84-0428 (1984).

38 D. Isaacs. A two-dimensional panel method for calculating slender-body theory loading (or loading for minimum vortex drag) on a body of arbitrary cross section. RAE TR 81003 (1983).

39 P. R. Ashill, P. D. Smith. An integral method for calculating the effect on turbulent boundary-layer development of sweep and taper. The Aeronautical Journal pp 45-51, Feb (1985).

40 P. D. Smith. An integral prediction method for three-dimensional compressible turbulent boundary layers. ARC R&M 3738 (1972).

41 M. D. Hodges, P. R. Ashill, P. D. Cozens, R. C. Lock. Application to a particular model of an approximate theory for determining the spanwise distribution of and total wave drag on a swept wing. UK MOD unpublished Report.

42 D. F. Myring. A theoretical study of body drag in subcritical axisymmetric flow. Aero. Qu., 27 (3) (1976).

43 T. J. Baker, F. A. Ogle. A computer program to compute transonic flow over an axisymmetric solid body. ARA Memo No 197 (1977).

44 P. D. Cozens. The wave drag coefficient of spherically blunted secant ogive fore-bodies of fineness ratio 1.0, 1.5 and 2.0 at zero incidence in transonic flow ESDU TDM 83017 (1983).

45 B. M. Patel. Calculation of wave drag of spherically blunted secant ogive forebodies at low supersonic speeds using Euler codes. UK MOD unpublished Report.

46 N. P. Weatherill, J. A. Shaw. The simulation of inviscid flow around military forebody geometries using the Euler equations. ARA Memo No 269 (1986).

47 A. J. Peace. Transonic flow calculations around isolated inlet configurations. The Aeronautical Journal pp 103-110 March 1986.

48 E. L. Goldsmith. Forces and pressure distributions at subsonic and supersonic speeds on circular section pitot intakes. ARA Memo in preparation.

49 J. Hodges. A method for calculating subsonic flows over axisymmetric afterbodies including viscous and jet effects. RAE TR 82097 (1982).

50 L. E. Putnam, J. Hodges. Assessment of NASA and RAE viscous-inviscid interaction methods for predicting transonic flow over nozzle afterbodies. AIAA-83-1789 (1983).

51 A. J. Peace. The calculation of axisymmetric afterbody flows with jet effects by a viscous/inviscid interaction method. ARA Report 67 (1986).

52 D. E. Reubush, J. F. Runckel. Effect of fineness ratio on boattail drag of circular-arc afterbodies having closure ratios of 0.5 with jet exhaust at Mach numbers up to 1.3. NASA TN D-7192 (1973).

53 N. P. Weatherill, J. A. Shaw, C. R. Forsey, K. E. Rose. A discussion on a mesh generation technique applicable to complex geometries. AGARD Symposium on Applications of computational fluid dynamics in aeronautics, Aix-en-Provence, France, April 1986.

54 N. P. Weatherill, C. R. Forsey. Grid generation and flow calculation for aircraft geometries. J Aircraft, Vol 22 No 10, Oct 1985.

55 W. R. Marchbank. The integration of computational fluid dynamics into the military aircraft design process. Paper 11 AGARD-CP-412 1986.

56 J. L. Fulker, P. R. Ashill. A theoretical and experimental evaluation of a numerical method for calculating supersonic flows over wing/body configuration. To be presented at AGARD FDP Conference 'Validation of computational fluid dynamics'.

57 D. S. Woodward. RAE unpublished work.

ACKNOWLEDGMENTS

The cooperation of all those who responded to requests for information is gratefully acknowledged as is the work by Mrs N E Rycroft and Mr G L Riddle in preparing the figures.

COMPUTATIONAL FLUID DYNAMICS DRAG PREDICTION – RESULTS FROM THE VISCOUS TRANSONIC AIRFOIL WORKSHOP

by

Terry L.Holst
Chief, Applied Computational Fluids Branch
NASA Ames Research Center
Moffett Field, CA 94035, USA

ABSTRACT

Results from the Viscous Transonic Airfoil Workshop held in January 1987, are compared with each other and with experimental data. Test cases used include attached and separated transonic flows for the NACA 0012 airfoil. A total of 23 sets of numerical results from 15 different author groups are included. The numerical methods used vary widely and include: 16 Navier-Stokes methods, 2 Euler/boundary-layer methods, and 5 potential/boundary-layer methods. The results indicate a high degree of sophistication among the numerical methods with generally good agreement between the various computed and experimental results for attached or moderately separated cases. The agreement for cases with larger separation is only fair and suggests additional work is required in this area.

INTRODUCTION

During the past 3 years the Viscous Transonic Airfoil (VTA) Workshop was planned, organized, and implemented. The workshop implementation was in two parts. The first part consisted of presentations at the AIAA 25th Aerospace Sciences Meeting at Reno, Nevada, in January 1987 by 15 author groups with a variety of different viscous airfoil numerical methods (Refs. 1-16). The second part of the VTA Workshop was the presentation of a compendium of results (Ref. 17) where the individual contributions were combined in a format to facilitate comparisons among both the various computations and selected experimental data. In this paper results from the VTA workshop obtained for the NACA 0012 airfoil are reexamined and analyzed with special emphasis on drag.

The individual author groups have computed a set of results for test cases involving a variety of different situations ranging from attached subcritical flows to transonic flows with both shock-induced and angle-of-attack induced separation. A complete set of instructions given to each author group, which lists all of the requested airfoil cases, required results, and result format, is reproduced in Ref. 17.

The methods used by the various authors vary from momentum-integral boundary-layer methods coupled with transonic potential inviscid codes to full Navier-Stokes methods. A quick-reference table showing authors, paper references, and methods used is given in Table 1. A total of 23 different sets of results were submitted by the 15 author groups as several authors decided to submit several sets of results. The majority of methods (a total of 16) utilize the Navier-Stokes equations. This is in direct contrast to the situation in 1980-81 at the Stanford Workshop on Complex Turbulent Flows (Ref. 18) where very limited results on airfoil calculations were submitted with Navier-Stokes methods. This suggests a strong trend toward the Navier-Stokes formulation, even though it can be computationally expensive. The remaining formulations are split between several categories: two are Euler/boundary-layer methods, and five are potential/boundary-layer methods. The boundary layer methods are divided between the momentum integral approach and the full boundary layer equation approach.

Major objectives to be addressed in this paper include the establishment of the abilities of viscous airfoil analysis methods to predict aerodynamic trends including drag and the establishment of the quantitative abilities of the various methods for predicting details of viscous airfoil flow fields. In short, the primary objective of this paper is CFD computer code validation. There are two types of errors which the validation process seeks to identify and hopefully eliminate. These include physical model errors and numerical errors. The physical models associated with CFD applications include the governing equations, the viscosity law, boundary conditions, the equation of state, and the turbulence model. Numerical errors associated with CFD applications are due to time and space discretization schemes, boundary condition implementation schemes, grid resolution, grid stretching, and artificial dissipation. Differences between two computed results that use different physical models are best evaluated by using accurate experimental data. Differences between two computed results that use the same physical models have to be numerical in nature by definition. Numerical errors can be effectively identified by numerical solution-to-solution comparisons. Grid refinement studies, outer boundary position studies, and code-to-code comparisons are examples of this type of error evaluation scenario. In actual practice physical model and numerical errors coexist in most applications. Thus, identification, evaluation, and removal of errors associated with CFD applications are best accomplished by a combined implementation of experimental and solution-to-solution comparisons. The purpose of the VTA Workshop in general, and this paper in particular, is to achieve this type of comprehensive code validation for the viscous transonic airfoil problem.

DISCUSSION OF RESULTS

The NACA 0012 airfoil is a symmetric, 12% thick airfoil which has an analytical definition given in Ref. 17. This airfoil, while not being state of the art in airfoil design, is extremely valuable as a standard because it has been tested extensively both experimentally and computationally. As a consequence, a range of experimental results taken from various sources can be compared with the present range of computational results.

Table 1 Summary of authors and numerical methods used in the Viscous Transonic Airfoil Workshop.

no.	author(s)[ref]	method description
1	Sugavanam[1]	NS, modified ADI, BL
2	Desai,Rangarajan[2]	NFP+LEBL+visc ramp, SLOR+grid sequencing
3	Dargel,Thiede[3]	NFP+MIBL+nonisentropic shock-point operator
4	Rumsey,Taylor,Thomas Anderson[4]	NS, AF, upwind FV, BL
5	Melnik,Brook,Mead[5]	CFP+LEBL, MG-ADI
6	Maksymiuk, Pulliam[6]	NS, diagonal-ADI, BL
7	Coakley[7]	NS, upwind-ADI, FV, CS
8	"	NS, upwind-ADI, FV, BL
9	"	NS, upwind-ADI, FV, JK
10	"	NS, upwind-ADI, FV, (q-ω)
11	Chen,Li,Alemdavoglu Mehta,Chang,Chen, Cebeci[8,9]	Euler+IBL, MG, FV, CS
12	"	NS, ADI, BL
13	"	FP+IBL, CS
14	King[10]	NS, ADI, CS
15	"	NS, ADI, BL
16	"	NS, ADI, JK
17	Huff, Wu, Sankar[11]	NS, ADI, BL
18	Matsushima, Obayashi, Fujii[12]	NS, LU-ADI, flux limiter, BL
19	Haase, Echtle[13]	NS, 3-step RK+RA, FV, CS
20	"	CFP+LEBL, MG-ADI
21	Kordulla[14]	NS, implicit pred-corr, BL
22	Drela, Giles[15]	Euler+MIBL, FV, Newton it
23	Morinishi,Satofuka[16]	NS, MG, RK, RA, BL

NS–Navier-Stokes, NFP–nonconservative full potential, CFP–conservative full potential, IBL–inverse boundary layer, LEBL–lag entrainment boundary layer, MIBL–momentum integral boundary layer, MG–multigrid, FV–finite volume, RK–Runge-Kutta, RA–residual averaging, BL–Baldwin-Lomax, JK–Johnson-King, CS–Cebeci-Smith

The first results for the NACA 0012 airfoil are pressure coefficient distributions at $M_\infty = 0.7$, $\alpha = 1.49°$, and $Re_c = 9\text{x}10^6$. These results, including 20 separate curves, are presented in Fig. 1 on a single set of axes without labels. For this case the flow is attached and just slightly supersonic near the leading edge upper surface. All methods produce very similar results with very little scatter and are in excellent agreement with the experimental data of Harris (Ref. 19). The measured experimental angle of attack for this case was 1.86°. Using a linear method for simulating wind-tunnel-wall interference, Harris determined the corrected angle of attack to be 1.49°. This is the angle of attack used to compute all the results displayed in Fig. 1. The consistency and accuracy of results for this case indicate that, at least for surface pressure associated with attached, weakly transonic flow, computational methods have attained a sophisticated level of development.

The second set of results computed for the NACA 0012 airfoil also consist of pressure coefficient distributions and are displayed in Fig. 2. These calculations were performed for $M_\infty = 0.55$, $\alpha = 8.34°$, and $Re_c = 9\text{x}10^6$. Again the angle of attack used in the computations (8.34°) is the corrected value obtained by Harris from the measured value (9.86°) using a linear analysis for wind-tunnel-wall effects. For this case the flow has a supersonic bubble well forward on the airfoil upper surface and is slightly separated at the foot of the shock. In addition, several authors reported boundary layer separation at the airfoil trailing edge. The angle of attack for this case is about one degree below the maximum lift value.

The computed results for this case are displayed in two different plots (all without labels). Computations utilizing inviscid-plus-boundary-layer methods (6 curves) are displayed in Fig. 2a, and computations utilizing Navier-Stokes methods (16 curves) are displayed in Fig. 2b. Both sets of computations are in good agreement with Harris' experimental data. However, the inviscid-plus-boundary-layer results show considerably more scatter for this case than the Navier-Stokes results. Most of the scatter is associated with the solution near the airfoil leading edge on the upper surface, where the large angle of attack causes a rapid expansion followed almost immediately by a shock wave. Perhaps the generally coarser streamwise spacing of the inviscid grids used in the inviscid-plus-boundary-layer methods, which averaged 137 points relative to an average of 243 points for the Navier-Stokes methods, is inadequate to capture the large gradients associated with the inviscid flow at the airfoil leading edge. The two solutions that significantly underpredict the peak $-c_p$ level at the upper surface leading edge (one result from Fig. 2a and one result from Fig. 2b) are from very coarse-grid calculations, and therefore, tend to support this observation.

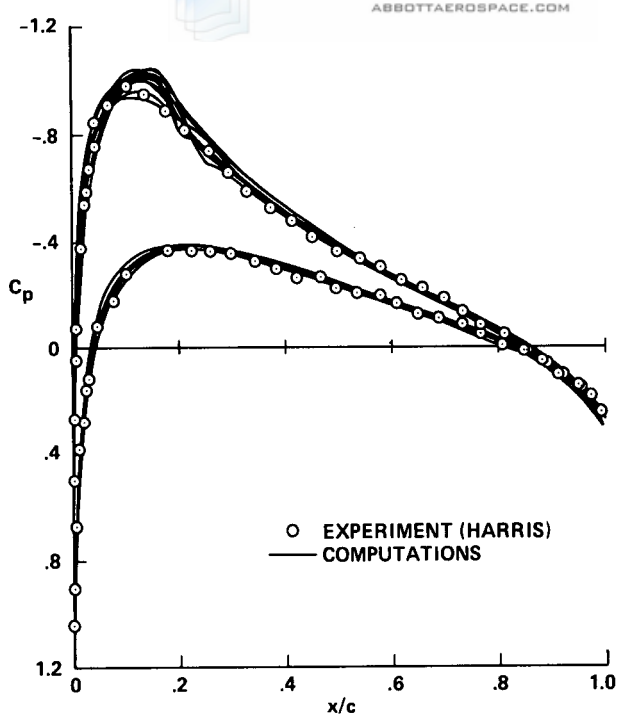

Fig. 1.- Comparison of pressure coefficient distributions for the NACA 0012 airfoil, $M_\infty = 0.70$, $\alpha = 1.49°$ (corrected), $Re_c = 9.0 \times 10^6$.

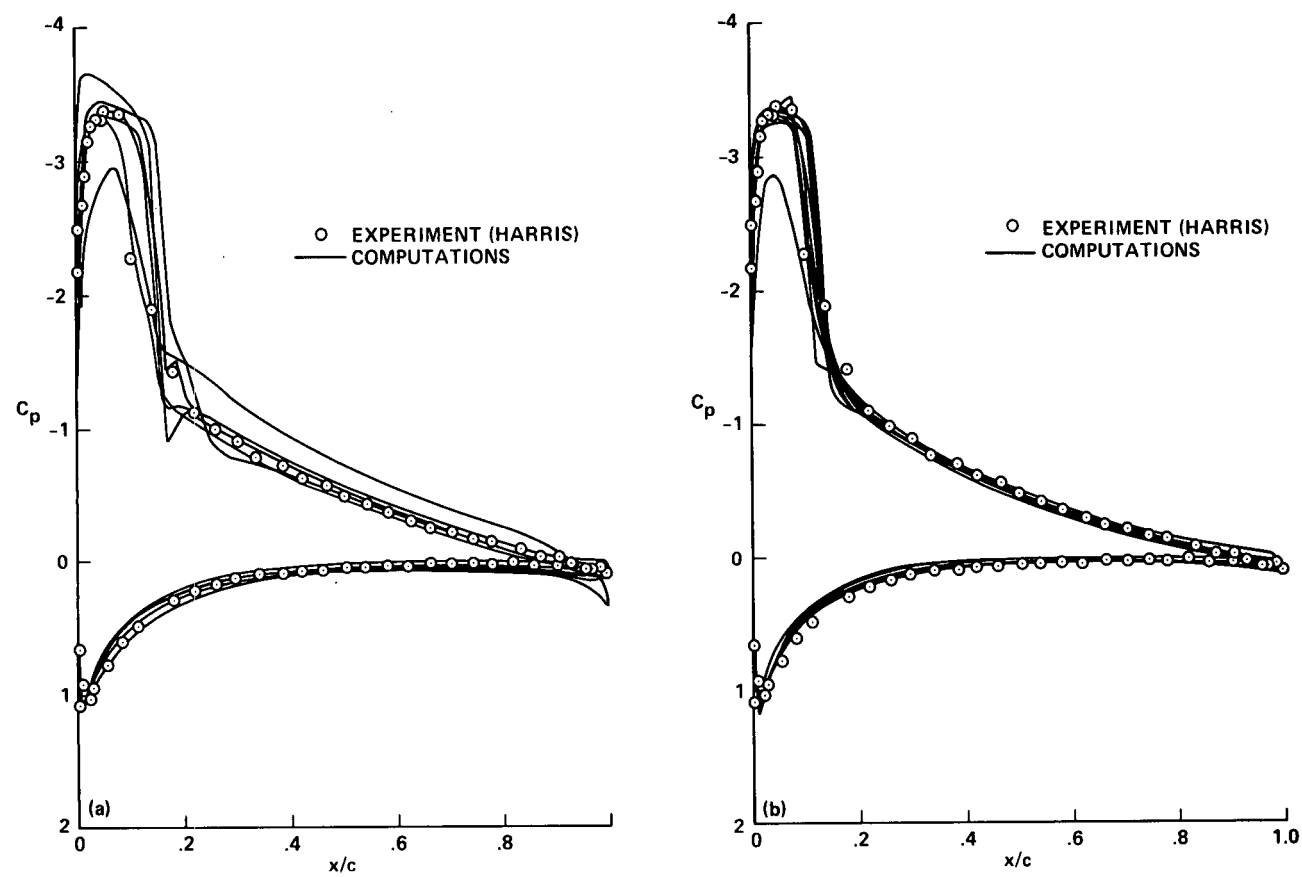

Fig. 2.- Comparison of pressure coefficient distributions for the NACA 0012 airfoil, $M_\infty = 0.55$, $\alpha = 8.34°$ (corrected), $Re_c = 9.0 \times 10^6$. a) Computations utilizing inviscid-plus-boundary-layer methods. b) Computations utilizing Navier-Stokes methods.

Comparisons of pressure coefficient distributions for the third NACA 0012 airfoil case are displayed in Fig. 3. The flow conditions for this case are $M_\infty = 0.799$, $\alpha = 2.26°$, and $Re_c = 9\text{x}10^6$. Again, the computational angle of attack (2.26°) is obtained from the measured angle of attack (2.86°) using a linear wind-tunnel-wall correction procedure. For this flow field a shock wave exists on the airfoil upper surface at about $x/c = 0.5$, which is strong enough to cause significant boundary layer separation. This case represents a severe test for all methods. The results are divided into five groups as follows: a) computations utilizing inviscid-plus-boundary-layer methods (6 curves), b) computations utilizing Navier-Stokes methods on coarse grids (4 curves), c) computations utilizing Navier-Stokes methods on fine grids (5 curves), d) Navier-Stokes computations with turbulence model variation due to King (Ref. 10; 3 curves), and e) Navier-Stokes computations with turbulence model variation due to Coakley (Ref. 7; 4 curves). The coarse-grid Navier-Stokes results were computed on grids ranging from 127 x 32 to 193 x 49, and the fine-grid results ranged from 257 x 57 to 265 x 101.

The inviscid-plus-boundary-layer results (Fig. 3a) show a significant amount of scatter especially at the shock wave and on the lower surface. Nevertheless, several of these methods do a good job in predicting both the position and strength of the shock wave. The

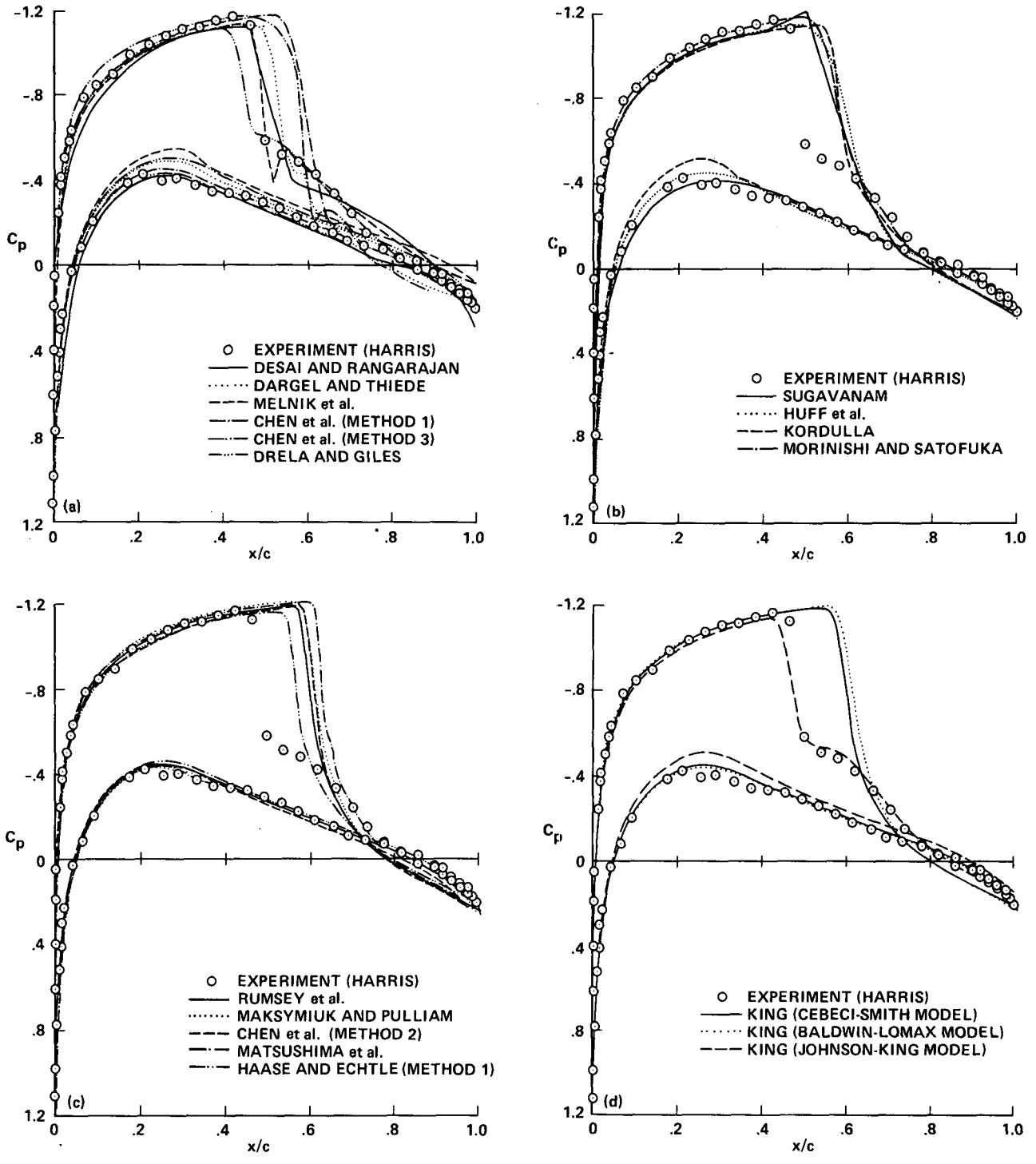

Fig. 3.- Comparison of pressure coefficient distributions for the NACA 0012 airfoil, $M_\infty = 0.799$, $\alpha = 2.26°$ (corrected), $Re_c = 9.0\text{x}10^6$. a) Computations utilizing inviscid-plus-boundary-layer methods. b) Computations utilizing Navier-Stokes methods on coarse grids. c) Computations utilizing Navier-Stokes methods on fine grids. d) Navier-Stokes computations with turbulence model variation due to King (Ref.10).

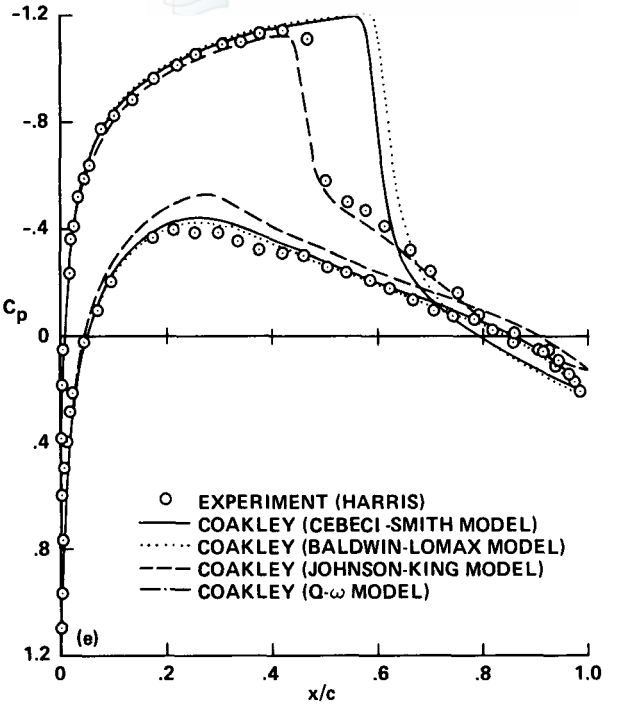

Fig. 3.- Concluded. e) Navier-Stokes computations with turbulence model variation due to Coakley (Ref.7).

coarse-grid Navier-Stokes results shown in Fig. 3b are generally in close agreement with each other but miss both the shock strength and position. The fine-grid Navier-Stokes results (Fig. 3c) are very similar to the coarse-grid results except the shock is slightly sharper. Thus, grid refinement is not the answer for obtaining good agreement for this case.

The turbulence model used in all but one of the nine.Navier-Stokes computations shown in Figs. 3b and 3c was the Baldwin-Lomax model (Ref. 20). In Fig. 3d King (Ref. 10) has computed results for three different turbulence models including Baldwin-Lomax, Cebeci-Smith (Ref. 21), and the newer Johnson-King model (Ref. 22). In Fig. 3e Coakley (Ref. 7) has computed results for four different turbulence models including Baldwin-Lomax, Cebeci-Smith, Johnson-King, and a two-equation model called Q-ω (Ref. 23). Note that the Q-ω and Cebeci-Smith results are identical and therefore are plotted as a single solid line. For the computations in Figs. 3d and 3e, only the turbulence model was allowed to vary, all other physical and numerical factors were held fixed. The Baldwin-Lomax, Cebeci-Smith, and Q-ω results from both codes produce results which are essentially identical to the other Navier-Stokes results (Figs. 3b and 3c). The shock is too strong and too far aft on the airfoil. However, the Johnson-King results are in excellent agreement at the shock, accurately predicting both shock position and strength. One drawback associated with the Johnson-King model computations is the under prediction of pressure on the airfoil lower surface. This, of course, will lead to a significant under prediction in lift relative to the experimental value. It is interesting to note that most of the inviscid-plus-boundary-layer results displayed in Fig. 3a, which agree well with the upper-surface shock strength and position, also under predict the lower-surface pressure distribution.

Figure 4 shows a comparison of 22 C_L vs α curves plotted without labels for the NACA 0012 airfoil at $M_\infty = 0.7$ and $Re_c = 9\text{x}10^6$. Experimental results from Harris with wind-tunnel-wall corrections included are also displayed. Most of the computed curves show good agreement with each other and with experiment at lower angles of attack. However, the overall comparison is disappointing at higher angles of attack. The scatter in the maximum lift value is particularly large. The $\alpha = 1.49°$ experimental point corresponds to the slightly-transonic solution shown in Fig. 1 where agreement is generally good. For angles of attack above this point the flow is more strongly transonic and eventually separates. In addition, several authors reported convergence difficulties or solution unsteadiness at these higher angles of attack. This may be a contributing factor to the large amount of scatter in the maximum C_L.

Drag polar comparisons are displayed in Fig. 5 for the NACA 0012 airfoil at $M_\infty = 0.7$ and $Re_c = 9\text{x}10^6$. As before, this set of comparisons is broken into several parts with experimental results of Harris included in each part for comparison. For $C_L \sim 0.2$ and lower, the flow field is subsonic. Drag values below this point correspond to pressure-plus-skin-friction drag and values above have, in addition, a wave-drag component. Since the pressure comparisons shown in Fig. 1 are all in good agreement, any disagreement in subcritical drag shown in Fig. 5 is probably due to disagreements in the skin-friction-drag component. However, since the pressure integration for drag can be quite sensitive, this ascertion should be studied in more detail by examining computed drag-component results.

Turbulence model variation has an effect on the drag polar as shown in Figs. 5e and 5f. For both figures, the newer Johnson-King turbulence model results overpredict the drag in comparison with experiment for the higher lift values, while the older models yield reasonable agreement. This trend is rather puzzling since the Johnson-King model yielded the best pressure distribution through the shock wave for the strongly separated case presented in Fig. 3. Perhaps the reason for poor drag polar agreement is associated with the under prediction of lower-surface pressure as predicted by the Johnson-King model in Figs. 3d and 3e. This would lower the lift, and if the drag is unaffected, produce the situation observed in Figs. 5e and 5f. However, several of the inviscid-plus-boundary-layer results

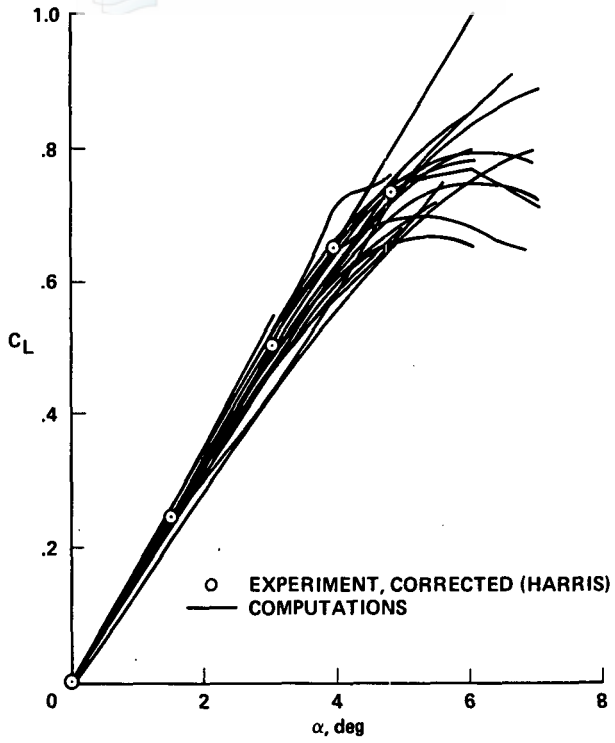

Fig. 4.- Comparison of lift coefficient versus angle of attack for the NACA 0012 airfoil, $M_\infty = 0.7$, $Re_c = 9.0 \times 10^6$.

presented in Figs. 5a and 5b also exhibit the same under prediction of pressure, but produce good drag polar results. This general area of drag prediction should be the subject of additional study.

Transonic drag-rise characteristics for the NACA 0012 airfoil at zero-lift conditions are displayed in Fig. 6. This set of comparisons is also broken into several parts and compared with a range of experimental data compiled by McCroskey (Ref. 24). All computations were performed at a Reynolds number based on airfoil chord of 9 million. The turbulent boundary layer was numerically "tripped" at $x/c = 0.05$ for those methods with trip or transition modeling and at the airfoil leading edge for those methods without. Each numerical curve shown in Fig. 6 is displayed with the computational points used to establish that curve (shown as solid circular symbols) when those points were available and when a small number of points (3 or 4) were used to establish the entire curve.

The range of experimental data displayed in Fig. 6 was established by looking at a large number of experiments (approximately 50). The six "best" sets of data, including Harris (Ref. 19), were selected, adjusted for Reynolds number effects, and plotted in Fig. 6 as a cross-hatched region. The different sets of experimental data, the selection process, and the Reynolds number adjustment procedure are

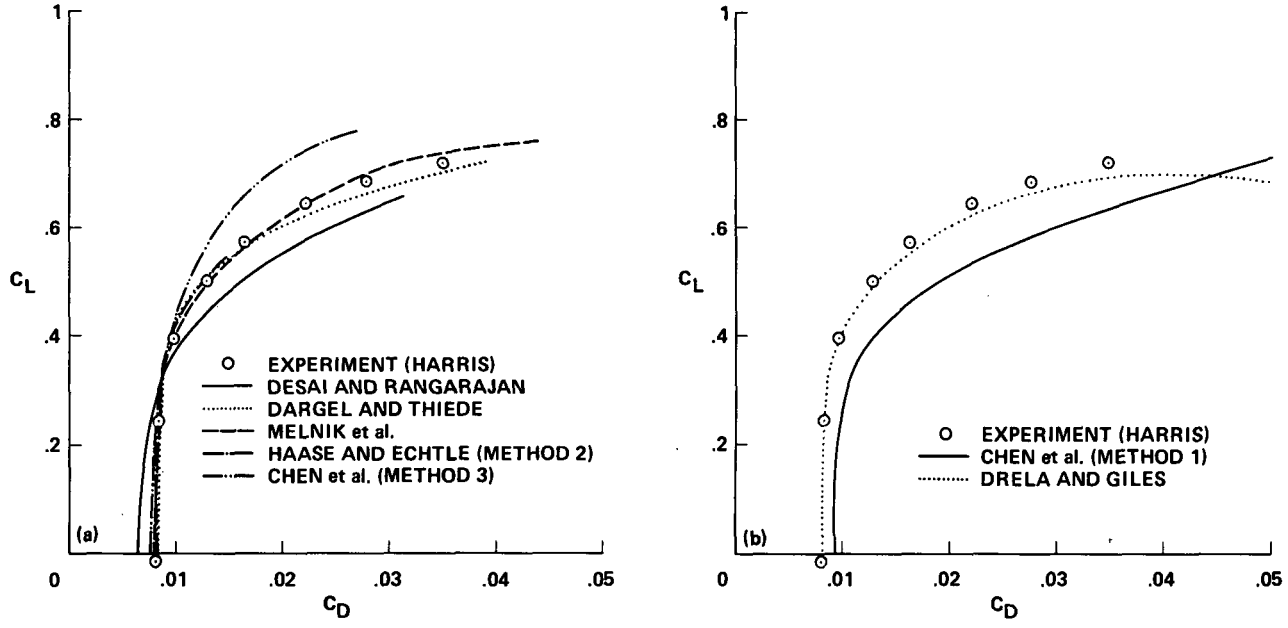

Fig. 5.- Comparison of lift versus drag polars for the NACA 0012 airfoil, $M_\infty = 0.7$, $Re_c = 9.0 \times 10^6$. a) Computations utilizing potential-plus-boundary-layer methods. b) Computations utilizing Euler-plus-boundary-layer methods.

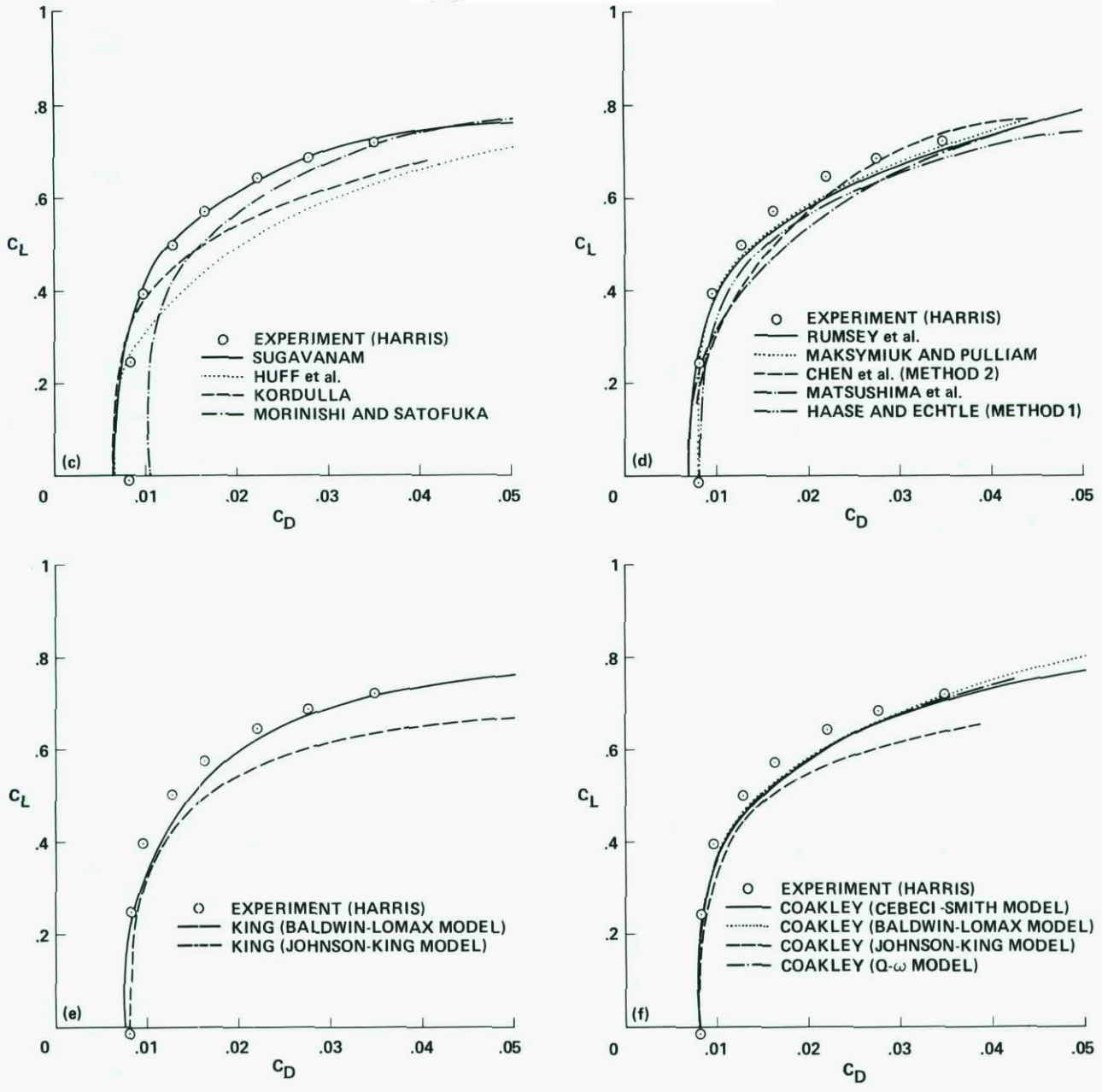

Fig. 5.- Concluded. c) Computations utilizing Navier-Stokes methods on coarse grids. d) Computations utilizing Navier-Stokes methods on fine grids. e) Navier-Stokes computations with turbulence model variation due to King (Ref. 10). f) Navier-Stokes computations with turbulence model variation due to Coakley (Ref.7).

described in McCroskey (Ref. 25). For this adjusted set of data, at a freestream Mach number of 0.7 the experimental drag value ranges from about 73 to 83 counts. For reference, Harris' highest Reynolds number tripped data produced a drag of about 75 counts.

The inviscid-plus-boundary-layer computations shown in Figs. 6a and 6b generally agree well with each other and with the experimental range of results. The drag-divergence Mach number is difficult to ascertain for some methods, especially the two Euler-plus-boundary-layer results shown in Fig. 6b. The scatter associated with the coarse-grid Navier-Stokes results (Fig. 6c) is quite large relative to the other computational and experimental results, especially at the subsonic Mach numbers, and suggests that the boundary layer grid refinement, or perhaps grid clustering, is a key parameter for drag calculations. The last two parts of Fig. 6 (Figs. 6e and 6f) show the effect of turbulence model variation on the drag-rise characteristics of the NACA 0012 airfoil. Except for relatively small variations in subsonic drag levels, there is virtually no variation in drag rise because of the turbulence models tested for this case.

Figure 7 shows computations (3 curves) compared with a range of experimental data, again compiled by McCroskey (Ref. 24), for the lift-curve slope ($dC_L/d\alpha$) plotted versus freestream Mach number. Values for $dC_L/d\alpha$ were obtained by computing the lift at $\alpha = 1.0°$. The units on $dC_L/d\alpha$ are therefore $(°)^{-1}$. This particular curve is significant because of its sensitivity to shock wave position and shock/boundary-layer interaction. The three computed results are in good agreement with the experimental range at lower free-stream Mach numbers, but deviate quickly. The single inviscid-plus-boundary-layer result starts deviation at about the drag-divergence Mach number. The two Navier-Stokes results qualitatively follow most of the experimental trends, including the severe shock-induced lift loss in the range $0.85 \leq M_\infty \leq 0.90$, but miss the appropriate levels, especially the minimum value of $dC_L/d\alpha$ at $M_\infty = 0.88$.

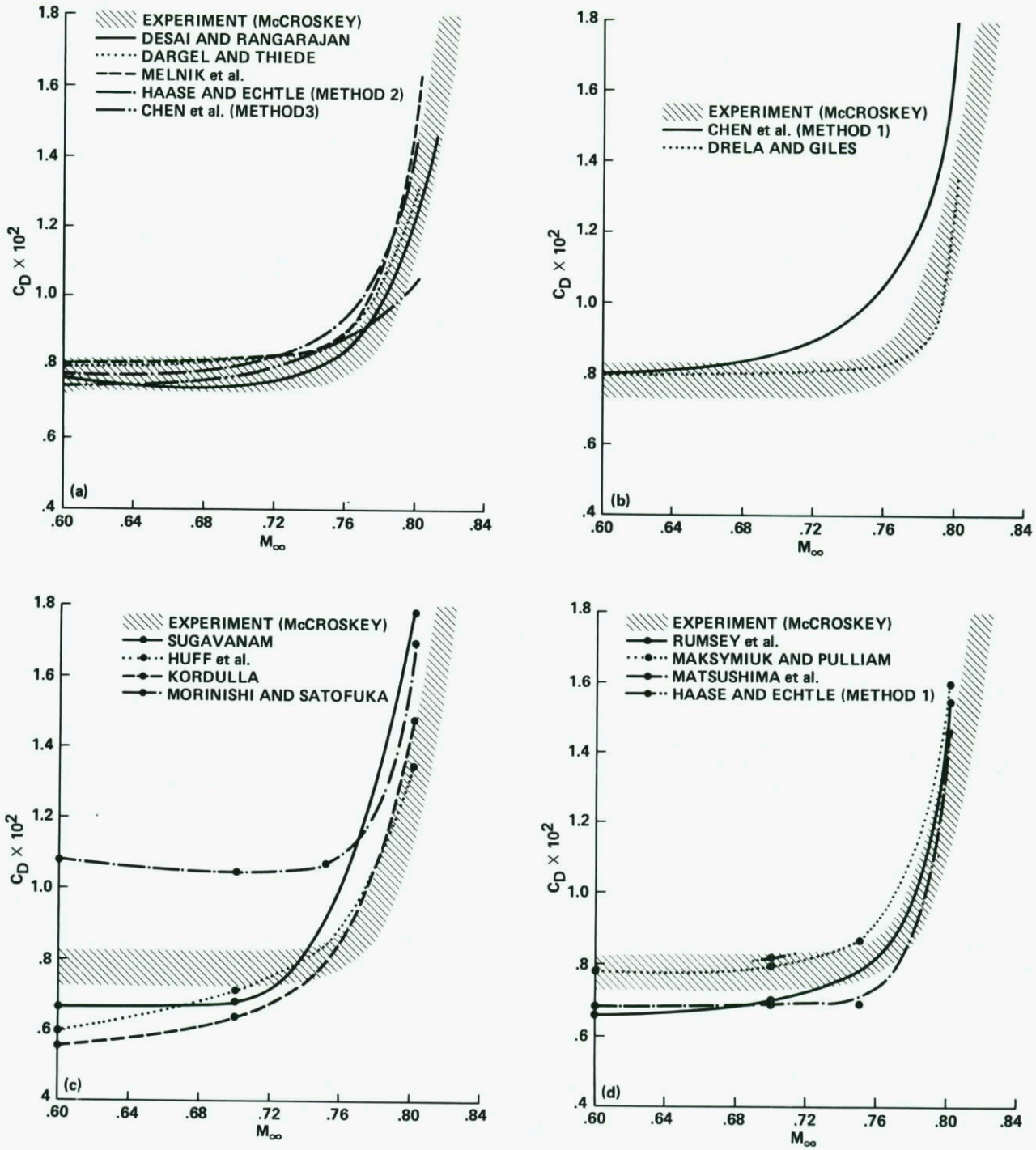

Fig. 6.- Comparison of computed and measured transonic drag-rise characteristics for the NACA 0012 airfoil, $\alpha = 0°$, $Re_c = 9.0 \times 10^6$. a) Computations utilizing potential-plus-boundary-layer methods. b) Computations utilizing Euler-plus-boundary-layer methods. c) Computations utilizing Navier-Stokes methods on coarse grids. d) Computations utilizing Navier-Stokes methods on fine grids.

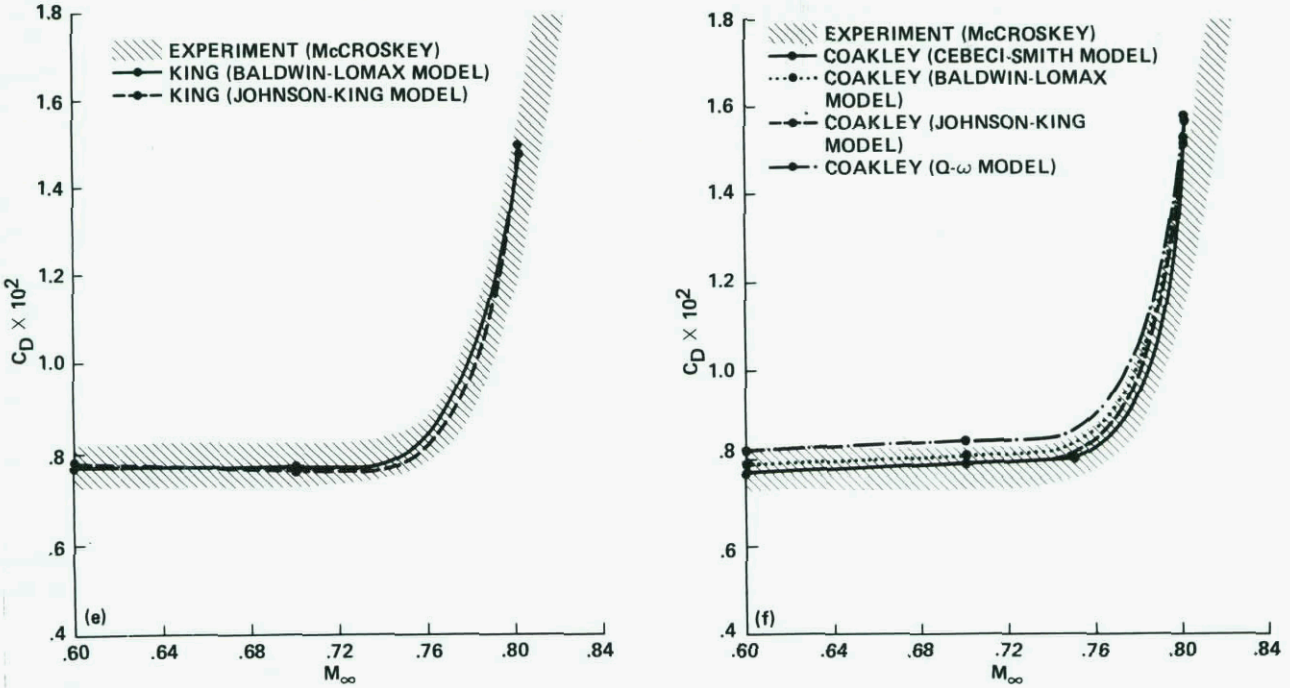

Fig. 6.- *Concluded.* e) Navier-Stokes computations with turbulence model variation due to King (Ref. 10). f) Navier-Stokes computations with turbulence model variation due to Coakley (Ref. 7).

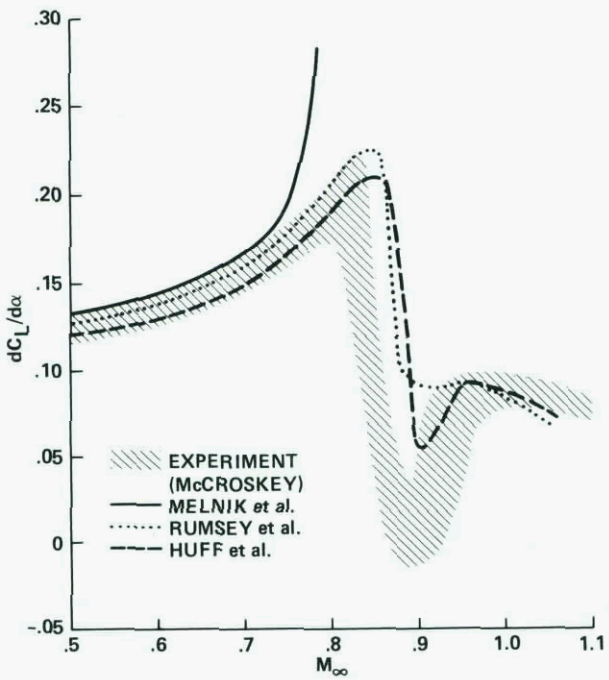

Fig. 7.- Comparison of computed and measured results for the lift-curve slope as a function of the freestream Mach number, NACA 0012 airfoil.

GRID REFINEMENT STUDY

As a part of the VTA Workshop, a grid refinement study was requested for the NACA 0012 airfoil solution presented in Fig. 1. The conditions for this solution are as follows: $M_\infty = 0.7$, $\alpha = 1.49°$, and $Re_c = 9x10^6$. This is a relatively easy solution with all CFD methods producing excellent agreement with each other and with experiment in terms of surface pressure (Fig. 1). Results of the grid refinement study are shown in Fig. 8 where the drag coefficient is plotted versus the inverse of the number of grid points on the airfoil chord (Δ). There are a total of six curves displayed in this figure, all without labels. The computational points defining each curve are displayed as solid circular symbols. The experimental drag level from Harris and a drag band representing the computational methods that reported drag levels for this case are also displayed. As desired, most of the curves approach a drag asymptote which falls in the lower end of the computational band near the experimental value ($C_D = 0.0079$). Of the curves presented, three have large slopes

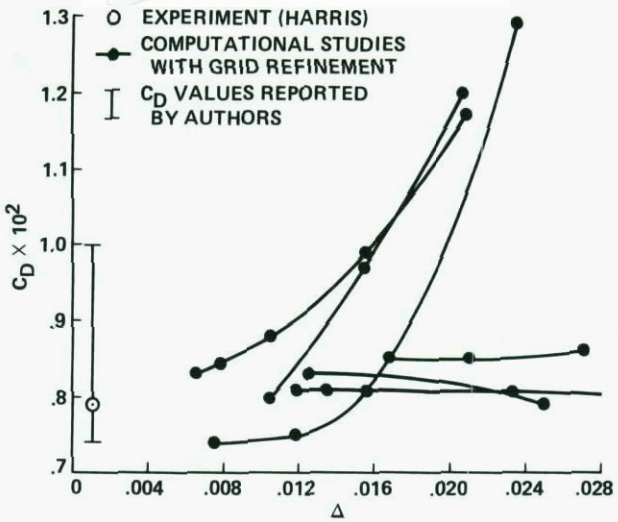

Fig. 8.- Computed drag coefficient versus average grid spacing on the airfoil upper surface (Δ) for the NACA 0012 airfoil (grid refinement study), $M_\infty = 0.7$, $\alpha = 1.49°$, $Re_c = 9.0 \times 10^6$.

and three have small slopes. The methods that produce small-slope results have reasonable drag levels even on coarse grids, which is a desirable characteristic. The methods that produce large-slope results have large drag errors when coarse grids are used. This is an alarming situation. Grid refinement checks such as the one in Fig. 8 are extremely important and can help calibrate the level of grid refinement required for applications and even uncover errors when the proper asymptotic behavior is not achieved.

COMPUTATIONAL STATISTICS

A relatively complete set of computational statistics for several of the cases just presented is given in Ref. 17. Of particular interest are the floating-point operation counts required for a solution from each of the individual methods. These statistics were not directly available from each author but were estimated from the statistics generally supplied by each author. The variation in per-solution operation count was quite large ranging from 4×10^7 to 6×10^{11}. The inviscid-plus-boundary-layer methods (Nos. 2, 3, 5, 11, 13, 20, and 22 from Table 1) have operation counts that range from about 4×10^7 to 2×10^{10}. This range is very large by itself and is primarily due to the wide diversity of methods within this category. The operation counts for the Navier-Stokes methods vary from about 2×10^{10} to 6×10^{11} and are due to variations in grid size and rates of convergence. From these statistics the inviscid-plus-boundary-layer methods appear to be about 30 to 500 times faster than the Navier-Stokes methods. However, caution should be exercised with this comparison because the Navier-Stokes methods generally utilized finer grids and produced most of the solutions for the more difficult cases, for example, cases involving maximum lift or drag. In addition, several of the Navier-Stokes methods were used time-accurately for unsteady solutions which increased the operation counts for these runs by several times.

CONCLUDING REMARKS

The Viscous Transonic Airfoil (VTA) Workshop has been held for the purpose of validating viscous transonic airfoil computations over a range of flow conditions. A total of 15 author groups have submitted 23 different sets of computed results. These results are compared with each other and experiment, when appropriate, in a series of plots with a variety of different results. The primary objective of this presentation is to establish method capabilities for predicting trends and individual flow field details. An additional purpose is the establishment of a data base which can be used for future computer code validation.

To a large extent the results obtained from the VTA Workshp are presented herein without concluding remarks. Specific conclusions about which methods are superior or inferior are left to the reader. Nevertheless, several general conclusions are easily identified and are now presented.

1. CFD methods for transonic, attached airfoil calculations have reached a sophisticated level of development. Most methods are capable of producing valuable results in the design environment, including the prediction of lift to within ±3% and drag to within ±5%. Other computed flow field data, including velocity boundary layer profiles and skin friction distributions, are in good agreement with each other and with experiment. Computational and experimental scatter for zero-lift drag-rise characteristics are comparable providing proper levels of grid refinement are utilized in obtaining the computational results.

2. CFD methods for transonic, separated airfoil calculations are not as well developed as the methods for attached flow computations. This is largely due to the lack of accurate turbulence modeling in regions of separated flow. Turbulence model inadequacies are the most important physical model error associated with the results contained in this report. Despite this major problem, recent progress in this area suggests hope for the future.

3. Many errors associated with CFD computer programs are solely numerical in nature. This type of error can be identified by various types of solution-to-solution comparison. Inappropriate grid clustering and refinement are the most important numerical errors associated with the results contained in this report. Establishment of "standard" levels of grid refinement is difficult because different methods have different requirements. However, grid refinement studies can be used to help eliminate these errors. More emphasis should be placed on solution-to-solution comparisons to aid in the evaluation and elimination of numerical errors.

ACKNOWLEDGMENTS

The time and effort of all the authors who participated in this workshop is deeply appreciated. Without their efforts an undertaking of this sort would not have been possible. In addition, the efforts of all the committee members who participated in the selection of test cases used in this workshop is deeply appreciated. A list of these individuals is as follows: Drs. Richard Barnwell, Leland Carlson, Norman Malmuth, Frank Marconi, Jr., William McCroskey, and William Van Dalsem.

REFERENCES

1. Sugavanam, A., "Transonic Viscous Flow Predictions with the Lockheed Navier-Stokes Code," AIAA Paper No. 87-0410, Jan. 1987.

2. Desai, S. S. and Rangarajan, R., "Viscous Tansonic Flow over Aerofoils Using Transonic Full Potential Equation in a System of Cartesian Coordinates," AIAA Paper No. 87-0411, Jan. 1987.

3. Dargel, G. and Thiede, P., "Viscous Transonic Airfoil Flow Simulation by an Efficient Viscous-Inviscid Interaction Method," AIAA Paper No. 87-0412, Jan. 1987.

4. Rumsey, C. L., Taylor, S. L., Thomas, J. L., and Anderson, W. K., "Application of an Upwind Navier-Stokes Code to Two-Dimensional Transonic Airfoil Flow," AIAA Paper No. 87-0413, Jan. 1987.

5. Melnik, R., Brook, J., and Mead, H., "GRUMFOIL: A Computer Code for the Computation of Viscous Transonic Flow Over Airfoils," AIAA Paper No. 87-0414, Jan. 1987.

6. Maksymiuk, C. M. and Pulliam, T. H., "Viscous Transonic Airfoil Workshop Results Using ARC2D," AIAA Paper No. 87-0415, Jan. 1987.

7. Coakley, T. J., "Numerical Simulation of Viscous Transonic Airfoil Flows," AIAA Paper No. 87-0416, Jan. 1987.

8. Chen, L. T., Li, S., and Chen, H., "Calculation of Transonic Airfoil Flows by Interaction of Euler and Boundary-Layer Equations," AIAA Paper No. 87-0521, Jan. 1987.

9. Chang, K. C., Alemdaroglu, N., Mehta, U., and Cebeci, T., "Further Comparisons of Interactive Boundary-Layer and Thin-Layer Navier-Stokes Procedures," AIAA Paper No. 87-0430, Jan. 1987.

10. King, L. S., "A Comparison of Turbulence Closure Models for Transonic Flows About Airfoils," AIAA Paper No. 87-0418, Jan. 1987.

11. Huff, D. L., Wu, J-C., and Sankar, L. N., "Analysis of Viscous Transonic Flow Over Airfoil Sections," AIAA Paper No. 87-0420, Jan. 1987.

12. Matsushima, K., Obayashi, S., and Fujii, K., "Navier-Stokes Computations of Transonic Flow Using the LU-ADI Method," AIAA Paper No. 87-0421, Jan. 1987.

13. Haase, W., Stock, H-W., and Echtle, H., "Computational Results for Some Test Cases of Viscous Transonic Flow Around Airfoils," AIAA Paper No. 87-0422, Jan. 1987.

14. Kordulla, W., "Using an Unfactored Predictor-Corrector Method," AIAA Paper No. 87-0423, Jan. 1987.

15. Drela, M. and Giles, M., "Viscous-Inviscid Analysis of Transonic and Low Reynolds Number Airfoils," AIAA Paper No. 87-0424, Jan. 1987.

16. Morinishi, K. and Satofuka, N., "A Numerical Study of Viscous Transonic Flows Using RRK Scheme," AIAA Paper No. 87-0426, Jan. 1987.

17. Holst, T. L., "Viscous Transonic Airfoil Workshop Compendium of Results," AIAA Paper No. 87-1640, June 1987.

18. Kline, S. J., Cantwell, B. J., and Lilley, G. M., Complex Turbulent Flows, Vol. II, 1980-81 AFOSR-HTTM-Stanford Conference on Complex Turbulent Flows, Stanford University, 1982.

19. Harris, C. D., "Two-Dimensional Aerodynamic Characteristics of the NACA 0012 Airfoil in the Langley 8-Foot Transonic Pressure Tunnel," NASA TM 81927, 1981.

20. Baldwin, B. S. and Lomax, H., "Thin Layer Approximation and Algebraic Model for Separated Turbulent Flows," AIAA Paper No. 78-0257, Jan. 1978.

21. Cebeci, T. and Smith, A. M. O., Analysis of Turbulent Boundary Layers, Academic Press, 1974.

22. Johnson, D. A. and King, L. S., "A Mathematically Simple Turbulence Closure Model for Attached and Separated Turbulent Boundary Layers," AIAA J., Vol. 23, No. 11, Nov. 1985, pp. 1684-1692.

23. Coakley, T. J., "Turbulence Modeling Methods for the Compressible Navier-Stokes Equations," AIAA Paper No. 83-1693, July 1983.

24. McCroskey, W. J., Private communication, October 1987.

25. McCroskey, W. J., "A Critical Assessment of Wind Tunnel Results for the NACA 0012 Airfoil," Paper No. 1, AGARD Fluid Dynamics Panel Symposium on Aerodynamic Data Accuracy and Quality: Requirements and Capabilities in Wind Tunnel Testing, Naples, Italy, Sept. 28-Oct. 2, 1987.

CFD DRAG PREDICTION FOR AERODYNAMIC DESIGN

by
Charles W. Boppe

Grumman Corporation
Aircraft Systems Division
Bethpage, NY 11714

SUMMARY

Consistent and accurate Computation Fluid Dynamics (CFD) prediction of absolute drag level for aircraft configurations is currently beyond reach. This is attributed to several elements characterizing state-of-the-art computer algorithms and hardware. With considerable research focused on the 2-D airfoil analysis problem, an exercise is conducted to quantify the implications for 3-D wings. Recent highlights in the U.S.A. which have advanced drag prediction capabilities or improved understanding of the problem are described. Examples are taken from the areas of computational physics, viscous airfoil simulation, component analysis, hypersonics, and conceptual design/configuration optimization. Primary attention is concentrated on aircraft but helicopter, missile, and automobile cases are also included. A near term solution to the CFD drag prediction problem can not be identified. Instead, means based on CFD's strengths are discussed which make computational methods valuable for drag reduction/prediction during aerodynamic design processes.

NOMENCLATURE

C_L	Lift Coefficient
C_D	Drag Coefficient
C_{D_i}	Lift-Induced Drag Coefficient
π	3.14159
C_p	Pressure Coefficient
M_∞	Freestream Mach Number
t/c	Airfoil/Wing Section Thickness-to-Chord Ratio
$\mathcal{R}$	Aspect Ratio
P	Pressure
X/L	Non-Dimensional Axial Distance
Λ	Sweep Angle
R_e, Rn	Reynolds Number
L/D	Lift/Drag Ratio
C_{D_o}	Zero-Lift Drag Coefficient
C_A	Axial Force Coefficient
C_M	Pitching Moment Coefficient
C_N	Normal Force Coefficient
α	Angle-of-Attack (Deg.)
Q	Heat Transfer Coefficient
TLNS	Thin Layer Navier-Stokes
q	Dynamic Pressure
BM	Bending Moment
FS	Fuselage Station
IN	Inch
KIP	1000 Pound Unit of Weight
T	Thrust
D	Drag
λ	Wing Taper Ratio (C_{TIP}/C_{ROOT})
X,Y,Z	Spatial Coordinates
d	Diameter
δ_F	Flap Deflection Angle (Deg.)
Count	Drag Coefficient Value of 0.0001
c	Chord Length

b	Span
SOB	Side of Body
$\bar{c}$	Average Chord
η	Wing Span Location (2 y/b)
P_T	Total Pressure
C_f	Friction Drag Coefficient
S_{WET}	Wetted Area
TOGW	Total Gross Weight (Vehicle)
I	Mass Injection Ratio

SUBSCRIPTS

av	Average
2-D	Two-Dimensional
3-D	Three-Dimensional
eff	Effective

1 - INTRODUCTION

An ever-present need to improve maneuvering performance and reduce fuel consumption of all powered aero-configured vehicles guarantees that the topic of drag prediction and reduction will remain a high priority for engineering design and analysis. Many conferences, meetings, and short courses have concentrated on elements of this subject. Several of the larger volumes which have resulted are itemized in Table 1.

Table 1 Drag Prediction/Reduction Reference Volumes

VOLUME	TITLE	DATE
AGARD CP-124	AERODYNAMIC DRAG	1973
AGARD AR-138	EXPERIMENTAL DATA BASE FOR COMPUTER PROGRAM ASSESSMENT	1979
AGARD CP-264	AIRCRAFT EXCRESCENCE DRAG	1981
AFWAL TM-84-203	PREDICTION OF AERODYNAMIC DRAG	1984
AGARD-R-723	AIRCRAFT DRAG PREDICTION	1985

R88-6099-023

Unfortunately, drag prediction difficulties, associated criticality in the design process, and commercial implications have evolved an environment wherein the free exchange of ideas and experiences is somewhat hindered save for university research and government lab activities. Several messages, however, form a consensus within existing literature. First, experimental techniques dominate publications dealing with absolute drag prediction. A majority of authors clearly believe that experimentation is practically the only means for both drag prediction and reduction. Second, a very small percentage of publications with central themes concentrating on CFD touch on the subject of drag. Instead, CFD research results focus on the prediction of flow field characteristics such as pressures, flow angularity, separation regions, shock wave patterns, wake visualization, etc. Third, research programs and aerodynamic configuration development programs do not generate drag and related phenomenological data of sufficient depth and quality to permit an organized attack on current deficiencies which could dramatically alter the state-of-the-art. This is true of both experimental and computational elements of these programs. It then becomes important to identify current capabilities and to use this information for focusing on areas of high potential pay-offs.

Industry configuration development programs have been in the past and are currently characterized by a drag build-up technique which is used for performance estimation purposes. The build-up technique varies from organization to organization and within an organization the technique varies from individual to individual since judgements are often required. In general, empirical data and organization design history will greatly influence this process. It is important to recognize that this classical approach to drag prediction is severely compromised when new aerodynamic configurations are being investigated for which little historical data base exists. Background for configuration drag build-up techniques can be found in Paterson's work[15] which covers subsonic and transonic aircraft applications with a slant towards transports. Jobe's report[3] provides transport and fighter aircraft drag estimation methodology. The supersonic speed regime is also included in Reference 3 along with data base information. Recent computational code results are identified which provide some indication of simulation accuracy for various drag components.

The magnitude of the total aircraft drag prediction problem can be illustrated in one sense by examining the various sources of excrescence drag on a typical fighter aircraft. Table 2 highlights the variety in antennas, lights/probes, and openings that might be encountered in fighter design.

TABLE 2 TYPICAL EXCRESCENCE DRAG

ANTENNAS (Exterior)	OPENINGS
1 Blade (APR-27) 10.32 $in.^2$	1 Fuel Dump – inc. in DECH Pod
2 Blade (AN/APX73) (AS1918/AR TACAN) 44 $in.^2$	1 Bleed Valve 2 in. - 4.5 in.
1 Blade (F-111) 32 $in.^2$ i = 30°	2 Engine Drains
1 ALQ-xxx DECM Pod (F-14)	18 Water/Fuel Drains 1/8 - 5/8 in. dia
4 Blade PDS 8 $in.^2$ each	5 Fuel Cell Vents (fuselage)
2 ECM pods (F-111) Tail/Wing	2 Refueling Sump Drains
	2 ECS Ground Cooling Louvers
	2 Oil Breathers 14 Holes @ 3
	Cockpit Safety, Gun Gas - Gas Purge
LIGHTS & PROBES	1 Ammo Vent, 1-Cockpit Exh.
	2 Oil Cooler, 2 ECS Exh.
2 Pitot Static Probes	2 Hyd. Oil Cooler Scoops
2 Total Temp Probes	2 Engine & IDG Oil Cooler
1 A-O-A Transmitter	1 EPU Intake & Exh Louver
2 Ball Nose Alpha Probes	1 APU Intake & Exh Louver
24 Static Discharge Probes	2 Bleed Air Heat Exchanger
1 Navigation Light	
1 Anti-Collision Light	
MISCELLANEOUS	
1 Windshield Rain Removal	
Access Door Hinges	
1 Arresting Hook	
R88-6099-024	

While on a large-scale, attention must be focused on global features of the configuration like the fuselage, wing, and trim surfaces which account for the main portion of friction, wave, and lift-induced drag ... it must also be apparent that absolute drag prediction for aircraft requires detailed attention to small-scale elements. This mixing of scales presents a significant problem for CFD which is somewhat constrained by today's supercomputers. The aircraft designer, however, recognizes that many of the small-scale geometric features listed in Table 2 are also beyond the range of successful ground test facilities using sub-scale models.

One obstacle to improving the ability to predict drag via CFD evolves from the typical dichotomy of critical task assignments. Researchers or methodology developers rarely participate in a project environment, the goal of which is to optimize a design or diagnose a problem. This appears to be, in part, attributable to personal preferences and an incompatibility related to skill requirements. As a result, the end-goal for many computational fluid dynamicists, or computational aerodynamicists; that of demonstrating that pressure fields agree with those from sub-scale testing – is not very satisfying for the project engineer responsible for an application involving aerodynamic performance.

It can be appreciated that subtle discrepancies between computed and experimental pressures will have different effects on drag and pitching moments obtained via pressure integration depending on local position and geometry. A small pressure anomaly near the middle of an aerodynamic configuration (where surface shaping is nearly aligned with the onset flow) will sum to produce a negligible contribution to total drag and if the location is near the moment center ... a negligible effect on overall pitching moment. If the pressure anomaly, even though small, is positioned aft on the configuration, say on a nozzle boattail, a significant drag effect will register due to integration on an aft-facing surface and significant moment effects can register since the moment arm is large.

Two additional examples of good pressure agreement not resulting in satisfactory engineering predictions are also included here for illustrative purposes. Consider the load prediction exercise sketched in Figure 1. Here, a fuselage forebody shape has been sketched. Pressure instrumentation might be positioned at sixteen fuselage axial stations. One can imagine that a computational solution might even touch upon all of the experimental data points as illustrated. To many, the pressure correlation shown here would be interpreted to be proof that a satisfactory solution or simulation is in hand. But fuselage bending moments, critical to satisfactory structural design, require a double integration of pressure ... the first (see Fig. 1-B) results in a shearing force distribution while the second (see Fig. 1-C) produces the fuselage bending moment. It may be surprising that a 36% bending moment discrepancy can be generated over the first quarter of the fuselage length. This has nothing to do with errors in the usual sense. Instead, it is a discrepancy caused by discretization.

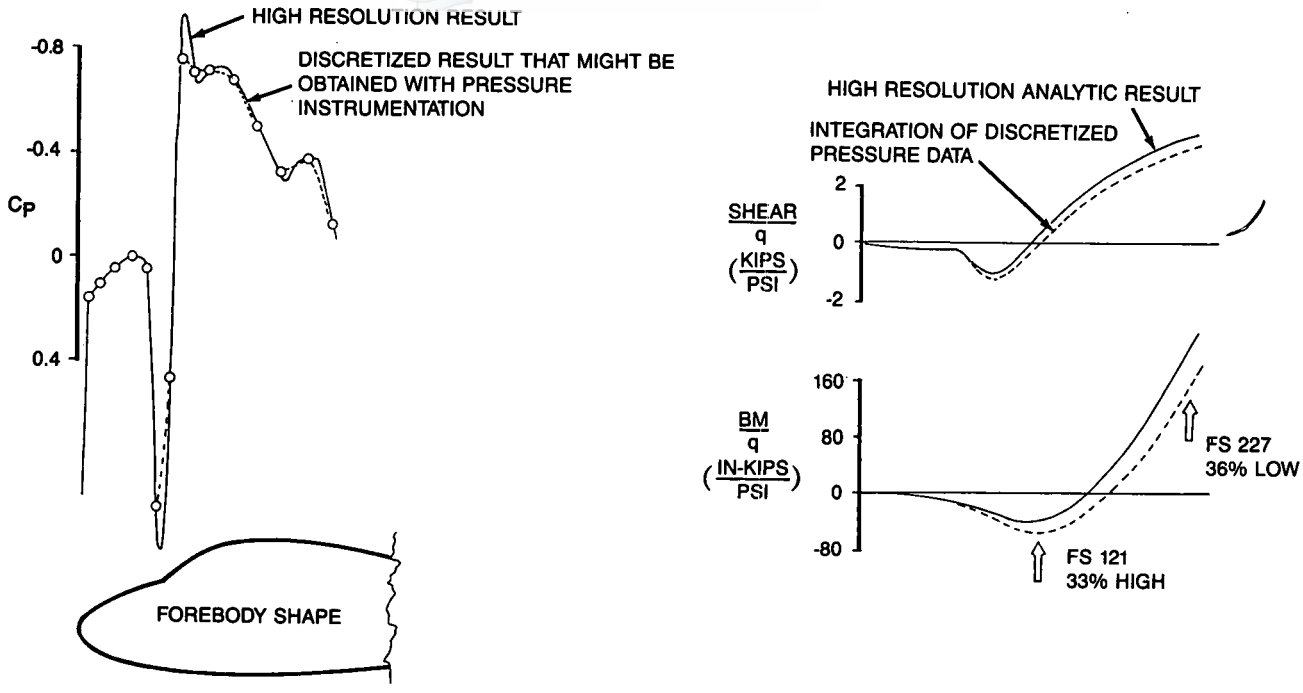

Figure 1 Effect of Pressure Distribution Discretization on Fuselage Shear & Bending Moment M = 0.7; $\alpha = 4°$

Heat transfer prediction problems are similar but the source of the difficulty is different. Figure 2 shows computations performed for a bent-nose biconic body shape at hypersonic conditions. The pressure comparison with test data appears to be very good but the accompanying heat transfer correlation is compromised. This type of discrepancy for Navier-Stokes code solutions is related to the convergence level achieved (see Section 2.6-D). These examples highlight two points. First, the most common means now used to validate CFD codes (pressure correlations) can be misleading for several elements of engineering applications. Second, drag forces are not the only source of difficulties for CFD codes. Problems can be identified on several different fronts, but the solution to one is likely to have beneficial implications for the others.

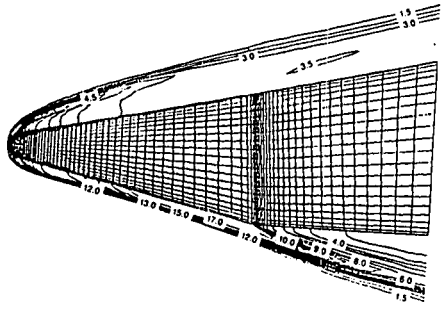

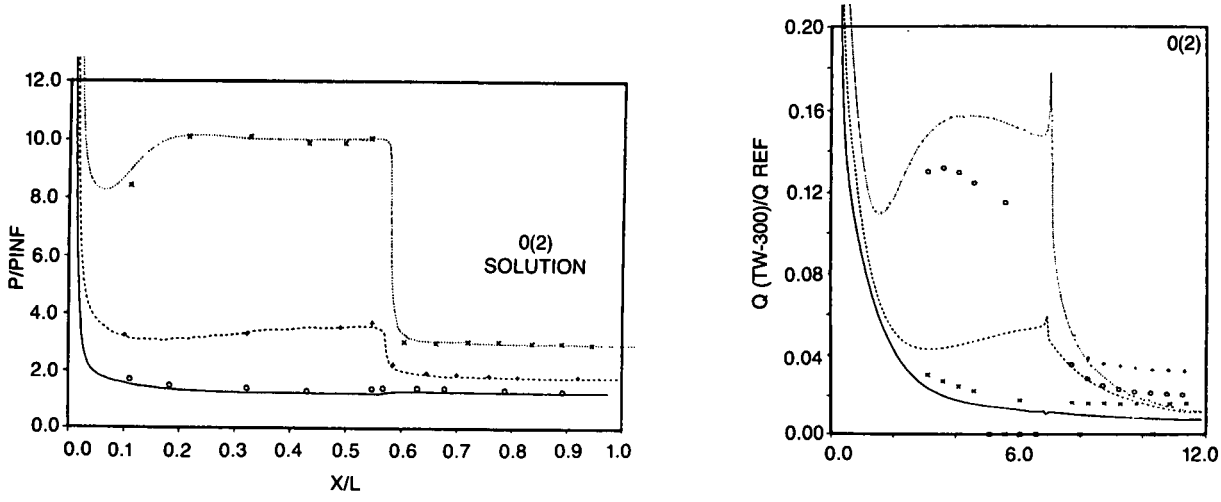

Figure 2 Pressure Field & Heat Transfer Computational (after 1/2 Hour on Cray X-MP)

Geometric complexity provides another source of difficulty for CFD. This was suggested earlier in the examination of the various sources of excrescence drag. Geometric complexity also takes the form of (1) complex lifting surface combinations, (2) multiple weapon/store carriage (with pylons and attachments), and (3) blended airframe-propulsion integration shaping. CFD simulations for these cases are hindered by a limited ability to generate very complex computing grid systems.

A final consideration deals with what might be called microphysics. This involves complexity in a flow feature sense as opposed to the aforementioned complexity in a geometric sense. Whether manifested alone or in combination with geometric complexity, the result is the same ... compromised simulation fidelity. Flow elements for consideration might include vortices, shock waves, mixing layers including entrainment, wake shear surfaces and turbulent separated flow regions. Detailed numerical simulation of these isolated flow features is difficult. Typical aircraft applications, however, include combinations of these elements as well as element interactions. Sufficient knowledge to treat all interaction combinations numerically is not in hand. Unfortunately, all of the flow elements listed affect drag levels so it becomes important to study computational physics if the primary interest is drag prediction via computational aerodynamics.

To evaluate the current state-of-the-art in CFD drag prediction for the United States, items from the aircraft, helicopter, and missile industry have been gathered. Aircraft applications concentrate primarily on problems related to the transonic flow regime, but hypersonic flow applications are increasing at a rapid pace. Helicopter technology focuses primarily on rotor airfoil drag prediction at transonic speeds and fuselage flow separation issues at subsonic speeds. Missile analyses are typically performed at supersonic speeds and the area of interest is usually base drag. Recent highlights in CFD drag prediction are identified along with the building blocks required to tackle future applications.

2 - DISCUSSION

It should be recognized upfront that the subtleties of aerodynamic drag are inherent in a number of flow field elements which can be easily observed such as ...

1) Vortices
2) Wakes
3) Shock Waves
4) Viscous Shear Layers
5) Turbulence
6) Base Flows
7) Heating Layers
8) Transition Regions.

But observation of these elements is not sufficient because difficult to observe microscale phenomena form the building blocks which determine element characteristics and effects. To further compound the drag prediction problem, aerodynamic flows typically involve interactions of these elements. Shock waves intersecting high-viscosity flow regions near surfaces, free vortices, wakes, and separation bubbles result in physical flow phenomena which are not well understood. As a result, CFD drag prediction depends now, and even more so in future, on a field called Computational Physics.

2.1 COMPUTATIONAL PHYSICS

Turbulence simulation continues to be the primary problem in computing fluid physics. A mix of large and small-scale fluid motion results in instabilities which impede numerical investigations. Further, attempts to enhance knowledge experimentally are compromised by a current inability to measure pertinent dynamic quantities. State-of-the-art test practice now is characterized by measurements which are in a sense "integrated" over both space and time.

In trying to enhance physical knowledge required to refine predictive capabilities, the physical constraints imposed by modern computers become apparent. Turbulent mixing layers, for example, might be better understood by modeling an inviscid vortex sheet, but consider this statement by Krasny(33):

> "A practical consequence for the present problem is that any consistent discretization of the vortex sheet equations will also have a short wave-length linear instability. In an actual computation, short wavelength perturbations are introduced spuriously by roundoff error and they may grow fast enough to destroy the calculation's accuracy. With a fixed machine precision, refining the mesh does not reduce the computational error since the discretization then resolves shorter wavelength modes which grow faster once they are perturbed by roundoff error."

Novel numerical schemes will be required to deal with constraints to establish this capability. Reference 33 describes a step in this direction.

Computer hardware limitation implications are also apparent in recent work by Rogallo and Moin(34) which highlights computational requirements for simulating the smallest eddies found in a turbulent channel flow at $Re = 10^4$. Approximately 5×10^{10} grid points coupled with 2000 time steps were needed to reach a steady state. For perspective, note that a majority of computations now being performed using Reynolds-Averaged Navier-Stokes formulations are based on grid systems featuring total point counts between 100,000 and 300,000 (500 to 1000 time steps). It is not clear at this point in time, how long it will take, or what technological breakthrough will make it possible to tackle aerodynamic applications with what is now perceived to be required resolution and cycle count.

2.2 AIRFOIL TECHNOLOGY EVALUATION

Establishing a foundation for understanding complete aircraft drag prediction capabilities might best be achieved by the examination of components in detail. For aircraft, the lifting wing and propulsion system present a major technical challenge in flow simulation. Limitations on drag prediction for 3-D lifting wings can be appreciated by studying simpler two-dimensional airfoil section predictions. Over the past 10-year period, a number of workshops[48,50] have been conducted to assess the ability of CFD to predict lifting airfoil flow fields. Holst[9] reports on the results of a recent workshop organized by the AIAA Fluid Dynamics Technical Committee. Twenty-three solution sets (70% N.S., 30% iterative B.L.) addressed the simulation of viscous flows for transonic airfoils.

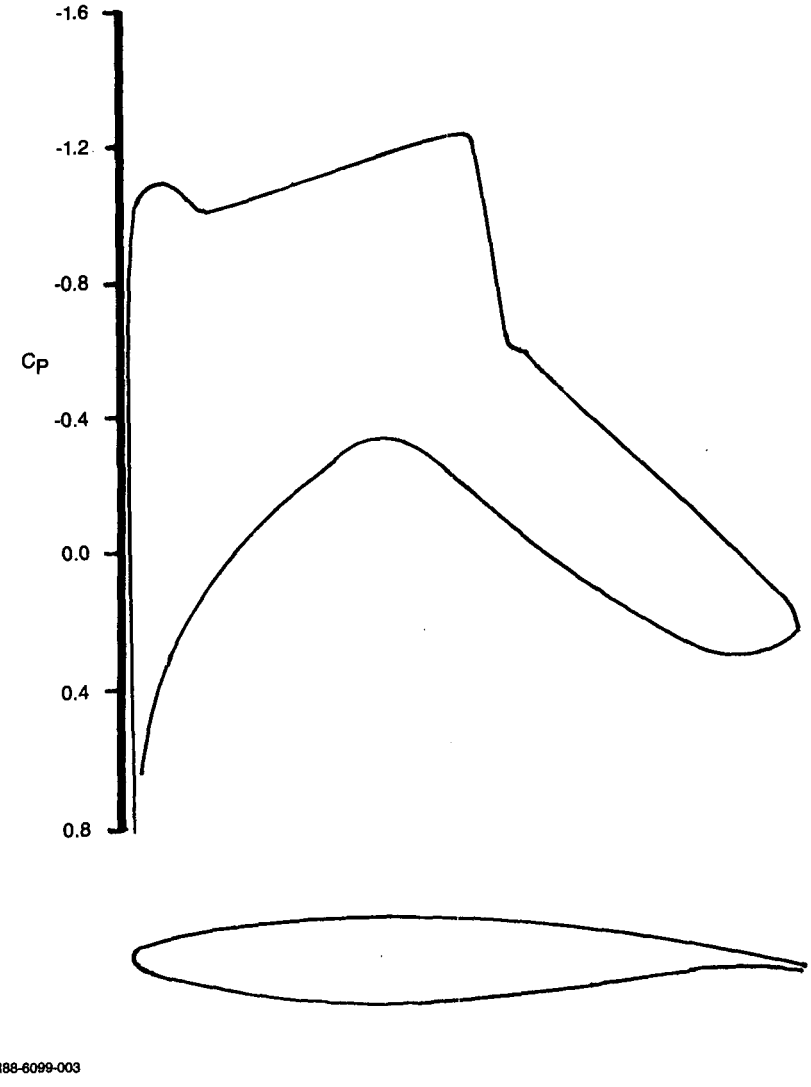

Figure 3 RAE 2822 Airfoil Pressure Distribution at M_∞ = 0.725, α = 2.9°

Several airfoil shapes were studied. Perhaps the most interesting airfoil, from an engineering design point of view, is the RAE 2822 airfoil (Figure 3). Test data for this section can be found in Reference 41. To form a drag rise curve with variable lift level data, Korn's relation*

$$M_\infty + \frac{C_L}{10} + t/c = K \qquad (1)$$

can be used. It provides an approximation of Mach/lift trades. The resulting drag rise curve for C_L=0.74 has been illustrated in Figure 4. Drag Divergence appears to occur near M_∞=0.7 which results in an "advanced airfoil" K-factor of 0.89. Conventional airfoil K-factors are near 0.87 while NASA-type supercritical sections with severe pitching moments exhibit K-factors near 0.95. A typical design point characterized by maximum M L/D occurs near M_∞=0.7 where this value is close to 59. Test data at M_∞=0.725 provides information nearest to what might be identified as a design condition. At this point, the shock wave is relatively strong but there is no evidence of appreciable flow separation. Code/experiment comparisons[9] reveal that on average, drag predictions disagree by approximately 5% and shock wave locations typically disagree by about 5% of chord length. These comparisons are compromised by some computational lift levels that are as much as 10% different than test data.

*Dr. David Korn (formerly of NYU – Courant Institute)

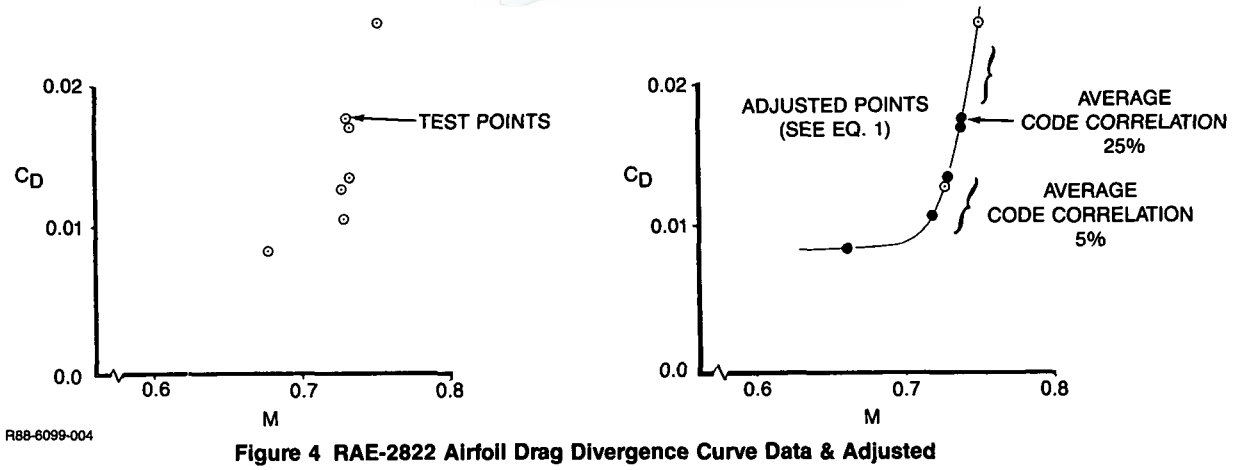

Figure 4 RAE-2822 Airfoil Drag Divergence Curve Data & Adjusted (C_l = 0.74)

It will be shown in the following Section that beyond-design-Mach conditions are important and the prediction of shock wave position is as critical for engineering applications as is the absolute level of 2-D drag predicted. RAE-2822 data at M_∞=0.74 illustrates a more severe case. Reference 9 reveals that average drag discrepancies are now on the order of 25% and shock positioning errors average close to 10% chord.

Understanding three-dimensional wing implications based on two-dimensional flow is important because "2-D" represents an upper limit for simulation fidelity. Three-dimensional flows are always more complex and computer hardware constraints guarantee that 3-D wing section resolution will be considerably less dense than that used for 2-D airfoil sections. This leads to transonic wing design/analysis implications based on the Reference 9 compendium of airfoil simulation results.

2.3 WING DESIGN/ANALYSIS IMPLICATIONS

Simple Sweep Theory has been used in the past to relate 2-D and 3-D airfoil characteristics. It was shown in Reference 4 that these simple cosine relations remain valid through the transonic regime providing that the effective sweep angle (Λ_{EFF}) is used instead of any geometric angle linked to the wing planform so ...

$$M_{2\text{-}D} = M_{3\text{-}D} \times \cos\Lambda_{eff} \quad (2)$$

$$C_{L_{2\text{-}D}} = C_{L_{3\text{-}D}} / \cos^2\Lambda_{eff} \quad (3)$$

$$t/c_{2\text{-}D} = \frac{t/c_{3\text{-}D}}{\cos\Lambda_{eff}} \quad (4)$$

$$C_{P_{2\text{-}D}} = C_{P_{3\text{-}D}} / \cos^2\Lambda_{eff} \quad (5)$$

$$C_{D_{2\text{-}D}} = C_{D_{3\text{-}D}} / \cos^3\Lambda_{eff} \quad (6)$$

At transonic conditions with shock waves present, the local shock wave sweep angle controls or becomes the effective sweep for 2-D/3-D relations.

To develop a physical feel for 2-D/3-D drag relations and shock sweep effects, a typical fighter and transport wing planform can be considered. Planform characteristics are ...

Transport Wing Planform	Fighter Wing Planform
$\mathcal{R}$ = 8	$\mathcal{R}$ = 3
λ = 0.4	λ = 0.2
Λ_{LE} = 25°	Λ_{LE} = 40°

These wing shapes have been sketched in Figure 5. The effective sweep for both planforms is approximately 19° if, for example, the baseline wing section is similar to that of RAE-2822 which features a shock wave at the 55% chord location. At the $M_\infty \sim 0.725$ design point (see Refs. 9 and 41), this 2-D section generates about 107 counts of drag. Using equation 6, a 5% discrepancy in drag measured in two dimensions translates to a 4 1/2 count error for wing (or 3-D) drag prediction.

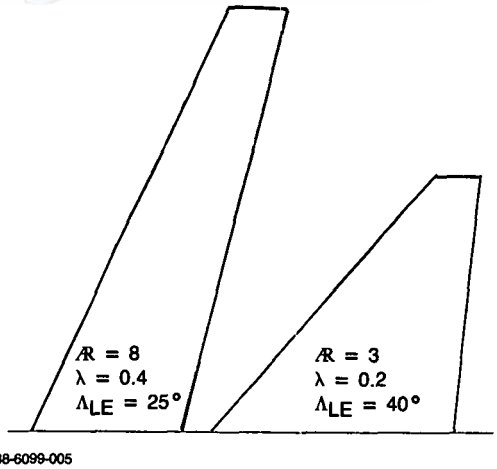

Figure 5 Transport & Fighter Wing Planforms

In the case of both the fighter and the transport wing, anomalies might cause shock sweep to be degraded by 5°. This new 14° shock or effective sweep level raises the 2-D Mach number to 0.75 and now the average 25% discrepancy in drag prediction applies to an airfoil (or 2-D) drag level of 242 counts. This translates into a 55-count drag discrepancy for a wing.

There are many examples where a 5 degree wing shock sweep variation occurs quite naturally and it may not be possible in some applications to design the problem away. A number of these situations have been illustrated in Figure 6. Note that the occurrences can be found on wings, canards, prop-fan blades, vertical tails, and winglets. For wing cases, the shock sweep impairment can be induced by canard downwash or nacelle, pylon, and fuselage interference. It may also be the simple result of load drop-off near the wing tip. The point here is that there are many local regions on a wing at transonic conditions where section drag discrepancies could be near 50 counts at what might be considered mild cruise conditions. Note that sectional drag integrated along the wing span will include a combination of 5% and 25% airfoil-type discrepancy regions. Integrated wing drag as a result might exhibit total 10 to 20% errors depending on configuration complexity and flow severity present in any given application. In an engineering sense, these 3-D drag prediction errors can be minimized by 1) selecting a 2-D code (or codes) which provide(s) accuracy better than the 5%/25% average used here for illustrative purposes and 2) calibrating the code for various classes of airfoil shapes. This calibration process can take the form of creating a Computational Airfoil Catalog (this has been the author's experience). The catalog would essentially be a compendium of high-value code simulations for various classes of airfoils (i.e., NASA Supercritical, NACA, Wortmann, Liebeck sections, etc.) where experimental comparisons can be archived. The aerodynamicist, approaching a design or analysis task involving new airfoil shapes, can identify CFD simulation idiosyncrasies or simulation discrepancy trends by observing like-shape correlations. Empirical biases can then be added to the CFD result. It is the author's experience that a majority of transonic cruise and maneuver design/analysis problems can be tackled using this modified CFD approach based on 2-D polar buildup and historical CFD/experiment adjustments. Absolute drag level prediction considerably closer than 5% can be achieved. Figure 7 illustrates a maneuver polar shape generated during the HiMAT program using this technique. Prior to this, polar estimating accuracy at high-lift can be identified to be approximately 60 counts.

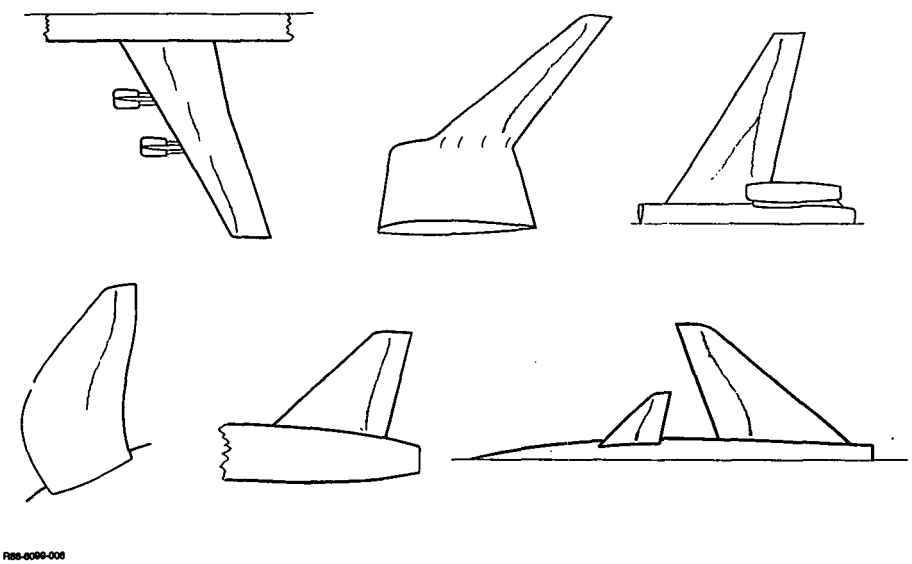

Figure 6 Shock Wave Unsweep Regions

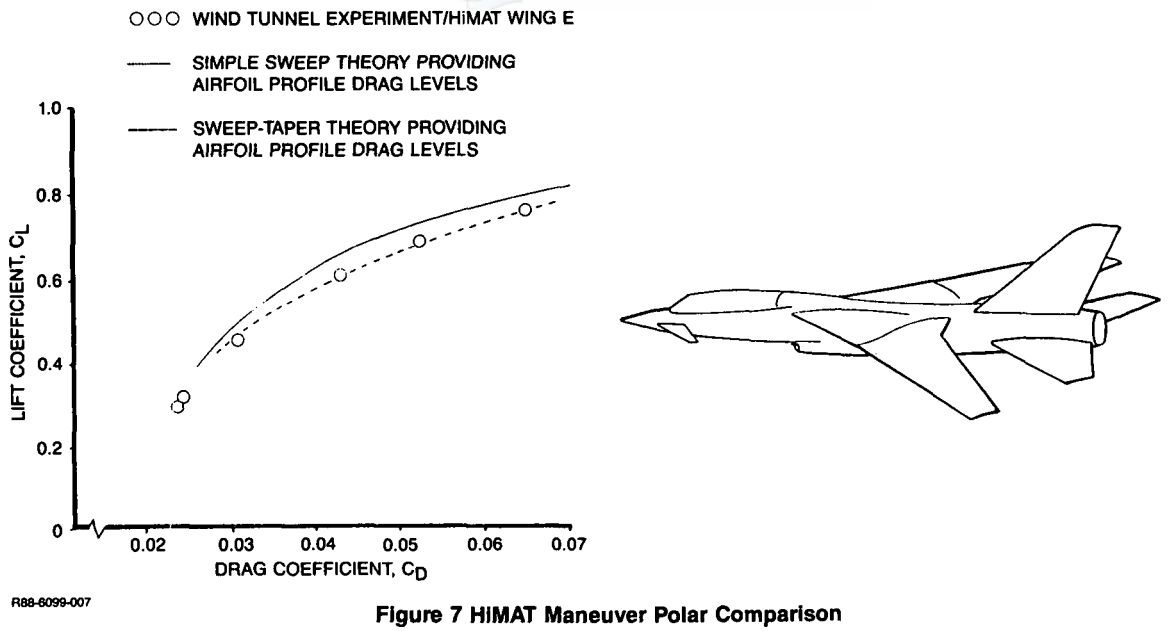

Figure 7 HIMAT Maneuver Polar Comparison

Before leaving this topic, it will be worthwhile to examine the generic fighter wing planform again, but this time using higher lift correlation results found in Reference 9 for the NACA-0012 airfoil (Figure 8). Figure 9-A shows the shock wave location on this planform when the shock wave chord location is 10% c. Here, the effective sweep angle is 37°. The average code/experiment drag discrepancy for $M_{2\text{-}D}$=0.55 and C_L ∿1.0 is 100 counts. Using Equation 6, the wing drag prediction discrepancy is approximately 51 counts. But in some cases at maneuvering conditions, shock wave sweep can effectively be lost completely as sketched in Figure 9-B. If this occurs, the full 2-D drag discrepancy level of 100 counts can register for the wing. Further aggravating this situation ... the 0° shock sweep results in an effective 2-D Mach number which is considerably higher than 0.55. The true "airfoil" drag error for wing performance estimates can easily grow to several hundred counts.

Understanding these limits based on 2-D CFD code performance is important because three-dimensionality further complicates the problem. Identifying the sources of 3-D drag prediction discrepancies can become quite difficult.

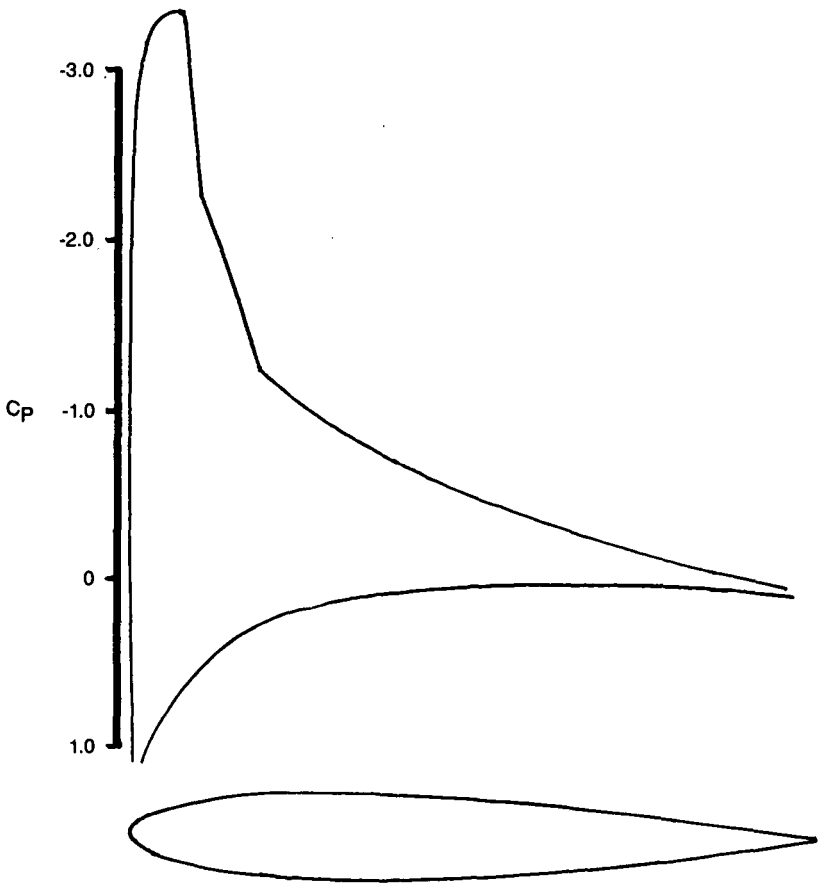

Figure 8 NACA 0012 Airfoil & Pressure Distribution at M = 0.55, α = 8.34°

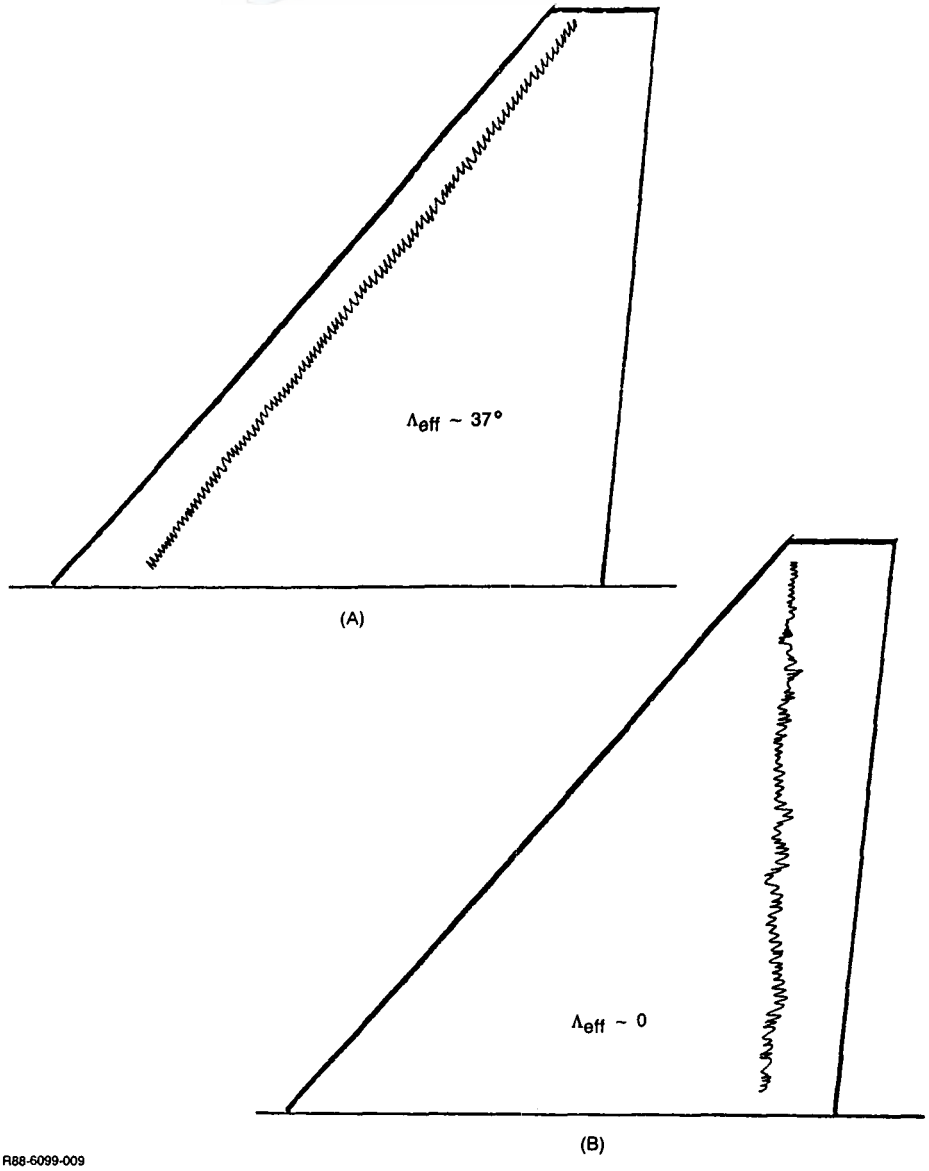

Figure 9 Fighter Planform Effective Sweep Variations

2.4 X-29 EXPERIENCE

For transport design, where aerodynamic configuration variations over the past decades have in most cases been subtle, small improvements in drag ... in the order of 1%, are important. Economic implications can be significant. Fighter design, however, has been characterized by change. Drag improvements much greater than 1%, typically at sustained and instantaneous maneuvering conditions, are sought.

Toward this end goal involving drag reduction, the CFD tool can provide a direct effect in projecting drag levels (absolute or incremental) or it can provide an indirect benefit by providing the designer with an understanding of fundamental flow physics not easily obtained by sub-scale test techniques. This is particularly important when configuration novelty results in a design environment for which little historical information is available. The X-29 configuration development effort would be categorized in this manner.

It was pointed out in the preceding section that by using CFD to enhance the estimation of conventional drag build-up techniques, advances in predictive capabilities could be achieved. Most important, the value of 2-D airfoil analysis methods was stressed based on HiMAT program experiences. Additional computational analyses performed during the HiMAT program[4] using a 2-D[30] potential flow/boundary layer scheme are shown in Figure 10. The 2-D/3-D flow simulation approach described in the preceding section was enhanced by decoupling the airfoil upper and lower surfaces. Upper surface pressures were best simulated by keying the conversion relations (eq. 2 and 3) to the upper surface shock wave sweep angle while lower surface simulations were improved by using a leading edge or quarter-chord sweep angle. This discovery was the result of numerical experimentation. From comparisons, it was reasoned that forward-swept wing planforms might yield transonic aerodynamic performance benefits when compared to more conventional aft-swept arrangements. Since a larger portion of the wing section load is carried on the lower surface in the form of higher pressures (due to lower leading edge sweep of a forward swept wing planform; recall eq. 5), reduced expansion requirements on the upper surface for any given total lift level would result in a weaker shock wave and thus ... lower wave drag. Also, it should be recognized that as angle-of-attack or speed is increased, the wing upper-surface shock

wave will move aft on the wing into a region of higher sweep because of planform taper (i.e., tip chord < root chord). Since airfoil (2-D) wave drag levels will surface as wing (3-D) wave drag via Eq. 6, drag benefits for transonic maneuvering could be identified. This was the basis for initiating the X-29 program.

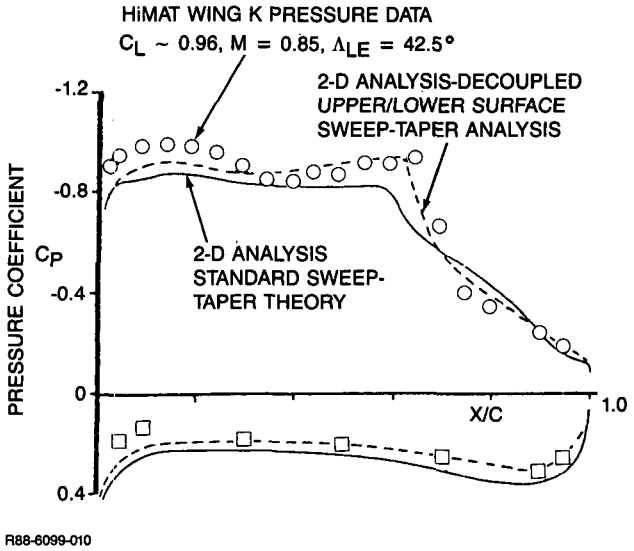

Figure 10 Effect of Decoupled Upper/Lower Surface Analysis for Airfoil K

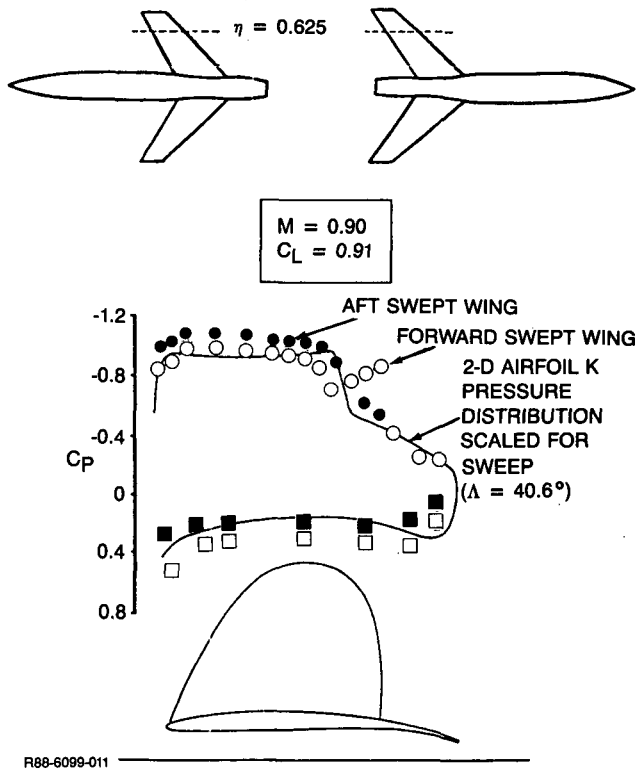

Figure 11 Test Result Showing Forward/Aft Sweep Effect on Upper/Lower Surface Load Sharing

Wind tunnel tests performed during the summer of 1977 confirmed these rationalizations based on CFD numerical experimentation. Figure 11 shows wing upper/lower pressures at comparable lift levels for the forward and aft-swept wing research models tested at M_∞=0.9. The upper/lower pressure shift can be identified. Drag polar comparisons have been included here as Figure 12. Note that maneuvering design point, (M_∞=0.9,C_L=0.9) benefits of about 40 counts were identified. But perhaps more interesting, drag benefits at higher lift levels quickly jump to several hundred counts.

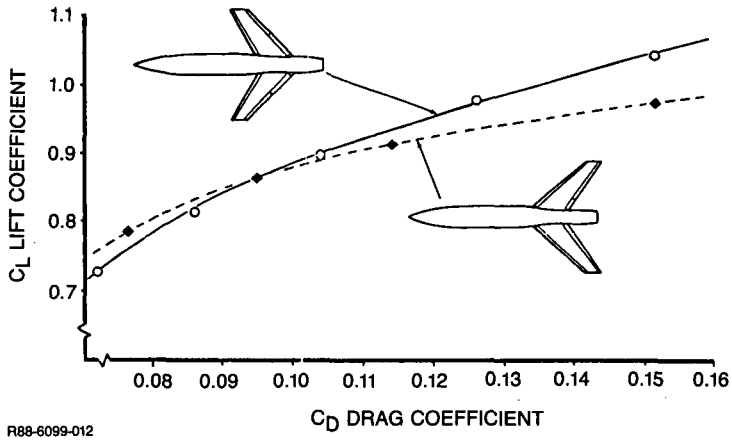

Figure 12 Forward/Aft Swept Wing Drag Comparison, AFFDL Wind Tunnel Test M_∞ = 0.9

Of course, the final proof rests with measured flight test performance. X-29 flight test results conducted over the past year with a calibrated engine are shown in Figure 13-A. All current fighter drag polar efficiency levels have been grouped into a band. Figure 13-A shows a subsonic polar efficiency comparison while Figure 13-B is a similar comparison for transonic conditions. The subsonic polar comparison reveals benefits linked to the X-29's configuration. Three sources of drag reduction might be identified, but only one deals with forward sweep. First, the X-29 three-surface arrangement provides negligible trim drag penalties. Second, two segment variable camber for the main wing trailing edge minimizes flow separation and camber drag penalties. Finally, it is conjectured that forward sweep yields a more favorable leading edge suction distribution. Note that for an aft swept wing, the drag-loading curve (which is a function of wing span location), reveal drag forces over most of the wing surface with particular concentrations at the

wing root (see Figure 14-A). The wing tip exhibits a suction or thrust component. For a forward swept wing, the opposite situation exists. Drag forces register across most of the span, particularly at the wing tip. The root, however, registers thrust (see Figure 14-B). On a weighted integral basis (see eq. 7) suction at the root could be considerably more beneficial than suction at the wing tip. Also, the wing root typically features thicker airfoil sections characterized by larger leading edge radii providing the appropriate forward-facing surface to absorb the full suction potential. Going back to Figure 13-A, a 24% improvement in polar efficency can be identified near $C_L = 1.0$ if comparison is made to the best conventional configuration polar shape. The interesting feature to be identified in Figure 13-B is that the transonic polar shape efficiency improvement (at a lift level comparable to that just noted for subsonic flow) is now 36%. This gain, which is greater when compressibility effects are present, is most likely attributable to the two aforementioned forward sweep drag reduction mechanisms [i.e., 1) upper/lower load sharing and 2) shock wave over-sweep at extreme conditions].

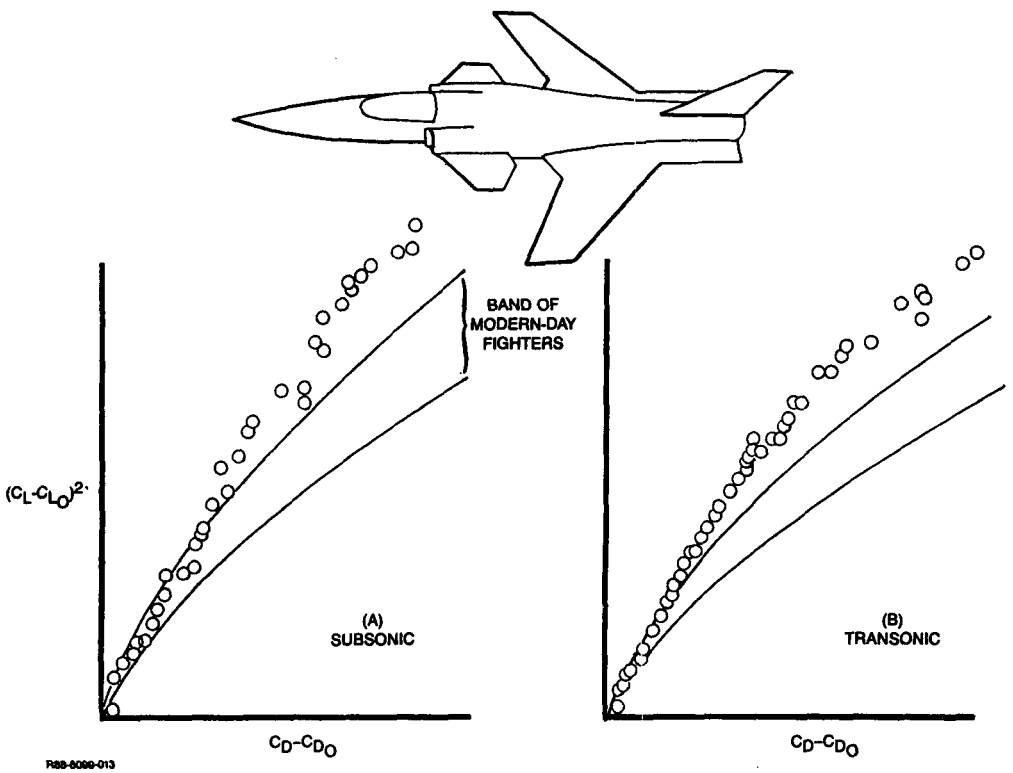

Figure 13 X-29 Drag Polar Efficiency Comparison at Subsonic & Transonic Speeds (All Aircraft Data Converted to $\mathcal{R} = 4$)

$$C_D = \sum \frac{cCd}{c_{av}} \tag{7}$$

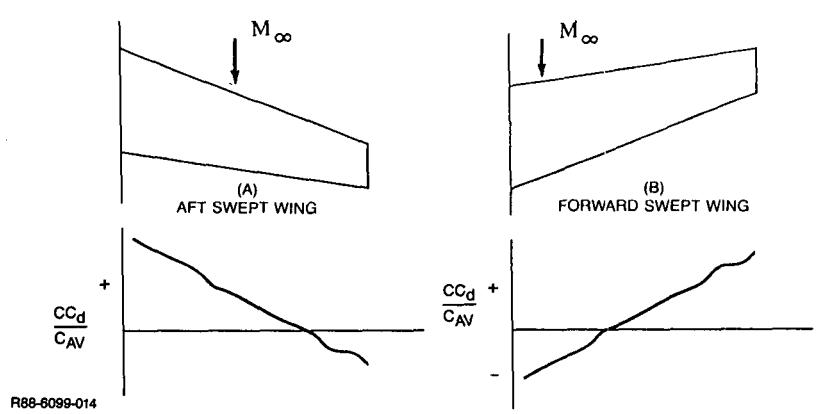

Figure 14 Forward/Aft Sweep Wing Drag Loading

This example, using the X-29, demonstrates how CFD can have an impact on drag prediction and design in an indirect sense. The benefit in terms of wing design procedure value and conceptual evaluation is underscored by the fact that X-29 performance levels were achieved after only 160 hours of configuration development wind tunnel testing were completed.

2.5 3-D ANALYSIS EXPERIENCE

Recent 2-D CFD code experience was used in Section 2.3 to establish upper bounds for 3-D CFD drag analysis of wing shapes at transonic speeds. Beyond this, experience indicates, as noted in Reference 1, that wing drag prediction accuracy via CFD for transports at cruise conditions is in the order of 10-30 counts. Often, variations on the order of several counts are sought. Successful project applications, wherein the favorable outcome of the program can be attributed to absolute drag prediction capabilities with this level of accuracy, are not in hand. But 3-D analyses, despite even current limitations, can play an important role during design/analysis by highlighting problem areas. As a result, it is often possible to optimize and attain close to an ideal aerodynamic solution even though absolute drag levels predicted are in error.

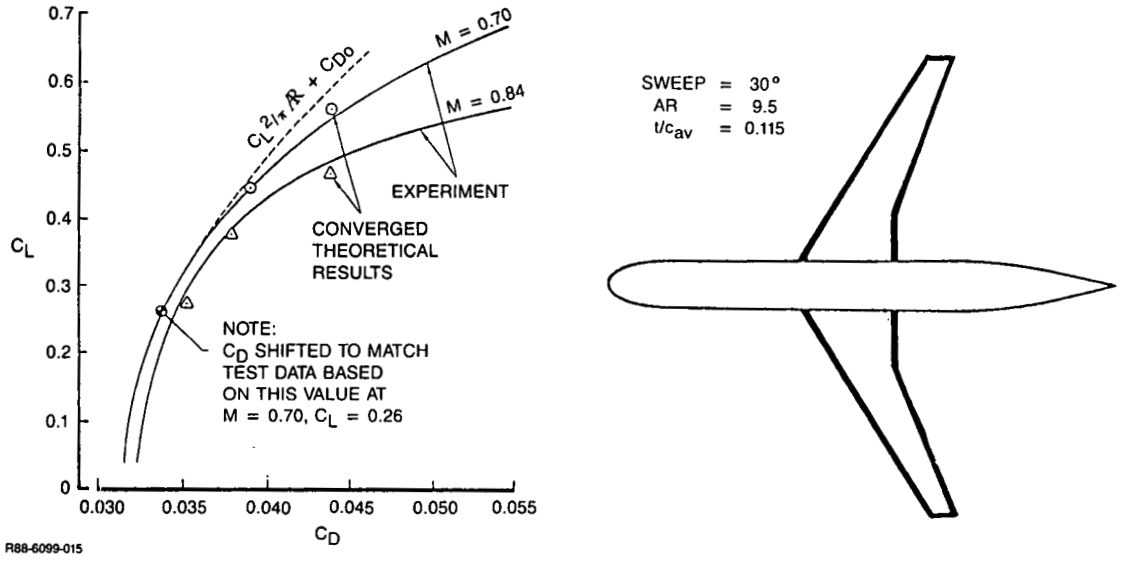

Figure 15 Comparison of Transport Model CFD & Experimental Drag Polar Shape (Boeing-Tinoco)

Figure 15 transport computations provided by Tinoco[11] using a full potential code coupled with a 3-D finite difference boundary layer method[45] demonstrates polar shape accuracy of about 10 counts over a range of $\Delta C_L \sim 0.3$ if the C_D levels are shifted by the CFD/test difference at the lower lift levels within the band. Perhaps most important, is the method's ability to predict the spanwise distributions of wave and profile drag as illustrated in Figure 16. This type of information, which can in fact be generated quite economically, allows the designer to refine known trouble spots within geometric constraints. Many wing shape concepts can be weeded out prior to commitment to expensive and time consuming sub-scale testing.

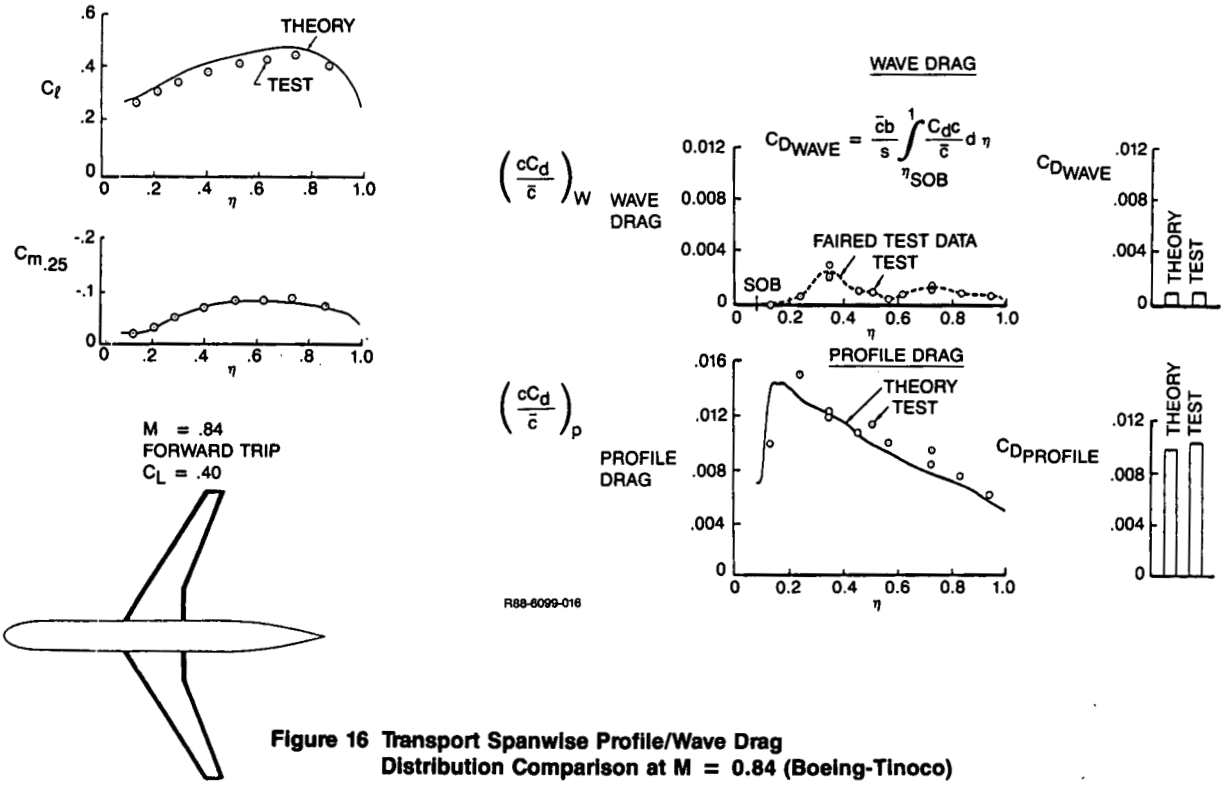

Figure 16 Transport Spanwise Profile/Wave Drag Distribution Comparison at M = 0.84 (Boeing-Tinoco)

2.6 RECENT U.S. HIGHLIGHTS – CFD AERODYNAMIC DRAG PREDICTION

Many references found in the list at the back of this paper identify key elements of CFD drag prediction. Here, an effort is made to highlight a number of items representing work accomplished over the past several years in the United States which have had an impact of CFD drag prediction. These examples include advances in...

A) Computational physics
B) 2-D viscous airfoil simulations
C) Component analysis
D) Hypersonics
E) Conceptual design
F) Configuration optimization – Detailed design.

The examples highlight drag prediction capabilities, both directly (items B, C, D, and E) and indirectly (items A and F).

2.6-A ADVANCES IN COMPUTATIONAL PHYSICS

A vortex sheet is a discontinuity in tangential velocity formed where two streams of differing velocity interface. For aircraft applications, vortex sheets can be identified in turbulent mixing layers, leading edge/wing tip/juncture vortices, wakes, and plumes. The detailed micro-physics of these phenomenon are not fully understood and it is not clear that near or mid-term research experiments will resolve these questions. It may be possible to answer some physics questions computationally by studying numerical mechanics models and comparing final outcome to more easily observed macro-physics test observations. Towards this end, vortex-sheet models of inviscid flow might provide insights needed to better understand turbulent mixing layers. Krasny's work[33] is worth noting.

As vortext sheets evolve computationally, a singularity develops which eventually compromises the sheet's analyticity. Further, computer round-off error enters the solution erroneously amplifying short wave length modes. Krasny[33] describes a desingularization process in which the exact equations describing vortex development are replaced by approximate equations featuring a smoothing parameter. The exact equations and solution are eventually obtained by letting the parameter degrade to zero. Figure 17-A shows a solution to the ordinary differential equations for single precision arithmetic. Figure 17-B is a similar plot for double precision arithmetic. Figure 17-C shows that the desingularization process has the same effect on computed vortex sheet structure as higher precision computing.

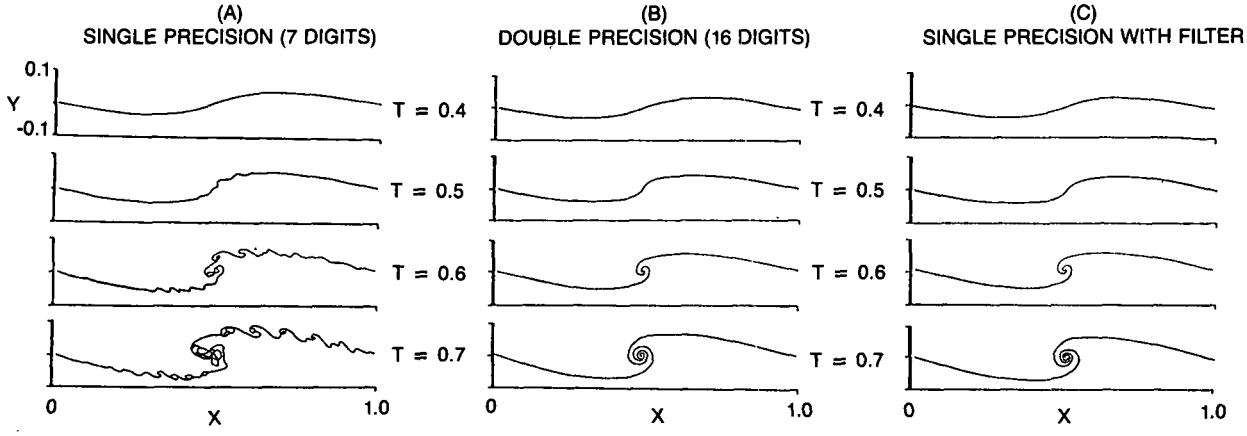

Figure 17 Vortex Sheet Stability (Krasny [33])

CFD predictions constrained by computing hardware involve limits on resolution (n-total number of points) and time step (Δt). Krasny's work offers potential for "numerical relief" which can be implemented to offset hardware constraints.

The work of Corcos and Sherman[32] is also pertinent. Here, the authors provide a numerical simulation for two-dimensional shear flow. It is postulated that complex fluid motions can be rationalized based on the understanding of a small number of elemental motions. Corcos and Sherman use the aforementioned shear layer instability characteristics to provide physical insight into shear layer roll-up and pairing along with the related strain history. Their analysis identifies three characteristics lengthscales for this micro-physics interaction phenomena.

Kim, Moin, and Moser[39] have enhanced the physical understanding of turbulence by performing channel flow computations for a grid of four million points. This numerical data-base will prove valuable for constructing turbulence closure models to be applied to more complex flows, the simulation of which is beyond the range of current supercomputers. A number of discrepancies are identified by comparisons to existing experimental data. Weaknesses in test techniques might, in part, explain the areas of disagreement for normal and shear stresses near the channel walls.

2.6-B 2-D VISCOUS AIRFOIL SIMULATION

Some criticize 2-D airfoil methodology development efforts because "We don't fly airfoils." In Section 2.3, however, a case was made for the value of 2-D design optimization providing that key 2-D/3-D relations are taken into account along the way. In the recent compendium of new airfoil analysis results[9], Holst cautiously leaves conclusions up to the reader. Clearly, there is no best method since different approaches demonstrate good accuracy in different areas. A code selected for one application may not be the best for another application. One global conclusion, however, might be drawn. Considering variety in section shape and conditions, and recalling that for two-dimensional codes shock wave chord location prediction is as critical as absolute drag level projected, it is apparent that the newer and quantitatively dominant (70%) Navier-Stokes schemes do not show any advantage in simulation fidelity. The N.S. schemes are also characterized by a one to two order-of-magnitude computer resource penalty when compared to the older potential/Euler zonal schemes.

One zonal scheme, that of Drela and Giles[10], displays a number of interesting characteristics. Drag prediction accuracy is good for all cases including those at the more extreme conditions ... those that might be encountered well into drag divergence. As noted before, shock sweep loses of about 5° might make predictions on this portion of the 2-D Mach/C_D curve important for wing drag prediction. The code also predicts low Reynolds number airfoil cases featuring transitioning separation bubbles. Maximum drag levels are predicted. It's economical.

This method is not like other codes in that its formulation is characterized by an Euler equation basic outer flow solution coupled with a two-equation integral boundary layer. The set of equations is solved by a global Newton iterative process. The laminar/turbulent boundary layer scheme incorporated is demonstrated to work well for strongly interacting cases. As a result, it is suspected that less reliance on empirical adjustments (see Section 2.3) would be required if this code were implemented. This code appears to have "The Right Stuff" and probably represents an advancement to the state-of-the-art.

2.6-C COMPONENT ANALYSIS

CFD development in the past has relied heavily on correlation studies for isolated components such as airfoils, wings, axi-symmetric bodies, spheres, cylinders, etc. For these types of shapes, geometric complexity is minimized simplifying gridding and the dominance of attached flow increases the probability that useful information will be extracted from the investigation. Success for these components is a prerequisite for graduation to more complete realistic aircraft shapes.

While complex configuration interference effects are important for optimization efforts, knowledge of component contributions and drag source breakdown for each component must also be a high priority. Tinoco[11] illustrates a recent case of nacelle drag prediction using an Euler code coupled with a 3-D finite difference boundary layer method developed by McLean[45]. Inlet mass flow ratio and exhaust pressure ratio effects are included in this simulation. Figure 18 shows the nacelle/strut geometry, gridding, and correlation achieved. For this attached flow case, a desirable 1-count drag accuracy level has registered. Further, the breakdown between wave and profile drag components is now thought to be correct.

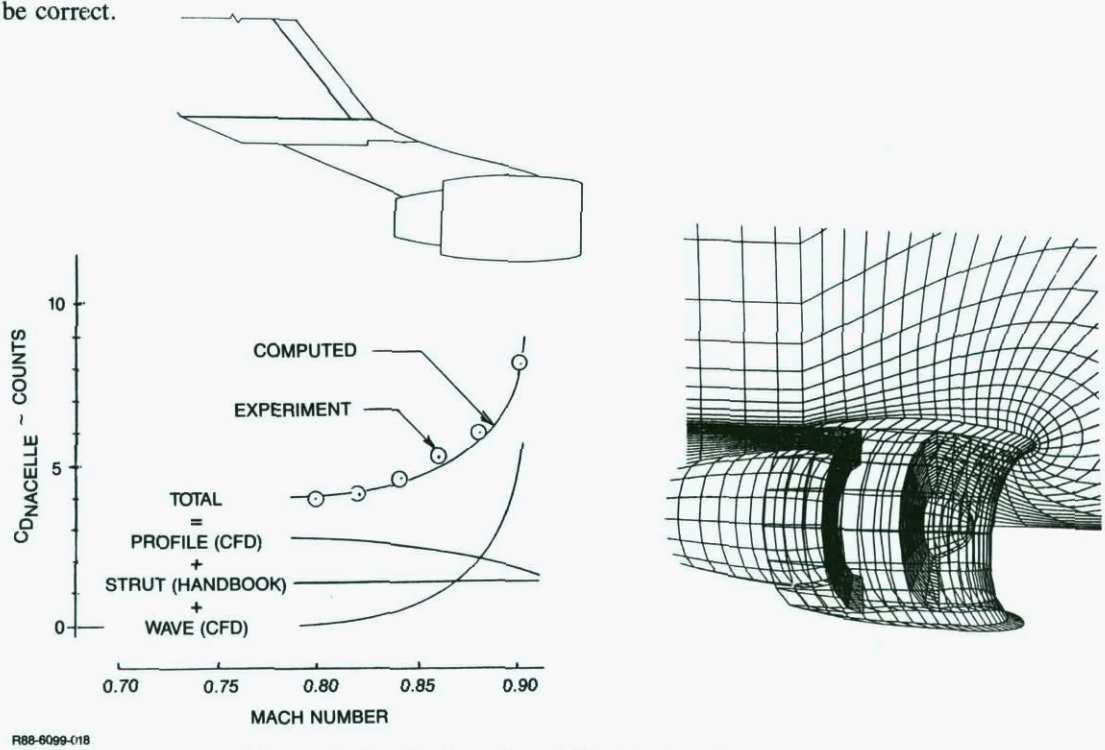

Figure 18 Nacelle Drag Correlation (Boeing-Tinoco)

2.6-D HYPERSONICS

Limits of current ground test facilities are expected to focus considerable attention on CFD as a means for designing future hypersonic vehicles and weapons. Powered hypersonic vehicles now being considered exhibit T-D levels over portions of mission trajectories that are quite small by current standards. Accurate drag prediction and minimization will be critical for success. This problem is compounded by aero-propulsion concepts for which the examination of isolated components provides only a basis or foundation for building complete configuration analyses.

Recent computations by Wilson and Davis[5] provide insights into the difficulties which can be expected. Their CFD calculations are performed using a version of Pulliam and Steger's[43] ARC3D code. This time-dependent 3-D Thin-Layer Navier-Stokes scheme has been modified to include equilibrium-air high-temperature effects. A key to obtaining good heat transfer and drag predictions is (1) the removal of all added dissipation near the body surface and (2) convergence levels that are two to three orders of magnitude beyond that required for good pressure correlation. Figure 19 shows the L/D correlation obtained over a ten-degree range of incidence for two different biconic shapes. The impact of convergence level on lift and drag can be identified in Figure 20.

MEASURED & CALCULATED AERODYNAMIC COEFFICIENTS
AT MACH 6 FOR BICONIC CONFIGURATIONS

	α (deg)		C_N	C_A	C_M	L/D
STRAIGHT BICONIC	0	EXPERIMENT	0.003	0.096	0.000	0.000
		TLNS	0.000	0.095	0.000	0.000
	5	EXPERIMENT	0.153	0.102	-0.005	1.250
		TLNS	0.152	0.102	-0.004	1.260
	10	EXPERIMENT	0.313	0.119	-0.010	1.670
		TLNS	0.325	0.120	-0.011	1.710
BENT-NOSE BICONIC	0	EXPERIMENT	0.108	0.119	0.021	0.908
		TLNS	0.110	0.118	0.020	0.932
	5	EXPERIMENT	0.248	0.140	0.017	1.460
		TLNS	0.266	0.144	0.017	1.510
	10	EXPERIMENT	0.414	0.178	0.015	1.530
		TLNS	0.433	0.184	0.011	1.540

R88-6099-019

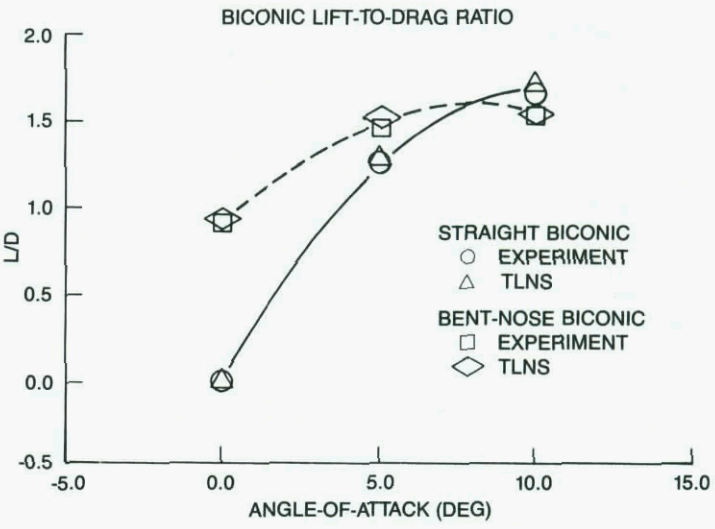

Figure 19 CFD/Test Drag Comparison for Hypersonic Forebodies

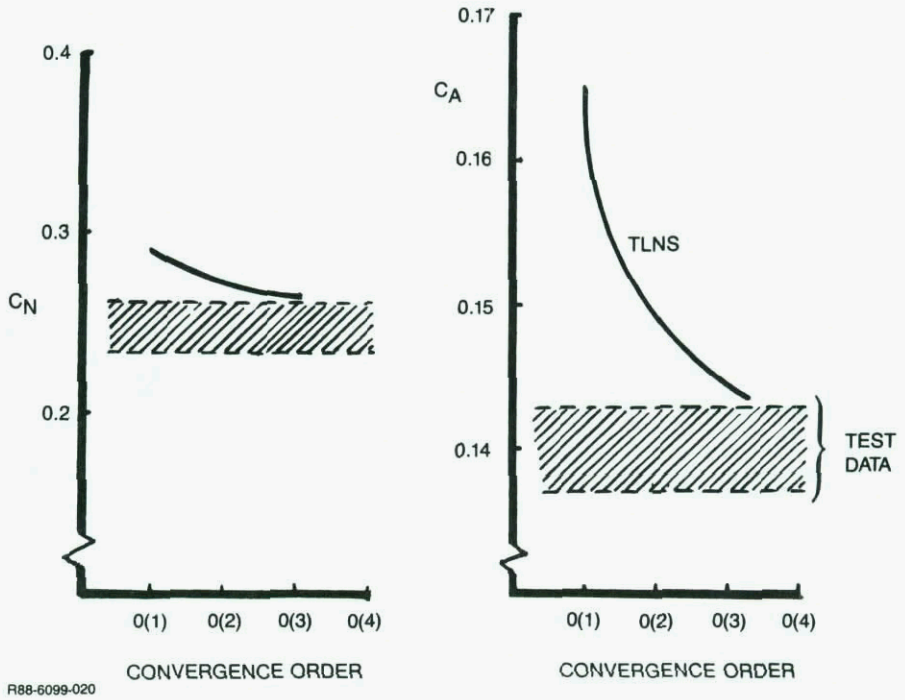

R88-6099-020

Figure 20 Bent-Nose Biconic Lift and Drag Correlation Vs. Convergence Level

Convergence level effects can also be identified using pressure and heat transfer correlations. Resources required for a solution of the Navier-Stokes equations can be assessed by listing the time required for order of magnitude reductions in the "L2 norm" parameter. This weighted maximum residual is based on the five flow parameters involved. The chart below (Table 3) provides a time/convergence relationship.

Table 3 Cray X-MP Convergence/Time Relationship
Hypersonic Forebody Analysis M = 10

L2 NORM ORDER	MINUTES CRAY X-MP
1	17
2	37
3	65
4	120
5	180

Figure 21 shows top, bottom, and side pressure correlation achieved on a bent-nose biconic shape at M=6.0. Note that very good agreement is achieved with the Order-2 solution. Further convergence to Order-3 only slightly improves the forward top centerline pressure level. Note that fourth and fifth Order solutions are not included in this figure.

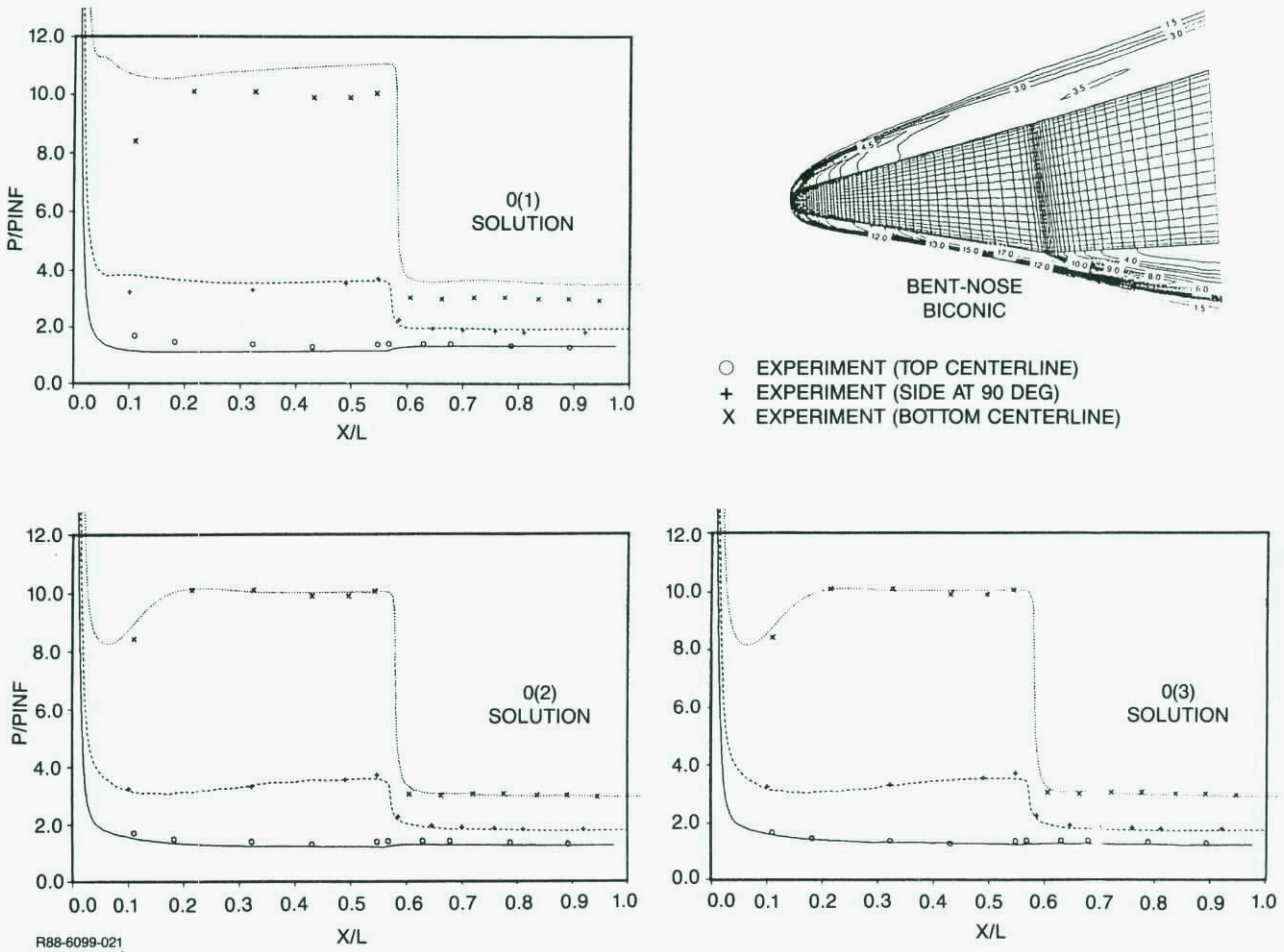

Figure 21 Effect of Convergence Level on Hypersonic Pressure Correlation M = 6

Unfortunately, existing experimental data does not permit both pressure correlation and heat transfer correlation to be examined together at the same flow condition or convergence level. Pressure data for this research forebody shape has been taken at M=6, $\alpha=5°$ while heat transfer data is available at M=10, $\alpha=0°$. Based on past experience, however, the comparison is still useful.

Heat transfer comparisons are quite different. Figure 22 shows correlations for Orders 2 through 5. Agreement is improving by Order-4 and some significant refinement is still identified for the Order-5 solution. The heat transfer comparison in Figure 22 is more aligned in character with drag levels shown in Figure 20. Considerably more resources are required to accurately predict drag or heat transfer levels.

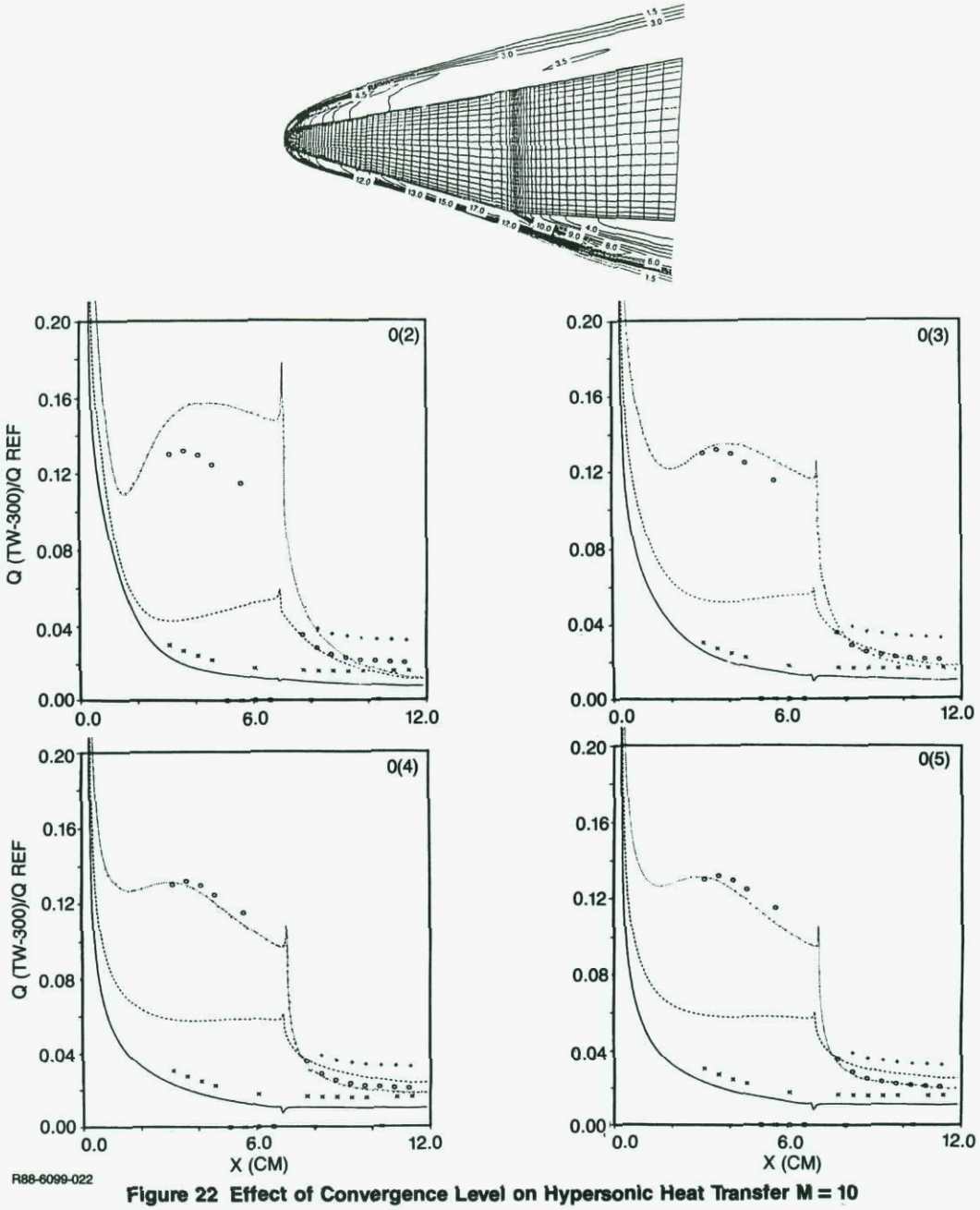

Figure 22 Effect of Convergence Level on Hypersonic Heat Transfer M = 10

2.6-E CONCEPTUAL DESIGN

Linearized methods are typically implemented during aircraft conceptual design efforts to estimate overall lift and wave drag characteristics. At this stage of the aircraft design process, many contour details have not been finalized and the application of very sophisticated CFD methods is impaired by fast response times characterizing the working environment. But computer methods such as the Harris Wave Drag Program[51] are easily applied during conceptualization for wave drag prediction. Techniques like this have been used for over 20 years. Volumetric wave drag in the Harris Program is computed based on an equivalent body form which is a function of Mach number. For fighter configurations, particularly during maneuvering, wave drag due to lift can be appreciable. While these effects are computed by CFD techniques typically during the detailed design phase, it is often not possible to modify the overall wing planform at that point in the design process.

Malmuth et al[18] describe a recently developed nonlinear area ruling procedure for predicting drag rise due to volume and lift. The low expense and simplicity of the scheme make it an attractive candidate for conceptual design work. Physical insight into the problem is derived from the formulation which features a lift component add-on to the equivalent body approach. Figure 23 shows calculations which illustrate the computed magnitude of wave drag due to lift generated on a fighter type planform at two incidence angles.

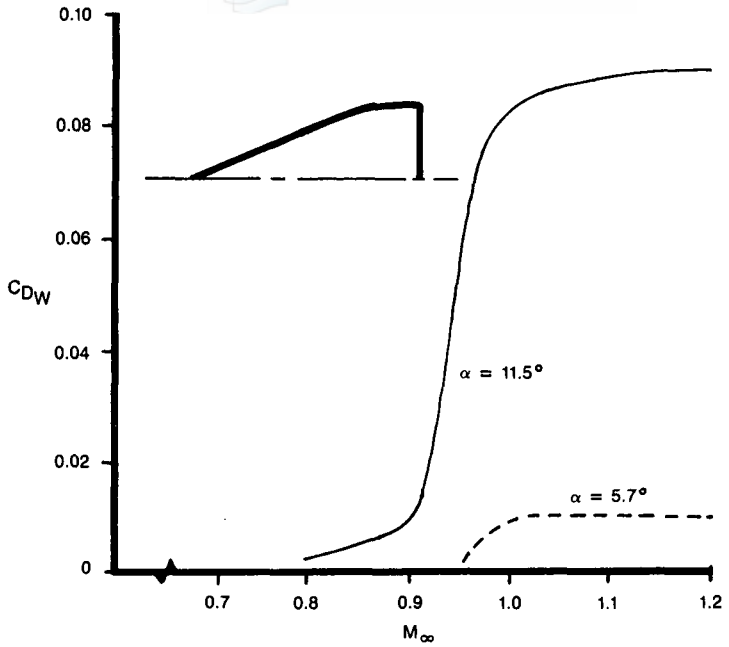

Figure 23 Wing Planform Wave Drag Due-to-Lift Prediction (Ref. 18)

2.6-F CONFIGURATION OPTIMIZATION - DETAILED DESIGN

Calibrated engine flight test data obtained during 1987 for the X-29 Forward Swept Wing Technology Demonstrator reveals unprecedented levels of drag polar shape efficiency. Also of interest is an Air Force turn radius performance comparison involving the X-29, F-16, and F-15 (see Reference 28). While performance levels might in part be attributable to forward sweep, it should be appreciated that the X-29 design featured roots anchored in CFD. The 160 hours of high-speed test time devoted to X-29 configuration development is approximately an order of magnitude less than that accumulated for aircraft with comparable design goals. Key to success was the achievement of a good design prior to first testing. The strength of the CFD approach is underscored as there was no historical data base upon which to evolve the design concept.

2.7 HELICOPTERS & TILT ROTORS

Drag prediction applications for helicopter and tilt-rotor vehicles focus primarily in three areas. First, rotor airfoil design and analysis problems are tackled using the same two-dimensional codes typically implemented for aircraft wing design. As is the case for propellers, rotor applications are "2-D" save for the spanwise flow effect induced by increasing dynamic pressure as the rotor tip is approached. The second and third areas involve component drag prediction in hover and forward flight.

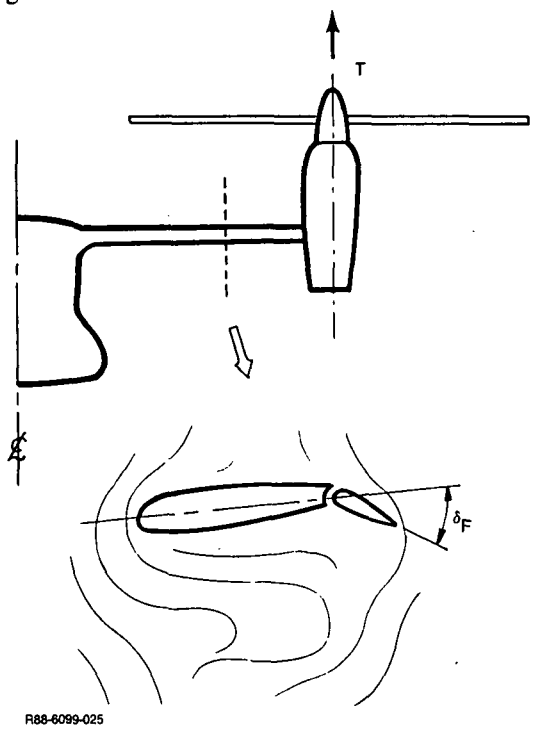

Figure 24 Rotor Downwash - Airfoil Interaction Schematic

Recent hover load/drag prediction efforts have been reported on by McCroskey, et al[26]. The problem has been sketched here as Figure 24. It is known that download, or vertical drag penalty due to rotor downwash for the XV-15 vehicle varies between 5% and 15% of TOGW. It becomes important then, to refine both lifting and non-lifting configuration elements to minimize the download magnitude. Unlike most aircraft drag prediction applications, this case involves drag coefficient levels that are very high ... on the order of 1.0. The key to this study involves blending the best features of sub-scale testing and CFD. For testing, Reference 26 itemizes the following strengths/weaknesses (see Table 5).

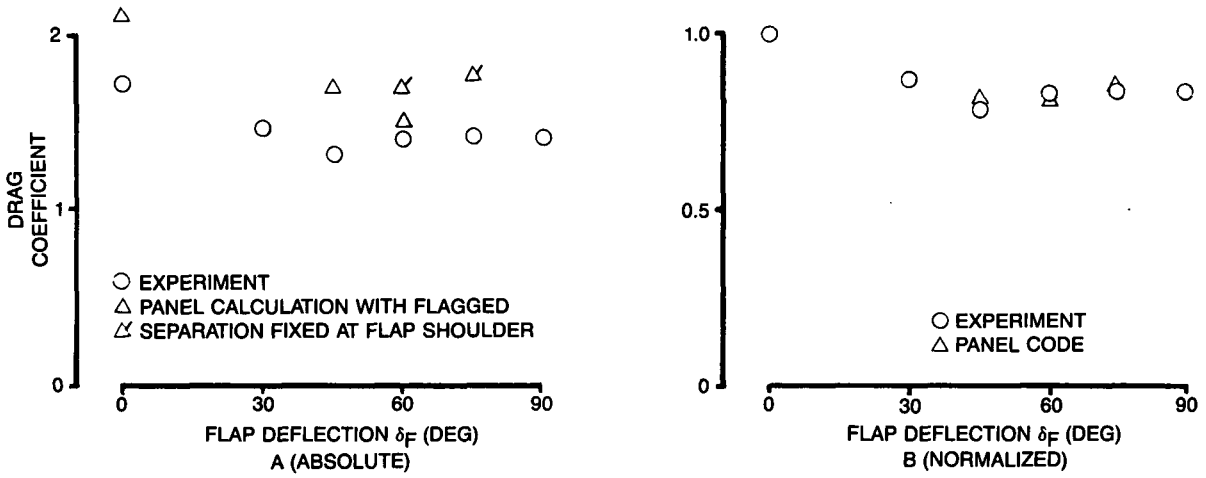

Figure 25 Measured/Calculated Drag vs Flap Deflection Angle (NACA 64A223M Airfoil)

Table 5 Tilt-Rotor Test Strengths/Weaknesses

Strength	Weakness
• Provides definitive facts about separated viscous flow	• Wind tunnel wall corrections • Re corrections • Measurement limitations

Strengths and weakness for CFD analyses were also highlighted as summarized in Table 6.

Table 6 Tilt-Rotor CFD Analysis Strengths/Weaknesses

Strength	Weakness
• Unlimited "measurements" w/no Re, wall problems • Model change/analysis speed and flexibility	• Physical modeling limitations • Formulation approximations • Low confidence in absolute values predicted

Figure 25-A shows that airfoil drag in crossflow varies with the flap deflection angle. The correlation between test data and the computer model is compromised by a shift in absolute drag level. This is quite common for many applications. If the curves are normalized, however, by the $\delta_F = 0$ drag valves, it can be seen (see Fig. 25-B) that proper trends are predicted. This trending was obtained using an unsteady panel method coupled with a free-streamline representation of the separated wake.

Consistent prediction of trends will result in successful computational component optimization despite the fact that absolute drag levels do not agree with test data. The computers speed and relatively low cost in this case permit a large number of shape/orientation combinations to be investigated. In this environment, out-of-the-ordinary solutions which would not be considered for testing based on past experience can surface enhancing the probability of success. The aforementioned airfoil download problem is illustrative in that the minimum drag does not occur when the flap deflection is 90° (minimum area normal to flow).

Efforts to predict more conventional free-stream drag components on helicopter fuselages have not reached this same level of success but it is rewarding to see that attempts are being made to overcome difficulties and the results are being reported. Reference 27 describes unsteady code panelization of a helicopter fuselage shown in Figure 26. Computational drag coefficients based on frontal area varied between 0.15 and 0.20 depending on which flow separation model was used. Test data indicated a C_D level of 0.13.

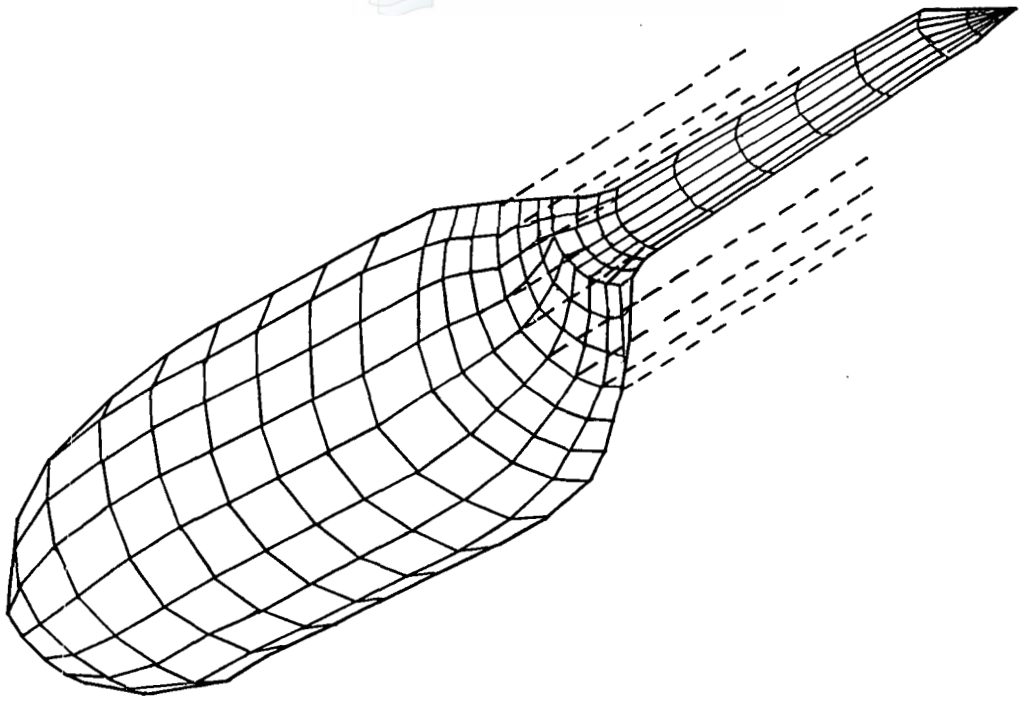

Figure 26 Helicopter Fuselage Panelization for Unsteady Flow Simulation

2.8 MISSILES & PROJECTILES

Computational methods developed for missile and projectile applications[16,19,23,46,47] are characterized by features that are common to aircraft methods. One exception, however, is the concentration on base drag prediction which for missiles (terminal phase of trajectory) and projectiles might vary between 10% and 99% of the total drag. As in the aircraft field, two groups with different approaches have formed. One, represented by Sahu[23,46,47] provides computational flow simulation results based on a thin layer Navier-Stokes formulation. Base drag correlations with test data at supersonic speeds typically agree to within 10%-15%. But is it important to note that testing for this type of data is often compromised by sting attachments interfering with re-circulation zones and lowering the base drag level.

A second approach taken by Wolfe and Oberkampf[22] for incompressible flow is characterized by a source/sink potential flow solution coupled with an integral boundary layer scheme and empirical adjustments based on boat-tail angle for base pressure. Projectile correlations for total drag are within $\pm 10\%$ of test data while cone and flare shapes agree to within $\pm 2\%$. 1% discrepancies are identified for finned non-lifting missiles.

One technique showing promise for projectile drag reduction involves base mass injection. Recent computations performed by Cavalerri[52] using a two-dimensional axi-symmetric Navier-Stokes code are instructive. Figure 27 computer results indicate that base pressure levels agree to within about 10% of test data. For this type of testing, however, experimental scatter is significant as can be seen in Figure 28. So, the levels and trending demonstrated are quite good. Projected trending in base drag as a function of the mass injection ratio can be found in Figure 29. This trending appears to represent an improvement when compared to that of older analysis tools. With this base comparison in hand, the computer simulation can now be implemented to identify the most promising injection arrangement for test evaluation/verification. The advantage of using the CFD tool in this case is that many injection schemes can be investigated. Since flow phenomenon involved are complex and little experience base exists, computer modeling often identifies valuable solutions that are not apparent or solutions that prior to analysis would be rated with a low probability of success.

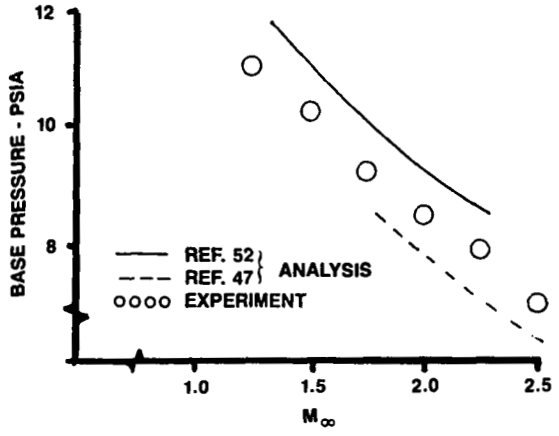

Figure 27 Effect of Mach Number on Base Pressure

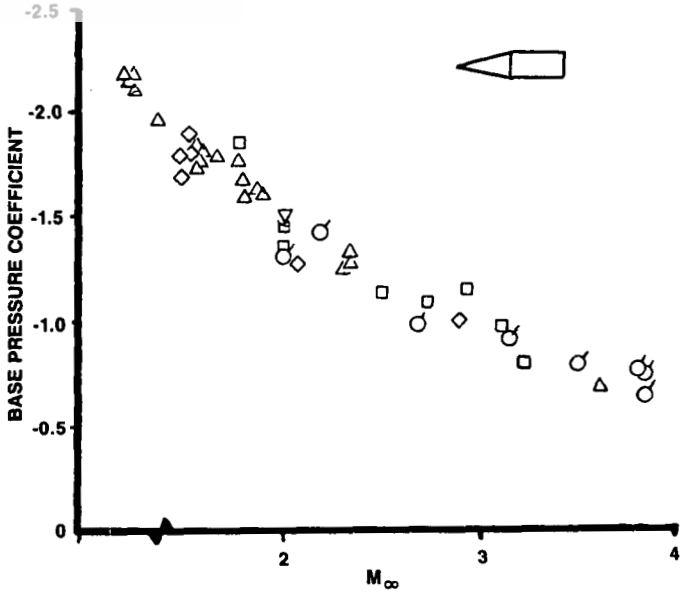

Figure 28 Base Pressure Test Data Scatter

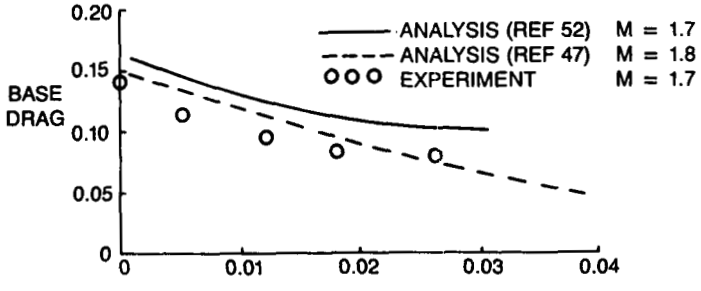

Figure 29 Effect of Mass Injection on Base Drag

2.9 AUTOMOBILES

In certain respects, the aerodynamics problems for automobiles are more complex than that for aircraft and missiles. This is related to the volume of separated and vortical flow that characterizes the application type. It in part, explains why drag computation for automobile applications cannot be found in the literature or by discussions with key applications engineers. The external aerodynamic problems are quite interesting, however, as they include drag reduction, noise suppression (wind), and handling qualities which are influenced by cross-winds and gusting. Industry investments at the present time are concentrating on more sophisticated wind tunnel testing which includes measurements of pressure, velocity components, and turbulence properties. The objective here is to refine and verify new computational method formulations.

3 - CONCLUDING REMARKS

Recent engineering and research advances in the United States addressing the CFD drag prediction problem have been reviewed. In addition, the impact of two-dimensional airfoil analysis accuracy level on wing design has been assessed. The most important conclusion to be drawn is that there are no simple answers to the CFD drag prediction problem. Accurate and consistent direct computation of absolute drag level for complete aircraft configurations is currently beyond reach. Reasons for this come from many sources. Assuming all small features of a particular problem could be modeled (recall excrescence drag - Table 2), it has been shown by Kim et al[39] that grid resolution required to resolve all flow details affecting total drag is insufficient ... by many orders of magnitude. Turbulence models do not completely resolve this problem. Matters are futher complicated by convergence levels required for drag computations. From the Wilson and Davis[5] work on hypersonic Navier-Stokes applications, it is found that residuals must be driven down two to three orders of magnitude beyond that required for reasonably acceptable pressure correlation. Finally, from Krasny's work[33], we find that elements of computational physics forming the cornerstones for computational aerodynamics, are sensitive to machine roundoff error. Machine accuracy must be improved or numerical schemes must be designed to circumvent this problem.

Advances on many fronts can be identified. Most solutions, however, will involve added expense. It should be recognized that once a solution to the CFD drag prediction is found ... the solution may not be affordable. Other means of accomplishing design and analysis tasks could be more competitive for future applications. As evidence that future economic issues exist, note that CFD methodology currently used for the majority of U.S. industry program applications represents ten-year-old technology. In other words, potential flow and Euler schemes with coupled boundary layer analyses dominate. While more sophisticated methods based on Navier-Stokes equations are now in use, these applications typically do not involve drag prediction. This appears to be a function of economics. Any approach requires approximations; for Navier-Stokes formulations, this comes in the form of a turbulence model. The engineer faced with an application is bounded by computing resource constraints in the same manner as sub-scale test and flight test resources are bounded. Current practice suggests that better drag results can be obtained by using CFD resources for resolution and iteration count applied to methods based on potential/Euler flow solvers as opposed to say Thin-Layer-Navier-Stokes solvers wherein resolution and convergence is somewhat compromised by large computer time/core requirements. When drag prediction is of primary interest, errors attributable to approximations in the flow governing equation(s) now appear to be less important than simulation fidelity errors linked to the turbulence model approximation. Skills required by both the CFD research scientist and application engineer have traditionally included mathematics, physics, theoretical methods, numerical analysis, and programming. Now it becomes important to add economics.

Despite these elements which limit direct CFD drag prediction applications, success in project environments has registered on many fronts. Most positive CFD application experiences build on CFD's strengths. As a result, drag prediction and reduction might be thought of as being dealt with indirectly. CFD characteristics to be exploited are listed below.

- Configuration/variable evaluation speed
- Virtually unlimited resolution power (compared to subscale testing)
- Relatively low cost (if properly handled)
- Uncompromised by many factors which limit sub-scale and flight test experimentation

Sub-Scale Test	Flight Test
Wall/Sting interf.	Turbulence
Scaling effects	On-board instrumentation limits
Model contour fidelity	Thrust measurement
Instrumentation accuracy & resolution	Unsteady environment
Power effects	True aircraft shape under load
Aeroelastic effects	Cost/time constraints
Turbulence	Data reduction complexity

As a result, we can expect that one of CFD's primary benefits will be an ability to enhance the traditional aircraft drag build-up process.

In closing it is judged that advances in future decades will remove the current obstacles hindering direct absolute CFD drag prediction. For the near term, by concentrating on CFD's current strengths, it is not necessary to wait for this to happen.

ACKNOWLEDGMENTS

In attempting to portray a current status picture of CFD drag prediction in the U.S.A., the author consulted with many colleagues in the aircraft industry and members of AIAA Applied Aerodynamics Technical Committee. In particular, the following individuals are acknowledged for sharing their personal experiences...

Ed Tinoco	–	Boeing
Woody Bonner	–	Rockwell
Frank Moore	–	NSWC-Dahlgren
Jerry Crusciel	–	Lockheed Missiles & Space
Dean Hammond	–	General Motors
Bill Brayman	–	General Dynamics
Terry Holst	–	NASA-Ames
Bob Melnik	–	Grumman
Warren Davis		
Jim Daywitt	–	General Electric
Preston Henne	–	Douglas
Bob Liebeck		
Walt Sturek	–	ABRL-Aberdeen

Also, the author wishes to thank Warren Davis of Grumman for assistance in preparing the hypersonic computations illustrating convergence level effects on pressure, heat transfer, and drag predictions.

Finally, the author expresses his appreciation to the AGARD Fluid Dynamics Panel for the invitation to participate in the AGARD meeting "Validation of Computational Fluid Dynamics."

REFERENCES

1. Slooff, J. W.; "Computational Drag Analyses and Minimization; Mission Impossible?" AGARD-R-723, May 1985.

2. Hunt, B., et al; "The Strengths and Weaknesses of Computational Fluid Mechanics in Aerodynamic Design and Analysis," Seminars on Computational Fluid Dynamics, VSSC, Trivandrum, India, Dec. 1981.

3. Jobe, C. E.; "Prediction of Aerodynamic Drag," AFWAL-TM-84-203, July 1984.

4. Boppe, C. W.; "Computational Aerodynamic Design: X-29, The Gulfstream Series, and a Tactical Fighter," SAE 851789, October 1985. (SAE Wright Brothers Award Paper . . . 1986).

5. Wilson, G. J. and Davis, W. H.; "Hypersonic Forebody Performance Sensitivities Based on 3-D Equilibrium Navier-Stokes Calculations," AIAA 88-0370, January 1988.

6. Boppe, C. W.; "Engine-Airframe-Store Integration; Computational Methods and Applications." Lectures notes for 1987 Purdue Short Course on Engine-Airframe Integration, July 1987.

7. Boppe, C. W., et al; "Detailed Keel-Winglet Design Considerations for Racing Yachts," Ancient Interface XVII, October, 1987.

8. Davis, W. H. Jr.; "Applied Transonics at Grumman," (Invited Paper) Transonic Symposium – Theory, Application, and Experiment, NASA-Langley Research Center, 19-21 April 1988.

9. Holst, T. L.; "Viscous Transonic Airfoil Workshop Compendium of Results," AIAA 87-1460, June 1987.

10. Drela, M. and Giles, M. B.; "Viscous-Inviscid Analysis of Transonic and Low Reynolds Number Airfoils," AIAA Paper No. 87-0424, Jan. 1987.

11. Tinoco, E. N.; "Transonic CFD Applications at Boeing," Transonic Symposium, NASA-Langley Research Center, April 1988.

12. Boppe, C. W.; "Computational Flow Simulation; Aerospaces CAE Middleman," Mechanical Engineering, Cover Story, August 1984.

13. Henne, P. A., Dahlin, J. A., and Peavey, C. C.; "Applied Computational Transonics-Capabilities and Limitations," Transonic Aerodynamics, Progress in Aeronautics & Astronautics, Vol. 81, 1982.

14. Anonymous; "Going With (And Computing) The Flow," Mechanical Engineering, December 1987.

15. Paterson, J. H. et al; "A Survey of Drag Prediction Techniques Applicable to Subsonic and Transonic Aircraft Design," AGARD CP-124, April 1973.

16. Wardlaw, A. B., Jr., et al; "Multiple Zone Strategy for Supersonic Missiles," Journal of Spacecraft, Vol. 24, No. 4, July-August 1987.

17. Rizzi, A. and Engquist, B.; "Selected Topics in the Theory and Practice of Computational Fluid Dynamics," Journal of Computational Physics, Vol. 72, pp 1-69, 1987.

18. Malmuth, N., et al; "Transonic Wave Drag Estimation and Optimization Using the Non-Linear Area Rule," AIAA 86-1798, June 1986.

19. Devan, L. and Kania, L. A.; "Nonaxisymmetric, Discontinuous Body, Second-Order, Linear, Supersonic Flow Prediction," AIAA 85-1810, June 1985.

20. Shevell, R. S.; "Aerodynamic Bugs: Can CFD Spray Them Away?," AIAA 85-4067, October 1985.

21. Flores, J., et al; "Simulation of Transonic Viscous Flow Over a Fighter-Like Configuration Including Inlet," AIAA 87-1199, June 1987.

22. Wolfe, W. P. and Oberkampf, W. L.; "Drag Prediction for Projectiles and Finned Bodies in Incompressible Flow," AIAA 85-0104, January 1985.

23. Sahu, J., et al; "Navier-Stokes Computations of Projectile Base Flow With and Without Base Injection," AIAA 83-0224, January 1983.

24. Barche, J.; "Experimental Data Base for Computer Program Assessment," AGARD AR-138, 1979.

25. Boppe, C. W., et al; "STARS & STRIPES; Computational Flow Simulations for Hydrodynamic Design," The Eighth Chesapeake Sailing Yacht Symposium Proceedings, pp 124-146, March 1987.

26. McCroskey, W. J., et al; "Airloads on Bluff Bodies, with Application to the Rotor-Induced Downloads on Tilt-Rotor Aircraft," Vertica Vol 9, No. 1, pp 1-11, 1985.

27. Clark, D. R. and Maskew, B.; "Use of Computer Models in Helicopter Drag Prediction," American Helicopter Society Specialist Meeting, Arlington, Texas, 25-27 February 1987.

28. Pitrof, S. M., (AFWAL), Private Communication.

29. Boppe, C. W.; "Future Requirements of Wind Tunnels for CFD Code Verification," AIAA 86-0753, March 1986.

30. Bauer, F., et al; "Supercritical Wing Sections II, a Handbook," Lecture Notes in Economics and Mathematical Systems, No. 108, Springer-Verlag, 1975.

31. Chakravarthy, S. R.; "The Versatility and Reliability of Euler Solvers Based on High-Accuracy TVD Formulations," AIAA 86-0243, January 1986.

32. Corcos, G. M. and Sherman, F. S.; "The Mixing Layer: Deterministic Models of a Turbulent Flow. Part 1. Introduction and the Two-Dimensional Flow," Journal of Fluid Mechanics, Vol. 139, pp 29-65, 1984.

33. Krasny, R.; "Desingularization of Periodic Vortex Sheet Roll-Up," Journal of Computational Physics, Vol 65, pp 292-313, 1986.

34. Rogallo, R. S. and Moin, P.; "Numerical Simulation of Turbulent Flows," Annual Review of Fluid Mechanics, Vol. 16, pp 99-137, 1984.

35. Hackett, J. E. and Sugavanam, A.; "Evaluation of a Complete Wake Integral for the Drag of a Car Like Shape," SAE Paper No. 840577, February 1984.

36. Anonymous; "Aircraft Excresence Drag," AGARD CP-264, 1981.

37. Kapryzynski, J. J.: "Drag of Supercritical Airfoils in Transonic Flow," AGARD CP-124, April 1973.

38. Addy, A. L., et al; "A Study of Flow Separation in the Base Region and Its Effects during Powered Flight," AGARD CP-124, April 1973.

39. Kim, J., et al; "Turbulence Statistics in Fully Developed Channel Flow at Low Reynolds Number," Journal of Fluid Mechanics, Vol. 177, pp 133-166, 1987.

40. Thomson, J. F., et al; Numerical Grid Generation-Foundations and Applications, North-Holland, New York, 1985.

41. Cook, P.H., et al; "Aerofoil RAE 2822 – Pressure Distributions, and Boundary Layer and Wake Measurements," AGARD AR-138, 1979.

42. daCosta, L. A.: "Application of Computational Aerodynamics Methods to the Design and Analysis of Transport Aircraft," ICAS 78.B201, September 1978.

43. Pulliam, T. and Steger, J.; "Implicit Finite-Difference Simulations of 3-D Compressible Flow," AIAA Journal, Vol. 18 (2), pp 159-167, February 1980.

44. Maskew, B.; "Predictions of Subsonic Aerodynamic Characteristics – A Case for Low-Order Panel Methods," AIAA Paper 81-0252 (1981).

45. McLean, J. D. and Randall, J. L.; "Computer Program to Calculate Three-Dimensional Boundary Layer Flows over Wings with Wall Mass Transfer," NASA CR-3123, 1978.

46. Sahu, J. and Nietubicz, C.J; "Numerical Computation of Base Flow for a Projectile at Transonic Speeds," AIAA 82-1358, August 1982.

47. Sahu, J.; "Supersonic Flow over Cylindrical Afterbodies with Base Bleed," AIAA 86-0487, January 1986.

48. Rizzi, A. and Vivind, H.; "Numerical Methods for the Computation of Inviscid Transonic Flows with Shock Waves - A GAMM Workshop, Friedr. Vieweg & Sohn, Braunschweig/Wiesbaden, 1981.

49. Covert, E. E.; Thrust and Drag; Its Prediction and Verification, Progress in Astronautics & Aeronautics, Vol. 98, AIAA, New York, 1986.

50. Kline, S. J., Cantwell, B. J., and Lilley, G. M.; Complex Turbulent Flows, Vol. II, 1980-81 AFOSR-HTTM-Stanford Conference on Complex Turbulent Flows, Stanford University, 1982.

51. Harris, R. V., Jr.; "An Analysis and Correlation of Aircraft Wave Drag," NASA TM X-947, 1964.

52. Cavalerri, R. J. and Posey, S. A.; "Effect of Injection Configuration on Base Drag Reduction," AIAA 88-0213, January 1988.

REPORT DOCUMENTATION PAGE

1. Recipient's Reference	2. Originator's Reference	3. Further Reference	4. Security Classification of Document
	AGARD-AR-256	ISBN 92-835-0516-6	UNCLASSIFIED

5. Originator
Advisory Group for Aerospace Research and Development
North Atlantic Treaty Organization
7 rue Ancelle, 92200 Neuilly sur Seine, France

6. Title
TECHNICAL STATUS REVIEW ON DRAG PREDICTION AND ANALYSIS FROM COMPUTATIONAL FLUID DYNAMICS: STATE OF THE ART

7. Presented at
the Laboratorio Nacional de Engenharia Civil, Lisbon, Portugal, on 5 May 1988.

8. Author(s)/Editor(s)	9. Date
Various THIBERT J.J. BUCCIANTINI G. SCHMIDT W. PAPAILIOU K.D.	May 1988

10. Author's/Editor's Address	11. Pages
Various	156

12. Distribution Statement
This document is distributed in accordance with AGARD policies and regulations, which are outlined on the Outside Back Covers of all AGARD publications.

13. Keywords/Descriptors

Computation
Fluid dynamics
Drag
Predictions
Numerical analysis

14. Abstract

This Report contains the papers presented at the AGARD Fluid Dynamics Panel Technical Status Review on "Drag Prediction and Analysis from Computational Fluid Dynamics: "State of the Art" held in Lisbon, Portugal on 5 May 1988. Speakers presented a state of the art review from their individual nation. The Program Chairman summarized the key conclusions from all the papers presented. It is recommended that the Fluid Dynamics Panel consider possibilities for further stimulation of progress in the field of CFD-based drag prediction and analysis.

AGARD Advisory Report No.256	AGARD-AR-256
Advisory Group for Aerospace Research and Development, NATO TECHNICAL STATUS REVIEW ON DRAG PREDICTION AND ANALYSIS FROM COMPUTATIONAL FLUID DYNAMICS: STATE OF THE ART Published June 1989 156 pages This Report contains the papers presented at the AGARD Fluid Dynamics Panel Technical Status Review on "Drag Prediction and Analysis from Computational Fluid Dynamics: "State of the Art" held in Lisbon, Portugal on 5 May 1988. Speakers presented a state of the art review from their individual nation. The Program Chairman summarized the key conclusions from all the papers P.T.O.	Computation Fluid dynamics Drag Predictions Numerical analysis

AGARD Advisory Report No.256	AGARD-AR-256
Advisory Group for Aerospace Research and Development, NATO TECHNICAL STATUS REVIEW ON DRAG PREDICTION AND ANALYSIS FROM COMPUTATIONAL FLUID DYNAMICS: STATE OF THE ART Published June 1989 156 pages This Report contains the papers presented at the AGARD Fluid Dynamics Panel Technical Status Review on "Drag Prediction and Analysis from Computational Fluid Dynamics: "State of the Art" held in Lisbon, Portugal on 5 May 1988. Speakers presented a state of the art review from their individual nation. The Program Chairman summarized the key conclusions from all the papers P.T.O.	Computation Fluid dynamics Drag Predictions Numerical analysis

AGARD Advisory Report No.256	AGARD-AR-256
Advisory Group for Aerospace Research and Development, NATO TECHNICAL STATUS REVIEW ON DRAG PREDICTION AND ANALYSIS FROM COMPUTATIONAL FLUID DYNAMICS: STATE OF THE ART Published June 1989 156 pages This Report contains the papers presented at the AGARD Fluid Dynamics Panel Technical Status Review on "Drag Prediction and Analysis from Computational Fluid Dynamics: "State of the Art" held in Lisbon, Portugal on 5 May 1988. Speakers presented a state of the art review from their individual nation. The Program Chairman summarized the key conclusions from all the papers P.T.O.	Computation Fluid dynamics Drag Predictions Numerical analysis

AGARD Advisory Report No.256	AGARD-AR-256
Advisory Group for Aerospace Research and Development, NATO TECHNICAL STATUS REVIEW ON DRAG PREDICTION AND ANALYSIS FROM COMPUTATIONAL FLUID DYNAMICS: STATE OF THE ART Published June 1989 156 pages This Report contains the papers presented at the AGARD Fluid Dynamics Panel Technical Status Review on "Drag Prediction and Analysis from Computational Fluid Dynamics: "State of the Art" held in Lisbon, Portugal on 5 May 1988. Speakers presented a state of the art review from their individual nation. The Program Chairman summarized the key conclusions from all the papers P.T.O.	Computation Fluid dynamics Drag Predictions Numerical analysis

presented. It is recommended that the Fluid Dynamics Panel consider possibilities for further stimulation of progress in the field of CFD-based drag prediction and analysis.

ISBN 92-835-0516-6

presented. It is recommended that the Fluid Dynamics Panel consider possibilities for further stimulation of progress in the field of CFD-based drag prediction and analysis.

ISBN 92-835-0516-6

presented. It is recommended that the Fluid Dynamics Panel consider possibilities for further stimulation of progress in the field of CFD-based drag prediction and analysis.

ISBN 92-835-0516-6

presented. It is recommended that the Fluid Dynamics Panel consider possibilities for further stimulation of progress in the field of CFD-based drag prediction and analysis.

ISBN 92-835-0516-6

AGARD

NATO OTAN

7 rue Ancelle · 92200 NEUILLY-SUR-SEINE

FRANCE

Telephone (1)47.38.57.00 · Telex 610 176

DISTRIBUTION OF UNCLASSIFIED AGARD PUBLICATIONS

AGARD does NOT hold stocks of AGARD publications at the above address for general distribution. Initial distribution of AGARD publications is made to AGARD Member Nations through the following National Distribution Centres.Further copies are sometimes available from these Centres, but if not may be purchased in Microfiche or Photocopy form from the Purchase Agencies listed below.

NATIONAL DISTRIBUTION CENTRES

BELGIUM
Coordonnateur AGARD — VSL
Etat-Major de la Force Aérienne
Quartier Reine Elisabeth
Rue d'Evere, 1140 Bruxelles

CANADA
Director Scientific Information Services
Dept of National Defence
Ottawa, Ontario K1A 0K2

DENMARK
Danish Defence Research Board
Ved Idraetsparken 4
2100 Copenhagen Ø

FRANCE
O.N.E.R.A. (Direction)
29 Avenue de la Division Leclerc
92320 Châtillon

GERMANY
Fachinformationszentrum Energie,
Physik, Mathematik GmbH
Karlsruhe
D-7514 Eggenstein-Leopoldshafen 2

GREECE
Hellenic Air Force General Staff
Aircraft Support Equipment Directorate
Department of Research and Development
Holargos, Athens, TGA 1010

ICELAND
Director of Aviation
c/o Flugrad
Reyjavik

ITALY
Aeronautica Militare
Ufficio del Delegato Nazionale all'AGARD
3 Piazzale Adenauer
00144 Roma/EUR

LUXEMBOURG
See Belgium

NETHERLANDS
Netherlands Delegation to AGARD
National Aerospace Laboratory, NLR
P.O. Box 126
2600 AC Delft

NORWAY
Norwegian Defence Research Establishment
Attn: Biblioteket
P.O. Box 25
N-2007 Kjeller

PORTUGAL
Portuguese National Coordinator to AGARD
Gabinete de Estudos e Programas
CLAFA
Base de Alfragide
Alfragide
2700 Amadora

SPAIN
INTA (AGARD Publications)
Pintor Rosales 34
28008 Madrid

TURKEY
Millî Savunma Bakanlığı (MSB)
ARGE Daire Başkanlığı (ARGE)
Ankara

UNITED KINGDOM
Defence Research Information Centre
Kentigern House
65 Brown Street
Glasgow G2 8EX

UNITED STATES
National Aeronautics and Space Administration (NASA)
Langley Research Center
M/S 180
Hampton, Virginia 23665

THE UNITED STATES NATIONAL DISTRIBUTION CENTRE (NASA) DOES NOT HOLD STOCKS OF AGARD PUBLICATIONS, AND APPLICATIONS FOR COPIES SHOULD BE MADE DIRECT TO THE NATIONAL TECHNICAL INFORMATION SERVICE (NTIS) AT THE ADDRESS BELOW.

PURCHASE AGENCIES

National Technical
Information Service (NTIS)
5285 Port Royal Road
Springfield
Virginia 22161, USA

ESA/Information Retrieval Service
European Space Agency
10, rue Mario Nikis
75015 Paris, France

The British Library
Document Supply Centre
Boston Spa, Wetherby
West Yorkshire LS23 7BQ
England

Requests for microfiche or photocopies of AGARD documents should include the AGARD serial number, title, author or editor, and publication date. Requests to NTIS should include the NASA accession report number. Full bibliographical references and abstracts of AGARD publications are given in the following journals:

Scientific and Technical Aerospace Reports (STAR)
published
Informati
NASA H
Washingt

Government Reports Announcements (GRA)

ISBN 92-835-0516-6